Hungarian University of Agriculture and Life Sciences

APPLICATION OF NON-DESTRUCTIVE TECHNIQUES IN QUALITY ASSESSMENT OF FRUITS AND VEGETABLES DURING POST-HARVEST STORAGE

Zinabu Hailu Siyum

Budapest

2025

PhD School/ Program

Name: Doctoral School of Food Science

Field: Food Science

Head: **Livia Simon Sarkadi, DSc**
Professor, D.Sc.
MATE, Institute of Food Science and Technology,
Department of Food Chemistry and Nutrition

Supervisors:

Dr. Baranyai László
Professor, Ph.D.
MATE, Institute of Food Science and Technology,
Department of Food Measurements and Process Control

Dr. Nguyen Le Phuong Lien,
Researcher, PhD
MATE, Institute of Food Science and Technology,
Department of Livestock Product and Food Preservation Technology

The applicant met the requirement of the Ph.D. regulations of the Hungarian University of Agriculture and Life Sciences, and the thesis is accepted for the defense process.

.....

Head of Doctoral School

.....

Supervisors

TABLE OF CONTENTS

LIST OF ABBREVIATIONS

ACS	Amino cyclopropane carboxylate synthase
ACO	Amino cyclopropane carboxylate oxidase
ANN	Artificial neural network
ANOVA	Analysis of Variance
BLE	Bluetooth Low Energy
CA	Controlled atmosphere
CCD	Charge-Coupled Device
CDF	Cauchy distribution function
CI	Confidence interval
CARS	Competitive adaptive reweighted sampling
CMOS	Complementary Metal-Oxide-Semiconductor
FAO	Food Agriculture Organization
FDA	Flexible discriminant analysis
GA	Genetic algorithm
GDF	Gaussian distribution function
GF	Gompertz function
GL	Gaussian–Lorentzian
HCSO	Hungarian Central Statistical Office
HSI	Hyperspectral imaging
LDA	Linear discriminant analysis
LD	Lorentzian distribution
LLBI	Laser light backscattering imaging
LS-SVM	Least squares-support vector machine
LV	Latent variables
MARS	Multivariate adaptive regression splines
MCP	Methylcyclopropene
MLR	Multi-linear regression
MSC	Multiplicative scatter correction

MVR	Multivariate regression
NDI	Normalized difference index
NIR	Near-infrared spectroscopy
PCA	Principal component analysis
PLS-DA	Partial least square discriminant analysis
PLS2-DA	Partial least squares 2-Discriminant analysis
PLSR	Partial least squares regression
QDA	Quadratic discriminant analysis
QI	Quality index
RH	Relative humidity
RPD	Residual prediction deviation
RMSEP	Root mean square error for predictions
SG	Savitzky-Golay
SNR	Signal-to-noise ratio
SNV	Standard normal variate
SPA	Successive Projections Algorithm
SSC	Soluble solid content
SVM	Support vector machine regression
USB	Universal Serial Bus
Vis-SWIR	Visible and short-wave infrared
VNIRS	Visible and near-infrared spectroscopy
WHO	World Health Organization
WL	Weight loss

1. INTRODUCTION

1.1 Background

Fruit and vegetables are essential for a healthy diet. They support immune function and reduce the risk of chronic diseases (Głąbska et al., 2020; Lara et al., 2020). As living standards improve, people are focusing more on the quality, taste, and nutritional value of fruits and vegetables (Mason-D'Croz et al., 2019; Pegiou et al., 2019). However, these horticultural products can deteriorate during storage due to temperature and time, affecting quality (Johnston et al., 2001; Ha et al., 2023). This can reduce shelf life. There's an increasing need for efficient methods to monitor and evaluate the quality of fruits and vegetables during postharvest storage. Traditional inspection techniques are often invasive, destructive, time-consuming, and not suitable for continuous, real-time evaluation. This indicates the need for rapid, nondestructive, and cost-effective methods to assess the quality and physiological status of fruits and vegetables (Costa and Lima, 2013; Nicolaï et al., 2007; Tian and Xu, 2022).

Optical methods, such as near-infrared (NIR) spectroscopy and laser light backscattering imaging (LLBI), have emerged as promising nondestructive techniques for postharvest quality assessment of fruits and vegetables. NIR spectroscopy typically operates within the 700–2500 nm wavelength range by measuring the light absorption to evaluate internal quality attributes, such as soluble solids content (SSC), firmness, and moisture content (Nicolaï et al., 2007; Tian and Xu, 2022). Conversely, LLBI utilizes laser diodes in the visible to near-infrared range to capture backscattered light, providing insights into tissue structure and surface properties based on scattering profiles (Qing et al., 2008; Baranyai and Zude, 2009; Mollazade et al., 2012). The NIR spectroscopy and LLBI are relatively low in cost and have faster acquisition times. Additionally, they have simpler hardware setups and better adaptability for real-time and industrial applications compared to other optical techniques such as hyperspectral imaging (HSI) (Qing et al., 2008; Baranyai and Zude, 2009; Mollazade et al., 2012; Wieme et al., 2022). However, these techniques face challenges related to noise, instrument limitations, and the heterogeneous nature of produce. For example, the water content of fruits and vegetables can overlap with other spectral bands, making interpretation difficult (Assaad, 2020; Bertran et al., 1999; Paz et al., 2008). To address these challenges, various spectral preprocessing methods, such as Savitzky-Golay filters, Standard Normal Variate (SNV), and derivatives, have been applied to improve signal quality (Nicolaï et al., 2007). Additionally,

advanced mathematical techniques, including genetic algorithms, optimization of loading weights in partial least squares regression (PLSR) models, and analysis of regression coefficients, have been employed to select sensitive wavelengths, further improving the calibration of predictive models in spectroscopic analyses (Yao et al., 2023; Zhang et al., 2018). When combined with chemometric models like PLSR, SVM, and MARS, these methods enhance the assessment of fruit and vegetable quality during storage (Hasanzadeh et al., 2022; Rinnan et al., 2009). Chemometric techniques are widely applied to predict various quality attributes of fruits and vegetables (Aline et al., 2023; Chauchard et al., 2004; Kashef, 2021). For instance, Zeb et al. (2023) applied LDA to classify the sweetness content of different orange varieties (*Blood Red, Mosambi, and Succari*), achieving a cross-validated accuracy of 56.7%. Liu et al. (2021) also applied PLSR to evaluate weight loss (R^2 = 0.96, RMSEP = 1.432%) and firmness (R^2 = 0.60, RMSEP = 2.453 N) in Chinese mini cabbage. The least squares support vector machine (LS-SVM) model was used to predict the firmness of pears, achieving an R^2 of 0.893 (Li et al., 2013). Alenazi et al. (2020) found that PLSR predicted the firmness of fresh tomatoes with an R^2 of 0.69. Additionally, Radzevičius et al. (2016) reported that simple linear regression predicted the SSC of tomatoes with an R^2 of 0.815.

Beyond NIR applications, laser light backscattering imaging (LLBI) has been used for the quality assessment of fruits and vegetables. Liu et al. (2020) used LLBI to classify peaches based on storage time with over 90% accuracy, while Daniels et al. (2021) used LLBI to classify grapes by color with 75% accuracy. LLBI has been used to detect decay in oranges due to fungal infection, achieving high accuracy (Lorente et al., 2015). Qing et al. (2007b) demonstrated that LLBI combined with PLSR could predict fruit firmness with R^2 = 0.81 and RMSEP = 5.44 N. Similarly, Romano et al. (2012) used digital imaging and laser diodes (532 nm and 635 nm) to monitor moisture content in bell peppers. They predicted moisture content using scattering area and light intensity, achieving R^2 = 0.86 and RMSEP =7.28 % for yellow peppers. The literature reports showed that non-destructive quality assessments using NIR spectroscopy and LLBI have been conducted at different geographical locations, using various measurement techniques, fruits and vegetables, and varying approaches to spectral and image processing, feature extraction, and calibration models. This work assessed the quality of popular Hungarian fruits and vegetables (i.e., asparagus, plum, and apple) using NIR spectroscopy, LLBI, and different calibration models.

2. LITERATURE REVIEW

2.1 Production and post-harvest storage of fruits and vegetables

Global fruit and vegetable production has steadily increased over the past decade (FAO, 2025). Similarly, in Hungary, the gross production value of fruits and vegetables has increased significantly over the past decade (FAO, 2025; KSH, 2025). However, to meet the dietary needs of an estimated 10 billion people by 2050, fruit and vegetable production will need to increase by 50-150% (Mason-D'Croz et al., 2019; Stratton et al., 2021). Due to the growth in population and increased health awareness, there has also been a rise in the consumption of fruits and vegetables globally. These horticulture items are abundant in bioactive substances that have major health benefits, such as flavonoids, carotenoids, anthocyanins, and phenolic compounds (Ruiz-López and García-Villanova Ruiz, 2023; Yahia et al., 2019). Regular consumption of these products plays an important role in the prevention of cardiovascular disease, diabetes, cancer, and mental disorders (Głąbska et al., 2020; Ju and Park, 2019). The World Health Organization (WHO) recommends a daily intake of at least 400 grams of fruits and vegetables for adults and children older than 10 years (WHO, 2025). Wang et al., (2014) also reported that higher consumption of fruits and vegetables was related to a lower risk of cardiovascular mortality. Additionally, the production, health benefits, and postharvest storage conditions of asparagus, plum, and apple are described in detail in the sections below:

2.1.1 Asparagus

Asparagus is highly valued for its distinct aroma, taste, and nutritional benefits, being low in calories, high in fiber, and rich in phytochemicals (Sergio et al., 2021). Traditionally, asparagus extracts have been used in medicine to treat conditions such as kidney and liver diseases, asthma, and cancer (Pegiou et al., 2019). However, post-harvest preservation remains a major challenge due to its high perishability and rapid deterioration, which results from its high respiratory and metabolic activity (Anastasiadi et al., 2020; Garrido et al., 2001). Storage conditions significantly impact asparagus quality. Storing asparagus at ambient temperatures accelerates chlorophyll breakdown, texture changes, and nutrient loss (Lipton, 2011; Villanueva et al., 2005). While storage above 10°C causes spear toughening, temperatures below 0°C for over 10 days can result in chilling injuries, such as loss of glossiness and wilting (An et al., 2008; Villanueva et al., 2005). Prolonged storage also leads to weight loss due to moisture evaporation from the product. The effect is more pronounced at higher storage temperatures. Increased temperatures not only accelerate weight loss

but also cause discoloration and deterioration of the visual quality of the product. For instance, 'Gijnlim' asparagus exhibited significant discoloration at 10°C (Boonsiriwit et al., 2021; Kitazawa et al., 2011) . In contrast, cold storage at 4°C helps preserve higher levels of chlorophyll and vitamin C, thereby extending both nutritional quality and shelf life (Boonsiriwit et al., 2021). Storage also affects the texture of asparagus, particularly its firmness and toughness. These changes are most noticeable in the lower portions of the spears, where an increase in toughness is attributed to the accumulation of lignin and other phenolic compounds in the cell walls, leading to tissue hardening (Jaramillo et al., 2007; Rodríguez et al., 2004). In addition to physical and biochemical changes, green asparagus is highly susceptible to microbial contamination, primarily from aerobic bacteria, yeast, and mold, which can cause significant deterioration during storage (Wang et al., 2021). The proliferation of these microorganisms is strongly influenced by storage temperature. The higher temperatures accelerating microbial growth leading to faster sensory degradation and reduced shelf life (Valero et al., 2006; Wang et al., 2021). The fresh green asparagus stored at 1–2 °C can remain fresh for up to 14 days. To prevent moisture loss, the relative humidity (RH) should be maintained between 92% and 99%. However, when RH drops as low as 66%, significant weight loss and accelerated quality deterioration occurs, leading to faster degradation of both visual and textural attributes (Fuchs et al., 2008, Villanueva,2005). In cold storage, asparagus is best kept at 0–2°C, with 95–100% relative humidity (RH), 10–14% CO_2, and oxygen levels above 10%, allowing storage for up to 2–3 weeks (Cantwell and Suslow, 2002).

2.1.2 Plum

Plum is a widely consumed stone fruit known for its attractive appearance, flavor, and aroma. According to the Food and Agriculture Organization (FAO, 2025), the leading plum-producing countries include China, Romania, Serbia, and Chile. It is highly valued for its rich nutritional content, containing phytochemicals, vitamins, minerals, and dietary fibers (Lara et al., 2020). Its health benefits include potential roles in anti-inflammatory, memory-improving characteristics, and chronic disease management (Igwe and Charlton, 2016; Lara et al., 2020). However, plums are climacteric fruits with a short shelf life. The ethylene production accelerates ripening, respiration, and senescence, leading to structural and biochemical changes (Khan, 2022; Kumar et al., 2018; Singh and Khan, 2010). Proper storage conditions are crucial for preserving plum quality. Storage at 0 °C to 2 °C provides the best retention of weight, firmness, soluble solids, and vitamin C, while also reducing microbial activity (Briano et al., 2015; Feng et al., 2024; Pimienta et al., 2020). In

contrast, prolonged exposure to temperatures below 2–5°C may cause skin pitting, staining, and flesh browning (Briano et al., 2015; Ding et al., 2010). Higher storage temperatures (above 15°C), however, accelerate microbial growth and increase spoilage risk. For instance, plums stored at 37°C exhibited significant quality deterioration (Cárdenas et al., 2024). Fungal infections are another major factor influencing plum decay, with their growth highly dependent on storage conditions such as temperature, time, and humidity (He et al., 2024; Szparaga et al., 2014). Argenta et al. (2003) stored 'Laetitia' plums at 1 °C and 80 ± 5% relative humidity for up to 50 days, followed by ripening at 23 °C and 75 ± 8% RH for approximately 22 days, using 1-methylcyclopropene (1-MCP) to delay ripening. Similarly, Kumar et al. (2018) reported that under cold storage conditions of 2 ± 1 °C and 85–90% relative humidity, the shelf life and quality of 'Santa Rosa' plums were preserved for up to 28 days. Typically, plums are stored at –1 °C to 0 °C with 90–95% RH to minimize water loss and shriveling. For extended storage, controlled atmosphere conditions with 1–3% O_2 and 2–5% CO_2 are used to slow respiration and ripening, maintaining quality for 2–5 weeks (Cantwell and Suslow, 2002).

2.1.3 Apple

Apple is among the most widely consumed fruits worldwide. The leading apple-producing countries are China, the United State of America (USA), Turkey, Poland, and India (FAO, 2025). China and the USA alone contribute around 50% of global apple production (Khan, 2022). Over the years, global apple production has increased significantly, driven by the introduction of new apple varieties and advancements in cultivation technologies (Sayin et al., 2010). It is also nutritionally rich. It contains phytochemicals such as quercetin, catechin, and chlorogenic acid. These compounds provide health benefits, including reducing the risk of chronic diseases (Hyson, 2011). However, proper storage conditions are essential to maintain apple quality and extend shelf life. Storage at 0°C has been found to better maintain firmness and color and extend the storage time of fresh-cut apples (Li et al., 2014) . In some cases, storage at 4°C may be more beneficial for certain apple varieties, as it helps reduce peel disorders and maintain internal ethylene concentration (Yoo et al., 2018). Additionally, low temperatures (0–4°C) preserve color, flesh hardness, and volatile compounds, maintaining better overall quality compared to higher temperatures (Zhang et al., 2022) . Conversely, higher storage temperatures (such as 20°C) speed up ripening and shorten shelf life by reducing acidity and firmness (East et al., 2008; Zhang et al., 2022). Cold storage is crucial for slowing down ripening, but it can also lead to storage disorders such as flesh breakdown and

browning (Hasan et al., 2024; Lee et al., 2019). During extended storage periods, wound sites on apples serve as entry points for microorganisms, leading to tissue breakdown and decay (Hamilton et al., 2022; Scheper et al., 2007). The fungal infections significantly reduce apple quality and marketable yield (Argenta et al., 2021; Leng et al., 2023). However, other literature suggests that apples are typically stored at 0–3°C to preserve their quality and extend shelf life. This range slows ripening and reduces the quality loss (Büchele et al., 2024; Prange and Wright, 2023). According to Sharma et al. (2013), 'Royal Delicious' apples stored under ambient conditions (22–28 °C and 52–68% RH) exhibited an extended shelf life of up to 35 days. In contrast, Lidster (1990) reported that 'McIntosh' apples stored at 3 °C in controlled atmosphere (CA) conditions for 198 to 255 days, under varying relative humidity levels (80% to 94%). Prange and Wright (2023) reviewed global storage recommendations for apples, suggesting optimal temperatures of 0–1 °C and RH of 90–95% for storage durations of 5–8 months, depending on cultivar sensitivity to chilling. Generally, apples are stored at 0–3 °C with 90–95% RH to minimize moisture loss and maintain firmness. They benefit significantly from CA storage, where oxygen levels are reduced to 1–3% and carbon dioxide is maintained at 0.5–2.5%, depending on the cultivar. Under these optimized conditions, some apple varieties can be stored for up to 9–12 months without significant quality loss (Büchele et al., 2024).

2.2 Quality assessment of fruits and vegetables

Quality assessment of fruits and vegetables is a comprehensive process that involves evaluating both external and internal attributes to ensure that consumer preferences and market standards are fulfilled (Kyriacou and Rouphael, 2018). While external quality is typically assessed visually, internal quality is commonly evaluated using destructive techniques, which include chemical, physical, and mechanical analyses (Jaywant et al., 2022; Lu, 2017). There are two techniques used to assess the quality of fruits and vegetables: traditional and non-destructive techniques. Although traditional techniques provide detailed and accurate results, the trend is shifting towards non-destructive techniques, which offer rapid, efficient, and comprehensive quality assessment without causing damage to the products (Abasi et al., 2018; Aline et al., 2023). The evaluation of quality changes in fruits and vegetables during storage using traditional techniques is presented in detail in the following sections: -

2.2.1 Ethylene production

Ethylene production in fruits typically increases with both temperature and storage duration, contributing significantly to accelerated ripening and softening. For example, plums stored at higher temperatures exhibit elevated ethylene levels. This level is driven by enhanced activities of ethylene biosynthetic enzymes such as ACS (1-aminocyclopropane-1-carboxylate synthase) and ACO (1-aminocyclopropane-1-carboxylate oxidase) (Khan et al., 2011). Melnyk et al. (2014) reported that apples stored at 2 °C for 180 days, ethylene emission varies by cultivar; 'Golden Delicious' showed the highest production (~60 $\mu L \cdot kg^{-1} \cdot h^{-1}$ at 150 days), while 'Idared' remained much lower (~4.4 $\mu L \cdot kg^{-1} \cdot h^{-1}$ at 180 days). Similarly, Wang et al. (2022) demonstrated that apples stored at 20 °C released ethylene more rapidly and in higher amounts (peak ~37.62 $\mu L \cdot kg^{-1} \cdot h^{-1}$ at 10 days) compared to those stored at 0 °C (peak ~26.46 $\mu L \cdot kg^{-1} \cdot h^{-1}$ at 35 days). Storage duration also plays a critical role, with longer periods resulting in higher ethylene levels (Shafiq et al., 2011). Moreover, cold-stored fruits often experience a spike in ethylene production when transferred to ambient temperatures, accelerating ripening and firmness loss. Persimmons stored at 1 °C showed a sharp ethylene surge upon warming, leading to chilling injury (Orihuel-Iranzo et al., 2010), a trend echoed in zucchini moved from 4 °C to 20 °C. Higher storage temperatures further rise ethylene synthesis, which has been related to increased chilling sensitivity (Liu et al., 2022; Whale and Singh, 2007; Megías et al., 2015). Ethylene surges are a central trigger for physiological ripening processes, including texture softening, color development, and sugar accumulation (Luo et al., 2009; Ravindra and Goswami, 2008). Ultimately, higher ethylene levels accelerate fruit senescence, thereby shortening shelf life (Kumar et al., 2018; Manganaris et al., 2008).

2.2.2 Respiration Rate

Respiration rate refers to the rate at which oxygen is consumed, and carbon dioxide is produced in stored plant tissues. Higher respiration rate is closely associated with faster deterioration of produce quality because it accelerates biochemical changes that compromise freshness and shelf life (Ravindra and Goswami, 2008). This rate is influenced by storage temperature and enzymatic activities, and it increases during ripening. For example, Singh and Khan (2010) found that respiration rates rise from a minimum level to a peak as the fruit matures and then decline as it overripens. Argenta et al. (2003) emphasized that lower storage temperatures help suppress ethylene production, slow the ripening process, and extend the shelf life of produce. Contrary, Singh and Khan (2010) reported that higher respiration rates lead to quicker starch depletion and softening

of the fruits. Additionally, Løkke et al. (2011) demonstrated that respiration rates can increase by two to three times with every 10°C rise in temperature, underlining the importance of controlled temperature in maintaining postharvest quality. However, respiration rate can be affected by cultivar type, harvest maturity, preharvest environment, storage temperature, atmospheric composition, and postharvest treatments (Singh and Khan, 2010). Studies on crops like tomato, pepper, cucumber, and zucchini reveal that respiration varies significantly among cultivars (Priss et al, 2017). In climacteric fruits such as papaya, apples, and plums, respiration rates increase over time and with rising temperatures after harvest (Torrieri et al., 2009; Martins et al., 2014; Singh and Khan, 2010). Furthermore, Choi and Jung (2014) observed that respiration rates increased more rapidly in 'Fuji' apples stored at higher temperatures. In contrast, low temperatures can slow the respiration rate during storage (Singh and Khan, 2010). The temperature dependence of respiration is further illustrated in specific crops. Green mature mangoes, for example, exhibit a sharp increase in CO_2 production from approximately 16.5 ml CO_2 kg^{-1} h^{-1} at 5 °C to around 55 ml CO_2 kg^{-1} h^{-1} at 30 °C, with a decline over time in closed systems due to oxygen depletion (Ravindra and Goswami, 2008). Similarly, pomegranate fruit and arils show higher respiration at warmer temperatures: whole fruit CO_2 production increases from about 5.7 ml CO_2 kg^{-1} h^{-1} at 5 °C to 18.5 ml CO_2 kg^{-1} h^{-1} at 15 °C, while fresh arils range between 2.7 and 9.0 ml CO_2 kg^{-1} h^{-1} over the same temperature range, with cultivar differences also influencing CO_2 evolution (Caleb et al., 2012). In fresh-cut Annurca apples, respiration is primarily driven by temperature, with CO_2 production rising from about 3.0 ml CO_2 kg^{-1} h^{-1} at 5 °C to approximately 11.0 ml CO_2 kg^{-1} h^{-1} at 20 °C (Torrieri et al., 2009).The CO_2 production of 'Golden' papaya stored at 13 °C also rose from 7.62 to 33.18 mL kg^{-1} h^{-1} over 30 days (Martins et al., 2014). on the other hand, Plums benefit from controlled atmosphere (CA) storage conditions typically 1–3% O_2 and 2–5% CO_2 which help sup-press respiration and delay ripening (Cantwell and Suslow, 2002). Lu et al. (2023) developed a mathematical model for modified atmosphere packaging (MAP) using low-density polyethylene (LDPE) film to extend the shelf life of green asparagus. Their active MAP system maintained an internal atmosphere of 6.5% oxygen (O_2) and 15.5% carbon dioxide (CO_2) during storage at 5 °C.

2.2.3 Weight Loss

Weight loss is a critical indicator of the postharvest quality of fruits and vegetables. It affects their appearance due to shrinkage. The rate of weight loss is influenced by storage conditions, such as temperature and humidity, which affect respiration and water transpiration (Van Dijk et al., 2006). Hasan et al. (2024) indicated that water loss is a factor affecting the postharvest quality and shelf life of apples. Additionally, Kassebi et al. (2022) reported that higher storage temperatures accelerate weight loss in 'Golden Delicious' apples. Tzoumaki et al. (2009) found that asparagus stored at 4 °C for 11 days lost 7.3% of its weight, while Villanueva et al. (2005) reported an 11.8% loss of weight at 2 °C in 14 days. Atmospheric humidity also plays a significant role in determining weight loss, as shown by Hung et al. (2011). Guerra and Casquero (2008) reported that weight loss is significantly affected by harvest maturity in plums. Fruit harvested earlier showed less weight loss during storage but had low eating quality after ripening compared to later-harvested fruit. Li et al. (2022) noted that 'French' plums stored at 1 °C and 90 % relative humidity experienced significant and progressive weight loss throughout the 35-day storage period. Crisosto et al. (2004) revealed that lower metabolic activity and reduced evaporation in colder storage conditions help preserve the structural integrity of fruits over extended periods. Wang et al. (2016) reported that storage temperature and harvest maturity affect the development of physiological disorders in 'Friar' plums, with rapid disorder development at 5 °C and 15 °C, delayed or suppressed disorders at 0 °C and 2 °C. Additionally, pectin solubilization at 5 °C and 15 °C contributed to gel-like flesh translucency. Zhao et al. (2022) reported that low-temperature storage of fruits and vegetables helps maintain their weight and reduces deterioration caused by the growth of spoilage microorganisms. For instance, apples stored at 2 °C showed minimal weight loss compared to those stored at higher temperatures (Sanad et al., 2023). Similarly, weight loss in tomatoes was significantly affected by transportation distance, storage temperature, and storage period (Al-Dairi et al., 2021).

2.2.4 Firmness

Firmness is a crucial quality attribute that influences consumer perception, marketability, and postharvest value of fruits and vegetables. It is primarily governed by the cell wall structure, tissue composition, and physiological changes occurring during postharvest storage (Huang et al., 2018; Mishra et al., 2022). A reduction in firmness is commonly attributed to enzymatic degradation of cell wall polysaccharides, particularly pectin, by enzymes such as polygalacturonase (PG), pectinesterase (PE), and cellulase (Anastasiadi et al., 2020; Garrido et al., 2001; He et al., 2022).

These enzymatic activities disrupt the structural integrity of plant cells, resulting in tissue softening and texture loss (Toscano et al., 2021; Wang et al., 2016). Low-temperature storage is widely recognized for its ability to preserve firmness by slowing down the conversion of protopectin to soluble pectin and suppressing enzymatic activity (Geng et al., 2020; Manganaris et al., 2008). However, transitions from cold to ambient conditions can accelerate firmness loss due to enhanced ethylene production and increased respiration rates (Matabura, 2022). In fruits like pears, the degradation of soluble pectin by polygalacturonase plays a critical role in softening during cold storage (Kaur and Dhillon, 2015). Similarly, firmness loss in blueberries is related to the increased water-soluble pectin and alterations in the cell wall matrix (Concepción et al., 2021). Moreover, the initial maturity stage at harvest significantly affects postharvest firmness retention. Earlier-harvested fruits generally maintain firmness longer than those harvested at advanced maturity stages, as reported in pears and apples (Kaur and Dhillon, 2014; Candan & Calvo, 2021; Moggia et al., 2017). The role of ethylene is also central to firmness loss, with high ethylene exposure accelerating cell wall breakdown, especially in climacteric fruits like apples (Tong et al., 2013; Concepción et al., 2021). In plums, cooler storage temperatures effectively delay softening and preserve textural quality over extended periods (Guo et al., 2022; Cocco et al., 2022). In contrast to most fruits, green asparagus exhibits firmness loss primarily due to water loss and the accumulation of lignin rather than enzymatic pectin degradation. The rise in lignification during storage contributes to increased toughness, reducing consumer acceptability and overall sensory quality (Toscano et al., 2021; Priss et al., 2024).

2.2.5 Soluble Solid Content (SSC)

Soluble Solids Content (SSC) is an essential quality attribute for fruits and vegetables. It plays a crucial role in determining their sweetness (Guo et al., 2019; Lie et al., 2016). Studies have shown that ripening increases SSC, driven by the conversion of starch into simple sugars and moisture loss during storage. Kodagoda et al. (2021) reported that temperature and time significantly affect the sugar content of fruits like plums, apples, and others. Lower initial SSC is associated with extended storage potential, as higher SSC results in faster metabolic activity and reduced shelf life (Guerra & Casquero, 2008; Crisosto et al., 2004). Additionally, Jha et al. (2012) demonstrated that SSC in apples increases as starch is converted to sugars during ripening (Cao et al., 2021; Tokala et al., 2022). For instance, the SSC of kiwi fruit increases during ripening due to the breakdown of starch into sugars (Xia et al., 2024). However, lower storage temperatures have been shown to decelerate

metabolic processes, thereby prolonging the retention of SSC. In tomatoes stored at low temperatures, SSC degradation was slower compared to those stored in ambient air (Valenzuela et al., 2011). Similarly, Phillips et al. (2021) reported that starch is converted to simple sugars when bananas ripen. On the other hand, peppers, SSC in peppers declined more rapidly during early storage (Díaz-Pérez et al., 2024). In mangoes, spatial variations within the fruit also influence SSC, with the shoulder region near the stem showing higher SSC compared to the tip (Mahayothee et al., 2020). Zhang et al. (2022) observed that the SSC in 'Gannan navel' oranges initially increased during early storage, reflecting enhanced sweetness as sugars accumulated. However, prolonged storage at ambient temperature (20°C) led to a gradual decline in SSC, likely due to sugar degradation and metabolic activity. Conversely, low-temperature storage (4°C) better preserved SSC levels over time. Tomar and Pradhan (2024) also reported that the SSC of Amla (*Phyllanthus emblica*) fruit stored at room temperature significantly increased, primarily due to moisture loss, while SSC changes under low-temperature conditions were insignificant.

2.2.6 Peel Color

Peel color is a key visual indicator of ripeness and quality in fruits and vegetables, governed by pigments like chlorophylls, carotenoids, and anthocyanins (Kapoor et al., 2022; Muhammad et al., 2024). These pigments undergo metabolic changes during ripening and storage, leading to visible color transitions (Kapoor et al., 2022; Schiavon et al., 2023). Anthocyanin accumulation, particularly in fruits like plums, plays a major role in deepening pigmentation (Kodagoda et al., 2021; Lorente et al., 2015). The hue angle and L* value based on the International Commission on Illumination (CIE) typically decrease with ripening, color development (Ozturk et al., 2015; Bizjak et al., 2012). The L* value represents the lightness of the color, ranging from 0 (black) to 100 (white). The hue angle (expressed in degrees) describes the actual color tone: 0° = red, 90° = yellow, 180° = green, and 270° = blue. High storage temperatures accelerate undesirable color changes (Neri et al., 2019), and prolonged storage may degrade pigmentation (Guerra et al., 2010). Controlled conditions help preserve color, as seen in blackberries and pitayas, where anthocyanin synthesis continues postharvest (Martineli et al., 2021, 2022; Schiavon et al., 2023). Aispuro-Hernández et al. (2019) showed that storage temperature directly affects grapefruit peel color via pigment composition. In pomegranates, Sarrwy et al. (2021) found that 10 °C storage enhanced anthocyanin content and red pigmentation, while 20 °C caused browning and 5 °C preserved color with reduced intensity.

2.3 Non-destructive quality assessment of fruits and vegetables

The growing consumer demand for high-quality fruits and vegetables has intensified the need for reliable, efficient, and scalable quality assessment methods (Ncama and Magwaza, 2022). Traditionally, external attributes like color and size are evaluated through visual inspection, yet this method is subjective and often inconsistent due to human perception and environmental factors (Nguyen et al., 2024; Tasioulas et al., 2024). To overcome these challenges, advanced tools integrating machine vision and machine learning now provide objective, repeatable assessments for automated sorting (Araujo et al., 2022; Bahaddou et al., 2024; Tian and Xu, 2023). Meanwhile, internal quality assessment has historically relied on destructive techniques such as chemical analysis and physicochemical testing (Jaywant et al., 2022; Fodor et al., 2024), which, while accurate, are labor-intensive, costly, non-repeatable, and unsuitable for high-throughput use (Tian and Xu, 2022; Jaywant et al., 2022). In contrast, non-destructive technologies such as NIR spectroscopy, LLBI, hyperspectral imaging, and machine vision enable a real-time, large-scale evaluation without damaging the product (Fodor et al., 2024; Baranyai and Zude, 2009; Wieme et al., 2022). These techniques not only reduce waste and operational costs (Luo et al., 2022; Jaywant et al., 2022) but also support continuous postharvest monitoring to preserve freshness (Aline et al., 2023; Shen et al., 2018). Unlike traditional sensory evaluation, which is subjective, non-destructive methods offer consistency through sensor-based measurement and machine learning algorithms (Akter et al., 2024; Elmetwalli et al., 2024). Additionally, traditional systems are often standalone and difficult to digitize, whereas non-destructive tools are designed for integration, automation, and data-driven decision-making across the supply chain (Fakhlaei et al., 2014). However, these advanced techniques also have their own limitations, such as complex data processing requirements, spectral overlapping, the need for skilled personnel, and relatively high costs (Fodor et al., 2024; Wieme et al., 2024). The strengths and weaknesses of these approaches are discussed in detail in Section 2.5.3. This section presents only a general comparison between conventional and non-destructive methods. A summary of their differences in terms of cost, speed, scalability, and integration is provided in Table 1.

Table 1: Comparison between traditional and Non-destructive measurement techniques

Attribute	Traditional measurements	Non-destructive measurements	References
Destructiveness	Often destructive, leading to sample loss	Non-destructive, allowing repeated measurements on the same sample	(Tian and Xu, 2022)
Speed	Time-consuming, especially for large-scale operations	Rapid and suitable for real-time monitoring	Fodor et al 2024
Subjectivity	Subjective, particularly in sensory evaluation	Objective and consistent, reducing human error	(Akter et al., 2024).
Cost	High costs due to labor, equipment, and sample destruction	Lower costs in the long run, with minimal labor and no sample destruction	(Jaywant et al., 2022; Luo et al., 2022)
Integration	Difficult to integrate with automated systems	Easily integrated into sorting lines and supply chain management systems	Fakhlaei et al., 2024
Data analysis	Requires specialized equipment and expertise	Can be combined with machine learning for enhanced accuracy and automation	(Elmetwalli et al., 2024; Salehi, 2020)

2.4 NIR spectroscopy and Laser light backscattering imaging (LLBI)

Near-infrared (NIR) spectroscopy and laser light backscattering imaging (LLBI) are modern, non-destructive techniques that are increasingly being used for postharvest quality assessment of fruits and vegetables. These methods leverage different regions of the electromagnetic spectrum, including 400-1000 nm (VNIR) and 900-1700 nm (NIR), as shown in Figure 1. These spectral ranges are widely utilized to evaluate both internal attributes, such as SSC, moisture content, and firmness, and external features, like color and texture (Gibertoni et al., 2022; Ravikanth et al., 2017). The basic principles, spectral preprocessing strategies, optimal wavelength selection, image analysis, calibration models, and comparison of both NIR spectroscopy and LLBI are discussed in the following sections.

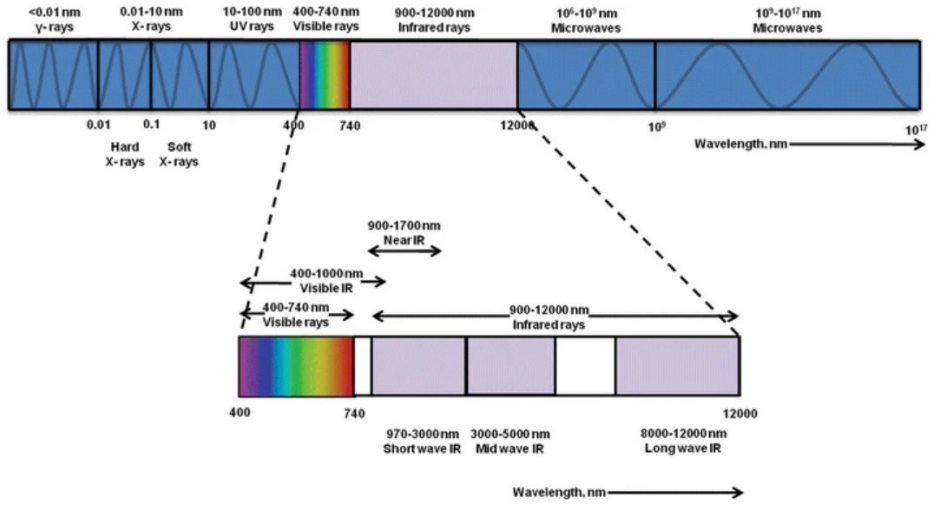

Figure 1: The electromagnetic spectrum (source: Ravikanth et al. 2017)

2.4.1 Near-infrared spectroscopy (NIR)

Basic principle

NIR spectroscopy is widely used for non-destructive quality assessment of fruits and vegetables due to its rapid, non-invasive, and cost-effective approach (Bureau et al., 2009; Hayati et al., 2020; Walsh et al., 2020). It assesses the quality of fruits and vegetables by measuring light absorption and diffuse reflectance in the near-infrared region. When NIR light interacts with a sample's surface, chemical components such as water, sugars, and proteins absorb light at specific wavelengths, while diffuse reflectance is influenced by tissue structures (Camps and Gilli, 2017 ; Tian and Xu, 2022). Absorption occurs due to C-H, O-H, and N-H bonds, while spectral features arise from overtones and combinations of molecular vibrations at infrared wavelengths (Wu et al., 2014)

Spectral Characteristics

The NIR absorption peak at 930–1080 nm is attributed to O–H stretching overtones in water and carbohydrates (Qing et al., 2007a), while the 970 nm band corresponds to the second overtone of O–H stretching in water. Additional peaks at 1190 nm and 1462 nm are linked to C–H and O–H first overtones, respectively (Mireei et al., 2010). Absorption at 840, 960, and 1440 nm is associated with O–H, and at 910, 1100, and 1700 nm with C–H overtones (Walsh et al., 2020), with 910 nm particularly sensitive to sugar content (Paz et al., 2008; Walsh et al., 2020). Subedi et al. (2012) also noted that absorbance near 1680 nm reflects CH_2 or O-H-containing compounds. However, water is the dominant absorber in the NIR region, complicating spectral interpretation (Nicolaï et al., 2007). Moreover, NIR spectra are affected by overlapping bands, low signal-to-noise ratios, and sample composition variability, requiring advanced pre-processing for accurate analysis (Magwaza et al., 2012).

Savitzky-Golay Smoothing

The Savitzky-Golay (SG) smoothing method is commonly used in spectroscopy to eliminate high-frequency noise while enhancing the signal-to-noise ratio (Yao et al., 2023). It works by generating an optimal estimate through averaging or fitting multiple data points within a designated window size (Magwaza et al., 2012; Yao et al., 2023). Unlike traditional smoothing techniques, SG filtering preserves the integrity of spectral shapes, ensuring that the important spectral features and chemical composition information remain intact (Costa and Lima, 2013; Rinnan et al., 2009). This method enhances data quality for further analysis without distorting critical spectral characteristics required

for fruit and vegetable quality assessments. The effectiveness of SG smoothing depends on the degree of the polynomial and the window size, both of which determine the extent of smoothing applied to the data. It enhances spectral clarity and peak detection but must be carefully configured (window size, polynomial order), as improper settings can flatten subtle but meaningful signals (Antonov, 2017).

Multiplicative Scatter Correction (MSC)

Multiplicative Scatter Correction (MSC) is a widely used spectral pretreatment method that enhances the robustness and accuracy of multivariate calibration models. It corrects the scatter level of each spectrum to match an average spectrum, aiming to eliminate deviations caused by sample size, texture, and undesirable scatter effect by the devices (Rinnan et al., 2009). Unlike SNV, which uses data from each spectrum, MSC standardizes every spectrum using the mean spectrum of all spectra. Jiang et al. (2012) found that MSC minimizes spectral variability in diffuse reflectance measurements caused by light scattering, sample thickness differences, and environmental noise. Lei et al. (2019) reported that MSC significantly enhances prediction accuracy by compensating for light scattering and baseline shifts due to physical sample differences. However, Fearn et al. (2009) noted that MSC relies on a stable reference spectrum and may perform poorly with nonlinearities and spectral outliers

Standard Normal Variate (SNV) Transformations

SNV is a row-oriented transformation that can remove scatter effects in spectral data, which arise from variations in sample particle size, surface roughness, or path length (Rinnan et al., 2009). In NIR spectroscopy, these scatter effects can obscure true chemical information by introducing baseline shifts or slope changes in the spectrum (Pokhrel et al., 2023; Rajkumar et al., 2022). SNV transformation works by standardizing each spectrum, setting its mean value to zero and standard deviation to one, thereby removing light-scattering effects and allowing for better sample comparisons. Each spectrum can be calibrated based on the average value of a spectrum that is subtracted from the original spectrum, and then the result is divided by the standard deviation. Thus, it plays a crucial role in making spectral data more uniform, reducing the impact of physical inconsistencies, and improving model accuracy in predicting fruit and vegetable quality attributes (Liu et al., 2021; Rinnan et al., 2009). However, it may have a potential loss of useful scattering

information and ineffectiveness to the biological variability (Kusumiyati et al., 2021; Mishra et al., 2021).

Use of Derivatives

Derivatives can remove both additive and multiplicative effects in spectra (Hasanzadeh et al., 2022; Rinnan et al., 2009). They are particularly useful for reducing baseline shifts and improving the resolution of overlapping peaks in complex spectral data (Hasanzadeh et al., 2022). The first derivative measures the slope of the spectral curve at each point, effectively removing constant baseline offsets. The second derivative measures the change in the slope, eliminating linear trends and improving spectral clarity (Liu et al., 2021; Rajkumar et al., 2022). In addition, these techniques are particularly valuable in distinguishing between closely related chemical compounds and resolving overlapping absorption bands. By highlighting underlying chemical variations, derivatives allow for more precise assessments of quality parameters, such as sugar content, moisture levels, and ripeness in fruits and vegetables (Liu et al., 2021; Rinnan et al., 2009). However, the effectiveness of these methods is challenged by spectral complexity, fruit variability, and environmental influences (Abderrahim et al., 2023 ;Mishra et al 2021). The comparison summary of the spectral pretreatment methods used in NIR spectroscopy is presented in Table 2.

Table 2: Strengths and weaknesses of common spectral preprocessing methods

Method	Strength	Weakness	References
Savitzky-Golay Smoothing	It preserves fine spectral detail better than traditional smoothing filters. Reduces noise while maintaining the shape of peaks.	Requires careful selection of window size and polynomial order. Over-smoothing may flatten small but meaningful peaks. Not effective if baseline drift or scattering is present	Antonov, 2017
Multiplicative Scatter Correction (MSC)	Effective for removing scatter effects, particularly in diffuse reflectance spectra.	Requires reference spectrum. Limited for non-linear effects tend to produce outliers in treated spectra	Fearn et al 2009

Standard Normal Variate (SNV)	Self-normalizes No reference needed Effective for removing baseline shifts and slope variations.	Being sensitive to noise may suppress useful variations. It may also interfere with the interpretation of spectra	Kusumiyati et al 2021 Mishra et al 2021
Derivatives (1st & 2nd order)	Improves resolution of overlapping features. Helps in baseline correction and subtle feature detection. Compensation for instrumental drift	Very sensitive to noise, especially higher-order derivatives. Needs smoothing before application to avoid amplifying noise.	Abderrahim et al 2023

Selection of Wavelengths

The NIR spectrum contains a full of information but often suffers from high dimensionality and nonlinearity, which can hinder model performance. Various wavelength selection methods have been developed to extract the most informative and relevant spectral variables to enhance the predictive accuracy and reduce the complexity of the model. The utilization of these methods minimizes redundancy, reduces calibration time, and improves model robustness. The Successive Projections Algorithm (SPA) has been shown to identify wavelengths with minimal collinearity and low redundancy (Liu et al., 2014; Wang et al., 2015). Competitive Adaptive Reweighted Sampling (CARS) is a method that selects a subset of wavelengths by eliminating variables with low regression coefficients through an iterative process involving adaptive reweighting and Monte Carlo sampling (Li et al., 2019; Yang et al., 2016). Meanwhile, the Genetic Algorithm (GA) acts as a global optimization strategy inspired by the principles of natural evolution. The GA starts with a randomly generated set of potential solutions and applies genetic operators such as selection, crossover, and mutation to evolve toward an optimal solution, typically minimizing RMSEP (Wang et al., 2015; Zhang et al., 2018)

2.4.2 Laser light backscattering imaging (LLBI)

Basic principles

Laser light backscattering imaging (LLBI) is a non-destructive optical technique used to evaluate the quality of fruits and vegetables by analyzing how light is reflected and scattered from their surface and internal tissues (Baranyai and Zude, 2009; Mollazade et al., 2012). Based on the principle of diffuse backscattering, LLBI measures the diffusely reflected light after it interacts with biological materials. The scattering behavior is influenced by the tissue's optical properties, geometry, and cellular structure, including factors such as water content, sugar, pigment levels, and surface roughness (Birth, 1978; Träger, 2012; Lu, 2017). As illustrated in Figure 2, diffuse reflection patterns vary depending on the nature of the medium (Lu, 2017).

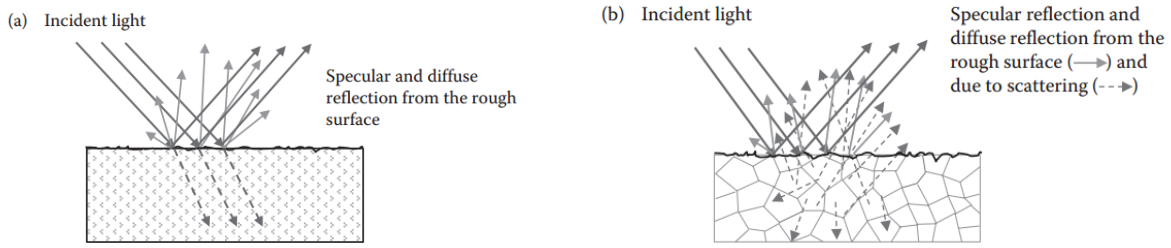

Figure 2: Diffuse reflection occurring on two types of medium (Source: Lu, 2017)

Agricultural products typically reflect only 4%–5% of incident light, with the rest being absorbed or scattered within the tissue (Birth, 1978). Reflectance accuracy can be compromised by surface curvature and requires correction for consistency. The reflected intensity follows Lambert's cosine law, being proportional to the cosine of the angle between the incident beam and the surface normal (Kienle et al., 1996). During LLBI measurement, a laser beam creates a 'halo' of backscattered light, which is captured by imaging sensors. Absorbed photons reveal chemical composition, while scattered light informs on texture, firmness, and mechanical traits (Lu, 2004; Baranyai and Zude, 2009; Mollazade et al., 2012). When integrated with spectral data, LLBI can also estimate attributes like soluble solids content (Qing et al., 2007b). LLBI operates in the visible and near-infrared wavelength range. It includes two primary approaches: monochromatic imaging and broadband imaging (Peng and Lu, 2006; Qing et al., 2008). The important factors in system design include the beam's wavelength, size, and angle of incidence. A smaller beam is preferred for localized analysis, as it simplifies quantification by reducing the scattering region (Lu, 2004). For instance, prior studies have used beam diameters and divergence angles such as 1.6 mm (0.024 rad) for apples

(Peng and Lu, 2005), 1.5 mm (<0.296 rad) for peaches (Peng and Lu, 2006), and 1 mm (<0.01 rad) for kiwifruit (Baranyai and Zude, 2009). The optimal angle of incidence ranges from 7° to 25° relative to the perpendicular to the surface of the materials (Qin and Lu, 2008; Qing et al., 2007b). This configuration (i.e., small beam size and optimal angle of incidence light) results in image symmetry around the point of incidence, which simplifies image processing. However, LLBI is typically limited to a single wavelength at a time, restricting its spectral coverage (Qing et al., 2007b).

Wavelength Selection

The selection of appropriate wavelengths for the target fruit or vegetable is an essential first step in Light Backscattering Imaging (LBI). Since there is a limited number of wavelengths that provide sufficient information about the internal chemical and mechanical properties of agricultural and food products, the effectiveness of LLBI analysis depends largely on the wavelengths that are chosen. The following methods can be applied to the selection of wavelengths:- A complete wavelength search (Lu, 2009), based on prior knowledge of the effective spectral ranges for particular fruit attributes (Lu, 2004) and selection based on NIR spectroscopy results, where wavelengths identified as important in Near-Infrared (NIR) spectroscopy studies are applied to LBI (Lu, 2004; Qing et al., 2007b).

Image processing

In Light Backscatter Imaging (LBI), enhancing the signal-to-noise ratio (SNR) and reducing image noise are essential for reliable analysis. Techniques such as radial averaging, profile averaging, and pixel binning are commonly applied to improve image quality and reduce random variability (Lu, 2004; Peng and Lu, 2005, 2006). Histogram-based thresholding is widely used to convert images to grayscale and define clusters for automated segmentation (Qing et al., 2007b). Backscattering images are then processed through feature extraction, including total pixel count, intensity values, and 2D texture features, to assess quality traits in agro-food products (Noh and Lu, 2007; Romano et al., 2010; Qing et al., 2007b; Mollazade et al., 2012).Theoretical models, such as the Lorentzian distribution, help characterize scattering profiles (Peng and Lu, 2005). Statistical descriptors, including mean, median, mode, standard deviation, skewness, and kurtosis, can also be extracted from pixel intensities to develop efficient classification and prediction models, supporting potential real-time applications (Zhu et al., 2021).

2.4.3 Classification models

Supervised classification models are valuable for assigning input data to predefined categories based on feature patterns, making them useful for detecting quality changes in fruits and vegetables (Lasalvia et al., 2022; Zhao et al., 2023). Partial Least Squares Discriminant Analysis (PLS-DA), derived from PLS regression, adapts regression techniques for classification by identifying latent variables that maximize separation between quality classes (Daniels et al., 2021; Lasalvia et al., 2022). PLS-DA handles complex, high-dimensional datasets effectively, optimizing the covariance between predictor variables and categorical outcomes, and performs well even in the presence of collinearity or noise (Wang et al., 2015; Zhao et al., 2023). This makes it particularly suitable for NIR and LLBI applications. In contrast, Linear Discriminant Analysis (LDA) is a classic statistical approach that projects data onto a subspace maximizing between-class variance while minimizing within-class variance, enabling discrimination of fruit quality changes (Vignati et al., 2023; Vitalis et al., 2021; Lorente et al., 2015). While less capable of handling non-linear relationships than PLS-DA, LDA remains effective when its assumptions align with the data. Model performance for both PLS-DA and LDA is commonly evaluated using confusion matrices, which provide the basis for metrics such as accuracy, precision, sensitivity, specificity, and F1-score (Pokhrel et al., 2023).

2.4.4 Prediction models

Supervised statistical models are widely used to predict fruit and vegetable quality attributes such as soluble solids content (SSC) and firmness (Wang et al., 2015). These models establish quantitative relationships between spectral predictors and target variables (Wang et al. 2015). Partial least squares regression (PLSR) is among the most widely adopted methods for spectral data analysis. It models the relationship between a set of predictor variables (i.e., spectral data) and a continuous response variable by projecting both into a lower-dimensional latent space that maximizes their covariance (Rosipal and Krämer, 2006; Vestergaard et al., 2021). This dimensionality reduction enhances model robustness and interpretability, making PLSR particularly effective in fruit and vegetable quality assessment applications. In addition, support vector machine (SVM) regression is applied to model both linear and non-linear relationships between predictors and responses (Kashef, 2021; Zareef et al., 2020). SVM constructs hyperplanes in high-dimensional feature spaces to predict continuous outcomes, and its ability to use kernel functions allows it to capture non-linear patterns in spectral data (Chidambaram and Srinivasagan, 2019; Kashef, 2021;

Zareef et al., 2020). This adaptability is particularly advantageous for assessing quality attributes that do not follow linear trends, such as textural changes or color evolution. Multivariate Adaptive Regression Splines (MARS) offers another approach for modeling nonlinear relationships. It works by partitioning the data into separate regions and fitting linear regression models within each region. The MARS algorithm automatically selects optimal knots and basic functions, allowing it to flexibly capture complex, time-dependent quality dynamics in postharvest produce (Akin et al., 2020). Furthermore, multivariate regression (MVR) is relevant when predicting multiple continuous outcomes simultaneously from a set of independent variables. Unlike univariate models, MVR accounts for interdependencies among multiple response variables, which is beneficial in scenarios where fruit quality is influenced by several interconnected factors (Seasholtz and Kowalski, 1992). To evaluate the predictive accuracy and reliability of these regression models, performance metrics such as the coefficient of determination (R^2), root mean square error of prediction (RMSEP), and residual predictive deviation (RPD) are commonly used. A high R^2 indicates a strong correlation between predicted and actual values, while a low RMSEP reflects minimal prediction error. An RPD value between 2 and 2.5 indicates that coarse quantitative predictions are possible, and a value above 2.5 corresponds to good prediction accuracy (Hemrattrakun et al., 2021; Nicolaï et al., 2007).

2.5 Applications of NIR spectroscopy and LLBI in postharvest quality assessment

Near-Infrared (NIR) spectroscopy and Laser light backscattering imaging (LLBI) have emerged as promising non-destructive techniques for monitoring the postharvest quality of fruits and vegetables throughout the supply chain. These techniques have been applied for applications such as ripening assessment, defect detection, and quality control, enabling rapid and accurate evaluations that help maintain product consistency and reduce losses (Liu et al., 2022; Pham et al., 2024; Li et al., 2018). By capturing internal and external quality attributes in real time, NIR and LLBI systems support decision-making during storage, transport, and retail stages. Specifically, NIR spectroscopy excels at assessing internal features like SSC, firmness, and moisture due to its penetrative capabilities across near-infrared wavelengths, while LLBI is particularly adept at characterizing surface textural properties and detecting bruises or cuts that may not be visible to the naked eye.

2.5.1 Quality monitoring using classification models

Near-infrared (NIR) spectroscopy and laser light backscattering imaging (LLBI), when combined with classification models, have proven to be powerful non-destructive tools for monitoring postharvest quality changes in fruits and vegetables. These methods are particularly useful in detecting changes due to factors such as temperature, storage time, and cultivar variation. For example, Li et al. (2018) utilized NIR spectroscopy in combination with a support vector machine (SVM) to classify apples based on variety and origin, achieving a prediction accuracy of 96.67%. Cortés et al. (2019) integrated principal component analysis (PCA) with quadratic discriminant analysis (QDA) for in-line apple variety classification, reporting 98% accuracy for red apples and 85% for yellow varieties. Similarly, Kanchanomai et al. (2022) employed QDA to classify seeded and seedless grape cultivars of the 'White Malaga' variety, attaining classification accuracies up to 95.44%. Sánchez et al. (2009) used a diode array/scanning monochromator NIR instrument (350–2500 nm) and PLS2-discriminant analysis (PLS2-DA) to evaluate quality changes in green asparagus stored at 2 °C for 28 days. Sampling at intervals of 0, 7, 14, and 28 days, the study achieved 100% classification accuracy, confirming the model's robustness in distinguishing freshness levels. Gabriëls et al. (2020) demonstrated the use of visible and near-infrared spectroscopy (VNIRS, 400–1000 nm) with artificial neural networks (ANN) to classify internal browning in 'Keitt' mangoes. Their model achieved an overall accuracy of 83.1%, with 86.3% sensitivity and 80.0% specificity, highlighting its potential for detecting internal disorders non-

destructively. Shen et al. (2018) explored the use of Vis/NIR spectroscopy (650–1690 nm) for assessing postharvest quality and storage duration of strawberries. Using partial least squares-discriminant analysis (PLS-DA), the study achieved classification accuracies between 93.3% and 97.4%, particularly when coupled with competitive adaptive reweighted sampling (CARS) for wavelength selection. The method proved effective for distinguishing storage durations based on changes in soluble solids content (SSC). On the other hand, in the LLBI applications, Lockman et al. (2019) used 658 nm and 705 nm laser diodes to monitor ripening in cocoa pods. Features like mean intensity, area, and shape descriptors were extracted from images and correlated with reference firmness and color measurements. Linear discriminant analysis (LDA) classified pods by ripeness stage with 90% accuracy at 658 nm and 95% at 705 nm. Zulkifli et al. (2019) applied LLBI at 658 nm to classify ripening stages in Berangan bananas. Using LDA, the model achieved 94.2% accuracy for binary classification (unripe vs. ripe), though performance dropped to 59.2% when distinguishing all six commercial ripening stages, indicating challenges in mid-stage classification. Adebayo et al. (2016) further demonstrated the power of LLBI with ANN models trained on optical parameters derived from Farrell's diffusion model using five laser wavelengths (532–1060 nm). Their model classified banana ripeness (stages 2–7) with 97.53% accuracy, with most misclassifications occurring only between adjacent stages. This study highlighted how absorption is related to chemical content (e.g., sugars, chlorophyll), while scattering reflects structural changes (e.g., cell wall breakdown). Lorente et al. (2013) and (2015) developed LLBI-based systems for early detection of citrus fruit decay. Infected oranges (Penicillium digitatum) were scanned using five wavelengths (532–1060 nm), and features from Gaussian–Lorentzian (GL) model fitting were extracted. Classification with LDA achieved 80.4% accuracy using 532 nm alone, which improved to 96.1% when all wavelengths were combined. The follow-up study achieved 93.4% overall accuracy by comparing both GL and physical diffusion models, confirming the advantages of multi-wavelength fusion and spatial modeling for decay detection. Yang et al. (2021) evaluated LBI at 520 nm for detecting chilling injury in kiwifruit. For the 'SunGold™' variety, flexible discriminant analysis (FDA) modeling based on four key LBI parameters achieved a 92% classification accuracy, while performance for 'Hayward' was lower at 58%.

2.5.2 Quality monitoring using prediction models

Table 3 summarizes the application of NIR spectroscopy and laser light backscattering imaging (LLBI) for the non-destructive assessment of fruit and vegetable quality, including weight loss, firmness, soluble solids content (SSC), and skin color. These techniques, often combined with multivariate regression models such as PLSR, SVM, and ANN. They vary in performance depending on the spectral range, produce type, and modeling strategy.

The near-infrared (NIR) spectroscopy has been used to detect variations in the water molecular structure that are closely associated with weight loss and other quality attributes (Gibertoni et al., 2022; Vitalis et al., 2023). For example, Rabasco-Vílchez et al. (2024) successfully applied NIR spectroscopy within the 700–1430 nm range, combined with partial least squares regression (PLSR), to estimate weight loss in strawberries. Their model achieved an R^2 of 0.82 and an RMSE of 4.07%. Moreover, Bonifazi et al. (2024) used visible and short-wave infrared (Vis-SWIR) spectroscopy (350–2500 nm) along with PLSR to predict weight loss in intact olive fruits. Their method achieving an R^2 of 0.96 and a cross-validated RMSE of 4.5%. They also observed that the prominent wavelengths, which were sensitive to weight loss at bands 700–800 nm (third overtone of O–H), 1400–1500 nm (first overtone of O–H), and 1900–2000 nm (i.e., combination of O–H stretch and bend). On the other hand, LLBI at 670 nm has been applied for monitoring moisture loss in banana a strong linear relationship ($R^2 > 0.93$) was observed between moisture content and the relative laser area across all pre-treatment groups (Romano et al 2010).

Flores-Rojas et al. (2009) used NIR spectroscopy (400–2500 nm) with modified PLSR to predict firmness as a shear force in asparagus, achieving an R^2 of 0.67 and an RMSEP of 7.81. However, high moisture content and the fibrous heterogeneity of the spears limited the model's accuracy. The prominent wavelengths influencing prediction included water absorption bands (970, 1450, 1940 nm) and cellulose-related C–H bonds (1160, 1790 nm). Similarly, Huang et al. (2018) found that tomato firmness prediction was hindered by internal complexity and high-water content. Beyond 1340 nm, strong water absorption reduced the signal-to-noise ratio, and overlapping spectral features were especially prominent at 970, 1180, and 1340 nm. In contrast, Chen et al. (2024) used Vis/NIR (350–1150 nm) with SwinT-PLS and CARS for peach firmness prediction, achieving high accuracy ($R^2 = 0.951$, RMSEP = 0.443 N/mm). For bananas, Ferreira et al. (2022) employed NIR (900–1700 nm) with SVM and reported $R^2 = 0.84$, RMSEP = 7.98 N. Additionally, they highlighted the visible range (660–727 nm) as useful for identifying biochemical and textural changes during

ripening. Besides, LLBI has also shown strong potential for firmness assessment. Qing et al. (2007b) used LLBI at 680–980 nm with PLSR for 'Elstar' apples, yielding $R^2 = 0.81$ and RMSEP = 5.49 N/cm²; similar results were obtained across 600–1100 nm ($R^2 = 0.79$). Peng and Lu (2005) used a Lorentzian distribution (LD) model on scattering images at 680, 880, 905, and 940 nm, achieving an excellent fit ($R^2 > 0.99$, SEE = 4.37). Firmness predictions were conducted across two independent datasets (Test 1 and Test 2), with multi-linear regression (MLR) models yielding R^2 values of 0.67 and 0.58, respectively, and standard errors of validation (SEV) of 6.39 N and 6.01 N. Similarly, Peng and Lu (2006) developed an MLR model using three parameters extracted from the Gompertz function (GF) of scattering profiles for predicting apple firmness, achieving an R^2 of 0.79. Meanwhile, Pratiwi et al. (2023) found that SSC prediction was more accurate in thinner-skinned fruits, achieving R^2 values up to 0.90 in sapodilla and 0.88 in banana, while thick-skinned fruits like dragon fruit and tomatoes yielded lower R^2 values (0.59–0.64). Similarly, Zeng et al. (2024) used NIR spectroscopy to predict SSC in intact apples by collecting diffuse reflectance spectra in the 900–1700 nm range. Among the tested models, the PLSR model preprocessed with Savitzky-Golay smoothing and multiplicative scatter correction (S-G + MSC) performed best, achieving $R^2 = 0.92$ and RMSEP = 0.54%. Yu and Yao (2023) developed a universal NIR model for SSC across several thin-skinned fruits (i.e., Fuji apples, Aksu apples, Korla pears, and Nanguo pears), achieving $R^2 = 0.93$, RMSEP = 0.60 %. Jiang et al. (2022) emphasized the impact of apple size on NIR accuracy, finding improved predictions when models were size-specific. Data fusion with fruit diameter and CARS-enhanced features further improved performance ($R^2 = 0.77–0.82$, RMSEP = 0.497–0.536%). Furthermore, Mariani et al. (2014) also demonstrated SSC prediction in jaboticaba using NIR reflectance (1000–2500 nm), achieving $R^2 = 0.71$ and RMSEP = 1.33 %. Praiphui et al. (2023) applied NIR (640–1050 nm) to mangoes, reporting $R^2 = 0.81$ and RMSEP = 1.07 %. Shen et al. (2018) used Vis/NIR (650–1690 nm) in online strawberry assessment with a CARS-PLSR model, achieving $R^2 = 0.733$ and RMSEP = 0.69%. Pratiwi et al. (2023) also showed Vis–SWNIR (400–1000 nm) was effective for sapodilla ($R^2 = 0.905$), banana ($R^2 = 0.885$), and guava ($R^2 = 0.769$), though less so for tomato ($R^2 = 0.646$) and dragon fruit ($R^2 = 0.596$), due to thick skin, high water content, and complex internal morphology. Qing et al. (2007b) evaluated LLBI (680–980 nm) for SSC in apples, achieving $R^2 = 0.79$ and RMSEP = 5.44%. Mozaffari et al. (2022) applied LLBI with a 650 nm laser and ANN models in apricots, achieving $R^2 = 0.96$ and RMSEP = 1.146 for SSC. Likewise, Adebayo et al. (2016) used LLBI with ANN and NIR wavelengths (830 and 1060 nm), achieving an accuracy ($R^2 = 0.92$- 0.96) for SSC. Furthermore,

while firmness and soluble solids content (SSC) contribute to internal quality attributes, skin color also plays a significant role in external attributes. Noh and Lu (2007) have predicted apple skin color (hue) using hyperspectral imaging and a neural network, achieving an R^2 of 0.88, while chroma was predicted with an R^2 of 0.54. They also highlighted the importance of selecting appropriate wavelengths to effectively capture anthocyanin variations during ripening. It agreed with the pigment dynamics reported by Chen (2015). Moreover, Vis/NIR spectroscopy has also been applied to other fruit types. In the case of tomatoes, Arruda De Brito et al. (2022) used Vis/NIR spectroscopy combined with PLSR to predict the a* color parameter, achieving a strong correlation (R^2 = 0.94, RMSEP = 2.89), further demonstrating the technique's robustness across different produce. In addition, Zulkifli et al. (2019) demonstrated the effectiveness of laser light backscattering imaging (LLBI) at 658 nm, where parameters such as mean intensity, diameter, backscattering area, and maximum intensity, when combined with stepwise multiple linear regression (MLR), could accurately predict peel color changes during banana ripening. Among the CIE Lab* color components, the b* value, representing yellowness, showed the highest predictive performance (R^2 = 0.85, RMSEP = 2.80), confirming its strong relationship with banana ripeness stages. Similarly, Li et al. (2018) used hyperspectral imaging to predict plum peel color non-destructively. They applied VNIR (600–975 nm) and SWIR (865–1610 nm) imaging systems to develop PLSR models from spectral data on both sides of the fruit. Notably, the b* value was again predicted with high accuracy in the VNIR region, particularly for the ‘Marjorie’s Seedling’ cultivar, where the model achieved an R^2 of 0.88, RMSEP of 2.01, and RPD of 2.98. The ‘Victoria’ cultivar and the combined-cultivar model also showed good predictive ability (R^2 = 0.72–0.73; RPD = 1.95). In contrast, predictions based on SWIR spectra resulted in lower accuracy (R^2 = 0.55–0.69; RPD = 1.34–1.52).

Table 3: Applications of NIR spectroscopy and LLBI in quality assessment of fruits and vegetables.

Techniques	Fruit/ vegetable	Parameter	Wavelength	Model	Performance (R^2, RMSEP)	Reference
NIR Spectroscopy	Strawberry	Weight loss	700–1430 nm	PLSR	$R^2 = 0.82$, RMSE = 4.07	Rabasco-Vílchez et al. (2024)
NIR Spectroscopy	Olive	Weight loss	350–2500 nm	PLSR	$R^2 = 0.96$, RMSEP = 4.5%	Bonifazi et al. (2024)
Vis/NIR Spectroscopy	Peach	Firmness	350–1150 nm	SwinT-PLS +CARS	$R^2 = 0.951$, RMSEP = 0.443 N/mm	Chen et al. (2024)
Vis/SWNIR Spectroscopy	Tomatoes	Firmness	400–1100 nm	PLSR	$R^2 = 0.899$	Huang et al. (2018)
NIR Spectroscopy	Bananas	Firmness	900–1700 nm	SVM	$R^2 = 0.84$, RMSEP = 7.98 N	Ferreira et al. (2022)
NIR Spectroscopy	Green asparagus	Firmness	400-2500 nm 350–2500 nm	PLSR	$R^2 = 0.55$–0.67	Flores-Rojas et al. (2009)
LLBI	Apple	Firmness	680–980 nm	PLSR	$R^2 = 0.81$	Qing et al. (2007b)
LLBI	Apple	Firmness	600–1100 nm	PLSR	$R^2 = 0.79$	Qing et al. (2007b)
LLBI	Apple	Firmness	680, 800,900, and 950 nm	PLSR	$R^2 = 0.90$	Peng and Lu (2006)
NIR Spectroscopy	Apple	SSC	900–2500 nm	PLS	$R^2 = 0.8757$, RMSEP = 0.4092%	Shen et al. (2021)

NIR Spectroscopy	Mango	SSC	600–1080 nm	PLSR	R^2 = 0.81, RMSEP = 1.07 %	Praiphui et al. (2023)
NIR Spectroscopy	Jaboticaba	SSC	1000-2500 nm	PLSR	R^2 = 0.71, RMSEP = 1.33 %	Mariani et al. (2014)
NIR Spectroscopy	Apple	SSC	900–1700 nm	PLSR	R^2 = 0.92, RMSEP = 0.54%	Zeng et al. (2024)
Vis/NIR Spectroscopy	Apple	SSC	470–1150 nm	PLSR	R^2 = 0.91, RMSEP = 0.508 %	Song et al. (2024)
NIR Spectroscopy	Banana	SSC	400–1000 nm	PLSR	R^2 = 0.88, RMSEP = 0.39 %	Pratiwi et al. (2023)
NIR Spectroscopy	Pear and apple	SSC	900–1700 nm	PLSR + GA	R^2 = 0.90, RMSEP = 0.73 %	Yu and Yao (2023)
NIR Spectroscopy	Apple	SSC	900–1700 nm	PLSR	R^2 = 0.77–0.82	Jiang et al. (2022)
LLBI	Apple	SSC	680–980 nm	PLSR	R^2 = 0.79, RMSEP = 4.14%	Qing et al. (2007b)
LLBI	Apricot	SSC	650 nm	ANN	R^2 = 0.963, RMSEP = 1.146%	Mozaffari et al. (2022)
LLBI	Banana	SSC	830, 1060 nm	ANN	R^2 = 0.92–96	Adebayo et al. (2016)
Vis/NIR Spectroscopy	Tomatoes	Skin color (a*)	396-1,131 nm	PLSR	R^2 = 0.94, RMSEP = 2.89	Arruda De Brito et al. (2022)

2.5.3 Comparison between NIR spectroscopy, LLBI, and HSI techniques

Hyperspectral Imaging (HSI), Near-Infrared Spectroscopy (NIR), and Laser light backscattering imaging (LLBI) are non-destructive techniques widely used for evaluating the quality of fruits and vegetables. HSI combines imaging and spectroscopy to generate a spatial-spectral 'hypercube', capturing a full spectrum at each pixel, which enables detailed analysis of surface and internal features (Wieme et al., 2022). It operates in reflectance, transmittance, or interactance modes, depending on the intended application (Nikzadfar et al., 202. It has been applied for SSC prediction in strawberries, oranges, and plums (Meng et al., 2021; Riccioli et al., 2021; Weng et al., 2020), as well as for detecting bruises and defects in pomegranates and loquats (Han et al., 2023; Okere et al., 2023). However, HSI is cost-intensive, requires powerful data processing systems, and is sensitive to surface texture and light variability (Ahmed et al., 2024; Benelli et al., 2020). In contrast, NIR spectroscopy evaluates internal quality by measuring the absorption of near-infrared light, which is sensitive to molecular bonds such as O–H, C–H, and N–H (Farag et al., 2022; Giordano et al., 2023). This allows for the estimation of soluble solids content, moisture, and dry matter. It can be used for monitoring ripeness, grading, and shelf-life (Kusumiyati et al., 2019). NIR is fast and scalable for industrial use but suffers from overlapping absorption bands, lacks spatial resolution, and depends on complex calibration models (Farag et al., 2022; Zhang et al., 2018). Meanwhile, LLBI analyzes how laser light scatters on and beneath the fruit's surface to assess firmness, texture, and mechanical damage (Adebayo et al., 2016; Pham et al., 2024). It is a low-cost and rapid method, making it practical for postharvest quality checks. However, LLBI is limited to surface and near-surface evaluation and is highly affected by sample curvature, shape, and ambient lighting (Mollazade et al., 2012; Pham et al., 2024). Overall, while each technique offers unique advantages, their suitability depends on specific application needs, required accuracy, and practical constraints of implementation. The summarized strength and weaknesses of the techniques is presented in Table 4.

Table 4: Comparison of advantages and limitations of HSI, NIR spectroscopy, and LLBI

Techniques	Strength	weakness	References
Hyperspectral Imaging (HSI)	Detailed chemical and spatial mapping detects internal and external defects	Expensive Multicollinearity Tedious data processing Not suitable for direct implementation in industries	Wieme et al., 2022 Ahmed et al., 2024
NIR Spectroscopy	High chemical prediction accuracy Fast and scalable Suitable for bulk sorting	Limited to surface analysis, sensitive to scattering effects, and requires sample preparation. Spectral overlapping requires advanced data processing and needs frequent calibration	Kusumiyati et al., 2019; Farag et al., 2022
Laser light backscattering imaging (LLBI)	Fast and cost-effective Easy to operate	Limited detection of internal defects, high dependence on image processing	Mollazade et al., 2012; Pham et al., 2024

3. RESEARCH GAP

After reviewing various literature, I identified some research gaps that can be used for further investigation. Traditional methods have high operating costs, product wastage, and are limited to integrated online operations. Advanced non-destructive techniques like hyperspectral imaging are costly to develop and maintain, hard to scale for industrial use, and produce complex datasets that are difficult to process and interpret (Wieme et al., 2022). Exploring cost-effective and easy-to-handle complementary techniques, such as NIR spectroscopy and LLBI, can provide comprehensive information for the quality assessment of fruits and vegetables during post-harvest handling. However, most studies have applied full-spectrum approaches and typically implement an independent predictive model, constraining flexibility and adaptability. The performance of NIR models is often affected by physical, biological, and environmental variability (Jiang et al., 2022; Pratiwi et al., 2023; Zhang et al., 2018). Exploring optimal spectral ranges and comparing linear and nonlinear models can enhance the robustness and accuracy of postharvest quality assessment across different conditions. On the other hand, the literature on Laser light backscattering imaging (LLBI) has predominantly focused on beam system configurations and characterizing the LLBI profile using radial averaging and histogram techniques. While these approaches have proven useful, there is potential for improvement by evaluating different LLBI systems with varied parameter settings, such as beam size, wavelength, and incident light angle. Exploring alternative LLBI system configurations and feature extraction methods could further enhance its effectiveness as a non-destructive technique for characterizing agricultural products.

4. RESEARCH OBJECTIVES

The objective of the work was to apply non-destructive techniques to assess quality changes in fruits and vegetables during post-harvest storage. The following goals were established:

1. To develop classification and prediction models using optimized and full NIR spectra to detect quality changes during storage

    - Applying different linear and non-linear models using the full spectral range provided by the handheld near-infrared (NIR) spectrometer (900–1700 nm).
    - Optimizing the full NIR spectra by analyzing the standard deviation (SD) of the normalized spectra and selecting high-SD wavelengths for multispectral analysis.

2. To compare different mathematical models in Laser light backscattering imaging (LLBI) for describing the signal and utilizing model coefficients for classification and prediction models

    - Emitting multispectral laser diodes (532–1064 nm) onto the sample surface and acquiring backscattering images.
    - Extracting features and characterizing peaks using various theoretical mathematical models.
    - Optimizing wavelengths based on the analysis of variance (ANOVA) of the extracted model coefficients.
    - Comparing the performance of both beam and line-based LLBI systems at a specific wavelength

3. To evaluate the applicability of the developed techniques for assessing quality changes in asparagus, plum, and apple during post-harvest storage

    - Applying reference measurement methods to investigate changes in quality attributes such as weight loss, firmness, SSC, and color in samples stored under different time and temperature conditions.
    - Applying the developed LLBI and NIR techniques to monitor quality changes in asparagus, plum, and apple during post-harvest storage.

5. MATERIALS AND METHODS

5.1 Materials

This study evaluated the postharvest quality of three horticultural products of plum, asparagus, and apple was collected from commercial orchards located in Csengőd, Kiskőrös, and Dunaszentmiklós, Hungary (Fig. 3). After harvest, the fruits and vegetables were packed in polypropylene crates and promptly transported to the Laboratory of the Department of Food Measurement and Process Control, Institute of Food Science and Technology, at the Hungarian University of Agriculture and Life Sciences. Upon arrival, all samples were visually inspected to ensure uniformity in size, ripeness, and the absence of visible defects or infections.

Initially, a total of 1,300 samples were used. This included 120 green asparagus spears (Eros') with an average mass of 36.88 ± 4.59 g, length of 20.42 ± 0.58 cm, diameter of 11.94 ± 3.52 mm, and firmness at the base, middle, and tip of 15.01 ± 2.78 N, 12.86 ± 3.64 N, and 10.86 ± 1.09 N, respectively. Additionally, 1,020 plums (510 per cultivar) were analyzed, with average firmness of 45.76 ± 6.97 N ('Stanley') and 44.74 ± 5.83 N ('Elena'), and SSC of 14.50 ± 1.03% and 14.95 ± 0.52%, respectively. Furthermore, 160 'Granny Smith' apples were evaluated, with SSC of 10.75 ± 1.09%, an average height of 72.97 ± 3.66 mm, a width of 66.25 ± 4.36 mm, and a starch index of 4.81 ± 0. 83.

Storage conditions were tailored for each product. Asparagus samples were randomly divided into three groups, packed in low-density polyethylene (LDPE) plastic bags with ventilation holes. They were stored at 2 °C, 10 °C, and 15 °C for 12 days. Each plum cultivar was divided into four groups and stored at 1 °C, 5 °C, 10 °C, and 15 °C for 24 days. Apples were divided into two groups and stored at 2 °C for up to 27 weeks and at 22 °C for 5 weeks.

Relative humidity (RH) in the storage was measured using a Sain Lang humidity meter and DL-120TH Voltcraft data loggers. Cold storage conditions (1–10 °C) were 90–95% RH, while ambient storage (22 °C) was 60–65% RH. Some samples in each treatment were removed from the experiment before the scheduled measurement due to decay. Decayed fruits were excluded from the groups in accordance with Regulation (EU) No 543/2011 (Article 3, Annex I, Part A).

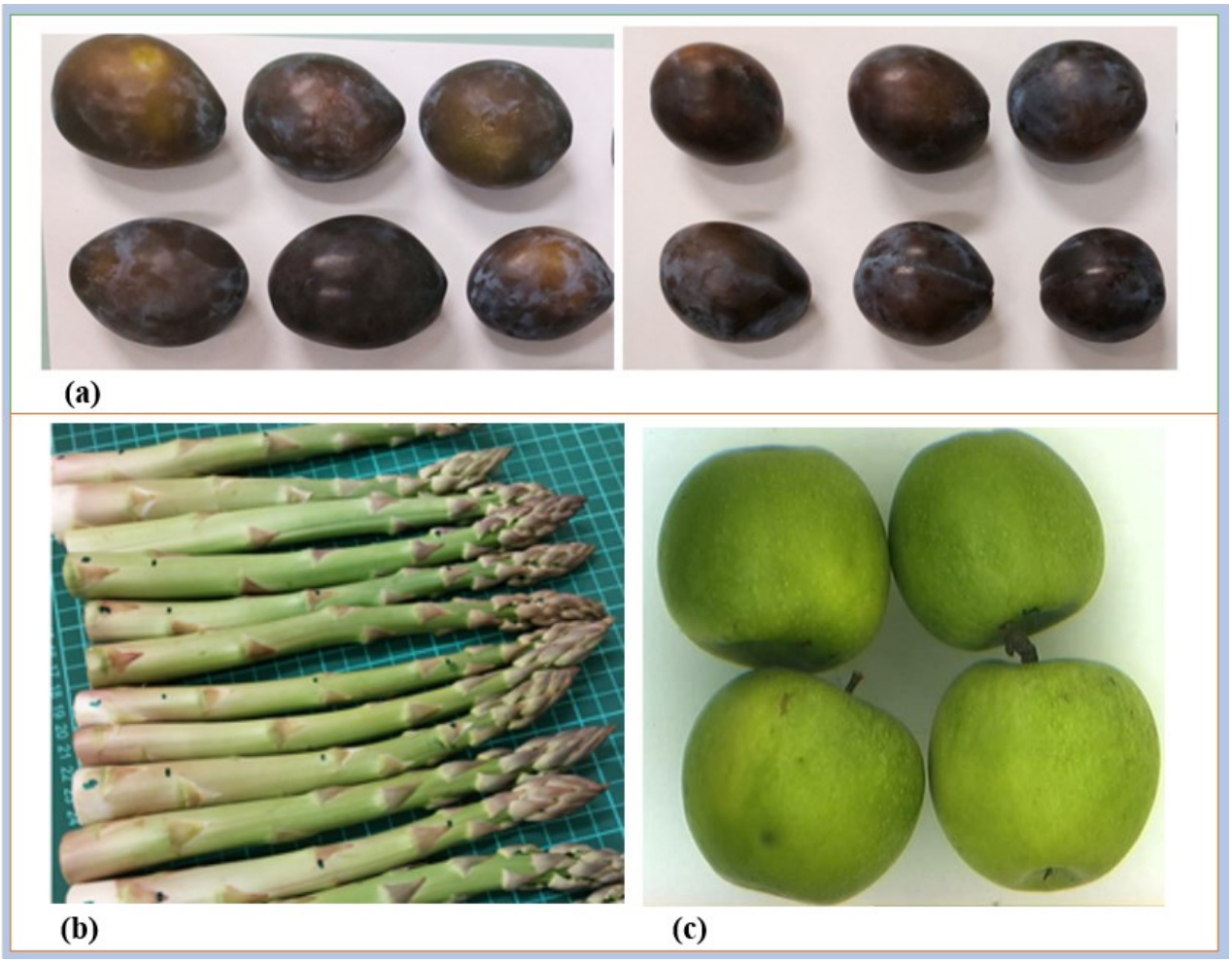

Figure 3: sample images for the materials (a) plums (i.e. 'Stanley' – left and 'Elena'- right) (b) green asparagus (i.e. *'*Eros'*)* and (c) apple (i.e. 'Granny Smith') used for the quality assessment using nondestructive techniques.

5.2 Measurement of quality attributes

5.2.1 Ethylene production

The ethylene production was measured by placing a standardized quantity (typically 1 kg) of the produce in a hermetically sealed container. The container was set for one hour, after that period the concentration of ethylene gas accumulated inside was recorded using an ICA-56 hand-held ethylene analyzer (International Controlled Atmosphere Ltd., United Kingdom) (Fig. 4). The resulting values were expressed as the volume of ethylene produced per kilogram of produce per hour (µL/Kg.h).

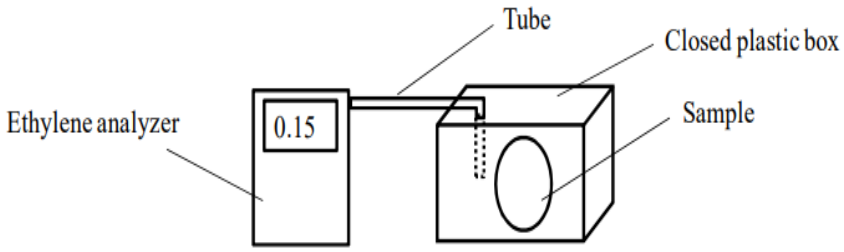

Figure 4: Schematic diagram of ethylene measurement

5.2.2 Respiration Rate

The respiration rate was measured by placing produce (typically 1kg) inside a sealed polymethyl methacrylate (plexiglass) container equipped with FY A600-CO2H carbon dioxide (CO_2) sensors connected to an Almemo 3290-8 data logger (Ahlborn Mess-und Regelungstechnik GmbH, Germany). The container was sealed to maintain a controlled environment, and CO_2 levels were measured in 1 hr. (Fig. 5). The results were reported as the volume of CO_2 produced per kilogram of produce per hour (mL/Kg.h)

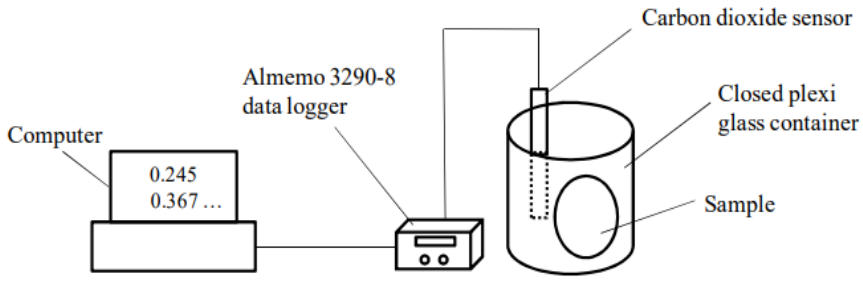

Figure 5: Schematic diagram of respiration measurement

5.2.3 Weight loss

Weight loss of fresh produce was determined using a digital balance (WLC 2/A2, RADWAG, Radom, Poland). The initial weight of each sample was recorded, followed by subsequent measurements over time. Weight loss was calculated as the difference between the current and initial weight, expressed as a percentage relative to the initial value. The weighing method varied depending on the type of produce: Green asparagus and Granny Smith apples were weighed individually, whereas plums were weighed in groups (i.e., 20 pieces per group)

5.2.4 Firmness

Asparagus

The firmness of the samples was measured using a texture analyzer (TA-XTplus, Stable Microsystems, Surrey, UK) equipped with a blade cutter (HDP/BSK) for the analysis of green asparagus samples. The test speed was set to 1 mm/s, with a 0.01 s delay between consecutive data points (Fig. 6a). Ten asparagus spears were tested at every 4-day interval from each storage temperature group. The maximum force (N) was recorded at three positions: the base, middle, and peak. Ten spears were used from each group on each measurement day, had four measurement days

Plum

The firmness was measured using a portable fruit firmness tester (FT 327, T.R. Turoni srl, Forlì, Italy) with a cylindrical probe with a diameter of 7.9 mm was used. The probe penetrated the peeled plums tissue of samples to a depth of 2 mm (Fig.6b). The maximum force (N) was obtained from two sides of each fruit. 20 fruits were used per 4-day interval across four storage temperature groups

Apple

Apple firmness was measured using a handheld fruit firmness tester (FT 327, T.R. Turoni srl, Forlì, Italy) mounted on a vertical stand for stability. A 7.9 mm cylindrical probe penetrated the peeled apple tissue to a depth of 10 mm. Maximum force (N) was recorded at three equatorial positions on each fruit. Twenty apples were measured every 9 weeks under cold storage (2 °C) and every 2 weeks at room temperature (22 °C)

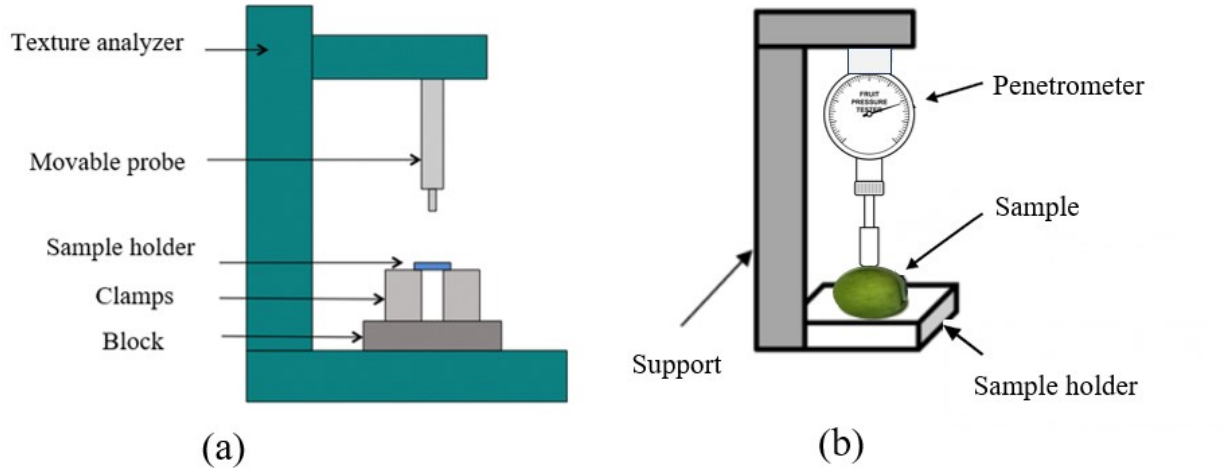

Figure 6: Schematic diagram of firmness measurement devices with different way

5.2.5 Soluble Solid Content (SSC)

SSC was measured using a handheld refractometer (PAL-1, Atago Co. Ltd., Tokyo, Japan; 0–53% range). Juice was extracted from each fruit, clarified of pulp, and one drop placed on the prism to record °Brix. Twenty plums were measured every 4 days across four storage temperatures, while twenty apples were sampled from each temperature group at every measurement point.

5.2.6 Peel Color

Minolta Chroma Meter

The peel color of plums was measured using a portable Minolta Chroma Meter CR-400 (Minolta Corporation, Osaka, Japan) (Fig.7a). The device was calibrated before each measurement session using a standard white calibration plate (CR-A43). Color measurements were taken at two opposite points along the equatorial section of each plum. Standard CIE color parameters (L*, a*, and b*) were recorded. The chroma (C*) value was calculated as $\sqrt{a^{*2} + b^{*2}}$ and hue angle value was calculated as the $\tan^{-1}$ of b*/a*.

Machine vision

A computer vision (CV) system was used to monitor peel color changes in asparagus and apples during storage. The system consisted of a high-performance color digital camera (Hitachi HV-C20 3CCD, Tokyo, Japan) operated in manual mode with default settings. The color temperature was

3200 K and was used for image acquisition. The camera was mounted 60 cm above the sample chamber, positioned perpendicular to the surface of the samples to ensure consistent top-down imaging and eliminate perspective distortion. LED lights (1m/1m LED light strips, 30LEDs, 2.8W) were arranged in a circular configuration around the inner ceiling of the chamber, providing uniform and diffuse illumination. This setup minimized shadows and reflections, ensuring consistent lighting across all samples. The color change in asparagus and apples during storage was evaluated (Fig. 7b). Four to five samples were placed on a white background, which also served as a color reference. Images were captured at a resolution of 768 × 576 pixels and processed using Scilab software (version 2024.0.1), following the image analysis method described by Nguyen et al. (2021). IP_hue spectra were extracted from each image to quantitatively assess color changes over storage time and temperature. The IP_hue represents a weighted histogram of hue angles, summarizing saturation across the image, with color changes indicated by peak displacement. The root mean square error (RMSE) between consecutive measurement days was calculated using the following formula:

$$RMSE_{A-B} = \sqrt{\frac{\sum_{i=1}^{n}(A_i - B_i)^2}{n}}$$

where A_i and B_i represent the saturation values at the i^{th} hue degree for two consecutive measurement days, and n is the total number of hue degrees (typically 360).

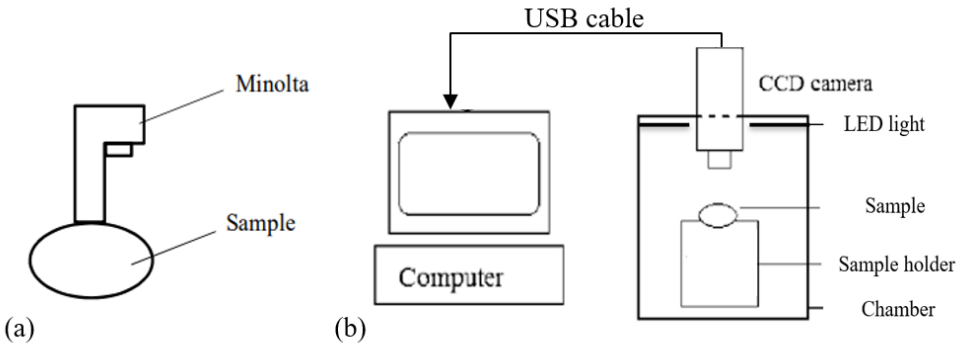

Figure 7: Schematic diagram of portable (a) Minolta Chroma Meter and (b) computer vision system

5.3 Non-destructive measurement techniques

5.3.1 NIR spectroscopy (NIR)

Fruits and vegetables are semi-transparent or opaque to radiation in the visible and near-infrared (NIR) regions, with NIR spectroscopy detecting absorption primarily from C-H, O-H, and N-H bonds in compounds like water, sugars, and pigments (Chandrasekaran et al., 2019). In this thesis work, a handheld NIR spectrometer was used. Its details are described below; -

NIR Spectra Acquisition

A handheld near-infrared (NIR) spectrometer (NIR-S-G1, InnoSpectra Co., Hsinchu, Taiwan) was used to collect absorption spectra in the 900–1700 nm wavelength range, with a spectral resolution of 4 nm. The device is based on digital light processing (DLP) technology and operates in reflectance mode. It features compact optics and is equipped with both Micro USB and Bluetooth Low Energy (BLE) interfaces, allowing data transfer either via USB or wirelessly to smartphones, tablets, or personal computers. Spectral acquisition was performed using the manufacturer's software (NIRScan) under ambient laboratory conditions. The device is internally calibrated and does not require an external white reference tile, as calibration is automatically managed by the internal system. During measurement, asparagus spears were positioned horizontally, and spectra were collected from three distinct locations along each spear: the base, middle, and tip. This approach was used to capture spatial variation in tissue composition along the spear. For plums and apples spectral data were collected from both opposite sides at the equatorial region. (as illustrated in Fig. 8). At each measurement location, two to three consecutive scans were performed to ensure repeatability and reliability. During scanning, the measurement window was fully covered by the sample surface to maintain a consistent contact area and minimize external light interference.

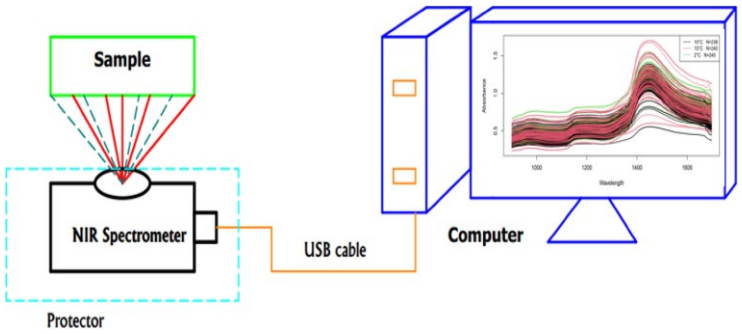

Figure 8: Schematic diagram about collecting the NIR absorption spectra in reflectance mode using a handheld spectrometer.

Pre-processing of NIR spectra

The spectral data was pre-processed using several techniques to correct for physical and chemical effects, such as non-zero baselines and scatter. These methods included Savitzky-Golay smoothing (i.e., polynomial, n=3 and window size, m =21) to reduce noise and Standard Normal Variate (SNV) to correct for scatter effects (Guo et al., 2019; Pandiselvam et al., 2022). These pre-processing techniques were applied to green asparagus, plums, and apple experiments to improve the quality of the spectra for subsequent analysis.

Selection of sensitive wavelengths

In this study, sensitive wavelengths were selected using a filter-based variable selection approach. The acquired spectra were pre-processed using SNV to remove the noise that is potentially produced by specular reflection and the device. The standard deviation of the normalized spectra was calculated column-wise to identify local maxima values, and significant wavelengths were manually selected. These wavelengths were considered important because they corresponded to changes in quality parameters such as WL, firmness, and SSC. Their relevance was further confirmed by calculating quality indices, including the normalized difference index (NDI) and quality index (QI), at the selected wavelengths. The reference wavelength was chosen based on the minimum standard deviation of the normalized full spectrum.

$$NDI = \frac{A_{selected} - A_{reference}}{A_{selected} + A_{reference}}, \qquad QI = \frac{A_{selected}}{A_{reference}}$$

Where $A_{selected}$ is NIR absorbance at the selected wavelength(s), $A_{reference}$ is NIR absorbance of the reference wavelength.

5.3.2 Laser light backscattering imaging (LLBI) system

Laser light backscattering imaging (LLBI) is a relatively novel technique that uses light absorption, scattering, and image processing in the visible and near-infrared range to assess the quality attributes of fruits and vegetables. In this method, a laser beam illuminates a point on the fruit's surface in a dark chamber, and the resulting light scattering provides valuable information about the fruit's mechanical and textural properties (Qing et al., 2007b; Qing et al., 2008; Baranyai and Zude, 2009).

Laser Module and Camera Specifications

Beam based LLBI

As shown in Fig. 9a, A laser beam imaging system with a 12-bit/pixel monochrome CMOS camera (MV1-D1312, Photon Focus, Lachen, Switzerland) with default settings was used to generate diffusely reflected signals. Laser diodes (3 mW) emitting at 532, 635, 780, 808, 850, and 1064 nm were used. The incident angle of the laser beams was set to 15°, focused within a circular area of Ø1 mm. Image acquisition was performed in a dark chamber to minimize external light interference and improve the signal-to-noise ratio. The system captured images at a resolution of 0.113 mm/pixel and a size of 512 × 512 pixels. The images were stored in raw binary format for analysis.

Line Based LLBI

A line laser imaging system was implemented to monitor quality changes in samples during post-harvest storage (Fig. 9b). The system comprised a dark chamber, a monochrome industrial camera (DMK38GX540-a, 1.2-inch Sony CMOS, GigE Interface (RJ45), Imaging Source, Bremen, Germany), and a 635 nm LM Laser KH93242 single-line laser module(1 mW power, 1 mm line thickness). The laser module was used to illuminate the samples, generating diffusely reflected signals for imaging. The camera lens was positioned 27 cm from the sample surface, and a laser module was mounted at an incident angle of 20° within a dark chamber to reduce direct reflections and geometric distortion. Digital images were captured at a resolution of 0.0325 mm per pixel to ensure spatial accuracy and minimize curvature-related effects.

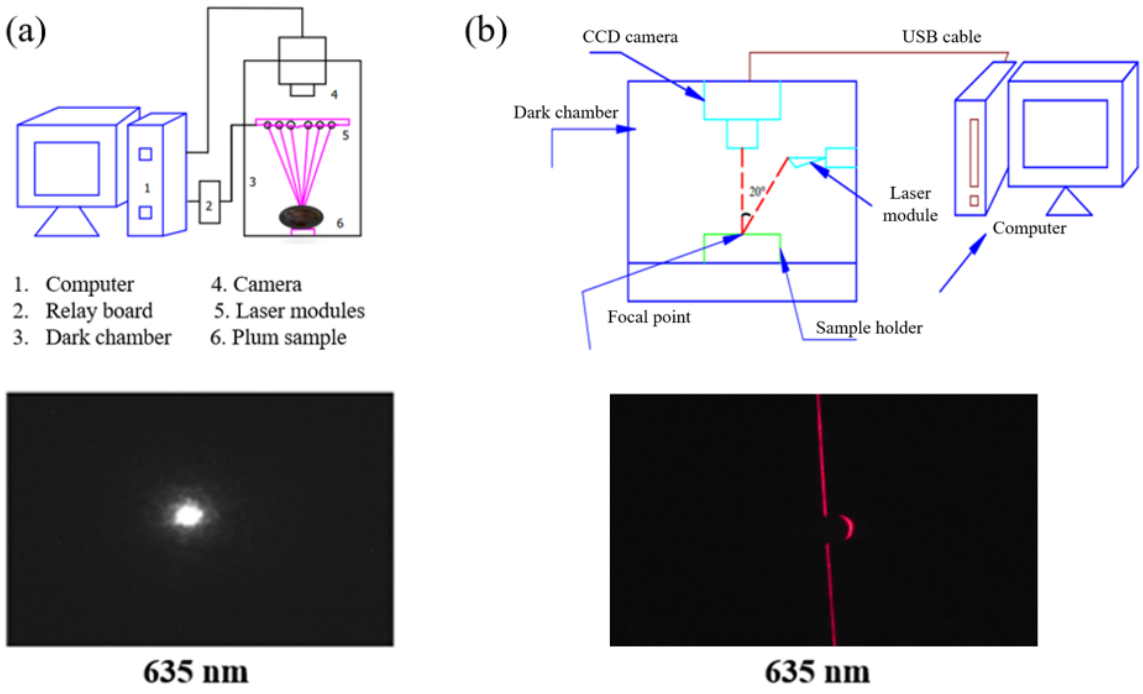

Figure 9: Laser light backscattering imaging System:(a) Beam-based system and (b) Line-based system with their respective sample of a backscatter image at 635 nm.

Description of LLBI profiles

An image processing algorithm was developed using Scilab (version 2024.1.0). Raw RGB image files were transformed into greyscales, resulting in a two-dimensional (2D) matrix of pixels with intensity values ranging from 0 to 255 . The incident (center) point was determined by calculating the intensity-weighted average of pixel positions. A 5-pixel-wide band crossing the incident point was selected as the region of interest (ROI). The 1D profiles were obtained from the intensity values within the ROI. Then, the 1D intensity profiles were modeled using the modified Cauchy distribution (CD) function (Eq. a) and the modified Gaussian distribution (GD) function (Eq. b), which are mathematically expressed as follows:

$$I_C = z_{1c} + \frac{z_{2c}\, {z_{3c}}^2}{(x-z_{4c})^2+{z_{3c}}^2} \qquad \text{(a)}$$

$$I_G = z_{1g} + z_{2g}\exp\left(-\frac{(x-z_{4g})^2}{2\,{z_{3g}}^2}\right) \qquad \text{(b)}$$

Where I_C and I_G denotes estimated light intensity; x denote the picture width ; z_{1c} and z_{1g} are the baseline intensity; z_{2c} and z_{2g} are amplitude; z_{3c} and z_{3g} are shape factors; and z_{4c} and z_{4g} are the location of the peak of CD and GD functions.

Image processing and feature extraction

The collected images were processed using Scilab (version 2024.1.0, Dassault Systèmes, Vélizy-Villacoublay, France). The coefficient parameters of the intensity profile were extracted using a signal approximation approach based on modified Cauchy distribution and Gaussian distribution function models. The coefficients derived from the model demonstrated strong performance in characterizing intensity profiles and were used to develop models for monitoring quality changes. The coefficients extracted from the line-based system at 635 nm, in combination with LDA, were used to detect quality changes of 4-day storage intervals. These coefficients combined with linear (MVR), and non-linear (MARS) models were used to estimate weight loss and firmness of green asparagus. Additionally, the coefficients from the beam-based system at optimal wavelengths, combined with LDA, were applied to detect quality changes in plums within 4-day storage intervals. These coefficients, combined with MVR, were used to estimate plum firmness, SSC, and skin color. On the other hand, coefficients directly extracted from the Cauchy model, measured at 635 nm using line- and beam-based systems, were used to estimate apple weight loss and firmness using SVM and MVR models. The MARS algorithm selects knots and basis functions adaptively, allowing it to capture non-linear relationships between predictors and responses (Akin et al., 2020) . The MARS model mathematically can be expressed as follows:

$$f\,(x) \;=\; \beta_0 \;+\; \sum_{i=1}^{n} \beta_i \, B_i(\,x) \qquad \text{(c)}$$

Where, β_0 is the intercept, β_i are the coefficients, $B_i(\,x)$ are basis functions, which are piecewise linear splines that fit different regions of the data. Whereas MVR is used to model the relationship between multiple predictors and a continuous dependent variable. Unlike simple regression models, which predict a single outcome, MVR simultaneously predicts multiple outcomes based on several independent variables (Seasholtz and Kowalski, 1992).

The general form of a multivariate regression model can be represented as:

$$Y = X\beta + E \qquad \text{(d)}$$

Where Y is the matrix of response variables, X is a matrix of predictor variables, β is the vector of coefficients, and E is the vector of errors.

5.4 Experimental design

The experiments of this research are schematically summarized in the flow chart shown in Fig. 10. Green asparagus (i.e., 'Eros'), plums (i.e., 'Stanley', 'Elena'), and apples (i.e., 'Granny Smith') were used for experimental work, treated at different storage temperatures and times.

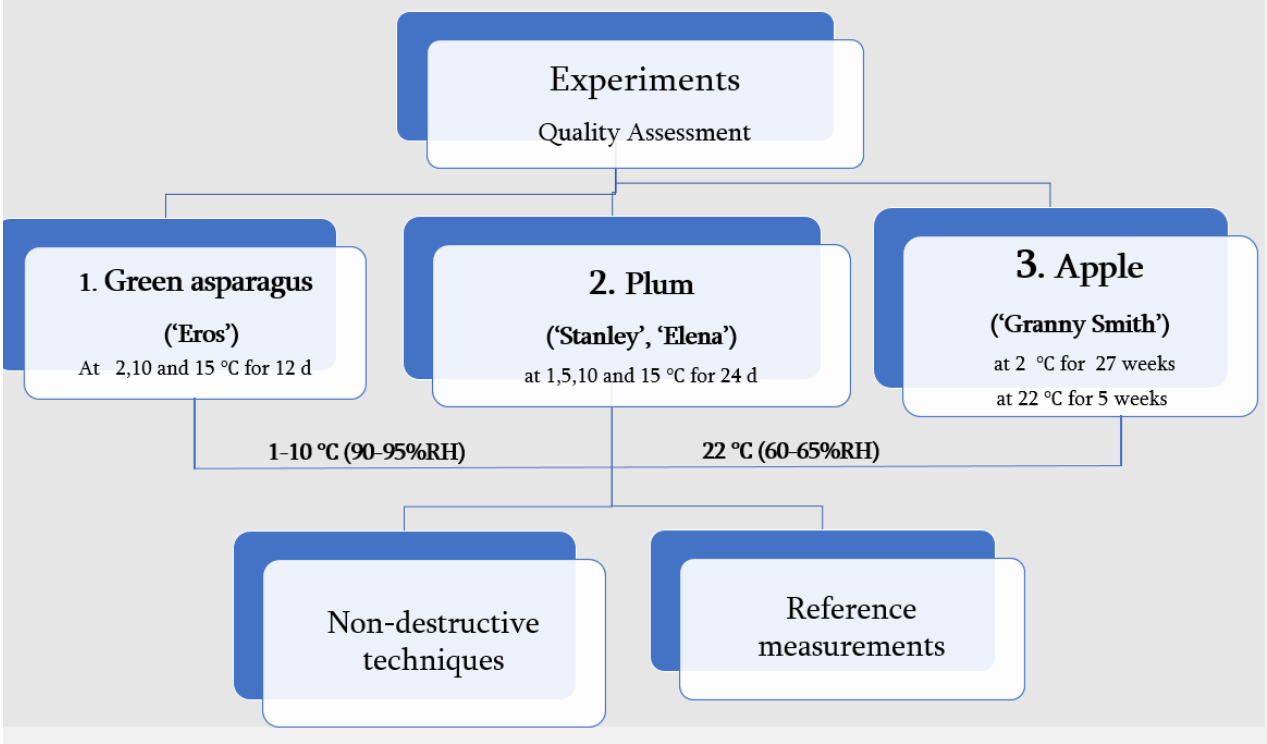

Figure 10: Overall experimental design of quality assessment of green asparagus, plum, and apple during post-harvest storage.

5.4.1 Quality assessment of green asparagus during post-harvest storage

Storage treatment

The LDPE-packed green asparagus spears (Eros') were stored at three different temperatures (2 - 10 ℃ with 90-95 RH% and 15 ℃ with default RH%). Measurements were taken at 4-day intervals, with 10 samples tested from each group at each time point. The samples were kept at room temperature for 12 h to maintain the surface temperature of the samples the same as the room temperature. First, non-destructive measurements were performed on each spear at three positions of the base, middle, and tip. Afterward, destructive analyses were conducted on the same tested spears, which were then removed from the sample pool. The over all quality assessment design presented in Fig 11.

Measurement

The weight loss and firmness of the green asparagus spears were measured using the methods described in Sections 5.2.3 and 5.2.4, respectively. The device used for NIR and the system for LLBI evaluations are detailed in Sections 5.3.1 and 5.3.2.

NIR spectroscopy

NIR spectra were collected non-destructively with two consecutive scans at three positions (base, middle, tip) of each asparagus spear, preprocessed with SNV, and analyzed to select sensitive wavelengths for NDI and QI calculation. A dataset of 684 observations across four storage times and three temperatures was split (80% training, 20% validation) to develop classification (PLS-DA, LDA) and prediction models (PLSR, SVM), with performance evaluated by metrics such as accuracy, sensitivity, specificity, precision, F1-score, and balanced accuracy (detailed in Annex Table 12.2). and R^2, RMSE, and RPD for prediction, validated by 100 bootstrap repetitions.

LLBI

Line-based LLBI was conducted at the wavelength of 635 nm, capturing three LLBI images from the base, middle, and peak of each asparagus spear. The Cauchy curve fitting method extracted LLBI parameters (i.e, amplitude, shape and FWHM) from the LLBI profile. A total of 344 observations were collected from asparagus spears stored at 2 °C, 10 °C, and 15 °C. MVR and MARS models were developed to predict weight loss and firmness, while LDA was applied to evaluate quality changes in the asparagus. The dataset was randomly split into two subsets, with 80% used for training and 20% for validation. Bootstrapping with 100 repetitions was performed to

evaluate model performance, generating statistical metrics such as mean and 95% confidence intervals for R^2, RMSE, and RPD.

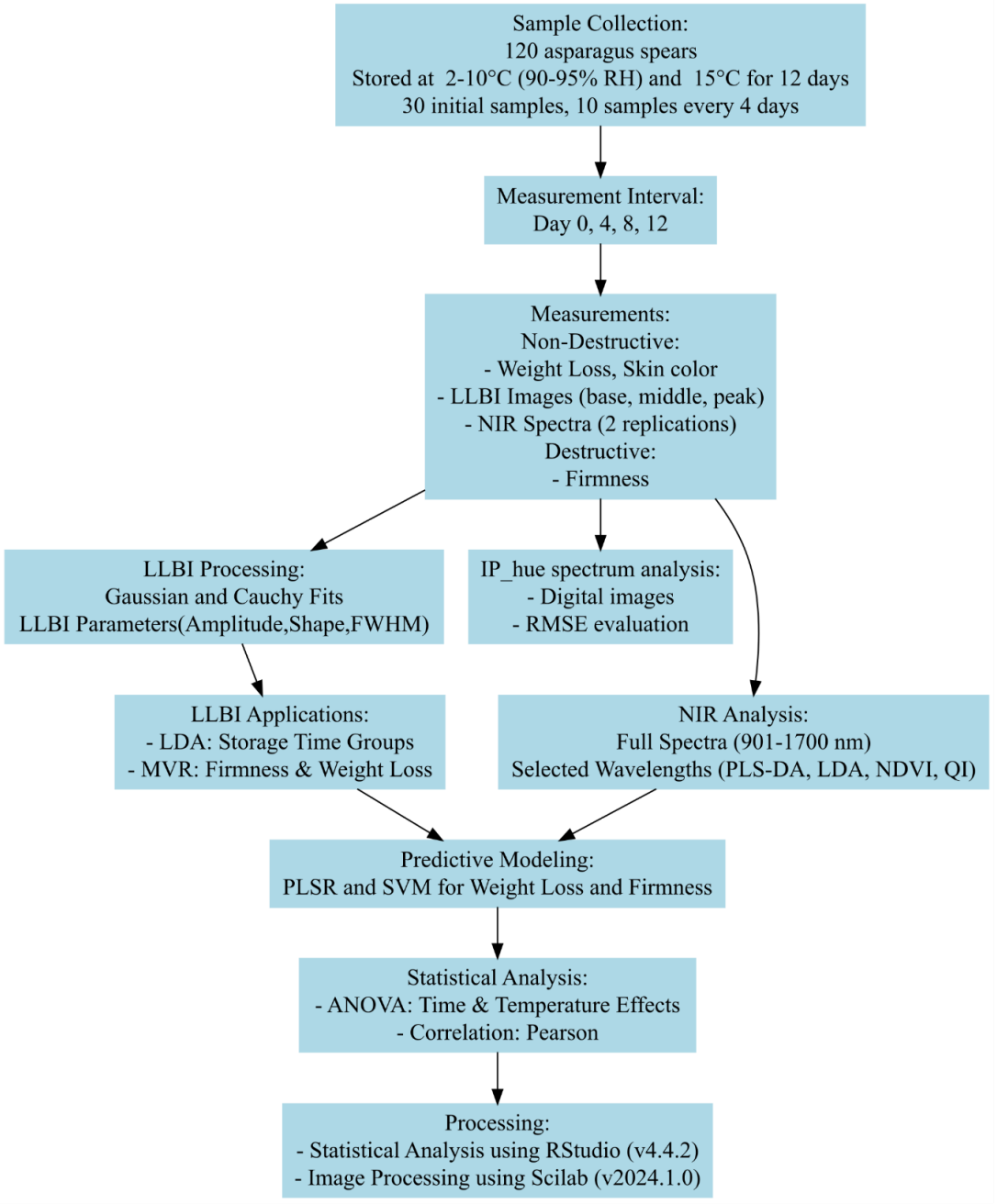

Figure 11: Assessment of quality changes in green asparagus using NIR Spectroscopy and LLBI techniques during post-harvest storage.

5.4.2 Quality assessment of Plums during post-harvest storage

Storage treatment

Two plum cultivars (Stanley' and 'Elena') were used in the study. A total of 510 fruits were selected for each cultivar, of which 30 were used for initial measurements. The remaining 480 fruits were randomly divided into four temperature groups (1 -10 °C with 90-95 RH%, and 15 °C) and stored for 24 days. Storage duration was recorded in days. On each measurement day, 20 fruits were taken from each temperature group, and they were kept for 12 h before the measurement to maintain the sample's surface temperature the same as the room temperature. Moreover, some groups were terminated early due to mold growth. Fig. 12 presents the overall assessment of quality changes in plums using NIR spectroscopy and LLBI techniques during postharvest storage.

Measurements

The physiological and quality changes of the plums were measured using the methods described in Sections 5.2.1 to 5.2.6. The device used for NIR and the system for LLBI evaluations are detailed in Sections 5.3.1 and 5.3.2.

NIR spectroscopy

Spectral data were collected from both sides of each fruit with three consecutive scans and preprocessed using SNV. Sensitive wavelengths were identified from the normalized spectra by calculating the standard deviation. Their sensitivity was also confirmed using NDI and QI indices. PLSR and SVM models were developed with both full spectra and selected wavelengths to predict weight loss and SSC, using a dataset of 2965 observations (1649 'Stanley' and 1316 'Elena'). Each dataset (combined, 'Stanley,' and 'Elena') was randomly split into 80% training and 20% validation, and model performance was evaluated with 100 bootstraps, reporting mean and 95% confidence intervals for R^2, RMSE, and RPD.

LLBI

Beam-based LLBI captured two images per plum from both sides across six wavelengths (532–1064 nm). Optimized wavelengths, identified via ANOVA and Tukey's test, highlighted sensitivity to quality changes. From 1,276 observations (Stanley' 569, 'Elena' 707), LDA classified samples by storage time, while MVR models predicted firmness, SSC, and skin color using two LLBI parameters at optimized wavelengths. Model performance was validated with 100 bootstraps, reporting R^2, RMSE, and RPD with 95% confidence intervals.

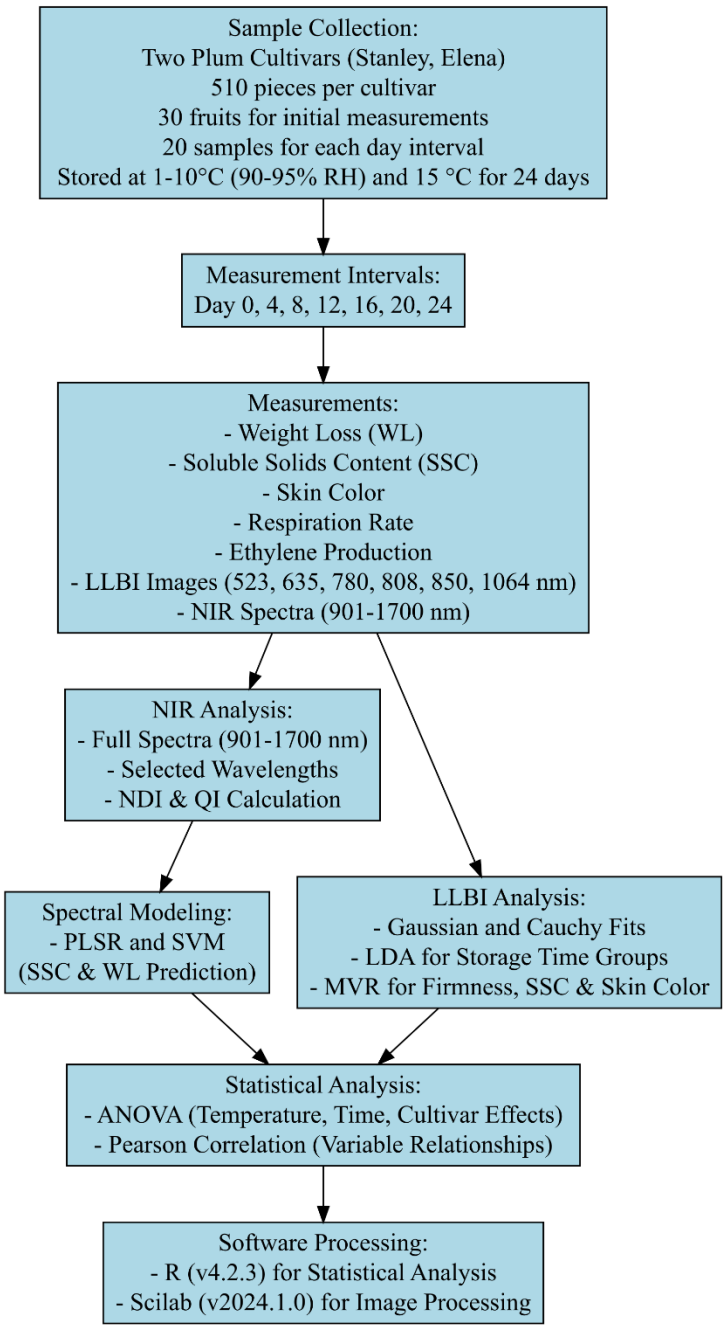

Figure 12: Assessment of quality changes in plums using NIR Spectroscopy and LLBI techniques during post-harvest storage.

5.4.3 Quality assessment of apple during post-harvest storage

Storage treatment

Similar to green asparagus and plums, the overall assessment of quality changes in ‘Granny smith’ apple using NIR spectroscopy and LLBI techniques during postharvest storage is presented in Fig. 13. A total of 160 apple samples were randomly divided into two groups. The first part was stored at room temperature (22 °C with 60-65 RH%) for 5 weeks and sampled at 2-week intervals. The second part apples were stored under cold conditions (2 °C with 90-95 RH%) for 26 weeks, followed by 1 week at 22 °C for shelf life, with sampling conducted at 9-week intervals.

Measurement

The physiological and quality changes of the ‘Granny Smith apples were measured using the methods described in Section 5.2.1. to 5.2.6 The device used for NIR and the system for LLBI evaluations are detailed in Sections 5.3.1 and 5.3.2

NIR Spectroscopy

A handheld NIR spectrometer (900–1700 nm) collected spectra from two opposite locations around the equator of each apple, with three consecutive scans per location. Spectra were preprocessed using SG smoothing and SNV. The significant wavelengths were identified from column-wise standard deviations. Additionally, NDI and QI indices for these wavelengths were calculated to confirm their sensitivity. PLSR and SVM models were developed using both the full spectra and the selected wavelengths, and their performance was compared. A total of 834 observations were collected. This dataset was randomly divided into two sheets, with 80% used for training and 20% for validation. Bootstrapping with 100 repetitions was employed to assess model performance, providing statistical metrics such as the mean and 95% confidence intervals for R^2, RMSE, and RPD, ensuring robust and reliable evaluation of the models

LLBI

Line-based LLBI images were captured from two opposite equatorial locations per apple. At 635 nm, LLBI profiles were fitted with a modified Cauchy model to extract amplitude, shape, and FWHM, which were used in MVR and SVM models. From 643 observations (line: 382, beam: 261). The dataset was randomly divided into two subsets, with 80% used for training and 20% for validation. Bootstrapping with 100 repetitions was performed, and model performance metrics (R^2, RMSE, and RPD) were evaluated using t-tests with 95% confidence intervals.

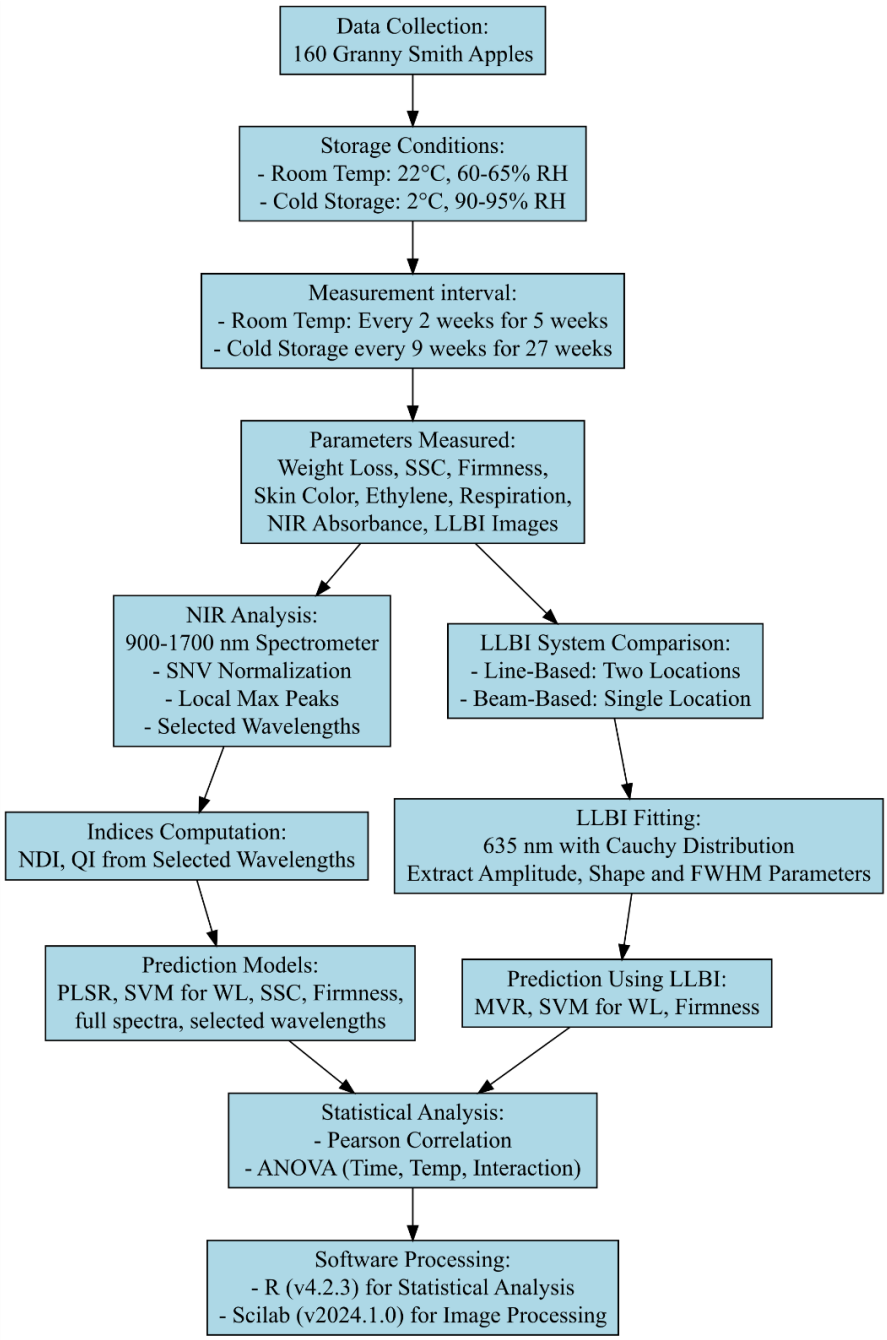

Figure 13: Assessment of quality changes in apple using NIR Spectroscopy and LLBI techniques during post-harvest storage.

5.5 Data analysis

The data analysis provides a comprehensive framework for the spectral analysis of horticultural products, employing both classification and prediction techniques to effectively assess and manage fruit quality. This integration of advanced spectral analysis with multivariate statistical methods enables precise control and improvement of post-harvest handling and processing procedures. In this dissertation, basic descriptive statistics on the quality parameters of the fresh produce during treatments were presented in plots, Analysis of Variance (ANOVA) was used to evaluate the effects of the treatments on these parameters. Moreover, classification and prediction models were applied to assess the association between quality parameters and the laser and NIR spectral variables. Partial Least Squares Discriminant Analysis (PLS-DA) and Linear Discriminant Analysis (LDA) were established to classify the samples based on their treatment groups, utilizing the 'plsdepot' (version 0.2.0) and 'mda' (version 0.5-3) packages. Additionally, Partial Least Squares Regression (PLSR), Multivariate Regression (MVR) Support Vector Machine Regression (SVM) and Adaptive Regression Splines (MARS) were built to predict the quality attributes of the samples using the 'pls' (version 2.8-2), 'aquap2' (version 0.4.2), 'e1071' (version 1.7-13), 'earth' (version 5.3.3) packages, respectively. All statistical analyses were performed using R software (version 4.2.3, R Foundation for Statistical Computing, Vienna, Austria).

6. RESULTS AND DISCUSSIONS

6.1 Green asparagus experiment during post-harvest storage

This section presents the results of NIR spectroscopy and line-based LLBI techniques used to monitor quality changes in green asparagus during storage. For NIR spectroscopy analysis, a total of 684 observations were generated by acquiring spectral data at three positions (base, middle, and peak) on each spear, using two scans per position. The collected spectra were preprocessed using standard normal variate (SNV), and sensitive wavelengths were manually selected based on the standard deviation of the normalized spectra. Normalized difference index (NDI) and quality index (QI) were calculated to validate the sensitivity of these wavelengths. Classification models (PLS-DA, LDA) and prediction models PLSR and SVM were developed using both full spectra and the spectra at selected wavelengths to evaluate changes in asparagus quality. PLS-DA was implemented using the 'plsdepot' package (version 0.2.0), while LDA was performed using the 'mda 'package (version 0.5-3) in R. For LLBI, 344 observations were obtained by capturing images at 635 nm from the same three positions on each spear. LLBI parameters (i.e., amplitude, shape and FWHM) were extracted using Cauchy curve fitting. MVR using 'pls' (version 2.8-2), and MARS with 'earth' (version 5.3.3) package in R. The models were developed to predict weight loss and firmness, while LDA was used to detect quality changes over time for the samples stored at different storage temperature groups. All datasets were randomly split into training (80%) and validation (20%) subsets. Model performance was evaluated using bootstrapped metrics (R^2, RMSE, RPD) with 95% confidence intervals

6.1.1 Weight loss

The box plot (Fig. 14) illustrates the significant impact of storage temperature and duration on weight loss in green asparagus. Weight loss increased significantly with both storage temperature and time (ANOVA, $P < 0.001$). Moreover, by day 12, the highest weight loss was observed in spears stored at 15 °C, followed by those stored at 10 °C.. Higher temperatures accelerated moisture loss due to increased respiration and transpiration, consistent with previous reports (Tzoumaki et al., 2009; Villanueva et al., 2005; Gantner et al., 2020). Spears stored at 15 °C also showed mold growth, likely from surface condensation (Hung et al., 2011).

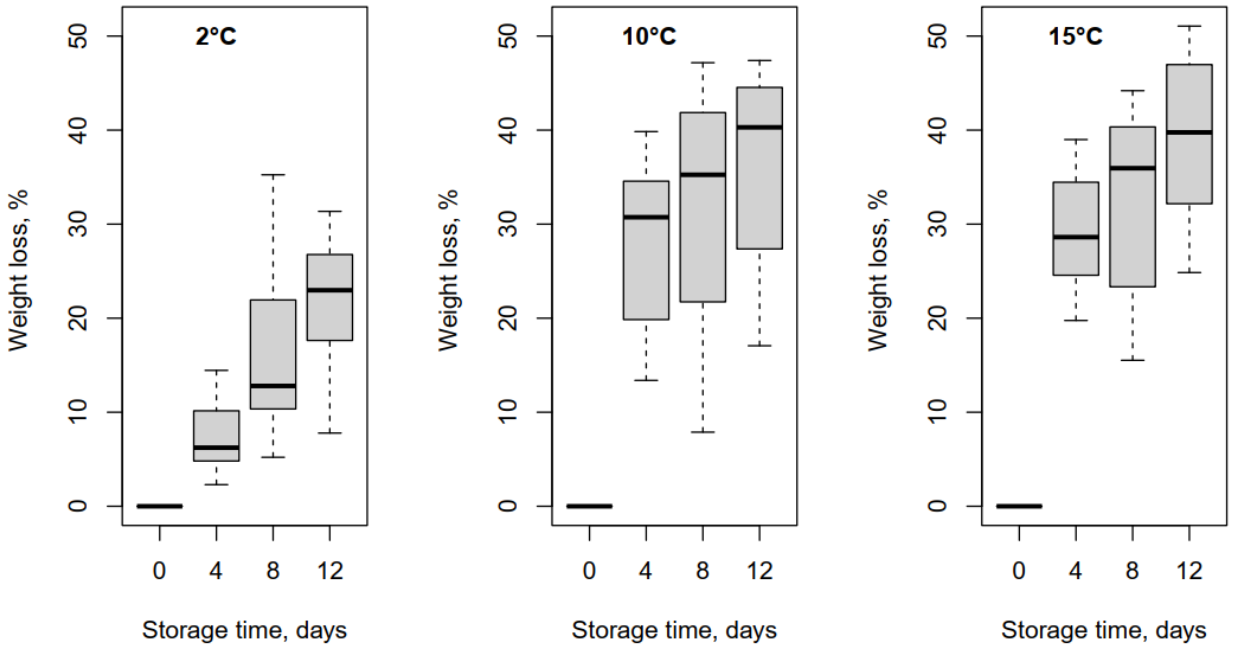

Figure 14: Changes in weight loss in the green asparagus samples stored at 2, 10, and 15 °C.

6.1.2 Firmness

The firmness of asparagus spears at the base increased over time across all storage temperatures and time (Fig.15). The increase was more pronounced at higher temperatures. ANOVA confirmed significant effects of temperature ($F = 862.10$), time ($F = 4751.08$), and spear position ($F = 168.087$, $p < 0.001$). Samples stored at 15°C showed the greatest firmness and variability, while lower temperatures preserved texture by reducing enzymatic and microbial activity. Higher temperatures accelerated moisture loss, chemical reactions, and deterioration, leading to reduced visual and textural quality. Firmness trends for the middle and peak positions of the spears are presented in Appendix Fig. 12.1.2. These observations align with previous reports showing that extended storage negatively affects texture, fiber, and organic compounds in asparagus, and that higher temperatures accelerate lignin development and firmness increases, whereas lower temperatures help maintain freshness and quality (Anastasiadi et al., 2020; Garrido et al., 2001; Villanueva et al., 2005; Lipton, 2011; An et al., 2008; Hung et al., 2011).

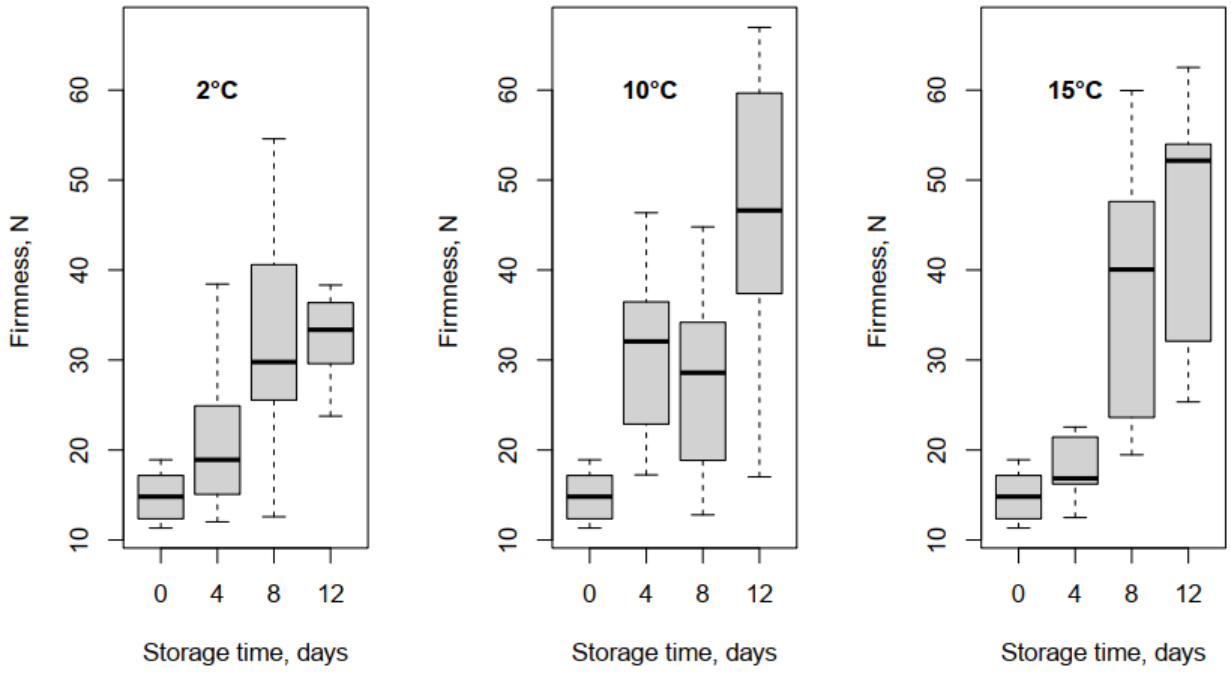

Figure 15: Changes in firmness in the base position of green asparagus samples stored at 2, 10, and 15 °C.

6.1.3 Peel color

Fig. 16 shows asparagus spear samples after 12 days of storage at different temperatures. Panels (a) to (c) present photographs of spears stored at 2 °C, 10 °C, and 15 °C, respectively, while panels (d) to (f) display the IP_hue spectra for each temperature group across their respective storage durations. Saturation and hue angle were used to evaluate color changes in green asparagus. As storage time and temperature increased, asparagus showed reduced freshness and quality, with discoloration, odor, and mold particularly evident at 15 °C. At 2 °C, hue spectra remained stable with minimal changes, while at 10 °C moderate shifts were observed. At 15 °C, the hue angle decreased markedly, shifting from yellow-green toward yellow, along with greater loss of saturation. These changes reflect chlorophyll breakdown, structural degradation, and accelerated enzymatic activity at higher temperatures. High moisture content and warmer storage conditions create an environment conducive to mold growth, leading to discoloration and surface blemishes (Sothornvit and Kiatchanapaibul, 2009; Villanueva et al., 2005). Additionally, these color changes

signify a decline in freshness and quality, with more pronounced changes at 10 °C compared to 2 °C (Gantner et al., 2020).

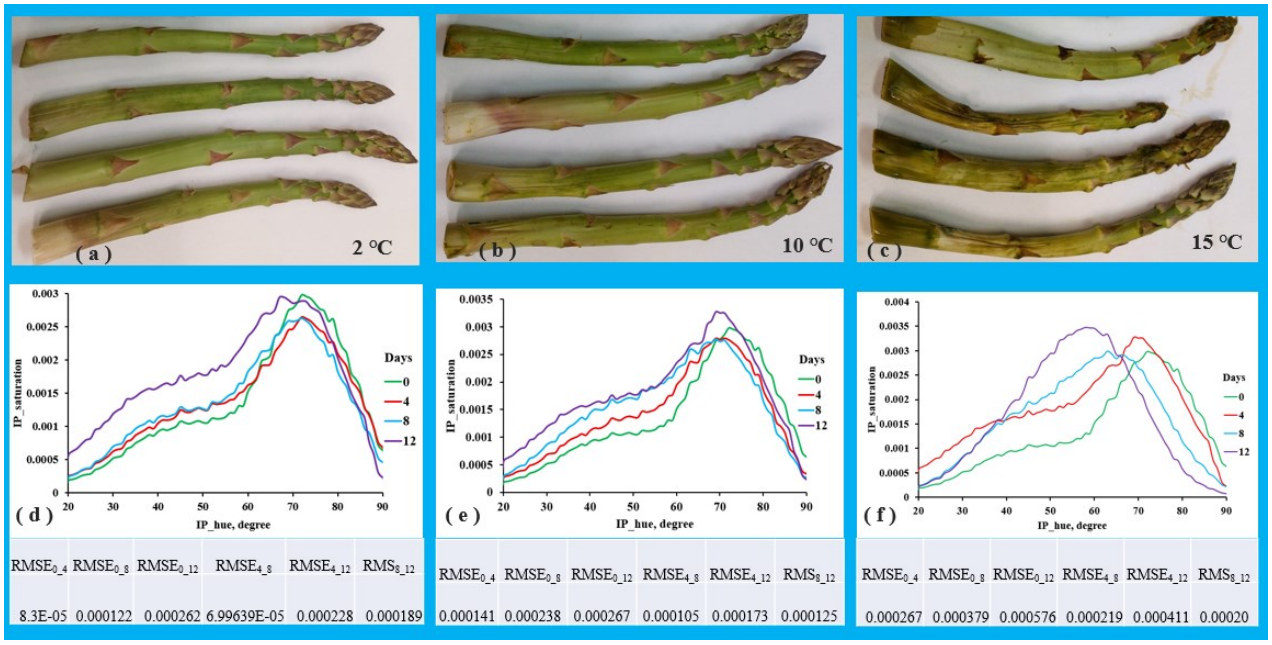

$RMSE_{0\_4}$	$RMSE_{0\_8}$	$RMSE_{0\_12}$	$RMSE_{4\_8}$	$RMSE_{4\_12}$	RMS_{8_12}
8.3E-05	0.000122	0.000262	6.99639E-05	0.000228	0.000189

$RMSE_{0\_4}$	$RMSE_{0\_8}$	$RMSE_{0\_12}$	$RMSE_{4\_8}$	$RMSE_{4\_12}$	RMS_{8_12}
0.000141	0.000238	0.000267	0.000105	0.000173	0.000125

$RMSE_{0\_4}$	$RMSE_{0\_8}$	$RMSE_{0\_12}$	$RMSE_{4\_8}$	$RMSE_{4\_12}$	RMS_{8_12}
0.000267	0.000379	0.000576	0.000219	0.000411	0.00020

Figure 16: Asparagus spears sample images arranged in front of the camera at the end of the experiment and hue spectra plot at storage temperatures of 2 °C (a & d), 10 °C (b & e), and 15 °C (c & f), respectively.

6.1.4 NIR spectroscopy

Spectral description

Fig. 17 shows (a) raw full-spectrum absorbance data for green asparagus stored at 2 °C, 10 °C, and 15 °C for 12 days in the 900–1700 nm range, (b) SNV-transformed normalization, (c) standard deviation of SNV, and (d) NDI_1252 box plots at 1696 nm showing changes in asparagus quality over time. The standard deviation highlights variability in absorbance across wavelengths, with higher variations at 907 nm, 923 nm, 1069 nm, 1442 nm, and 1696 nm, related to quality changes. The reference wavelength at 1252 nm showed the minimum standard deviation across the spectra. The NDI_1252 at 1696 nm declines over time, with higher fluctuations at higher temperatures, possibly due to increased metabolic and enzymatic activities. The absorbance peak at 1442 nm shows a greater change at 15 °C, likely due to temperature-related changes in spears structure or composition. Higher temperatures break down cells, leading to increased water loss. This weakens the interaction of light with internal water and cellular components, resulting in more pronounced changes in the spectrum of light absorption. Moreover, the enzymes responsible for the degradation

of structural polysaccharides, such as pectin and cellulose, are also stimulated by elevated temperatures (Villanueva et al., 2005). The literature reports that the NIR absorption peaks at this wavelength correspond to molecular vibrations of CH, OH and NH, likely influencing the spectral readings (Camps and Gilli, 2017).

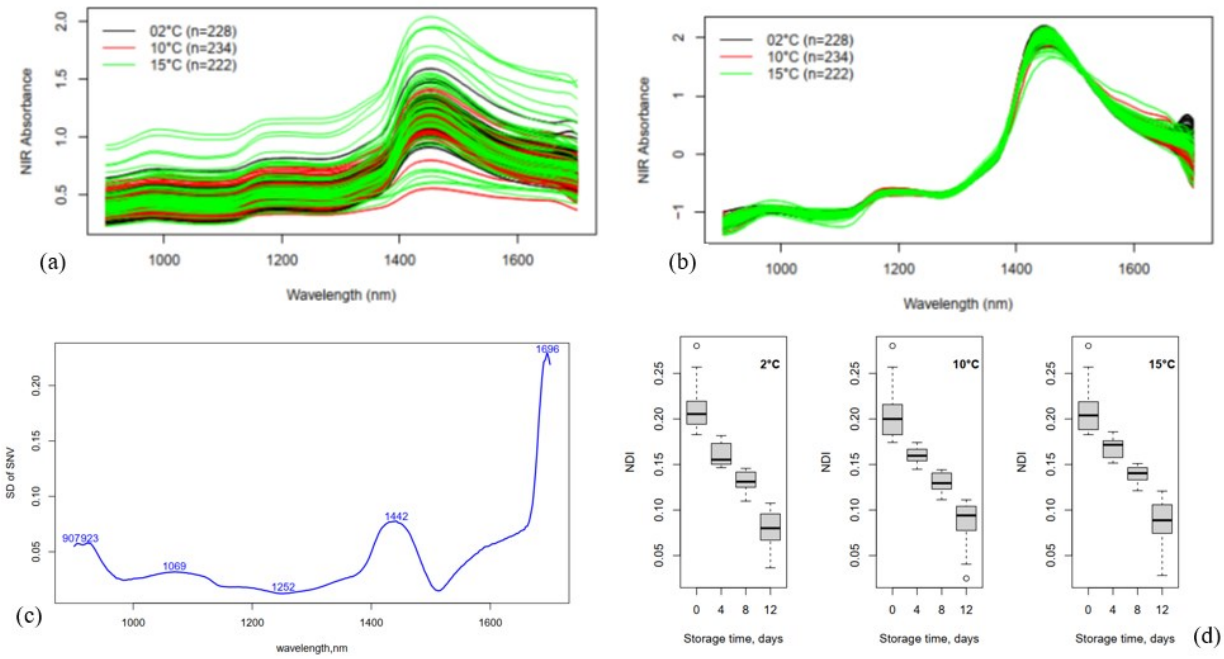

Figure 17: NIR analysis techniques: raw spectra (a), SNV (b), SD of SNV (c) and sample NDI_1252 at 1696 nm (d) of different storage time and temperature

Storage time significantly impacted both the NDI_1252 and QI indices across all wavelengths (Table 5). NDI_1252 of all selected wavelengths shows slightly higher F-values than QI across most wavelengths, except at 1442 nm, indicating greater sensitivity to time changes. Storage temperature has minimal effect on NDI_1252, except at 1442 nm and 1696 nm, while QI indices are more influenced by temperature, especially at longer wavelengths. In addition, interaction effects are significant at shorter wavelengths but decrease at longer wavelengths.

Table 5: F-values for the effects of storage time, storage temperature, and their interactions on NDI_1252 and QI indices at selected wavelengths.

Parameters	Factor	907 nm	923 nm	1069 nm	1442 nm	1696 nm
Asparagus NDI	Time(A), days	94.611^{s}	104.5^{s}	135.721^{s}	570.095^{s}	1622.416^{s}
	Temperature(B)	1.845	2.015	0.566	7.455^{s}	6.933^{s}

	Interaction (A× B)	417.271[s]	497.67[s]	491.082[s]	0.382	3.976
	Time(A), days	74.888[s]	89.378[s]	112.651[s]	685.056[s]	1251.284[s]
	Temperature(B)	3.973	3.3	5.451[a]	11.176[s]	13.47[s]
Asparagus QI	Interaction (A× B)	399.197[s]	467.909[s]	498.399[s]	3.209	0.704

NB: "s', $p<0.001$, "a" $p<0.05$

The correlation analysis between NIR absorbances, weight loss, and firmness further explains these relationships (Table 6). A significant correlation was observed between NIR absorbances at specific wavelengths, such as between NIR-907 and NIR-1069 (r = 0.998). Both NIR-907 (r = 0.928) and NIR-1069 (r = 0.923) exhibit significant correlations with firmness. Similarly, a significant correlation is observed between NIR absorbance at these wavelengths and weight loss (r = 0.829). The absorbance at longer wavelengths, such as NIR-1442 and NIR-1696, exhibited significant correlations with firmness (r = 0.453 and r = 0.607, respectively) and weaker correlations with weight loss (r = 0.233 and r = 0.439, respectively). This may be due to the longer wavelengths that penetrate deeper into the tissue and capture more complex changes. These interactions are less directly associated with properties on the surface such as firmness and weight loss, which leads to lower correlation values (Camps and Gilli, 2017). Additionally, the presence of overlapping absorption bands in the spectra may explain the lower level of significance observed between 907 nm and 1069 nm. Furthermore, these wavelengths may be sensitive to similar molecular vibrations, such as O-H and C-H bonds in water or organic compounds.

Table 6: Pearson's correlation matrix between NIR absorbance of the selected wavelength, weight loss, and firmness for green asparagus

	NIR_907	NIR_923	NIR_1069	NIR_1442	NIR_1696	Firmness, N	WL, %
NIR_907		0.526	0.998	0.509	0.67	0.928	0.829
NIR_923	s		0.523	0.878	0.834	0.499	0.21
NIR_1069	a	s		0.51	0.672	0.923	0.829
NIR_1442	s	s	s		0.9	0.453	0.233
NIR_1696	s	s	s	s		0.607	0.439
Firmness, N	s	s	s	s	s		0.755
WL, %	s	s	s	s	s	s	

NB: "s' $p<0.001$ and "a" $p<0.05$

Classification based on storage time and temperature

Fig. 18 compares PLS-DA and LDA models for detecting quality changes in asparagus stored at 15 °C for 12 days. PLS-DA used full spectra, while LDA relied on selected wavelengths. LDA outperformed PLS-DA, achieving accuracies of 76.9% (15 °C), 74.3% (10 °C), and 60.4% (2 °C) (Appendix Tables 12.2.2 and 12.2.3), with clearer class separation in score plots. This improvement is due to feature selection, which reduces spectral noise and emphasizes informative wavelengths. Lower accuracy at 2 °C reflects slower physiological changes and weaker spectral differences. Similar findings were reported by Sánchez et al. (2009), who achieved over 81% accuracy using PLS-DA on asparagus stored at 2 °C for 28 days.

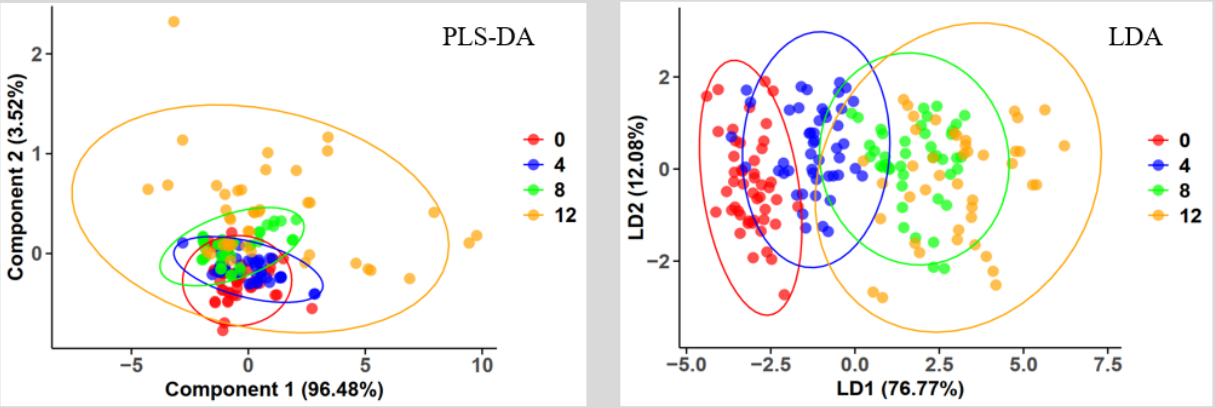

Metric	Validation set (n=45, LV=5) Mean	CI95 min	CI95 max
Accuracy	51.9%	42.2%	54.4%
Sensitivity	57.4%	38.9%	74.8%
Specificity	86.2%	82.2%	90.5%
Precision	51.0%	41.1%	63.7%
F-score	57.9%	44.1%	75.3%
Balanced Accuracy	72.7%	62.3%	74.4%

Metric	Validation set (n=45,LV=5) Mean	CI95 min	CI95 max
Accuracy	76.9%	67.4%	88.1%
Sensitivity	77.0%	65.9%	89.5%
Specificity	92.5%	89.3%	96.3%
Precision	76.4%	66.3%	87.8%
F-score	76.0%	65.6%	87.6%
Balanced Accuracy	84.7%	77.7%	92.9%

Figure 18: Comparison of PLS-DA and LDA models for detecting quality changes in Green Asparagus across four-day storage intervals using full and selected spectra for 15 ℃ storage groups.

On the other hand, Fig. 19 compares the quality detection efficiency of the PLS-DA and LDA models for green asparagus stored at three different temperatures (2°C, 10°C, and 15°C) on the 12th day of storage. Both models were constructed using five latent variables (LV = 5). The PLS-DA model, which used the full NIR spectrum, achieved a mean accuracy of 42.8%, with a sensitivity of 42.6% and a balanced accuracy of 58.3%. The score plot for PLS-DA shows an overlap between temperature groups. In contrast, the LDA model, constructed using selected NIR wavelengths, demonstrated

superior performance across all metrics. The LDA model achieved a mean accuracy of 87.7%, a sensitivity of 89.4%, and a balanced accuracy of 91.9%. The score plot for LDA reveals well-separated clusters for each temperature group. The PLS-DA plot shows overlap between the storage temperature groups, indicating that the full NIR spectra may not be discriminatory enough for detecting quality changes. The performance table reveals that PLS-DA has relatively good specificity (74.0%) but struggles with classification, as shown by its low precision and F-score. In contrast, the LDA plot shows clear separation between the temperature groups, particularly for samples stored at 2 °C, and demonstrates better performance. LDA achieves 87.7% accuracy, 89.4% sensitivity, and 94.4% specificity, with a balanced accuracy of 91.9%, indicating it effectively detects quality changes and classifies samples into temperature groups.

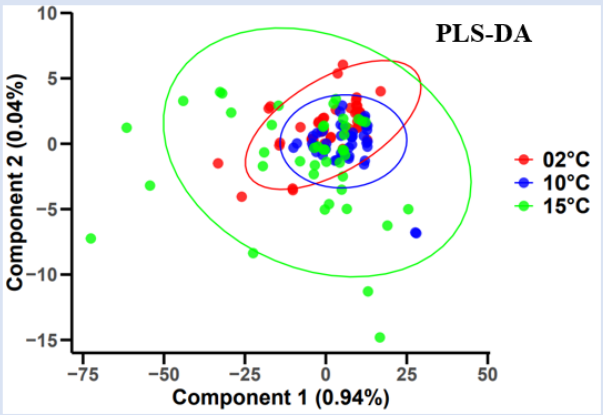

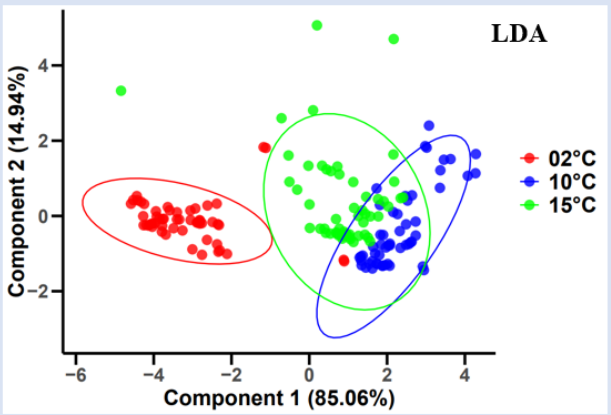

Metric	Validation (n=32, LV=5) Mean	CI95 min	CI95 max
Accuracy	42.8%	41.6%	43.9%
Sensitivity	42.6%	41.3%	44%
Specificity	74.0%	73.2%	74.8%
Precision	42.8%	41.6%	43.9%
F-score	42.7%	41.4%	43.9%
Balanced Accuracy	58.3%	57.3%	59.4%

Metric	Validation (n=32, LV=5) Mean	CI95 Min	CI95 Max
Accuracy	87.7%	87.0%	88.5%
Sensitivity	89.4%	88.8%	90.0%
Specificity	94.4%	94.1%	94.7%
Precision	87.7%	87.0%	88.5%
F-score	87.5%	86.7%	88.2%
Balanced Accuracy	91.9%	91.4%	92.4%

Figure 19: Comparison of PLS-DA and LDA models for detecting quality changes in Green Asparagus across three storage temperature groups using full and selected spectra**.**

Prediction of Weight Loss and Firmness

Figure 20 presents a comparison of the performance of PLSR and SVM models using the full NIR spectra and spectra at selected wavelengths for predicting weight loss (%) and firmness (N) in green asparagus. Each model was evaluated using both the full NIR spectra (left column) and selected wavelengths (right column).Scatter plots show predicted versus measured values, with data points

color-coded by storage temperature: blue represents samples stored at 2°C, orange corresponds to 10°C, and green indicates 15°C.The temperature-dependent variation significantly influenced the performance of the predictive models. In particular, the blue data points exhibited signs of overfitting. In contrast, the orange and green data points showed underfitting. The cross-validated performance metrics are summarized in Table 7. The SVM model showed relatively improved predictive accuracy when using selected wavelengths compared to PLSR model for both parameters. For weight loss, the model achieved with R^2 =0 .768, RMSE =5.690, and RPD= 2.080. for firmness, the model achieved R^2 of 0.829, RMSE= 5.380 N, and RPD =2.322. These results indicate that focusing on informative spectral regions combined with nonlinear regression models enhances model performance. Previous research by Flores-Rojas et al. (2009) applied PLSR to full NIR spectral data to estimate shear force in green asparagus, reporting moderate predictive ability ($R^2 < 0.67$), with limitations largely attributed to the product's high moisture content and tissue heterogeneity. In a similar study, Pérez-Marín et al. (2002) used NIR spectroscopy to estimate cutting force, achieving $R^2 = 0.840$.

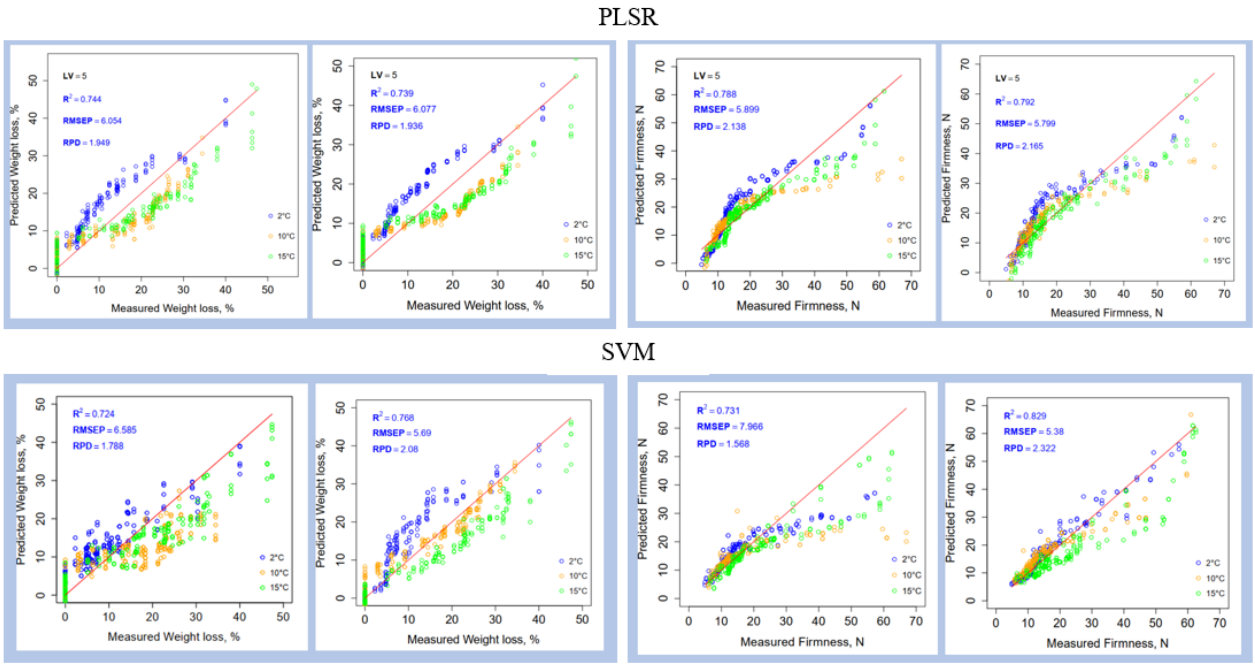

Figure 20: PLSR (top) and SVM (bottom) models for prediction of weight loss (left) and firmness (right) using full spectra (left) and selected wavelengths (right).

Table 7. Cross-validated performance metrics of the PLSR and SVM models for predicting asparagus weight loss and firmness (N = 684, LV = 5)

Datasets	NIR	Parameters	R2			RMSE			RPD		
			Mean	CI95min	CI95max	Mean	CI95min	CI95max	Mean	CI95min	CI95max
PLSR	Full	WL	0.744	0.738	0.751	6.054	5.973	6.136	1.949	1.923	1.975
		Firmness	0.788	0.780	0.795	5.899	5.748	6.049	2.138	2.105	2.172
	Selected	WL	0.739	0.733	0.745	6.077	6.006	6.149	1.936	1.912	1.960
		Firmness	0.792	0.787	0.798	5.799	5.688	5.910	2.165	2.137	2.193
SVM	Full	WL	0.724	0.717	0.732	6.585	6.505	6.664	1.788	1.768	1.807
		Firmness	0.731	0.719	0.743	7.966	7.760	8.171	1.568	1.545	1.591
	Selected	WL	0.768	0.762	0.775	5.690	5.616	5.764	2.080	2.053	2.108
		Firmness	0.829	0.822	0.835	5.380	5.270	5.491	2.322	2.281	2.362

6.1.5 Laser light backscattering imaging (LLBI)

LLBI Profile Description

The amplitude, shape, and FWHM parameters of the LLBI profile were extracted using the modified Cauchy and Gaussian distribution function models. Curve fitting across all sample images (n = 344) showed that the Cauchy model (R^2 = 0.78, RPD = 2.29) outperformed the Gaussian model (R^2 = 0.53, RPD = 1.96). As illustrated in Fig. 21, the modified Cauchy model provided a superior fit to the observed LLBI data, particularly for amplitude and Shape, and was therefore selected for further analysis

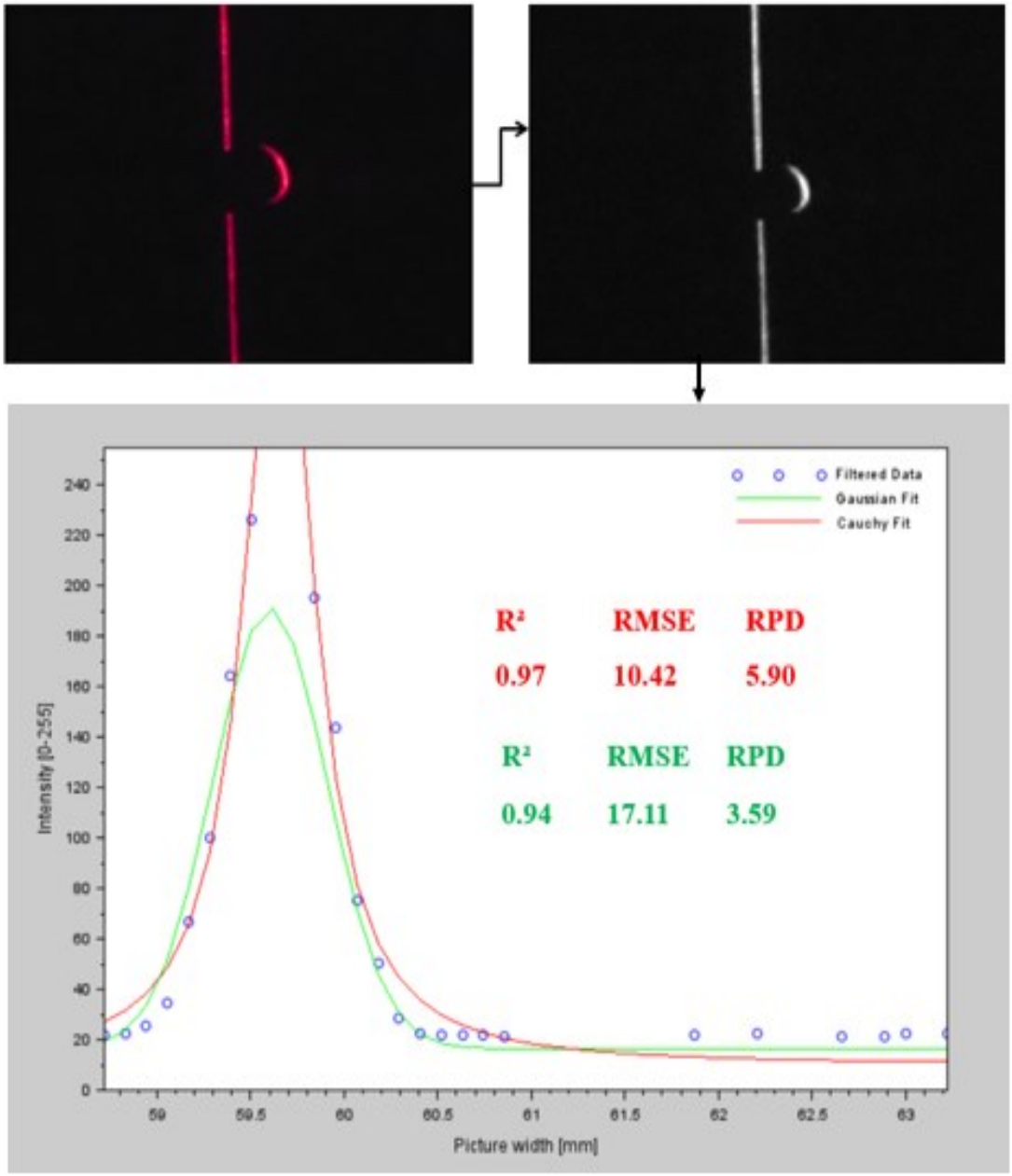

Figure 21: Sample illuminated images with a line laser at 635 nm (top left), followed by the grayscale image (top right), and curve-fitted profile using Gaussian and Cauchy models (bottom).

Fig. 22 shows that amplitude and shape parameters consistently increase with both time and temperature. Amplitude values indicate scattering intensity, while the shape parameter reflects light distribution size within the asparagus tissue. These changes are linked to physiological processes

like water loss, cell wall degradation, and tissue senescence. ANOVA results indicate significant effects of storage time on amplitude ($F = 641.172$, $p < 0.001$) and shape ($F = 431.757$, $p < 0.001$). Pearson's correlation analysis (Table 8) shows strong correlations between amplitude and shape ($r = 0.816$), amplitude and weight loss ($r = 0.809$), and shape with firmness ($r = 0.928$). Previous studies support that moisture loss and structural degradation affect light distribution in tissues, with firmer vegetables blocking light penetration (Romano et al., 2008; Hashim et al., 2018)

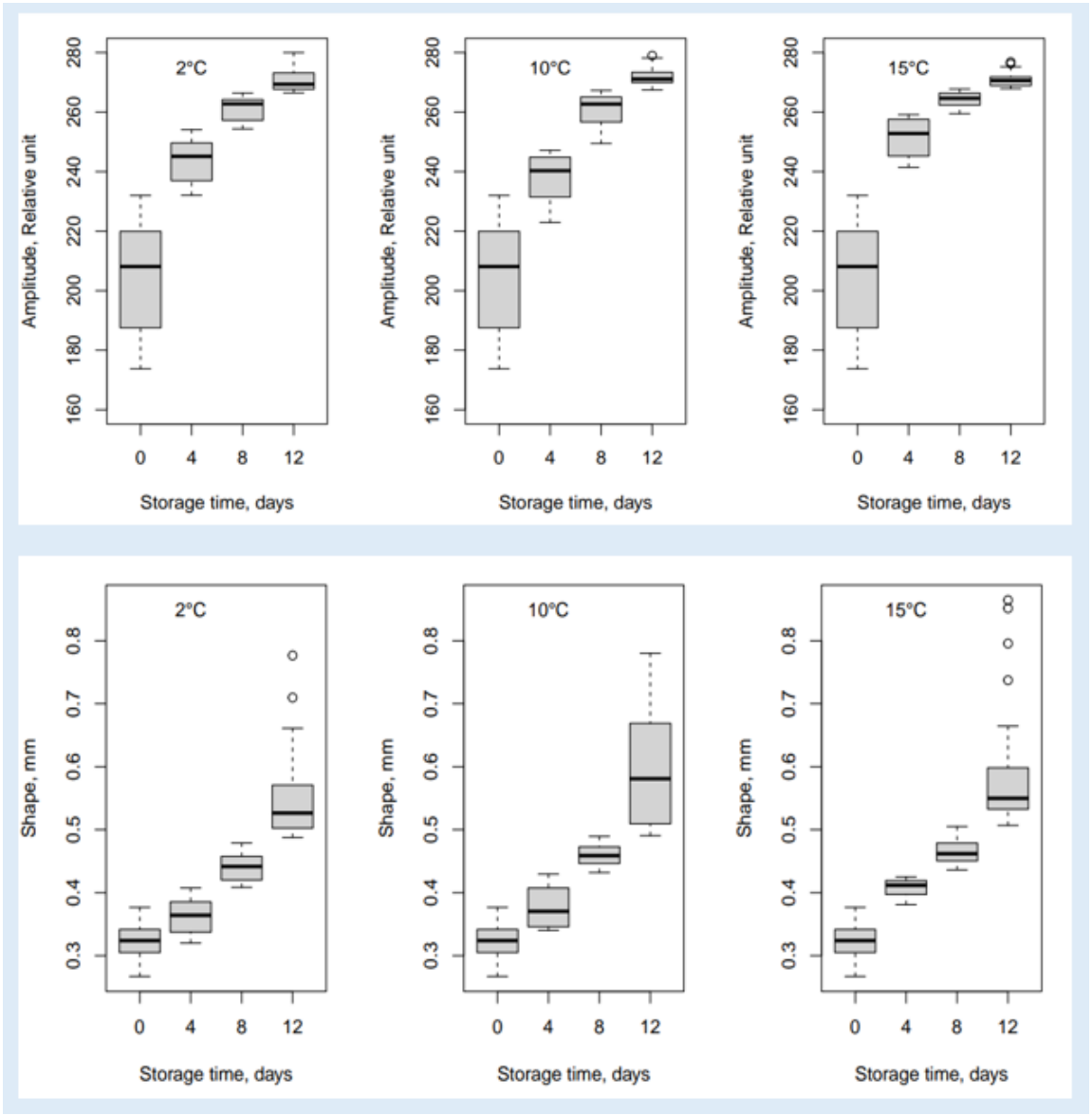

Figure 22: Changes in amplitude and shape parameters of modified Cauchy-Fitted LLBI Profiles for green asparagus at different storage times and temperatures

Table 8: Pearson's correlation coefficient between variables (n=344).

Variables	Amplitude, RU	Shape, mm	WL, %	Firmness
Amplitude, RU		0.816	0.809	0.654
Shape, mm	s		0.843	0.928
WL, %	s	s		0.748
Firmness, N	s	s	s	

's' , $p<0.001$

Classification of storage time and temperature groups

To assess the effect of storage time on asparagus quality, an LDA model was developed across all temperature groups (Fig. 23). The overall detection accuracy was 85.4% in training and 79.7% in validation. Individually, performance improved with temperature: 81.4% at 2 °C, 89.6% at 10 °C, and 93.4% at 15 °C (Appendix Fig. 12.1.3). This demonstrates the model's strong potential for real-time freshness classification, especially at higher temperatures. Previous studies also support the effectiveness of LDA in food quality monitoring. Pham et al. (2023) applied LLBI at 635 nm with LDA to starch-coated asparagus, achieving 70.5% accuracy. Lockman (2019) used LDA with LLBI at 650–705 nm to classify copepod maturity, reporting 90–95% accuracy. Zulkifli et al. (2019) combined LLBI (658 nm) with LDA for banana ripening stages, achieving above 90% accuracy.

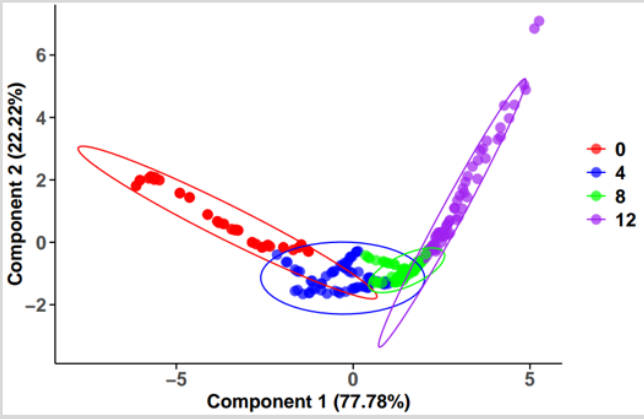

Training set(n=275, accuracy =85.4%)				
	0d	4d	8d	12d
0d	82.89	17.11	0	0
4d	1.61	85.48	12.9	0
8d	0	2.67	97.33	0
12d	0	0	25.81	74.19
Validation set (n=69, accuracy =79.7%)				
	0d	4d	8d	12d
0d	85.71	14.29	0	0
4d	0	81.82	18.18	0
8d	0	6.67	93.33	0
12d	0	0	38.89	61.11

Figure 23: LDA plot on the training set (left) and the confusion matrix (right) for storage time groups of green asparagus

Prediction of Weight Loss and Firmness

Fig. 24 presents regression results for predicting weight loss and firmness using LLBI parameters with Multivariate Regression (MVR) and Multivariate Adaptive Regression Splines (MARS). MARS outperformed MVR, showing tighter clustering around the regression line across all temperature groups (Table 9). While MVR struggled to balance predictions, especially across different temperatures, MARS better captured nonlinear variations, though slight dispersion remained at 15 °C.

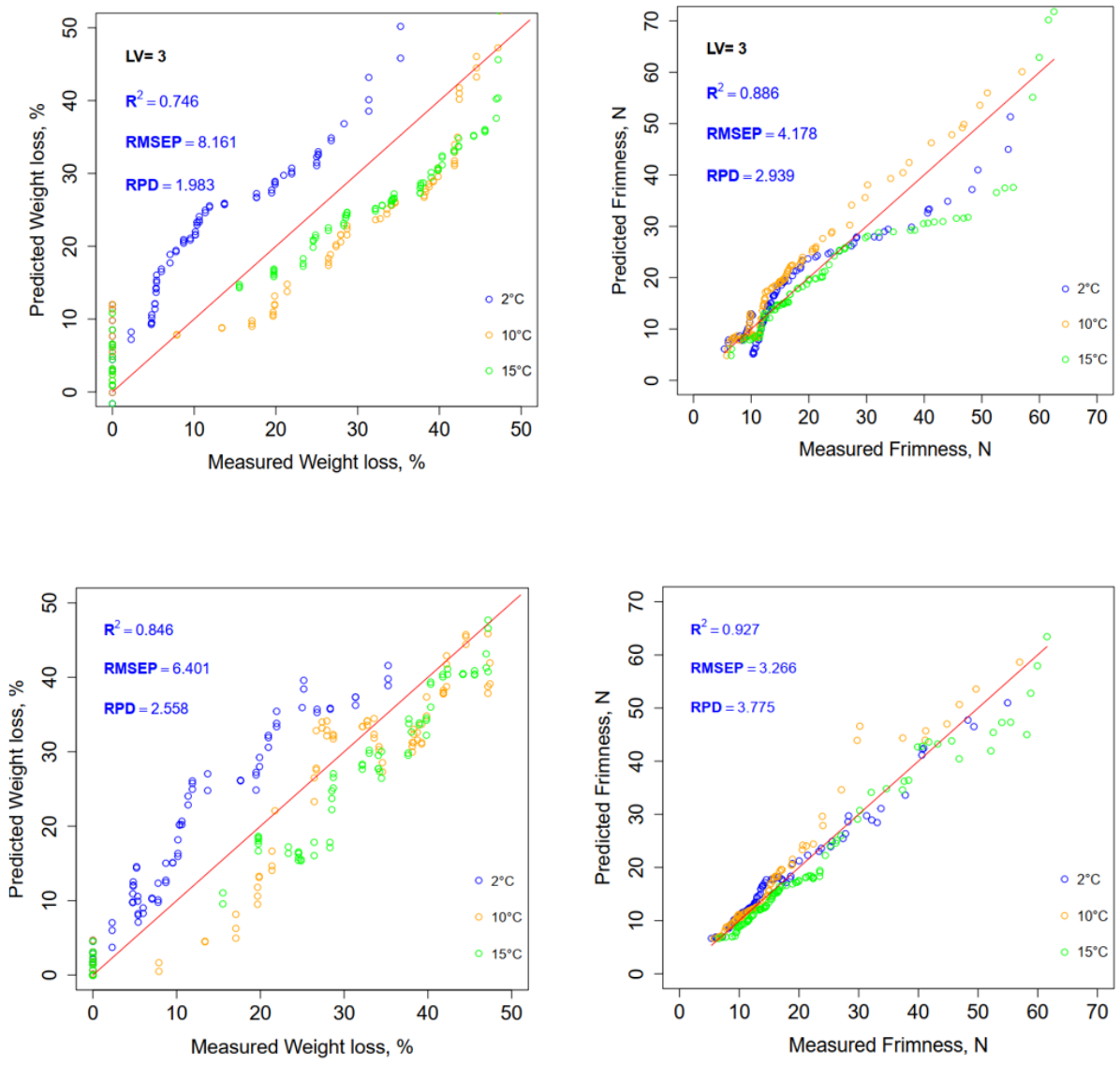

Figure 24: MVR (top) and MARS (bottom) for predicting weight loss (left) and firmness (right).

The MARS model showed higher performance compared to the MVR model across all metrics. For weight loss, MARS achieved a higher R^2 = 0.846, RMSE = 6.401% and a higher RPD = 2.558 . Similarly, for firmness, MARS showed superior performance with an R^2 = 0.927, RMSE = 3.266 N, and RPD = 3.775. Compared with previous studies, Qing et al. (2007b) reported that firmness prediction using frequencies of gray scale intensities and PLSR achieved R^2 = 0.81 and RMSECV = 5.44 N. This high correlation and reasonable RMSECV indicates good predictive performance, although the RMSECV is higher than the RMSEP achieved by MARS in this study. Similarly, Peng and Lu (2006) also found that LLBI parameters provided good fruit firmness predictions using multilinear regression, with r = 0.896 and SEP = 6.50 N. Romano et al. (2012) reported that scattering area and light intensity were able to predict moisture content changes of yellow bell pepper during drying. The logarithmic regression model was applied, and it achieved R^2=0.86 and RMSEP = 7.28%. Compared to existing literature, the current study demonstrates that LLBI combined with MARS is highly effective in predicting the weight loss and firmness of green asparagus during storage.

Table 9: Cross- validated Performance metrics of MVR and MARS models (n=344) for predicting WL and firmness.

Models	Parameters	R^2			RMSE			RPD		
		Mean	CI95min	CI95max	Mean	CI95min	CI95max	Mean	CI95min	CI95max
MVR	WL	0.746	0.739	0.753	8.161	8.084	8.238	1.983	1.955	2.011
	Firmness	0.886	0.882	0.890	4.178	4.075	4.280	2.939	2.883	2.994
MARS	WL	0.846	0.840	0.851	6.401	6.312	6.489	2.558	2.514	2.603
	Firmness	0.927	0.922	0.932	3.266	3.140	3.391	3.775	3.634	3.915

6.2 Assessment of quality changes in plums during post-harvest storage

In this section, the results obtained from physiological assessments, near-infrared (NIR) spectroscopy, and beam-based LLBI techniques are presented to evaluate the quality attributes of plum fruits during storage. For NIR spectroscopy analysis, a total of 2,965 observations were produced by acquiring spectral data from both sides of each fruit using three consecutive scans, followed by SNV preprocessing and manual selection of five prominent wavelengths. NDI and QI indices were calculated to validate spectral sensitivity. PLSR and SVM models were developed using the R packages 'pls' (version 2.8-2) and 'e1071' (version 1.7-13), respectively. These models were calibrated using both the full spectra and selected wavelengths to predict weight loss and soluble solids content in green asparagus. For LLBI, 1,276 observations were obtained by capturing images at six wavelengths (532, 635, 780, 808, 850, and 1064 nm) from both sides of each fruit. Optimized wavelengths were identified through ANOVA and Tukey's post hoc analysis. LDA and MVR models were used to detect the quality changes by classifying samples into their storage time groups and predicting firmness, SSC, and skin color, respectively. The datasets included samples from two cultivars (Stanley' and 'Elena') and were split into training and validation subsets. Model performance was evaluated using bootstrapped metrics (R^2, RMSE, RPD) with 95% confidence intervals.

6.2.1 Ethylene production

The rate of ethylene production increased with both storage temperature (F-value = 321.80 and 109.11; $P < 0.001$) and storage time (F-value = 170.42 and 69.03; $P < 0.001$) in both 'Stanley' and 'Elena' plums. However, the ethylene production of plums stored at 1 °C significantly differed from those stored at higher temperatures. The 'Stanley' plums showed a relatively higher rate of ethylene production than the 'Elena' plums across the temperature groups (Fig. 25). Similar studies have shown that plums, as climacteric fruits, experience a significant increase in ethylene production during ripening (Luo et al., 2009; Ha et al., 2023). In climacteric fruits, ethylene triggers ripening events such as fruit softening, chlorophyll breakdown, color development, and sugar accumulation (Ravindra and Goswami, 2008). These processes accelerate ripening, producing a relatively short shelf life (Kumar et al., 2018; Manganaris et al., 2008).

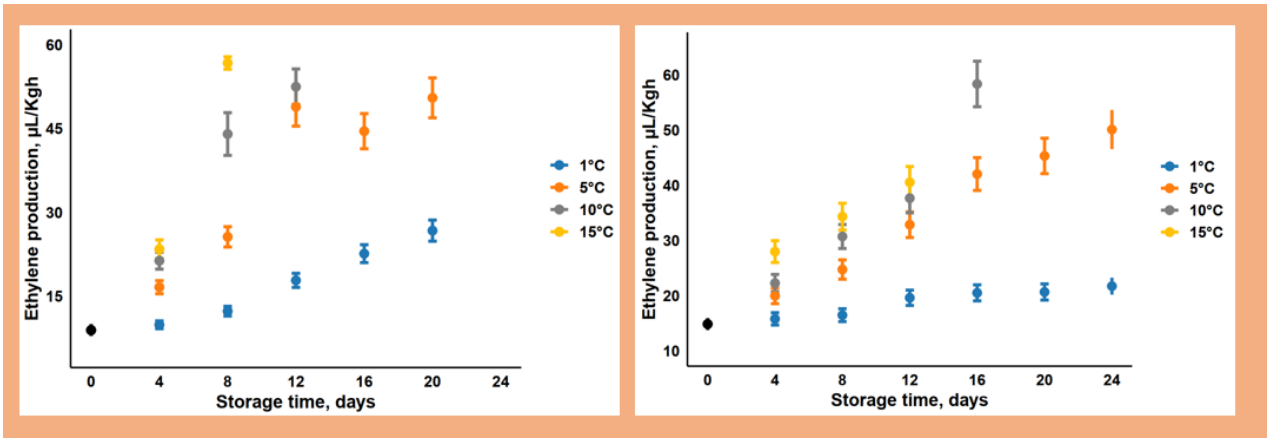

Figure 25: Ethylene production rate of 'Stanley' (left) and 'Elena'(right) during storage at different time and temperature groups. Results are presented as mean ± SD.

6.2.2 Respiration rate

The respiration rate of both 'Stanley' and 'Elena' plums increased with both storage temperature (F-value = 195.04 and 565.46; $P < 0.001$) and storage time (F-value = 816.80 and 269.53; $P < 0.001$). 'Stanley' plums stored at 10 °C and 15 °C exhibited higher respiration rates compared to those stored at 1 °C and 5 °C, while 'Elena' plums showed the highest respiration at 15 °C (Fig. 26 left). Respiration peaked at 8 days for 'Stanley' and 12 days for 'Elena', then declined after 20 days (Fig. 26 right). Respiration rates ranged from 6.41 to 18.65 mL/ Kg.h influenced by temperature, duration, and enzymatic activity. Singh and Khan (2010) reported that respiration increases to a peak and declines as the fruit ripens, while lower temperatures suppress ethylene production and slow ripening, extending shelf life (Argenta et al., 2003).

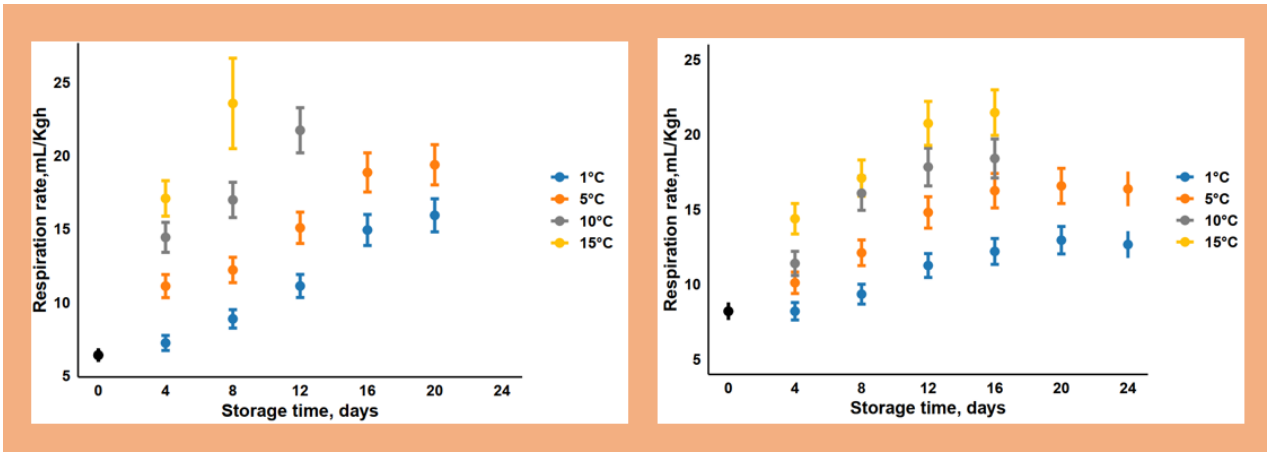

Figure 26: Respiration rate 'Stanley' (left) and 'Elena'(right) during storage at different time and temperature groups. Results are presented as mean ± SD

6.2.3 Weight loss

Table 10 summarizes plum weight loss (WL) across different storage temperatures and times. 'Stanley' plums showed greater WL than 'Elena', with ANOVA confirming significant effects of storage time, temperature, and cultivar ($F = 6.06 \times 10^{28}$, 1.88×10^{28}, 1.21×10^{28}; $p < 0.001$). WL increased notably after 12 days due to ripening-related water loss, enzymatic activity, and respiration. Moisture evaporation led to wilting, shriveling, and softening, consistent with prior reports on pre- and post-ripening weight loss (Guerra and Casquero, 2008; Zora and Ahmad, 2010; Van Dijk et al., 2006). Changes in water molecular structure also correlate with WL, as reported in previous studies (Gibertoni et al., 2022; Vitalis et al., 2023).

Table 10: Weight loss (Mean ± SD) of 'Stanley' and 'Elena' plums at different storage temperature and time.

Variables	Days	Cultivars	Storage temperatures			
			1 °C	5 °C	10 °C	15 °C
Weight Loss, %	0	Stanley	0 ± 0.00^{Aa}	0 ± 0.00^{Aa}	0 ± 0.00^{Aa}	0 ± 0.00^{Aa}
		Elena	0 ± 0.00^{Aa}	0 ± 0.00^{Aa}	0 ± 0.00^{Aa}	0 ± 0.00^{Aa}
	4	Stanley	1.37 ± 0.11^{Ab}	1.61 ± 0.09^{Bb}	1.96 ± 0.10^{Cb}	2.63 ± 0.12^{Db}
		Elena	1.74 ± 0.20^{Ab}	2.14 ± 0.16^{Bb}	2.66 ± 0.19^{Cb}	3.25 ± 0.20^{Db}
	8	Stanley	2.48 ± 0.13^{Ac}	3.28 ± 0.12^{Bc}	3.92 ± 0.12^{Cc}	4.70 ± 0.15^{Dc}
		Elena	3.15 ± 0.19^{Ac}	4.00 ± 0.29^{Bc}	5.14 ± 0.19^{Cc}	6.03 ± 0.21^{Dc}
	12	Stanley	3.66 ± 0.12^{Ad}	4.71 ± 0.17^{Bd}	6.19 ± 0.18^{Cd}	NA
		Elena	4.38 ± 0.17^{Ad}	5.19 ± 0.17^{Bd}	7.30 ± 0.16^{Cd}	8.99 ± 0.21^{Dd}
	16	Stanley	4.72 ± 0.19^{Ae}	6.23 ± 0.14^{Be}	NA	NA
		Elena	5.50 ± 0.18^{Ae}	6.59 ± 0.26^{Be}	10.2 ± 0.23^{Ce}	12.95 ± 0.22^{De}
	20	Stanley	5.91 ± 0.19^{Af}	7.84 ± 0.19^{Bf}	NA	NA
		Elena	7.13 ± 0.18^{Af}	8.71 ± 0.15^{Bf}	NA	NA
	24	Stanley	NA	NA	NA	NA
		Elena	9.31 ± 0.20^{Ag}	11.24 ± 0.19^{Bg}	NA	NA

NB: "NA" indicates data were not available; Different upper-case letters within a row indicate significant differences between storage temperatures for a given cultivar and storage time. Different lower-case letters within a column indicate significant differences between a given cultivar's storage times at a given cultivars and temperature (Tukey's test; $p < 0.05$).

The variation in plums' weight loss is influenced by storage temperature and duration, which accelerate enzymatic activities that enhance ripening due to increased respiration rates. Singh and Khan (2010) describe how oxygen consumption and carbon dioxide production rates initially increase, peak, and then decline as the fruit becomes overripe. Additionally, ripening leads to water loss in the fruit, causing undesirable effects like wilting, shriveling, and softening (Guerra and Casquero, 2008; Li et al., 2022). This is likely due to reduced metabolic activity and decreased evaporation, which help preserve the fruit's structural integrity over a longer period (Crisosto et al., 2004; Wang et al., 2016).

6.2.4 Firmness

Table 11 shows that plum firmness declined steadily over time for both cultivars, with samples stored at 15 °C exhibiting the fastest softening, followed by 10 °C. ANOVA confirmed significant effects of storage time ($F = 8992.12$), temperature ($F = 1927.80$), and cultivar ($F = 3142.06$; $p < 0.001$). Firmness loss is driven by ripening, enzymatic degradation of cell wall polysaccharides (polygalacturonase and pectinesterase), and moisture loss, while lower temperatures slow these processes by preserving cell wall integrity and delaying pectin breakdown. Genetic traits and physiological maturity also contribute to cultivar-specific differences in firmness. Previous studies reported that firmness variability is strongly influenced by cultivar genetics, ripening stage, and enzymatic activity, with lower storage temperatures mitigating softening and extending shelf life. For instance, Cetin and Saraçoğlu (2023) and Hend et al. (2009) highlighted the role of genotype and maturation in texture changes, He et al. (2022) and Wang et al. (2016) emphasized the role of enzymatic cell wall degradation, while Geng et al. (2020) and Manganaris et al. (2008) demonstrated that cold storage preserves firmness by slowing pectin breakdown. Moisture loss during storage also contributes to softening and textural deterioration (Huang et al., 2018; Mishra et al., 2022).

Table 11: Firmness (Mean ± SD) of 'Stanley' and 'Elena' plums at different storage temperatures and time

Variables	Days	Cultivars	Storage temperature			
			1 °C	5 °C	10 °C	15 °C
Firmness, N	0	Stanley	45.76 ± 6.98^{Aa}	45.76 ± 6.98^{Aa}	45.76 ± 6.98^{Aa}	45.76 ± 6.98^{Aa}
		Elena	44.16 ± 7.88^{Aa}	44.16 ± 7.88^{Aa}	44.16 ± 7.88^{Aa}	44.16 ± 7.88^{Aa}
	4	Stanley	30.62 ± 8.62^{Ab}	19.16 ± 4.58^{Bb}	15.07 ± 3.48^{Cb}	9.65 ± 2.42^{Db}
		Elena	37.27 ± 7.22^{Ab}	30.11 ± 5.60^{Bb}	26.51 ± 6.95^{Cb}	25.29 ± 7.88^{Db}
	8	Stanley	29.70 ± 4.14^{Ac}	13.70 ± 3.77^{Bc}	10.53 ± 3.64^{Cc}	7.16 ± 1.88^{Dc}
		Elena	36.95 ± 8.15^{Ac}	24.50 ± 5.67^{Bc}	15.78 ± 5.69^{Cc}	11.50 ± 5.46^{Dc}
	12	Stanley	29.16 ± 4.69^{Ac}	10.25 ± 1.96^{Bd}	7.39 ± 1.63^{Cd}	NA
		Elena	32.60 ± 5.47^{Ad}	21.38 ± 6.84^{Bd}	14.14 ± 4.41^{Cd}	7.82 ± 4.77^{Dd}
	16	Stanley	25.96 ± 4.77^{Ae}	8.16 ± 1.55^{Be}	NA	NA
		Elena	30.09 ± 8.90^{Ae}	14.25 ± 2.83^{Be}	10.30 ± 2.47^{Ce}	7.60 ± 1.94^{De}
	20	Stanley	30.35 ± 5.86^{Af}	8.47 ± 2.27^{Bf}	NA	NA
		Elena	32.77 ± 3.06^{Af}	13.90 ± 3.91^{Bf}	NA	NA
	24	Stanley	NA	NA	NA	NA
		Elena	10.71 ± 1.64^{Ag}	9.39 ± 4.16^{Bg}	NA	NA

NB: "NA" indicates data were not available; Different upper-case letters within a row indicate significant differences between storage temperatures for a given cultivar and storage time. Different lower-case letters within a column indicate significant differences between storage times at a given cultivar and storage temperature (Tukey's test; $p < 0.05$).

6.2.5 Soluble solid content (SSC)

Table 12 shows that SSC significantly increased with both storage time and temperature, with ANOVA revealing significant effects for both factors ($F = 124779.90$ and 4632.10; $p < 0.001$), as well as significant differences between cultivars ($F = 250701.30$; $p < 0.001$). Higher storage temperatures accelerated SSC increases, as seen in samples stored at 15 °C, which also had the highest SSC values. SSC is an indicator of sweetness, and ripeness of the fruits (Guo et al 2019; Lie et al 2016) and it can be influenced by sugar concentration, moisture loss, and cultivar characteristics (Kodagoda et al., 2021; Wang et al., 2016). Cold storage prolongs shelf life by reducing metabolic processes and evaporation, while higher temperatures lead to faster ripening and potential spoilage (Crisosto et al., 2004; Manganaris et al., 2008; Guerra and Casquero, 2008).

Table 12: SSC (Mean ± SD) of 'Stanley' and 'Elena' plums at different storage temperatures and time

Variable	days	Cultivar	Storage temperatures			
			1 °C	5 °C	10 °C	15 °C
SSC, %	0	Stanley	14.50 ± 0.07^{Aa}	14.50 ± 0.07^{Aa}	14.50 ± 0.07^{Aa}	14.50 ± 0.07^{Aa}
		Elena	14.95 ± 0.22^{Aa}	14.95 ± 0.22^{Aa}	14.95 ± 0.22^{Aa}	14.95 ± 0.22^{Aa}
	4	Stanley	14.49 ± 0.08^{Ab}	14.96 ± 0.11^{Bb}	15.19 ± 0.02^{Cb}	15.34 ± 0.05^{Db}
		Elena	15.71 ± 0.09^{Ab}	16.04 ± 0.18^{Bb}	16.48 ± 0.09^{Cb}	16.76 ± 0.17^{Db}
	8	Stanley	15.5 ± 0.08^{Ac}	15.69 ± 0.07^{Bc}	15.9 ± 0.07^{Cc}	16 ± 0.00^{Dc}
		Elena	17.19 ± 0.14^{Ac}	17.55 ± 0.05^{Bc}	17.72 ± 0.07^{Cc}	17.87 ± 0.05^{Dc}
	12	Stanley	16.05 ± 0.05^{Ad}	16.19 ± 0.02^{Bd}	16.36 ± 0.1^{Cd}	NA
		Elena	17.9 ± 0.02^{Ad}	18.06 ± 0.05^{Bd}	18.1 ± 0^{Cd}	18.1 ± 0.00^{Dd}
	16	Stanley	16.54 ± 0.05^{Ae}	16.73 ± 0.07^{Bd}	NA	NA
		Elena	18.26 ± 0.1^{Ae}	18.54 ± 0.11^{Be}	18.79 ± 0.08^{Ce}	19 ± 0.08^{De}
	20	Stanley	16.96 ± 0.12^{Af}	17.59 ± 0.22^{Be}	NA	NA
		Elena	19.36 ± 0.14^{Af}	19.71 ± 0.09^{Bf}	NA	NA
	24	Stanley	NA	NA	NA	NA
		Elena	20.11 ± 0.15^{Ag}	20.2 ± 0^{Bg}	NA	NA

NB: "NA" indicates data were not available; Different upper-case letters within a row indicate significant differences between storage temperatures for a given cultivar and storage time. Different lower-case letters within a column indicate significant differences between storage times for a given cultivar and storage temperature (Tukey's test; $p < 0.05$)

6.2.6 Peel Color

Table 13 shows the chroma and hue values of two plum cultivars measured using the Minolta Chroma Meter during storage at different temperatures and times. Both chroma and hue were significantly affected by storage conditions, with greater changes observed at higher temperatures. The 'Stanley' cultivar experienced a greater decline in chroma, and more noticeable hue shifts compared to 'Elena', indicating its higher sensitivity to temperature-induced color changes. Lower temperatures (1 °C and 5 °C) slowed hues and chroma changes, but 'Stanley' showed a sudden decline in hue at 5 °C, likely due to water loss and advanced ripening. Two-way ANOVA confirmed that chroma was most influenced by cultivar (F = 1498.539), followed by storage time (F = 1433.125), and temperature (F = 273.025), while hue was primarily affected by time (F = 1803.530) and temperature (F = 244.233). The reduction in chroma and hue shifts were attributed to biochemical changes during ripening, with anthocyanin accumulation playing a role in hue changes, particularly under cold stress (Wang et al., 2020; Robertson et al., 1991). Furthermore, the presence and transformation of pigments such as chlorophylls, carotenoids, and anthocyanins during the ripening process lead to changes in skin or peel color (Muhammad et al., 2024).

Table 13: Changes in chroma and hue angle of the two plum cultivars at different storage times and temperatures.

Variables	Days	Cultivars	Storage temperatures			
			1 °C	5 °C	10 °C	15 °C
Chroma	0	Stanley	9.82 ± 2.10^{Aa}	9.82 ± 2.10^{Aa}	9.82 ± 2.10^{Aa}	9.82 ± 2.10^{Aa}
		Elena	9.032 ± 0.83^{Aa}	9.032 ± 0.83^{Aa}	9.032 ± 0.83^{Aa}	9.032 ± 0.83^{Aa}
	4	Stanley	7.28 ± 0.32^{Ab}	6.75 ± 0.52^{Ab}	6.63 ± 0.43^{Cb}	5.72 ± 0.47^{Bb}
		Elena	7.83 ± 0.50^{ABb}	8.24 ± 0.65^{Ab}	7.07 ± 0.49^{BCb}	6.73 ± 0.31^{Cb}
	8	Stanley	5.89 ± 0.36^{Ac}	5.66 ± 0.26^{Ac}	5.44 ± 0.26^{Bc}	4.39 ± 0.47^{Bc}
		Elena	6.78 ± 0.19^{ABc}	7.21 ± 0.11^{Ac}	5.83 ± 0.26^{BCc}	5.82 ± 0.27^{Cc}
	12	Stanley	5.01 ± 0.25^{Ad}	4.74 ± 0.26^{Ad}	4.44 ± 0.60^{Bd}	NA
		Elena	6.20 ± 0.16^{ABd}	6.67 ± 0.20^{Ad}	5.10 ± 0.17^{BCd}	4.95 ± 0.29^{Cd}
	16	Stanley	3.91 ± 0.34^{Ae}	4.02 ± 0.22^{Ae}	NA	NA
		Elena	5.61 ± 0.17^{ABe}	6.05 ± 0.13^{Ae}	4.24 ± 0.51^{BCe}	3.86 ± 0.49^{Ce}
	20	Stanley	2.73 ± 0.45^{Af}	3.01 ± 0.46^{Af}	NA	NA
		Elena	5.05 ± 0.19^{ABe}	5.54 ± 0.18^{Ae}	NA	NA
	24	Stanley	NA	NA	NA	NA
		Elena	4.26 ± 0.47^{ABf}	4.57 ± 0.40^{Af}	NA	NA
Hue angle, degree	0	Stanley	40.05 ± 27.29^{Aa}	40.05 ± 27.29^{Aa}	40.05 ± 27.29^{Aa}	40.05 ± 27.29^{Aa}
		Elena	20.9 ± 17.89^{Aa}	20.9 ± 17.89^{Aa}	20.9 ± 17.89^{Aa}	20.9 ± 17.89^{Aa}
	4	Stanley	17.88 ± 15.03^{Ab}	30.71 ± 10.71^{Bb}	19.68 ± 12.97^{Cb}	-21.98 ± 22.17^{Db}
		Elena	6.67 ± 4.41^{Ab}	-20.2 ± 17.96^{Ab}	-37.53 ± 26.63^{BCb}	-36.36 ± 28.91^{Cb}

8	Stanley	38.81 ± 17.42^{Ac}	26.27 ± 6.19^{Bc}	-16.14 ± 14.42^{Cc}	-20.87 ± 27.65^{Dc}
	Elena	-8.47 ± 6.12^{ABc}	-35.47 ± 21.41^{Ac}	-48.42 ± 22.24^{BCc}	-45.57 ± 25.60^{Cc}
12	Stanley	37.65 ± 17.09^{Ad}	18.08 ± 4.32^{Bd}	2.23 ± 19.29^{Cd}	NA
	Elena	$- 9.43 \pm 8.28^{ABd}$	-39.28 ± 14.27^{Ad}	-56.63 ± 16.47^{BCd}	-66.04 ± 15.25^{Cd}
16	Stanley	-1.18 ± 28.42^{Ae}	-13.8 ± 12.69^{Be}	NA	NA
	Elena	-22.18 ± 12.18^{ABe}	-44.9 ± 10.20^{Ae}	-52.67 ± 18.53^{BCe}	-60.32 ± 14.63^{Ce}
20	Stanley	12.58 ± 25.44^{Af}	-11.98 ± 13.76^{Bf}	NA	NA
	Elena	-4.63 ± 2.92^{ABe}	-37.55 ± 12.37^{Ae}	NA	NA
24	Stanley	NA	NA	NA	NA
	Elena	-13.60 ± 3.29^{ABf}	-50.26 ± 8.10^{Af}	NA	NA

NB: "NA" indicates data were not available; Different upper-case letters within a row indicate significant differences between storage temperatures for a given cultivar and storage time. Different lower-case letters within a column indicate significant differences between storage times for a given cultivar and storage temperature (Tukey's test; $p < 0.05$)

In addition, the changes in the skin color parameters of plums can be attributed to pigment transformations driven by biochemical processes such as anthocyanin accumulation and chlorophyll degradation. Anthocyanin accumulation, which increases during ripening, is a key driver of the bright red coloration in plums, as highlighted by Fiol et al. (2021). Furthermore, chlorophyll degradation during ripening enhances the visibility of anthocyanins, leading to the transition from green to red (Wang et al., 2022). Among anthocyanins, cyanidin 3-O-glucoside plays a dominant role in the color change process, while carotenoids contribute secondarily by imparting yellow to orange hues (Chen, 2015). Additionally, plums are rich in carotenoids, with their concentrations significantly higher in the skin compared to the flesh (Kaulmann et al., 2016; Rezaei Kalaj et al., 2016; Deng et al., 2023).

6.2.7 NIR spectroscopy

Spectral description

Fig. 27 illustrates how storage temperature influences the spectral properties of plum samples. The raw NIR spectra (900–1700 nm) in Fig. 27(a) show distinct absorbance trends based on temperature, with notable changes after SNV correction in Fig. 27(b), particularly around ~1650 nm. The standard deviation of the SNV spectra in Fig. 27(c) highlights sensitive wavelengths (909, 1064, 1323, 1447, and 1650 nm), with the reference wavelength at 1532 nm showing the minimum standard deviation across the spectra. The wavelengths exhibiting significant variation may reflect physiological and biochemical changes in plums. These variations are likely linked to temperature-induced changes in metabolic activities and water dynamics. Previous studies indicate that

absorbance at these wavelengths corresponds to specific chemical bonds, with variations associated with sugar concentration, water absorption, and the overtones of C-H and O-H bonds (Paz et al., 2008; Walsh et al., 2020). Moreover, the NIR absorbance at 975 nm is useful for determining SSC (Mireei et al., 2010), while bands at 1330 nm, 1376 nm, and 1418 nm are associated with water absorption (Paz et al., 2008 ;Walsh et al., 2020). In addition, NIR peaks at 900, 906, and 910 nm with sugar-related third overtone absorption in fresh fruits and vegetables (Walsh et al., 2020; Wang and Xie, 2014). Variations in absorbance intensity at 1060 nm have been linked to changes in sugar concentration (Qing et al., 2007a), while intensity variations around 1680 nm are associated with the degradation organic compounds

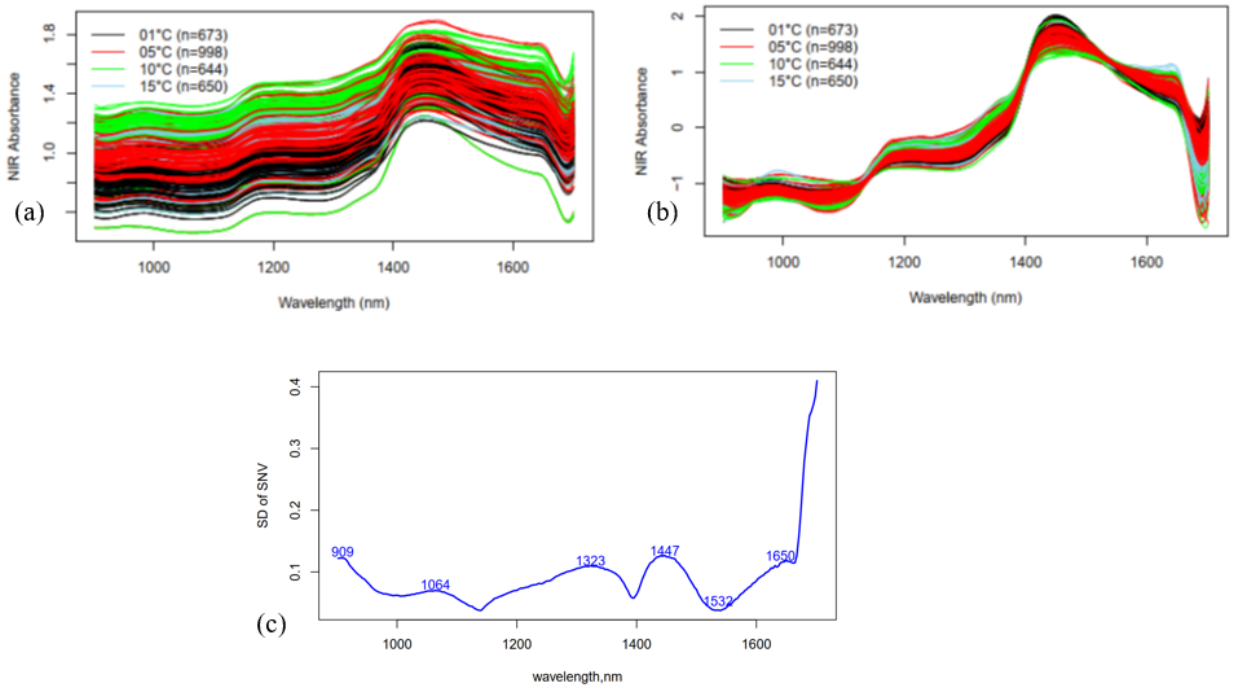

Figure 27: Full NIR raw spectra (a), Normalized spectra by SNV (b), and the standard deviation (b) of the normalized spectra (c)

The two-way ANOVA for plum NDI_1532 and QI (Table 14) shows that NDI_1532 is more sensitive to temperature across all wavelengths, with higher F-values compared to QI. While both parameters are significantly affected by time, NDI_1532 shows greater sensitivity at longer wavelengths (1447 and 1650 nm), reflecting its ability to capture structural changes over time. Shorter wavelengths like 909 nm and 1064 nm exhibit consistent responses for both indices, but the

effects are greater at longer wavelengths. NDI_1532 is more influenced by cultivar differences, especially at 1447 nm and 1650 nm, while QI is unaffected by cultivar variations. These findings suggest that NDI_1532 is more suitable for structural assessment, while QI is better for biochemical quality monitoring.

Table 14: Effects of storage time, temperature, cultivar, and their interactions on NDI_1532 and QI indices across selected wavelengths (N = 2994)

Parameters	Factor	909 nm	1064 nm	1323 nm	1447 nm	1650 nm
Plum NDI	Time (A)	114.874[s]	112.518[s]	93.052[s]	167.692[s]	251.372[s]
	Temperature (B)	25231.130[s]	25347.471[s]	25107.612[s]	16536.74[s]	21561.623[s]
	Cultivar (C)	2.792	0.321	2.371	55.71[s]	37.745[s]
	A × B	12168.716s	12099.964[s]	12341.622[s]	8719.549[s]	11202.127[s]
	A × C	0.235	0.144	2.522		0.073
	B × C	54.225[s]	53.622[s]	38.065[a]	18.812[a]	40.114[s]
	A × B × C	6.505[s]	6.574[s]	8.628[a]	5.865[s]	7.911[s]
Plum QI	Time (A)	5343.298[s]	5470.481[s]	5394.634[s]	4815.256[s]	5266.945[s]
	Temperature (B)	4.821	5.997[s]	5.743[s]	8.972[s]	6.01[s]
	Cultivar (C)	0.103	0.252	0.014	0.734	0.13
	A × B	2335.702[s]	2362.81[s]	2382.915[a]	2073.68[s]	2394.11[s]
	A × C	250.616[s]	243.783[s]	255.313[a]	241.384[a]	261.289[s]
	B × C	6.495[s]	6.445[s]	5.986[s]	8.188[s]	6.217[s]
	A × B × C	223.425[s]	229.678[s]	231.384[s]	205.436[s]	230.844[s]

's' $p < 0.001$

Pearson's correlation analysis (Table 15) showed significant relationships between NIR absorbance at selected wavelengths, weight loss (WL), and soluble solids content (SSC) ($p < 0.001$). Shorter wavelengths (909, 1064, 1323 nm) were strongly positively correlated with each other and with 1650 nm, while 1447 nm showed a strong negative correlation with these wavelengths. SSC correlated positively with WL ($r = 0.868$) and with absorbances at 1650 nm ($r = 0.803$), 1323 nm ($r = 0.741$), 1064 nm ($r = 0.681$), and 909 nm ($r = 0.647$), indicating sugar accumulation during ripening. In contrast, SSC was negatively correlated with 1447 nm ($r = -0.734$), reflecting sensitivity to structural changes and water loss in fruit cells. Similarly, WL showed strong positive correlation with 1650 nm ($r = 0.822$) and negative correlation with 1447 nm ($r = -0.755$), highlighting moisture loss and cell wall degradation during maturation. These results align with previous reports demonstrating that NIR absorbances reflect fruit water content, sugar accumulation, and ripening-induced structural changes (Cen and He, 2007; Walsh et al., 2020).

Table 15. Pearson's correlation values among parameters (N = 2964)

	SNV normalized NIR readings					SSC	WL
	909 nm	1064nm	1323 nm	1447 nm	1650 nm		
909 nm		0.974	0.966	-0.915	0.930	0.647	0.693
1064 nm	s		0.984	-0.943	0.956	0.681	0.715
1323 nm	s	s		-0.962	0.978	0.741	0.757
1447 nm	s	s	s		-0.962	-0.734	-0.755
1650 nm	s	s	s	s		0.803	0.822
SSC, %	s	s	s	s	s		0.868
WL, %	s	s	s	s	s	s	

NB: Upper triangle shows the correlation values, while the bottom triangle shows the significance level. 's' $p <$ 0.001

Prediction of WL and SSC

Fig. 28 compares the performance of SVM models in predicting SSC and WL of 'Stanley' and 'Elena' plums using full NIR spectra versus selected wavelengths, with PLSR and SVM metrics summarized in Table 16. For SSC, PLSR improved from $R^2 = 0.661$, RMSE = 1.130%, RPD = 1.717 (full spectra) to $R^2 = 0.747$, RMSE = 0.981%, RPD = 1.991 (selected wavelengths). For WL, PLSR improved from $R^2 = 0.676$, RMSE = 1.768%, RPD = 1.758 to $R^2 = 0.738$, RMSE = 1.582%, RPD = 1.954. The SVM model outperformed PLSR, with SSC prediction reaching $R^2 = 0.844$, RMSE = 0.781%, RPD = 2.499 and WL prediction $R^2 = 0.917$, RMSE = 0.884%, RPD = 3.492 using selected wavelengths. This demonstrates that SVM combined with feature selection provides superior accuracy for estimating SSC and WL in plums.

Table 16: Cross-validation performance metrics of SVM and PLSR models for predicting SSC and WL using full NIR spectra and spectra at selected wavelengths (n=2964)

Category	Model	R^2			RMSE			RPD		
		Mean	CI95min	CI95max	Mean	CI95min	CI95max	Mean	CI95min	CI95max
Full spectra	SSC PLSR	0.661	0.657	0.665	1.130	1.119	1.140	1.717	1.706	1.728
	WL PLSR	0.676	0.672	0.680	1.768	1.751	1.785	1.758	1.746	1.769
	SSC SVM	0.720	0.716	0.725	1.052	1.040	1.064	1.857	1.843	1.871
	WL SVM	0.727	0.722	0.731	1.648	1.627	1.670	1.869	1.853	1.886
Selected wavelengths	SSC PLSR	0.747	0.741	0.752	0.981	0.967	0.994	1.991	1.969	2.013
	WL PLSR	0.738	0.734	0.742	1.582	1.565	1.599	1.954	1.938	1.969
	SSC SVM	0.844	0.840	0.848	0.781	0.768	0.794	2.499	2.463	2.535
	WL SVM	0.917	0.916	0.919	0.884	0.876	0.894	3.492	3.459	3.526

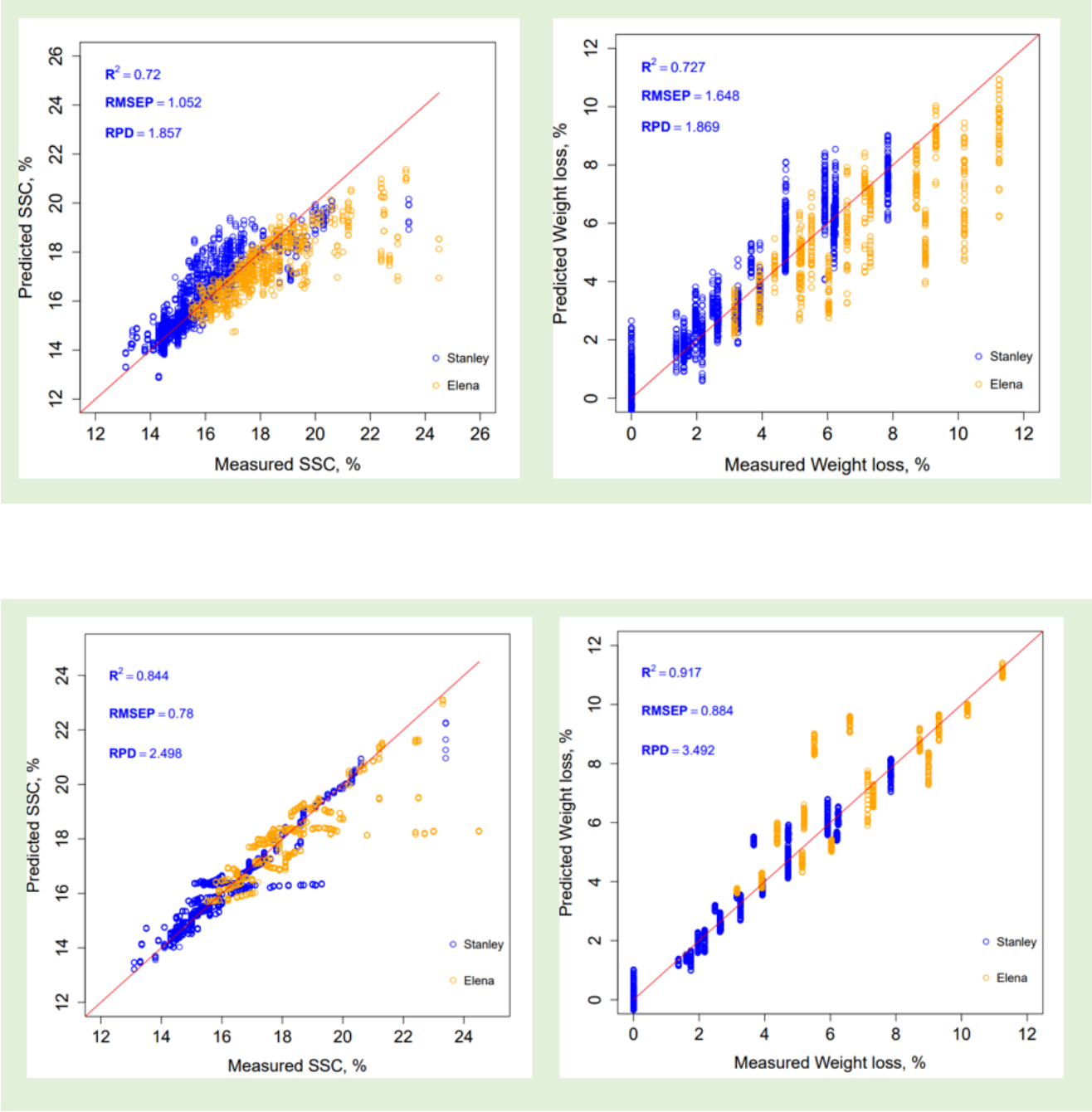

Figure 28: SVM prediction results for SSC (left) and WL (right) using full NIR spectra (top) and selected wavelengths (bottom).

The SVM model performance observed in this study aligns with previous reports (Table 17). For SSC prediction, Costa and Lima (2013) achieved $R^2 = 0.817$ for the 'Angeleno' plum, while a

combined PLSR model across nine cultivars reached $R^2 = 0.720$, RMSEP = 0.860. Golic and Walsh (2006) reported multi-variety PLSR models with $R^2 > 0.85$ for plums. SSC prediction in 'Bergarouge' apricots using PLSR reached $R^2 = 0.96$, RMSEP = 1.0% (Camps and Christen, 2009), and Carlini et al. (2000) predicted SSC in 'Ravenna' cherries with $R^2 = 0.97$, RMSEP = 0.490% using 600–1100 nm spectral data. Moreover, a PLS-SVM model predicted pear firmness with $R^2 = 0.893$, RMSEP = 0.476 (Li et al., 2013), confirming the effectiveness of SVM-based approaches for fruit quality assessment.

Table 17. Performance of SSC prediction of plums in single and multi-cultivar models.

Plum cultivar	LV	Model	R^2	RMSEP	Reference
Pioneer	10	PLSR	0.959	0.520	(Costa and Lima, 2013)
Pioneer, Laetitia, and Angeleno	12		0.946	0.610	
Laetitia	10		0.905	0.453	
Angeleno	10		0.817	0.569	
African Pride, Black Diamond, Fortune, Laetitia, Larry Anne, Late Royal, Prime Time, Sapphire, and Songold	n.a.	PLSR	0.720	0.860	(Paz et al., 2008)
Black Diamond, Golden Globe, Golden Japan, Fortune, Friar, and Santa Rosa	n.a.	PLSR	0.68	1.22	(Pérez-Marín et al., 2010)
Plums	5	PLSR	0.66	1.13	*

n.a. – information is not available ; '*' -current study

In this study, both SVM and PLSR models using the spectra at selected wavelengths for WL and SSC showed performance comparable to the results reported in the literature for multi-cultivar models. For example, for SSC, multi-cultivar models established with full spectra showed results like those observed in previous studies by Paz et al. (2008) and Pérez-Marín et al. (2010) (Table 17). The promising performance of the presented models confirms the effectiveness of wavelength selection and highlights the usability of the multi-spectral NIR technique for postharvest quality assessment of plums.

6.2.8 Laser Back Scattering Imaging

Description of backscattering profiles

Fig. 29 shows sample images illustrating the change in diffuse reflectance of 'Elena' plums at different storage conditions across all wavelengths. The light attenuation varied by wavelength both before and after storage. Before storage, the diffusively illuminated surface areas were marked with green circles. After storage, the images were marked with orange (1 °C) and red (15 °C) circles. Higher light attenuation was observed in plums stored at higher temperatures. This could be due to the increased enzymatic activity at higher temperatures, leading to increased SSC and degraded pigments, which affect the light absorption properties.

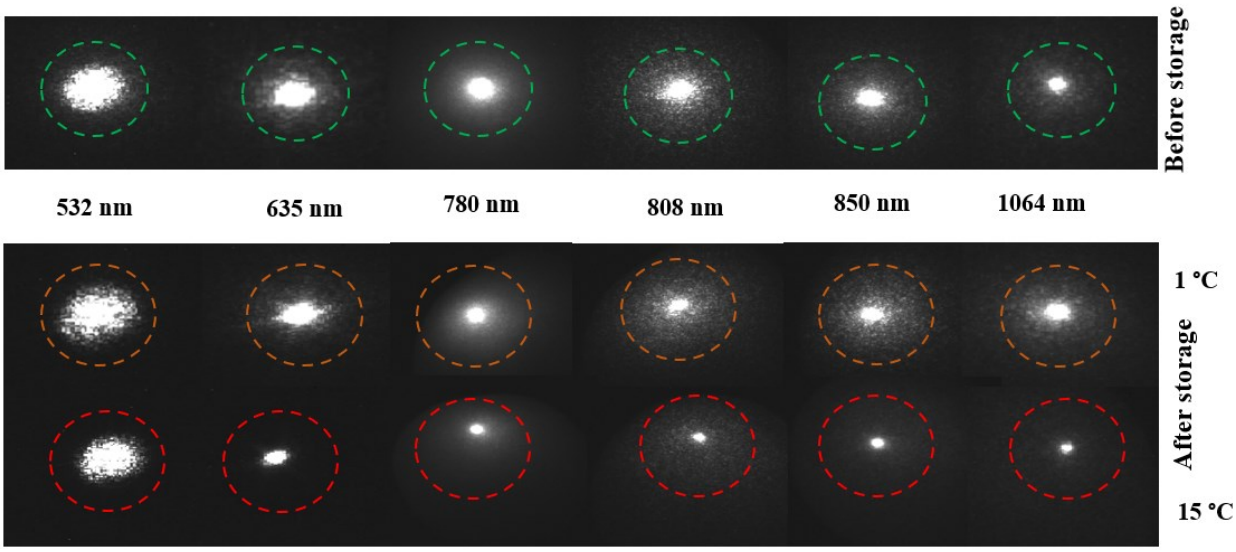

Figure 29: Changes of diffuse reflectance of 'Elena' plums under different storage conditions at all wavelengths.

Selection of sensitive wavelengths

Fig. 30 shows changes in amplitude and shape values across six wavelengths, with a significant impact of wavelength on both metrics, as confirmed by a one-way ANOVA ($F = 623.86$ for amplitude, $F = 2321.50$ for shape, $p < 0.001$, $n = 7825$).The amplitude values derived from the Cauchy distribution fitting of the LLBI backscatter profiles exhibited their highest values at 532 nm, with a gradual decrease observed across longer wavelengths (780–1064 nm). This trend likely reflects higher scattering efficiency and detector sensitivity at shorter wavelengths. In contrast, the shape parameter reached its minimum at 635 nm and showed an increasing trend in the 780–850 nm range, suggesting a wavelength-dependent variation in the spectral width or distribution of the

backscattered signal. These observations suggest the importance of 532 nm and 780 nm as potential wavelengths for monitoring plum quality during postharvest storage. , the change at these wavelengths correlate with firmness, soluble solids content (SSC), and color changes, agrees with literature indicating 532 nm is useful for evaluating skin color (Chen, 2015;Rezaei Kalaj et al., 2016) and 780 nm for assessing firmness and SSC (Baranyai and Zude, 2009; Romano et al., 2011; Hashim et al, 2014).

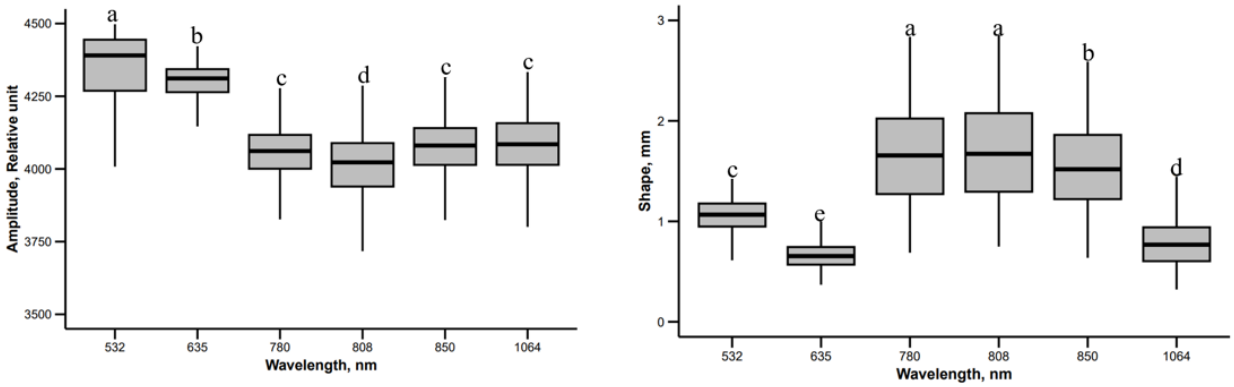

Figure 30: Change of the amplitude (left) and shape (right) values across different wavelengths during postharvest storage. Different letters on top of the boxes indicate significant differences (Tukey's post-hoc test, $p < 0.05$).

Fig. 31 compares the performance of the Gaussian and Cauchy distribution models for fitting LLBI profiles of plums at 532 nm and 780 nm. The modified Cauchy distribution (CD) with amplitude and shape of profile parameters demonstrated relatively better predictive power, achieving average values of R^2 above 0.96 and RPD above 4.5, in comparison to the Gaussian distribution, which achieved average R^2 below 0.70 and RPD below 4.5. Excluding top and bottom 5% of the intensity range led to a decline in both models' performance (Fig. 32 right), but the Cauchy model still performed better. Thus, LLBI parameters derived from the fully fitted Cauchy distribution at 532 nm and 780 nm were used for further analysis.

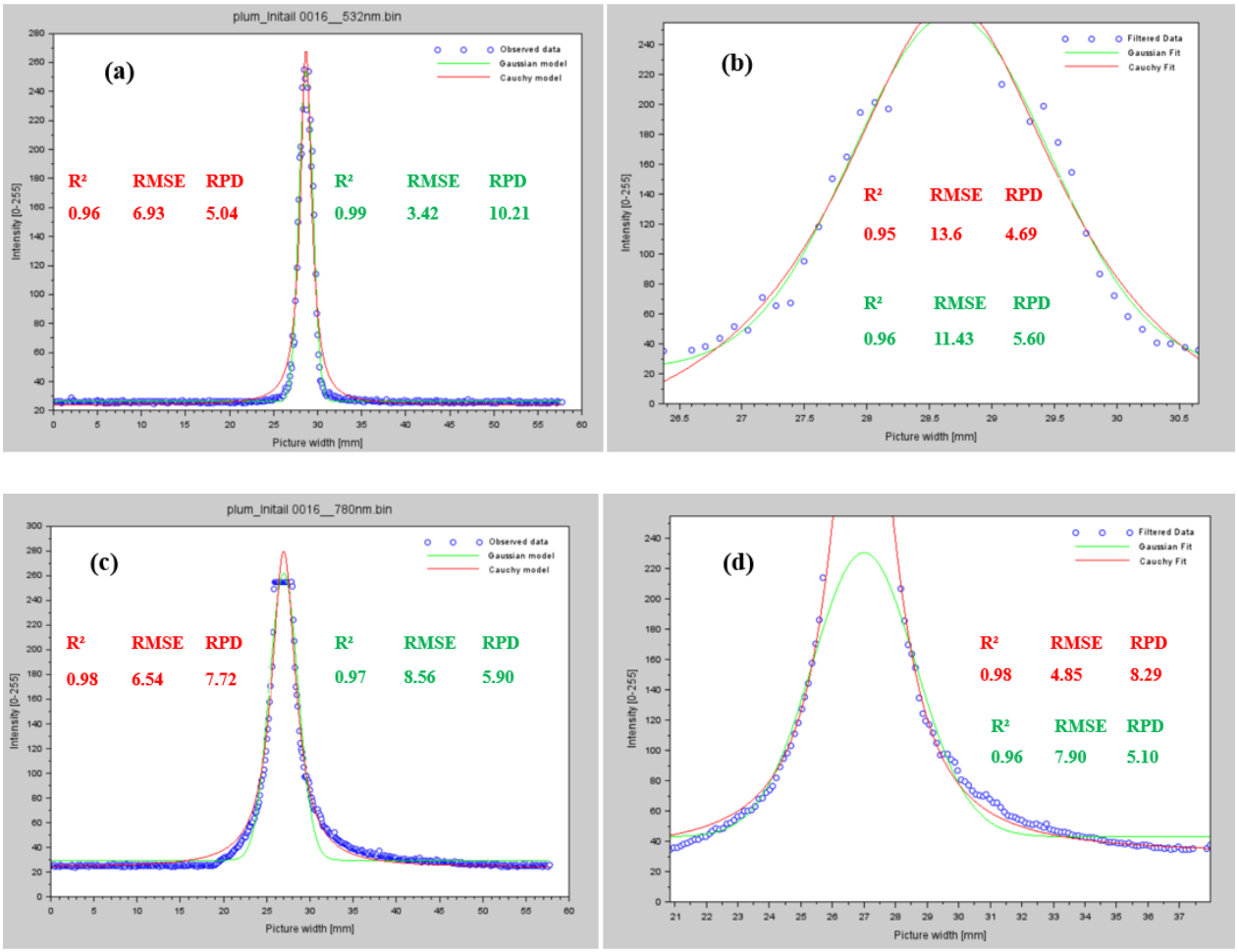

Figure 31: Sample curve fittings of GD (Gaussian Distribution) and CD (Cauchy Distribution) functions for the full (left) and partial (right) scattering profile of plum samples at 532 nm (top) and 780 nm (bottom).

The two-way ANOVA revealed that storage time, temperature, and cultivar type significantly affected amplitude and shape values in LLBI profiles (Table 18), with stronger effects observed at 780 nm than at 532 nm. The deeper tissue penetration of 780 nm made it more sensitive to internal structural changes like moisture loss and tissue softening, while 532 nm was more responsive to surface-level properties, including texture and pigmentation (Romano et al., 2012; Rezaei Kalaj et al., 2016). As storage time increased, these changes amplified the amplitude sensitivity, with stronger interaction effects at 532 nm, especially for surface properties, leading to hue shifts to red

and purple tones. The amplitude variation at 532 nm is likely due to changes in anthocyanin content, which affects light scattering as the fruit ripens, with cultivar-specific surface attributes influencing the results (Rezaei Kalaj et al., 2016). Studies have also shown that carotenoids, identifiable in the green/yellow regions, correlate with hyperspectral absorbance data (Falcioni et al., 2023). The sharper LLBI profile peaks observed during fruit ripening result from changes in the fruit's internal structure and composition (Mozaffari et al., 2022; Rezaei Kalaj et al., 2016). As fruits ripen, cell wall breakdown and softening create air spaces, leading to sharper peaks. Additionally, changes in pigments (such as reduced chlorophyll and increased anthocyanins or carotenoids) affect light absorption and scattering (Rezaei Kalaj et al., 2016). Water loss and structural modifications further enhance light scattering, contributing to the sharper LLBI peaks (Romano et al., 2008).

Table 18: F- value of two-way ANOVA results of the measured parameters (n=1276).

Factor	**Amplitude**		**Shape**	
	532 nm	**780 nm**	**532 nm**	**780 nm**
Storage time (A)	370.80^{s}	263.63^{s}	650.93^{s}	587.51^{s}
Storage temperature (B)	46.17^{s}	71.75^{s}	160.06^{s}	93.89^{s}
Cultivar (C)	465.16^{s}	9.80^{s}	412.30^{s}	2611.99^{s}
Interaction(A×B)	29.79^{s}	20.95^{s}	39.96^{s}	19.89^{s}
Interaction (A×C)	277.71^{s}	60.11^{s}	171.69^{s}	140.81^{s}
Interaction (B×C)	28.16^{s}	3.23	8.20^{s}	15.93^{s}

NB: "s", $p < 0.001$

The Pearson correlation analysis (Table 19) also supports the results of ANOVA. There is strong correlation between amplitude and shape coefficients at 532 nm (r = 0.787). The amplitude at 780 nm showed positive correlation with firmness (r = 0.607) and chroma (r = 0.661), but a negative one with SSC (r = -0.609), suggesting that increased SSC increase absorption and decrease peak intensity. The shape at 532 nm was highly correlated with chroma (r = 0.748) and firmness (r = 0.600). Shape at 780 nm was most strongly associated with firmness (r = 0.720) and chroma (r = 0.670) and was inversely associated with SSC (r = -0.570). Correlations meet expectations that plums with higher firmness have lower SSC and higher chromaticity. Previous studies have also reported that photon scattering is influenced by the density of tissue structure (Romano et al., 2011; Hashim et al., 2014). Although significant correlation was found between the huge angle and selected coefficients, this parameter obtained the lowest values. The observed difference between coefficients of 532 nm and 780 nm might be attributed to the rough surface.

Table 19: Pearson's correlation between variables (n=1276)

	Amplitude		Shape, mm					
Variables	532nm	780nm	532nm	780nm	Firmness, N	SSC, %	Chroma	Hue, degree
Amplitude (532nm)		0.680	0.787	0.239	0.434	-0.498	0.541	-0.102
Amplitude(780nm)	s		0.859	0.355	0.607	-0.609	0.661	0.419
Shape(532nm)	s	s		0.451	0.600	-0.604	0.748	0.229
Shape(780nm)	s	s	s		0.720	-0.570	0.670	0.256
Firmness, N	s	s	s	s		-0.824	0.817	0.351
SSC, %	s	s	s	s	s		-0.858	-0.377
Chroma	s	s	s	s	s	s		0.375
Hue, degree	s	s	s	s	s	s	s	

NB: correlation values are above the diagonal, while significance indicators are below (s', $p < 0.05$)

Classification of sample groups

Linear Discriminant Analysis (LDA) models using four LLBI parameters at 532 nm and 780 nm detected storage time-related quality changes in 'Stanley' and 'Elena' plums. Using all temperature groups, accuracy was 61.3% for 'Stanley' and 77.3% for 'Elena' (Fig. 32). When calibrated for individual temperatures, accuracy increased to 92.3% for 'Stanley' and 91.9% for 'Elena' at 1 °C and reached 100% for both cultivars at 5 °C (Appendix Fig. 12.1.7). These results demonstrate that LLBI effectively captures cumulative structural and compositional changes during storage. Previous studies reported similar trends: mid- to late-ripening stages in fruits like apples and watermelons show pronounced structural changes, enabling precise classification (Romano et al., 2011; Mohd Ali et al., 2017). Zulkifli et al. (2019) classified banana ripeness using LLBI at 658 nm and LDA with 94.2% accuracy, while Lorente et al. (2015) classified orange quality at 532 nm with 93.4% accuracy.

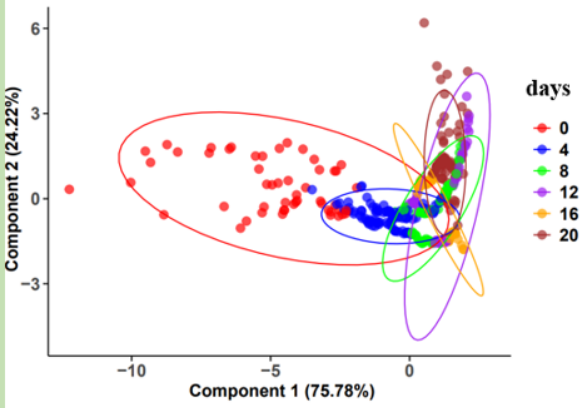

Training set (n= 455), average accuracy = 65.1%

	0d	4d	8d	12d	16d	20d
0d	72.55	27.45	0	0	0	0
4d	1.69	80.51	17.80	0	0	0
8d	0	23.76	65.35	0.99	0	9.90
12d	0	0	41.33	17.33	14.67	26.67
16d	0	0	28	0	58	14
20d	0	0	0	0	3.33	96.67

Validation set (n= 114), average accuracy= 61.3%

0d	88.89	11.11	0	0	0	0
4d	0	91.67	8.33	0	0	0
8d	0	36.67	46.67	10.00	0	6.67
12d	0	17.65	41.18	29.41	0	11.76
16d	0	0	71.43	0	21.43	7.14
20d	0	0	10.00	0	0	90.00

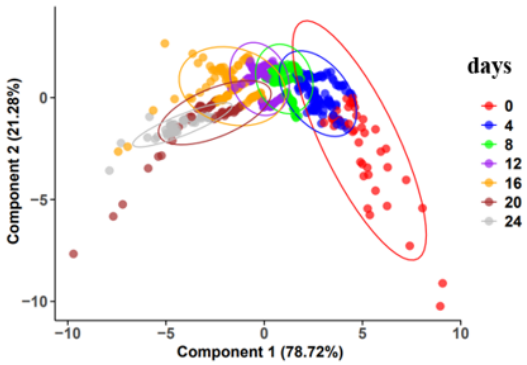

Training set (n= 566), average accuracy =79.5%

	0d	4d	8d	12d	16d	20d	24d
0d	61.36	38.64	0	0	0	0	0
4d	1.19	89.29	9.52	0	0	0	0
8d	0	4.72	87.74	7.55	0	0	0
12d	0	0	14.16	77.88	7.96	0	0
16d	0	0	0	20.83	75	0	4.17
20d	0	0	0	3.90	5.19	77.92	12.99
24d	0	0	0	0	0	21.74	78.26

Validation set (n=141), average accuracy= 77.3%

0d	62.5	37.5	0	0	0	0	0
4d	0	72.73	27.27	0	0	0	0
8d	0	4	88	8	0	0	0
12d	0	0	17.39	78.26	4.35	0	0
16d	0	0	0	27.27	72.73	0	0
20d	0	0	0	0	0	80	20
24d	0	0	0	0	0	8.33	91.67

Figure 32: LDA plot on training set and the confusion matrix for storage time groups of 'Stanley' (top) and 'Elena' (bottom) plums.

Prediction of quality parameters

The regression plots (Fig. 33) and validation results (Table 20) show the performance of MVR models calibrated using both two-cultivar and cultivar-specific datasets. Two LLBI parameters at 532 nm and 780 nm were used to estimate firmness, soluble solids content (SSC), chroma, and hue. For firmness, the two-cultivar model achieved R^2 = 0.632, RMSE = 3.924 N, and RPD = 1.653,

while cultivar-specific models performed better: 'Stanley' (R^2 = 0.769, RMSE = 3.049 N, RPD = 2.084) and 'Elena' (R^2 = 0.726, RMSE = 3.375 N, RPD = 1.932). The Durbin-Watson test indicated autocorrelation (DW = 0.344, p < 2.2e-16). Previous studies reported by Qing et al. (2007b) showed apple firmness predicted across multiple cultivars with R^2 = 0.81, Li et al. (2018) reported firmness prediction for 'Victoria' plums with R^2 = 0.73 and RPD = 1.90, and Mohd Ali et al. (2017) achieved R^2 = 0.882 for watermelon firmness using PLSR. Similarly, Lu (2004) and Qing et al. (2008) reported R^2 ≈ 0.87 for apple firmness prediction using light backscattering and PLSR.

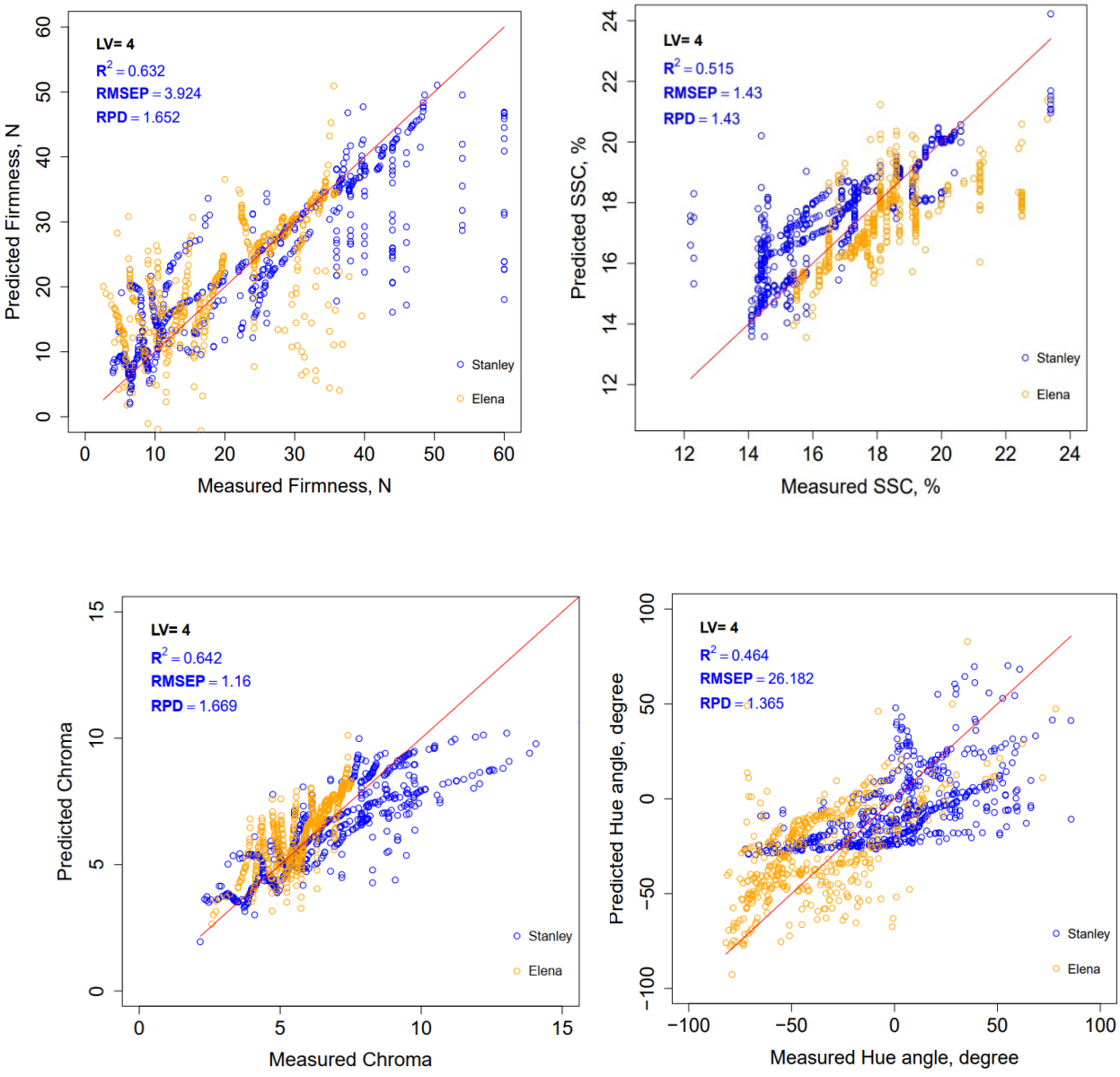

Figure 33: MVR Prediction of firmness (top-left), SSC (top-right), chroma (bottom-left) and hue angle (bottom-right).

Similar pattern was observed for SSC with higher accuracy of cultivar specific models for 'Elena' (R^2 = 0.818, RMSE = 0.873%, RPD = 2.366) and 'Stanley' (R^2 = 0.769, RMSE = 0.983, RPD = 2.117). All quality indices confirmed this pattern. Cultivars achieved close performance indices, but hue angle showed the largest difference. This might reflect the different color development of the cultivars involved. Qing et al. (2007b) reported that LLBI achieved an R^2 of 0.79 for SSC prediction in 'Elstar' apples using PLSR, while Qing et al. (2008) found an R^2 of 0.88 for SSC prediction in 'Pinova' apples. Additionally, Li et al. (2018) demonstrated that SWIR hyperspectral imaging in the wavelength range of 865–1610 nm effectively predicted SSC in 'Victoria' and 'Marjorie's Seedling' plums. The PLSR model achieved an R^2 value of above 0.8. On the other hand, the MVR model was effective in cultivar-specific models compared to multi-cultivar models for color parameter predictions. The model predicted chroma for 'Elena' with an R^2 of 0.866 and hue with an R^2 of 0.731 for 'Stanley' (Table 20). Similar studies, such as Noh and Lu (2007), reported predicting apple skin hue using LLBI with an R^2 of 0.88, while Udomkun et al. (2014) achieved an R^2 of 0.92 for predicting dried papaya color using MVR. Li et al. (2018) demonstrated that hyperspectral imaging in the 600–975 nm range with PLSR could predict plum color with R^2 values above 0.7 and RMSE below 3.16

Table 20: Cross validation performance metrics of MVR model 'Stanley' (n=114) and 'Elena' (n=141) and all samples together (n=255)

Variable	Cultivar	R^2			RMSE			RPD		
		Mean	CI95Min	CI95Max	Mean	CI95Min	CI95Max	Mean	CI95Min	CI95Max
Firmness, N	All	0.632	0.624	0.640	3.924	3.875	3.974	1.653	1.635	1.671
	Stanley	0.769	0.753	0.786	3.049	2.900	3.198	2.084	2.011	2.157
	Elena	0.726	0.714	0.738	3.375	3.308	3.443	1.932	1.889	1.974
SSC, %	All	0.515	0.507	0.523	1.431	1.417	1.445	1.436	1.424	1.448
	Stanley	0.769	0.757	0.781	0.983	0.954	1.013	2.117	2.056	2.179
	Elena	0.818	0.810	0.826	0.873	0.853	0.893	2.366	2.314	2.418
Chroma	All	0.642	0.636	0.649	1.160	1.146	1.175	1.669	1.654	1.685
	Stanley	0.835	0.826	0.844	0.883	0.859	0.907	2.498	2.429	2.567
	Elena	0.866	0.858	0.873	0.634	0.614	0.655	2.766	2.694	2.838
Hue, degree	All	0.465	0.457	0.473	26.183	25.955	26.411	1.366	1.356	1.376
	Stanley	0.731	0.722	0.740	16.623	16.384	16.863	1.933	1.902	1.965
	Elena	0.521	0.510	0.533	23.073	22.775	23.371	1.442	1.425	1.460

6.3. Assessment of quality changes of apples during post-harvest storage

This section also discusses the results of physiological measurement, NIR spectroscopy, and LLBI techniques applied to assess quality attributes of 'Granny smith' apples stored under different temperature conditions. In NIR spectroscopy analysis, a total of 834 observations were made by acquiring spectral data from two locations around equatorial part of each apple using three consecutive scans per location. The apples were rotated 180 degrees between scans to ensure full surface coverage. Spectral data in the 900–1700 nm range were preprocessed using SNV, and five significant wavelengths were manually selected based on the standard deviation of the normalized spectra. NDI and QI were computed to assess the sensitivity of selected wavelengths. PLSR and SVM models were developed using the R packages 'pls' (version 2.8-2) and 'e1071' (version 1.7-13), respectively. These models were calibrated using both full spectra and selected wavelengths to predict weight loss, firmness, and SSC. For LLBI, 643 observations were collected using both line-based (n = 382) and beam-based (n = 261) systems. LLBI images were captured at 635 nm, and the resulting profiles were fitted using the Cauchy Distribution model to extract amplitude and shape parameters. These parameters were used to develop MVR and SVM models for predicting weight loss and firmness. All datasets were randomly divided into training (80%) and validation (20%) subsets. Model performance was evaluated using bootstrapped metrics (R^2, RMSE, RPD) with 95% confidence intervals.

6.3.1 Ethylene production

The ethylene production rate in apples varied with storage temperature and time (Fig. 34). Apples stored in cold storage and then exposed to room temperature showed an increasing trend in ethylene production, while those stored at room temperature initially increased and then declined after 2 weeks. By the end of the storage period, apples in shelf-life conditions produced around 50 µL/ Kg.h, while those stored at room temperature had a final rate of 25 µL/ Kg.h. ANOVA indicated significant effects of storage temperature and time on ethylene production ($F = 171.985$ and 111.961; $p < 0.001$). Cold storage inhibits ethylene production but enhances the peel's ethylene-forming capacity, whereas warmer temperatures accelerate ripening and ethylene production. These findings align with previous studies showing that ethylene production in apples follows a climacteric pattern, with an initial increase, a peak, and a decline (Rudell et al., 2000; Wang et al., 2022).

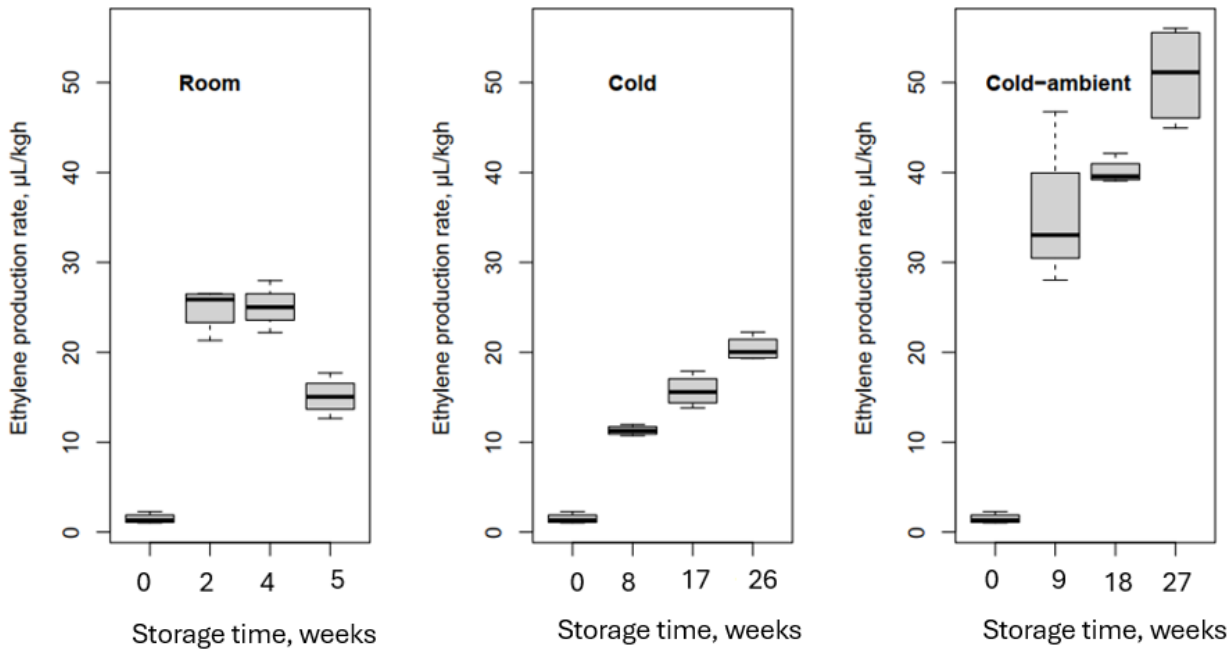

Figure 34: Ethylene production rate of 'Granny Smith' apples under different storage time and temperature

6.3.2 Respiration Rate

The respiration rate in apples followed a similar pattern to ethylene production. Apples stored in cold storage and then exposed to room temperature showed an increasing respiration rate over time, while those stored continuously at room temperature increased initially and then declined (Fig. 35). ANOVA indicated significant effects of storage temperature and time on respiration ($F = 83.665$ and 49.668; $p < 0.001$). The highest respiration rate was observed in apples subjected to cold storage followed by room temperature shelf life, peaking at 18.50 mL/ Kg.h. Apples stored at cold temperatures had lower respiration (11.88 mL/ Kg.h), while those stored at room temperature peaked at 6.20 mL/ Kg.h after two weeks before declining. This pattern aligns with the climacteric nature of apples, where respiration increases, peaks, and then declines as the fruit ripens (Singh and Khan, 2010; Choi and Jung, 2014; Løkke et al., 2011).

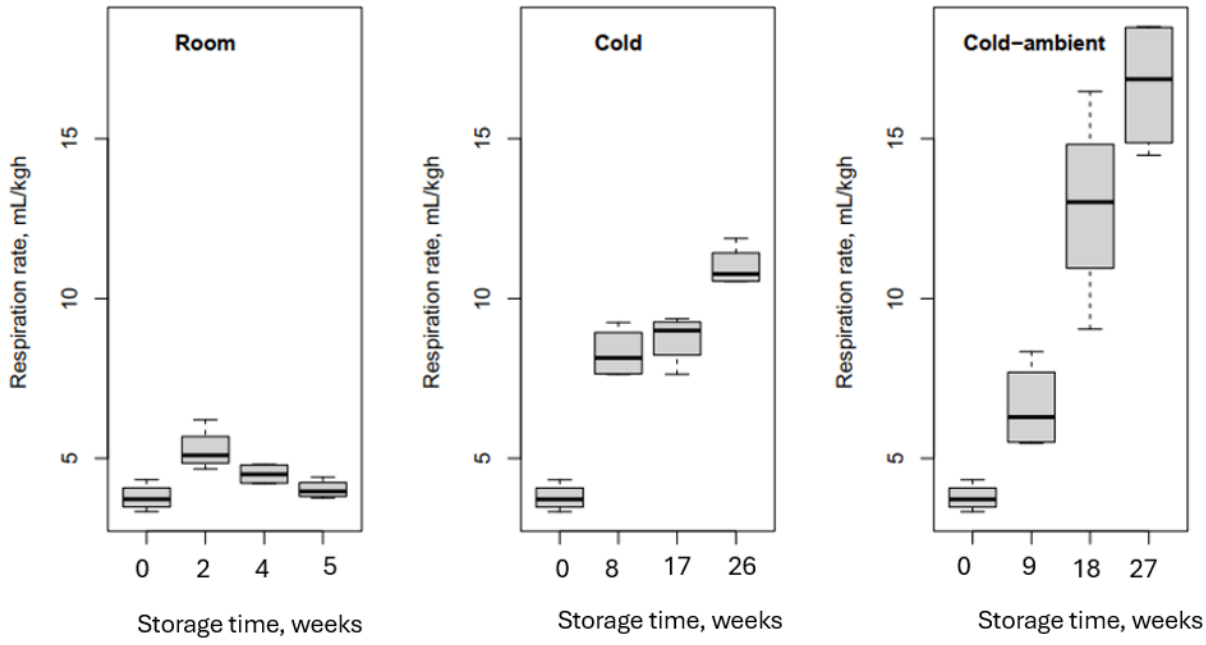

Figure 35: Respiration rate of 'Granny Smith' apples under different storage time and temperature

6.3.3 Weight loss

The weight loss of apples during storage increased over time (Fig. 36), with apples stored at cold temperatures showing lower weight loss than those stored at room temperature. ANOVA confirmed significant effects of storage time and temperature on weight loss (F-value = 571.58 and 216.57; $p < 0.001$). Higher temperatures accelerate respiration and water loss, leading to faster weight loss, while lower temperatures slow respiration and preserve freshness. Previous studies have shown that higher temperatures increase respiration and water loss, and accelerate weight loss (Guerra & Casquero, 2008; Singh and Khan, 2010). Cold storage helps to control microbial deterioration and preserves fruit (Zhao et al., 2022). However, moving apples from cold storage to room temperature further accelerates water loss (Kassebi et al., 2022; Hasan et al., 2024). During this transition, apples may experience temperature shock. The sudden temperature change leads to internal condensation and increases water activity inside the fruit, creating an environment where the fruit becomes more vulnerable to mechanical stress, including vibrations. Additionally, this temperature shift softens the fruit, making it more susceptible to physical damage (Wei et al., 2019; Fang and Wakisaka, 2021).

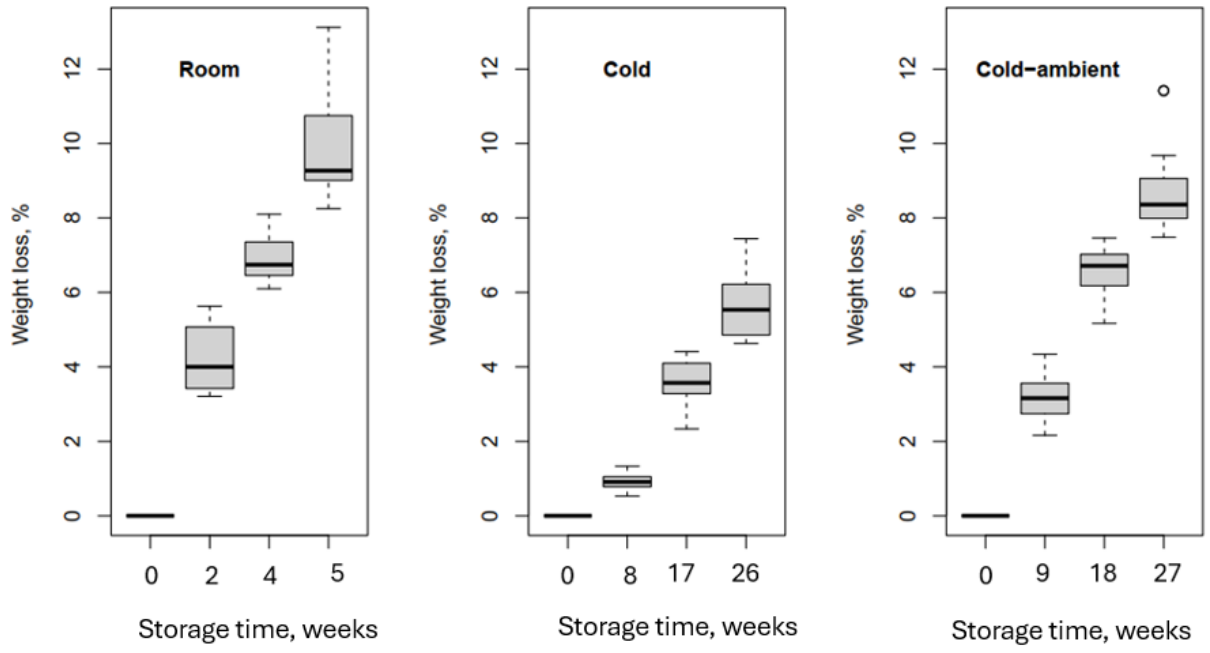

Figure 36: Change of weight loss of 'Granny Smith' apple at different storage time and temperature.

6.3.4 Firmness

The firmness of apples decreased over time in both cold storage and cold-to-ambient storage conditions (Fig. 37). Apples stored under cold-to-ambient conditions showed a faster reduction in firmness compared to those stored solely at ambient temperatures. ANOVA revealed that both storage time and temperature significantly affected firmness (F-value = 1469.8 and 2561.2, respectively; $p < 0.001$), with temperature having a more substantial impact. This may be due to temperature-induced changes in cellular structure, such as cell wall breakage and pectin degradation. Previous studies suggest that cold-to-ambient storage accelerates ethylene production and respiration rates, hastening ripening (Matabura, 2022). Metabolic changes during ripening lead to cell wall breakdown and tissue softening (Johnston et al., 2001; Geng et al., 2020). In addition, Singh, et al. (2011) reported that prolonged storage can alter the expression of ethylene-related genes, leading to increased ethylene production and a reduction in firmness as apples ripen.

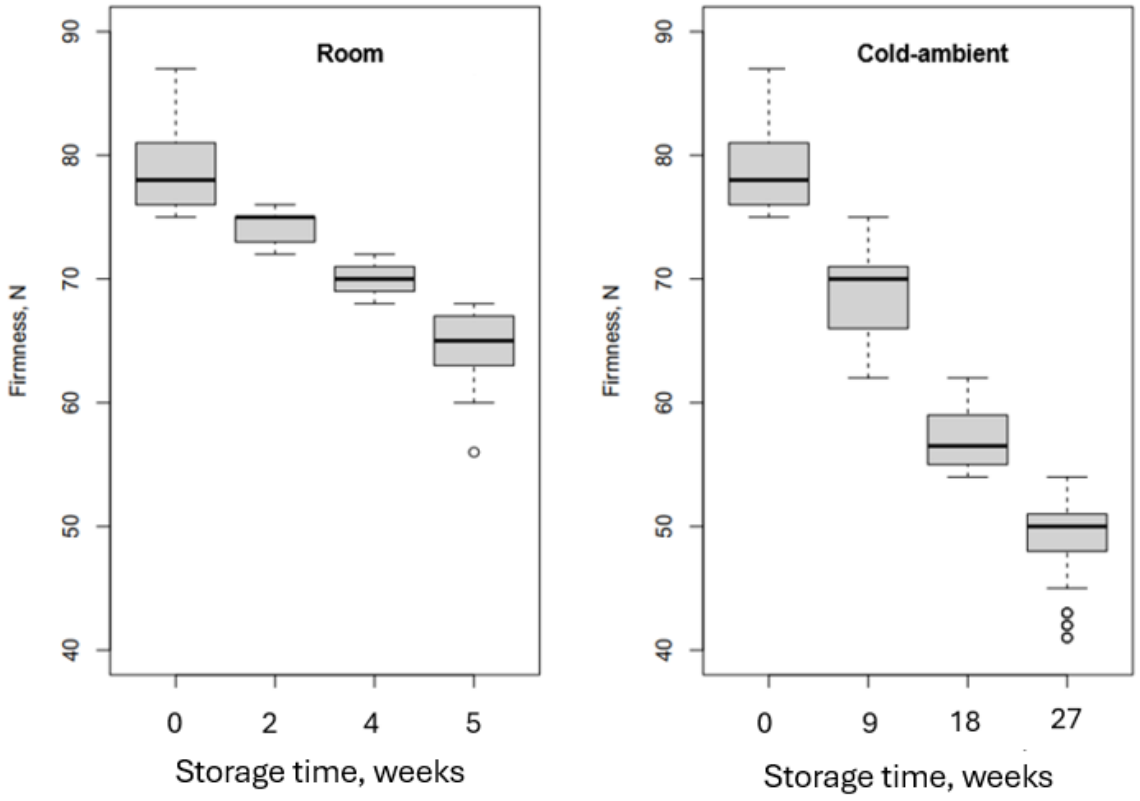

Figure 37: Change of Firmness of 'Granny Smith' apple at different storage time and temperature

6.3.5 Soluble solid content (SSC)

The SSC of the apples increased over time and with rising temperatures (Fig. 38). ANOVA revealed that the effects of storage time and temperature were significant (F-value = 354.3 and 16.8, respectively; $p < 0.001$). The increase in SSC is primarily due to the conversion of starch into sugars during ripening. This process is supported by findings by Jha et al.(2012), who noted that SSC in apples undergoes cyclic changes: initially decreasing as sugars convert to starch, followed by an increase as starch is reconverted into sugars during prolonged storage. In cold storage, the conversion of starches to sugars is slowed, and the respiration rate and ethylene production remain low. However, when apples are moved to ambient temperature, these processes accelerate, rapidly increasing SSC. Therefore, temperature and storage duration can significantly influence sugar accumulation in apples, thereby affecting SSC (Cao et al., 2021; Tokala et al., 2022).

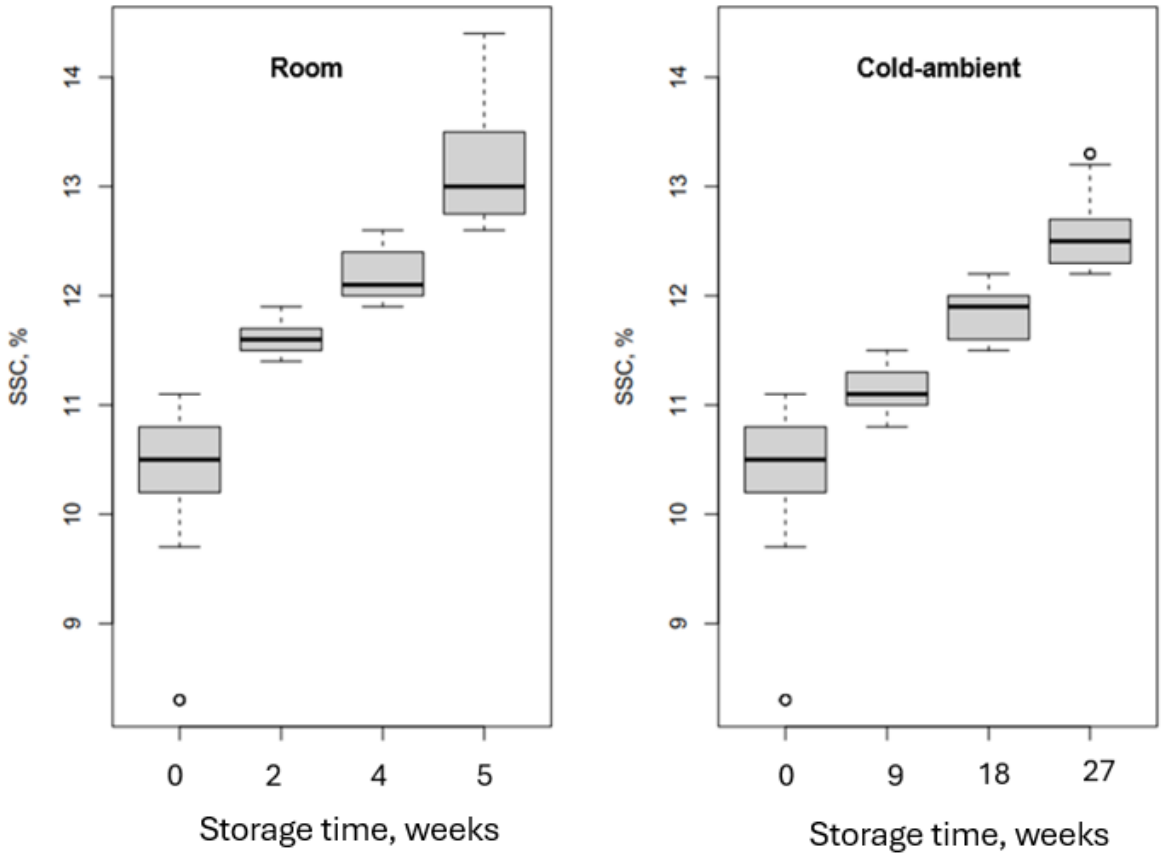

Figure 38: Change of SSC of 'Granny Smith' apple at different storage time and temperature

6.3.6 Peel color

The hue spectra of 'Granny Smith' apples were measured using machine vision, with four apples per image and nine images per temperature group. The average hue spectra values for each temperature group across the storage period are shown in Fig.39. The first plot captures the initial ripening phase of apples over 0, 2, 4, and 5 weeks. The RMSE values between these intervals are relatively low, with the highest being 0.003068 between days 4 and 5 weeks. This suggests that color changes are gradual during early ripening. The IP _hue spectra graph shows a steady shift, indicating increasing pigmentation and hue transformation.

Additionally, apples stored at cold temperatures showed minimal color change, though noticeable changes developed gradually over time (Appendix Fig. 12.1.9). In contrast, samples kept at ambient room temperature for an additional week per measurement exhibited color changes and defects after 9 weeks. The RMSE values also reflected increasing differences, with the highest (0.004004)

observed between the curves at 9 and 27 weeks. Related literature reported that the hue angle effectively measures apple color development, with a decrease in hue angle correlating with increased red pigmentation in varieties like 'Fuji' and 'Idared' apples (Ozturk et al., 2015; Bizjak et al., 2012). Whale and Singh (2007) reported these changes are due to chlorophyll degradation and increased the concentration of other pigments like carotenoids. The higher storage temperatures accelerate enzymatic browning, leading to a more orange-red color (Neri et al., 2019), while prolonged storage can cause undesirable color changes (Guerra et al., 2010). Matsumoto et al. (2021) observed that physiological disorder retaining green color with low brix values.

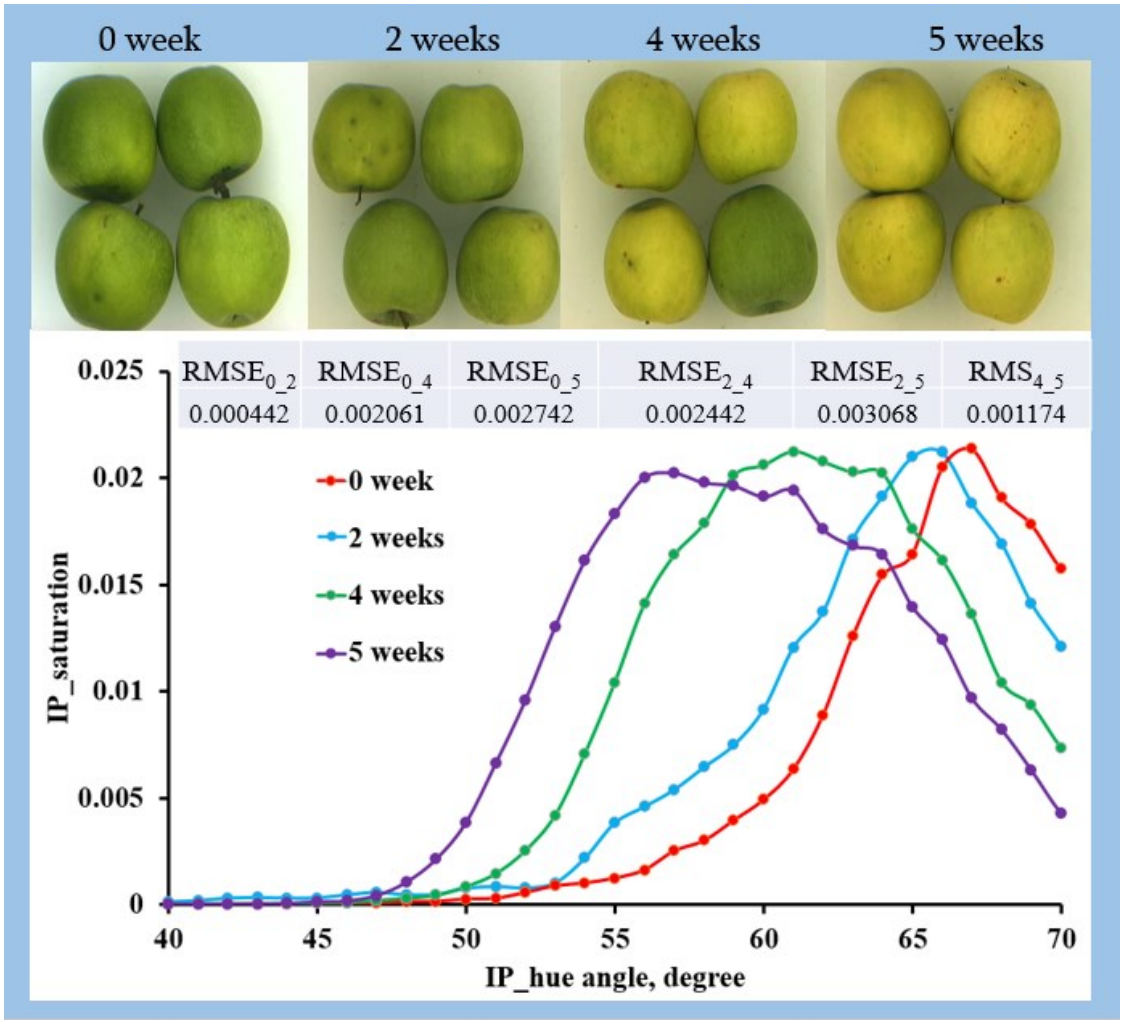

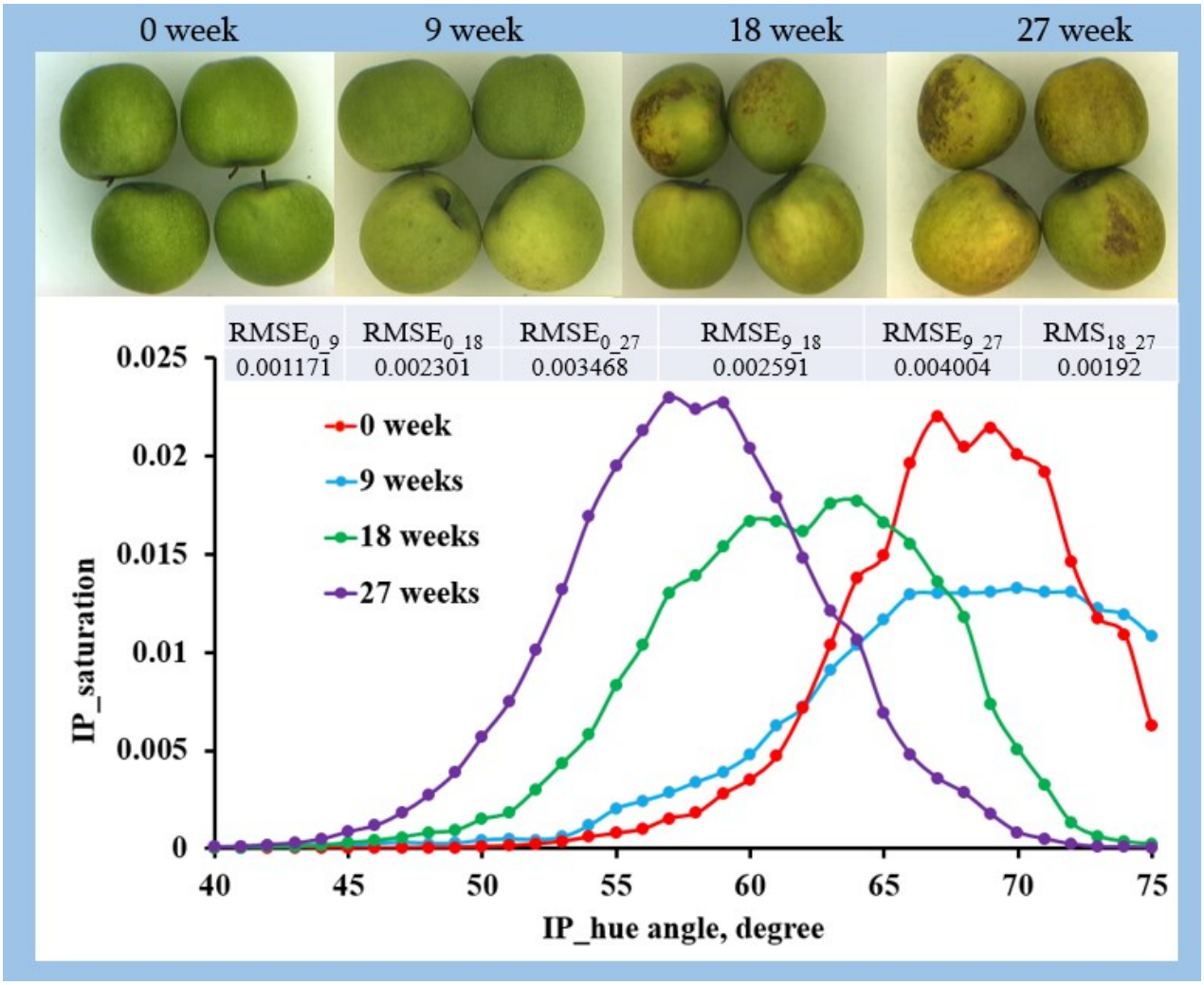

Figure 39: Changes in skin color and corresponding hue spectra of 'Granny Smith' apples under different storage durations and temperatures: Hue-saturation at room storage (top) and cold storage-ambient (bottom).

6.3.7 NIR spectroscopy

Fig. 40 illustrates the raw spectra (a), spectra normalized by SNV (b), SD of normalized spectra (c), and apple NDI_1531 at 1650 nm (d). The higher standard deviation of the normalized spectra was observed at 908, 1080, 1358, 1450, and 1650 nm (Fig. 40c), with the reference wavelength at 1531 nm showing the minimum standard deviation across the spectra. The deviations at these wavelengths reflect temperature and time-induced changes in apple quality attributes such as firmness, SSC, and weight loss. NDI_1531nm at 1650 nm value at both room temperature (22 °C)

and cold storage (2 °C), apples showed a noticeable increase in variability of NDI values in the first 4 days and 67 days, respectively. This is likely to reflect differences in the physiological responses among individual apples. Some fruits had already begun to deteriorate, while others remained intact, resulting in a wider spread of values. With prolonged storage, variability decreased as most apples reached a more uniform state of deterioration, leading to narrower NDI ranges. The 1650 nm wavelength in NIR spectroscopy is highly sensitive to changes in fruit tissue properties, including moisture, sugars, organic compounds, and cell structure integrity (Subedi et al., 2012; Walsh et al., 2020). The two-way ANOVA confirmed significant effects of storage temperature, time, and their interaction on both NDI_1531nm at 1650 nm and QI, with particularly high F-values indicating strong sensitivity. While 1450 nm and 1358 nm also showed high responsiveness, their effects were slightly lower (Table 21). Additionally, absorbance at 908 nm is associated with sugar-related third overtone absorption (Paz et al., 2008; Walsh et al., 2020).

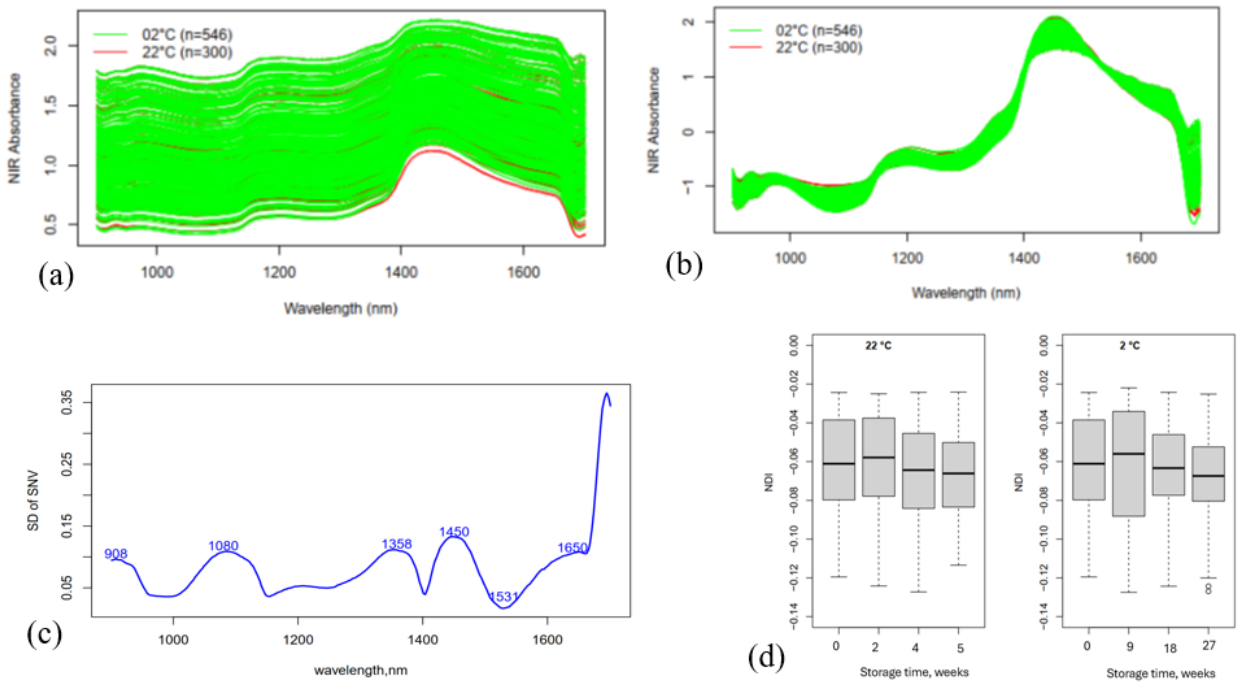

Figure 40: Full NIR raw spectra (a) Normalized spectra by SNV (b) and the standard deviation (b) of the normalized spectra (c) and (d) apple NDI_1531 at 1650 nm.

Furthermore, absorbance at 1080 nm is associated with changes in sugar content during ripening, driven by C-H stretching vibrations (Eisenstecken et al., 2015; Workman and Weyer, 2007). At 1360 nm and 1658 nm, variations correspond to firmness loss caused by pectin and cellulose degradation, with higher temperatures accelerating softening (Baltazar et al., 2020; Cetin and Kavdir, 2017). Absorbance at 1658 nm, linked to C=O stretching vibrations, indicates ripeness and cell wall breakdown (Buyukcan and Kavdir, 2017; Wu et al., 2014). At 1450 nm, water absorption changes highlight moisture and weight loss during storage, intensified at higher temperatures (Bobelyn et al., 2010; Ignat et al., 2014).

Table 21: ANOVA results showing the effects of storage time (days), temperature (°C) and interaction on apple NDI_1531 and QI (n=834)

	Factor	908 nm	1080nm	1358nm	1450nm	1650nm
Apple NDI	Storage time (A)	1297.53^{s}	1203.749^{s}	1843.885^{s}	1941.101^{s}	1961.863^{s}
	Temperature(B)	1065.269^{s}	1009.629^{s}	1576.809^{s}	1765.275^{s}	1805.046^{s}
	Interaction (A× B)	2751.275^{s}	2592.136^{s}	3905.025^{s}	4244.262^{s}	4346.353^{s}
Apple QI	Storage time (A)	1537.144^{s}	1458.867^{s}	1974.701^{s}	1875.882^{s}	2073.146^{s}
	Temperature(B)	1263.259^{s}	1225.476^{s}	1690.205^{s}	1706.297^{s}	1907.081^{s}
	Interaction (A× B)	3266.739^{s}	3149.307^{s}	4168.064^{s}	4112.744^{s}	4579.414^{s}

'^{s}' $p<0.001$

Pearson correlation analysis (Table 22) revealed strong relationships between NIR absorbances and apple quality parameters during storage. Significant positive correlations were found between 908 nm and 1080 nm (r = 0.844), 1080 nm and 1358 nm (r = 0.999), and 1358 nm and 1450 nm (r = 0.976). The 1650 nm wavelength showed the highest sensitivity, with strong correlations to weight loss (r = -0.87) and SSC (r = -0.843). Negative correlations were observed between weight loss and 908 nm (r = -0.873) and 1080 nm (r = -0.883), capturing moisture loss. Firmness correlated positively with 908 nm (r = 0.828) and 1650 nm (r = 0.818), while SSC showed negative correlations with 908 nm (r = -0.851) and 1450 nm (r = -0.806). Weight loss and SSC were strongly positively correlated (r = 0.936), whereas firmness and SSC showed a moderate negative correlation (r = -0.754).

Table 22. Pearson's correlation values between NIR readings, WL and firmness for apples (n = 834) at different storage times and temperatures

	1080 nm	1358 nm	1450 nm	1650 nm	WL, %	Firmness, N	SSC, %
908 nm	0.844	0.839	0.809	0.991	-0.873	0.828	-0.851
1080 nm		0.999	0.974	0.854	-0.883	0.785	-0.843
1358 nm	s		0.976	0.850	-0.879	0.775	-0.836
1450 nm	s	s		0.823	-0.835	0.690	-0.806
1650 nm	s	s	s		-0.87	0.818	-0.843
WL, %	s	s	s	s		-0.824	0.936
Firmness, N	s	s	s	s	s		-0.754

's' $p < 0.001$; the upper triangle shows the correlation values, while the bottom triangle shows the significance level.

Prediction models

The comparison of PLSR and SVM models (Table 23) using bootstrapped validation highlights the clear advantage of selected wavelength approaches (Fig. 41) over full spectra. SVM consistently outperformed PLSR for weight loss, firmness, and SSC. For weight loss, PLSR with selected wavelengths achieved $R^2 = 0.893$, RMSE = 1.116%, and RPD = 3.046, while SVM further improved predictions to $R^2 = 0.955$, RMSE = 0.708%, and RPD = 4.85. For firmness, PLSR yielded $R^2 = 0.823$, RMSE = 4.545 N, and RPD = 2.39, whereas SVM achieved $R^2 = 0.958$, RMSE = 2.201 N, and RPD = 5.09. For SSC, PLSR reached $R^2 = 0.791$, RMSE = 0.440%, and RPD = 2.20, while SVM significantly outperformed it with $R^2 = 0.937$, RMSE = 0.250%, and RPD = 3.93. These results indicate that SVM combined with selected wavelengths provides better predictive accuracy for apple quality parameters, outperforming both PLSR and full-spectrum approaches. Previous studies support these findings, such as Li et al. (2013) using NIR and LS-SVM ($R^2 = 0.891$, RMSEP = 0.624), Zhang et al. (2021) with Vis-NIR and PLSR (R = 0.82, RMSEP = 0.71), and Ignat et al. (2014) with NIR (850–1888 nm) and PLSR ($R^2 = 0.60$, RMSEP = 1.2, RPD = 1.7).

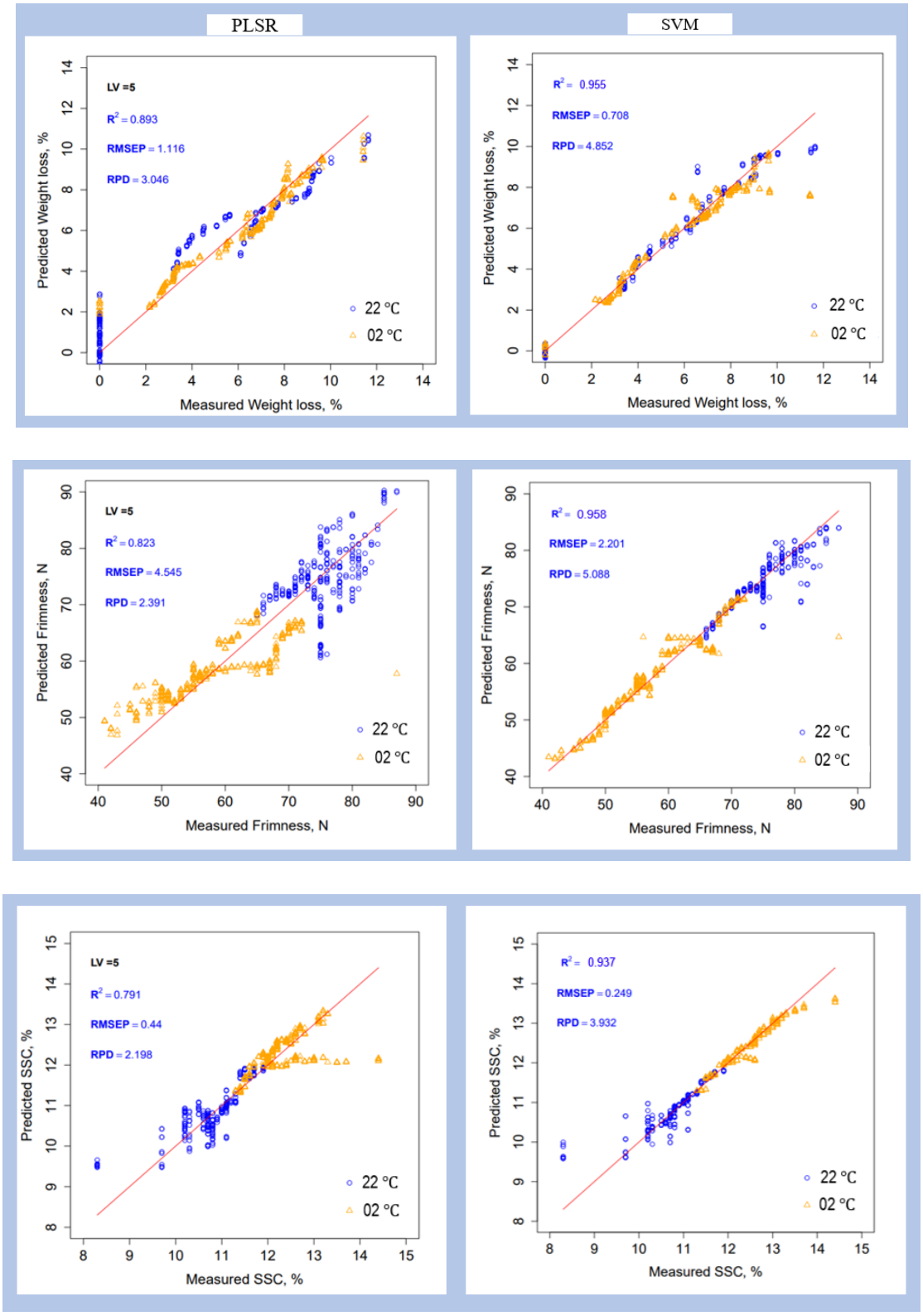

Figure 41: PLSR (left) and SVM (right) models using a set of selected wavelengths for prediction results of WL, firmness, and SSC (top-bottom)

Moreover, the selected wavelengths provided significant enhancements in predictive accuracy over the full spectra in SSC predictions. With PLSR, the full spectra yielded R2 of 0.488, RMSE of 0.70%, and RPD of 1.39, while the selected wavelengths achieved an R^2 of 0.791, RMSE of 0.44%, and RPD of 2.20. For SVM, the selected wavelengths (R^2=0.937, RMSE = 0.25%, RPD = 3.93) significantly performed better than the full spectra (R^2=0.613, RMSE = 0.62%, RPD = 1.56). Previous studies have also reported the use of various calibration techniques for predicting the SSC of fruits. Fan et al. (2020) predicted apple SSC using NIR and PLSR with R^2 = 0.690, RMSEP = 0.604% and RPD = 1.794. In addition, Li et al. (2013) used NIR and LS-SVM to predict Pears SSC with R^2 = 0.916 and RMSEP = 0.250%, while Sun et al. (2009) reported on apples SSC predictions using LS-SVM with R^2 = 0.88 and RMSEP = 0.80%. The current study's SVM model performs better in predicting weight loss, SSC, and firmness than that described in the cited literature.

Table 23: Cross-validated SVM and PLSR model performance metrics of 'Granny Smith' apples in validation set (n=167)

Category	Model		R^2			RMSE			RPD		
			Mean	CI95min	CI95max	Mean	CI95min	CI95max	Mean	CI95min	CI95max
Full spectra	SSC	PLSR	0.488	0.478	0.498	0.697	0.687	0.706	1.395	1.381	1.409
	WL	PLSR	0.549	0.539	0.558	2.280	2.255	2.305	1.490	1.475	1.505
	Firmness	PLSR	0.600	0.592	0.609	6.830	6.757	6.903	1.583	1.565	1.600
	SSC	SVM	0.613	0.603	0.623	0.620	0.609	0.631	1.556	1.538	1.575
	WL	SVM	0.692	0.684	0.701	1.910	1.877	1.934	1.782	1.756	1.808
	Firmness	SVM	0.756	0.750	0.762	5.430	5.368	5.489	2.004	1.979	2.028
Selected wavelengths	SSC	PLSR	0.791	0.785	0.798	0.440	0.431	0.450	2.198	2.163	2.234
	WL	PLSR	0.893	0.890	0.895	1.116	1.102	1.130	3.046	3.012	3.081
	Firmness	PLSR	0.823	0.818	0.829	4.545	4.483	4.608	2.391	2.354	2.428
	SSC	SVM	0.937	0.934	0.940	0.250	0.240	0.259	3.933	3.819	4.047
	WL	SVM	0.955	0.953	0.958	0.708	0.689	0.727	4.852	4.716	4.987
	Firmness	SVM	0.958	0.955	0.962	2.201	2.117	2.286	5.088	4.891	5.284

6.3.8 Laser light backscattering imaging (LLBI)

The modified Cauchy distribution (CD) function provided strong curve-fitting for LLBI parameter extraction, with average performance of $R^2 = 0.970$ and RPD = 6.08 for the beam system, and $R^2 = 0.884$ and RPD = 3.145 for the line system. In a single laser signal image at 635 nm (Fig. 42), the beam-based profile showed a strong fit ($R^2 = 0.97$), though filtering increased RMSE (5.50 to 12.63) and slightly reduced RPD (5.66 to 5.07). The line-based profile also fit well ($R^2 = 0.98$, RMSE = 3.60), but filtering reduced R^2 to 0.97 and raised RMSE to 9.26. Full data fitting results were used for subsequent analyses.

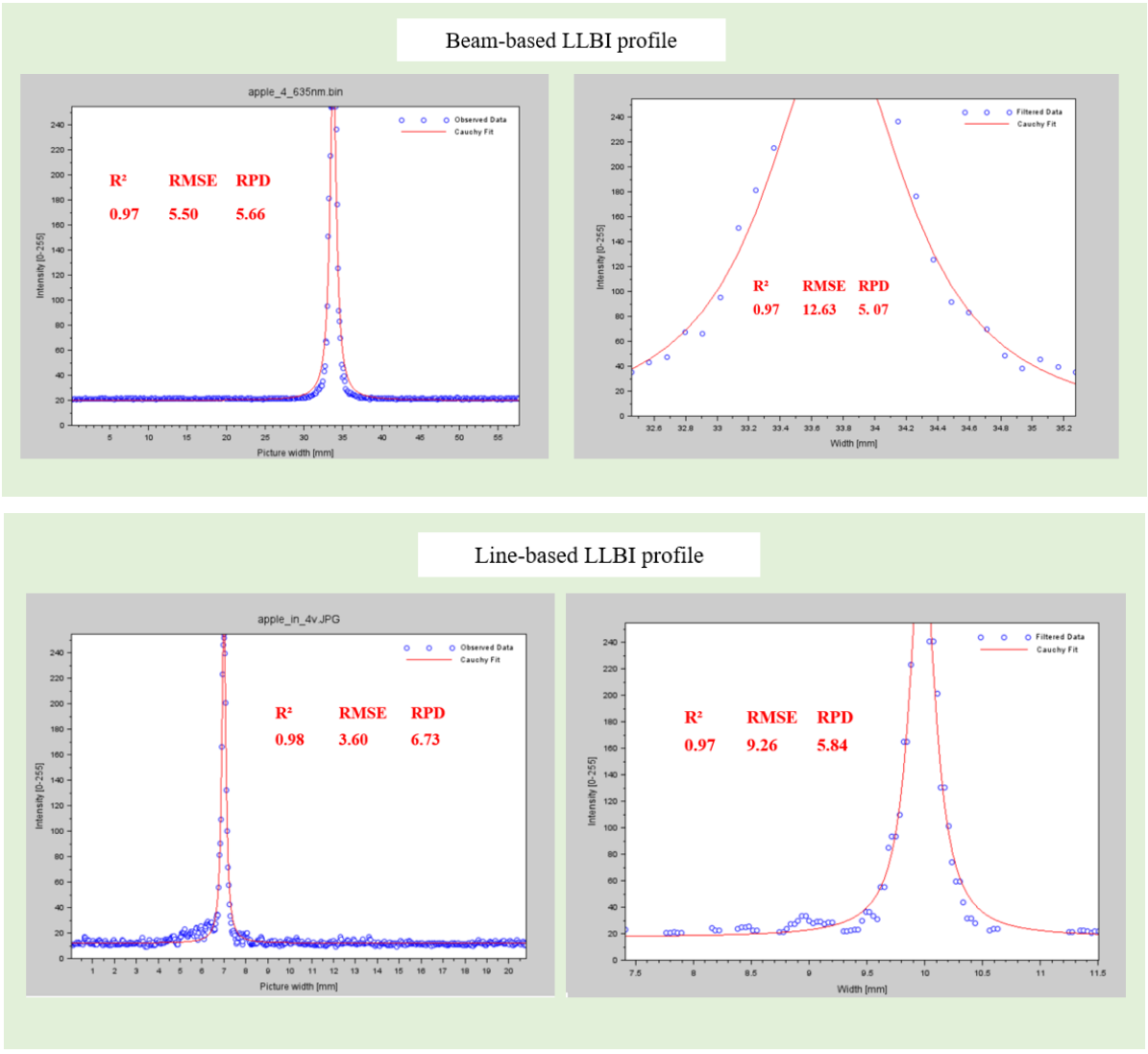

Figure 42: Sample curve fittings of modified Cauchy Distribution functions for the full (left) and partial (right) scattering profiles of apple samples at 635 nm using beam-based LLBI profiles (top) and line-based LLBI profiles (bottom).

Figure 43 shows the changes in amplitude and shape values from the modified CD model for different storage systems. The amplitude decreased, while the shape increased, for apples stored at room temperature and cold-ambient temperature. Different measurement approaches lead to differences in shape and amplitude values. This is due to changes in apple structure during storage (Baranyai and Zude, 2009; Lorente et al., 2015). Room temperature accelerates structural and biochemical changes, resulting in higher shape values more rapidly than cold-ambient storage. The changes in shape and amplitude have been related to chlorophyll loss and carotenoid pigment emergence, which reduce scattering widths at 635 nm (Hashim et al., 2014; Rezaei Kalaj et al., 2016). As apples ripen, diminished chlorophyll absorption and increased carotenoids lead to greater backscattering, reflecting ripening progress and storage conditions (Rezaei Kalaj et al., 2016). These structural changes alter light absorption and scattering behaviors (Hashim et al., 2014; Romano et al., 2011).

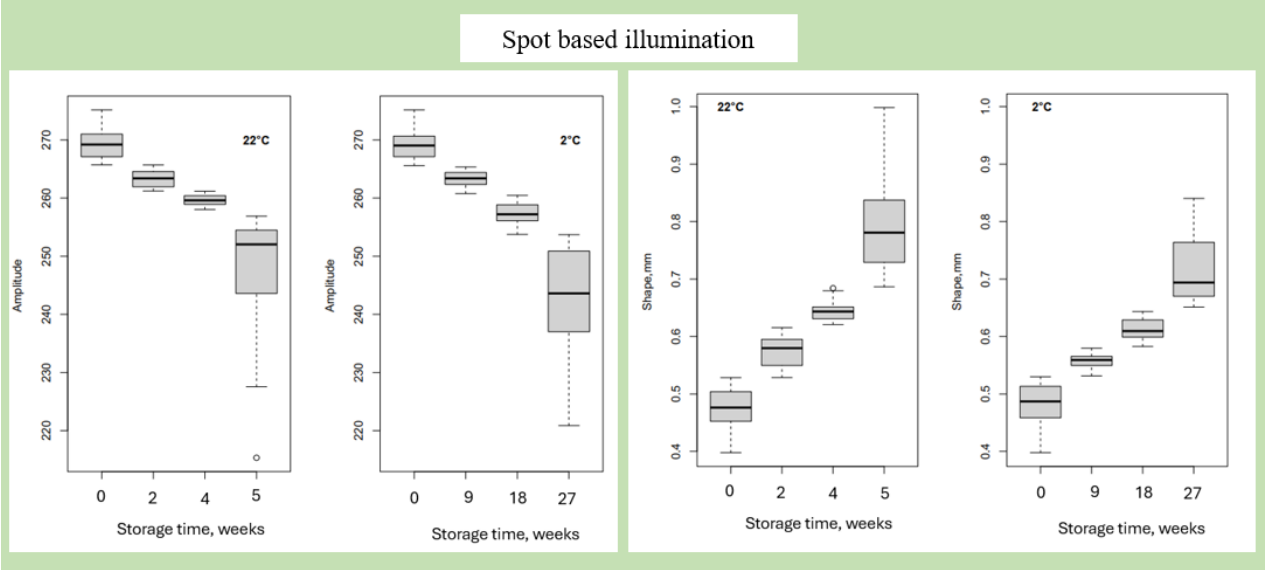

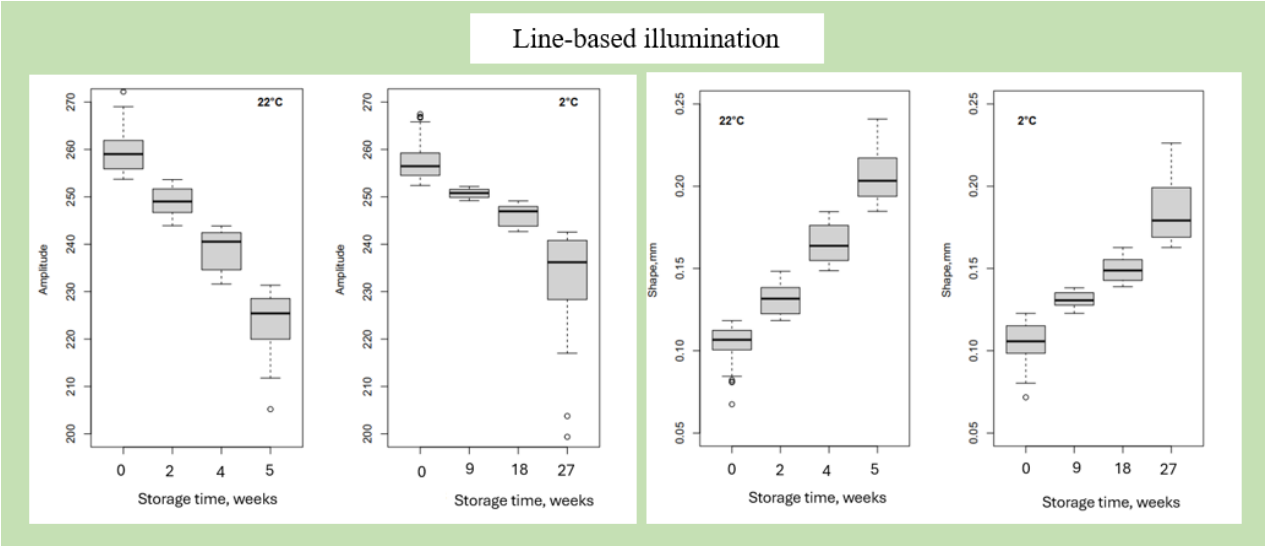

Figure 43: Change of amplitude (left) and Shape (right) from spot based (top) and line (bottom) illumination type in 'Granny smith' apple samples stored at different storage times and temperatures.

Table 24 shows the two-way ANOVA results for the effects of storage time, temperature, and their interactions on amplitude and shape values. Storage temperature significantly impacted amplitude (F = 477.176. Similarly, time and temperature interactions were significant for amplitude (F = 45.506) and shape (F = 292.44).

Table 24: Two- way ANOVA results showing the effects of storage time, temperature, and their interaction on the amplitude and shape values (N= 643).

Factor	LLBI parameters	
	Amplitude	Shape
Time (A)	471.252[s]	1590.99 [s]
Temperature (B)	477.176 [s]	14582.91 [s]
Interaction A × B	45.506 [s]	292.44 [s]

'[s]' $p<0.001$

Table 25 shows significant correlations between storage time, firmness, weight loss, and LLBI parameters. Amplitude positively correlated with firmness (r = 0.828 with beam, r = 0.684 with line) and negatively with weight loss (r = -0.883 with beam, r = -0.891 with line) and shape (r = -0.968 with line), indicating that higher amplitude reflects firmer fruits with less moisture loss and surface shrinkage. Shape negatively correlated with firmness (r = -0.726 with beam, r = -0.745 with

line) and positively with weight loss (r = 0.946 with both beam and line), suggesting that ripening-induced softening and moisture loss alter fruit structure.

Table 25: Pearson's correlation coefficients between storage time, firmness, weight loss, and LLBI profile variables measured using beam-based (n=261) and line-based (n=382) laser systems.

	System	Amplitude	Shape, mm	Firmness, N	Weight loss, %	Time, days
Amplitude	beam		-0.928	0.828	-0.883	-0.560
	line		-0.968	0.684	-0.891	-0.380
Shape, mm	beam	s		-0.726	0.946	0.328
	line	s		-0.745	0.946	0.477
Firmness, N	beam	s	s		-0.762	-0.836
	line	s	s		-0.720	-0.869
Weight loss, %	beam	s	s	s		0.443
	line	s	s	s		0.525

NB: upper triangle shows the correlation values, while the bottom triangle shows the significance level (s' $p < 0.05$)

Prediction models

The performance of MVR and SVM models was evaluated for predicting weight loss and firmness of 'Granny Smith' apples using LLBI-derived parameters under spot and line illumination (Fig. 44, Table 26). SVM consistently outperformed MVR, effectively capturing both surface and subsurface changes. With three LLBI parameters from modified Cauchy fitting, SVM achieved high predictive accuracy for weight loss ($R^2 > 0.96$) and firmness ($R^2 > 0.91$). Line illumination enhanced weight loss prediction ($R^2 = 0.971$, RMSE = 0.608%, RPD = 6.035), while spot illumination gave the best firmness prediction ($R^2 = 0.940$, RMSE = 2.626 N, RPD = 4.100). Earlier studies reported lower accuracies: Lu (2004) used neural networks ($R^2 = 0.87$) for firmness; Qing et al. (2007b, 2008) applied PLSR with R^2 of 0.81–0.87 for 'Elstar' and other apples; Peng and Lu (2005) employed twelve Lorentzian parameters across four wavelengths, reaching r = 0.76 and SEV = 6.01 N; and Romano et al. (2011) predicted apple moisture during drying with a linear LLBI model ($R^2 = 0.89$, RMSECV = 8.9%). In comparison, the present SVM-based approach shows superior performance, with the beam-based SVM best for firmness ($R^2 = 0.969$, RMSEP = 1.919 N, RPD = 5.728) and the line-based SVM best for weight loss ($R^2 = 0.972$, RMSEP = 0.603%, RPD = 6.115

Beam LLBI

MVR

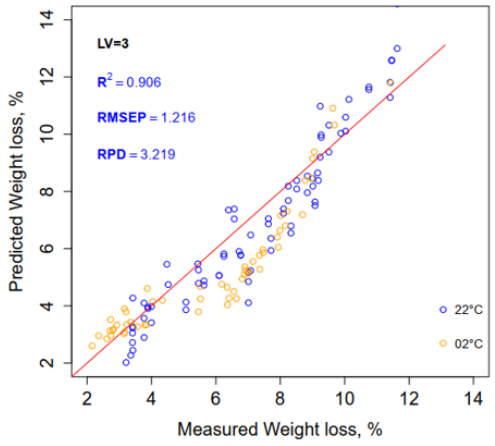

SVM

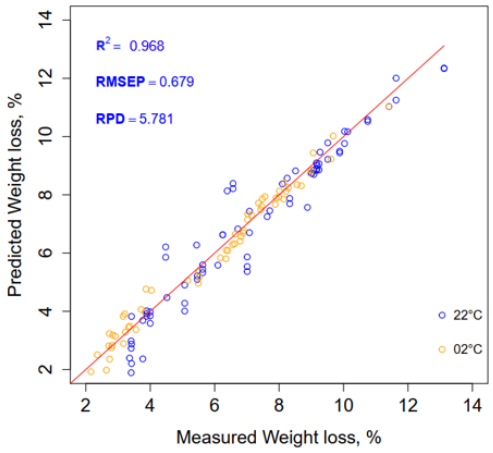

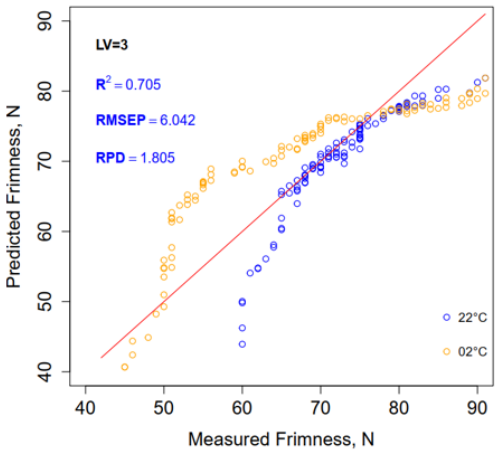

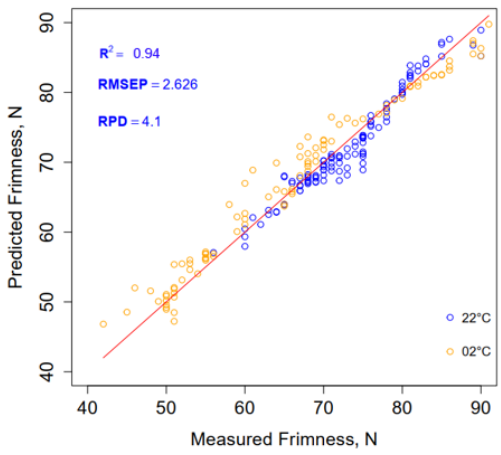

Line LLBI

MVR

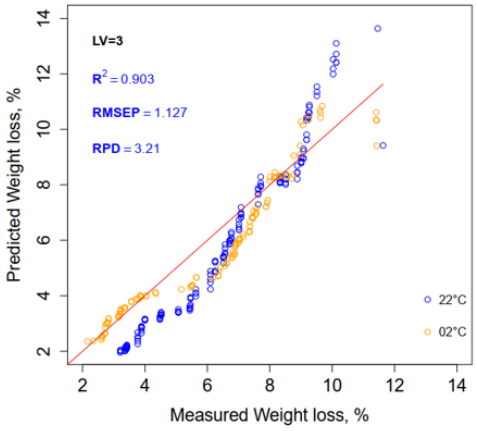

SVM

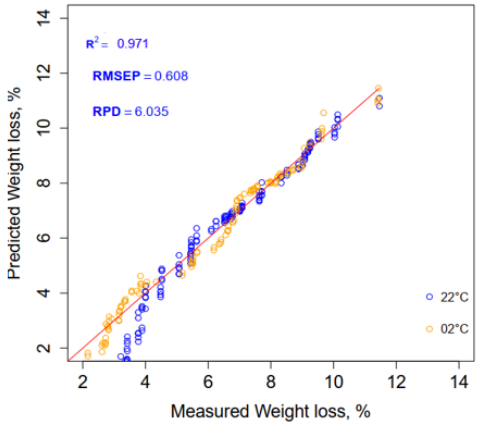

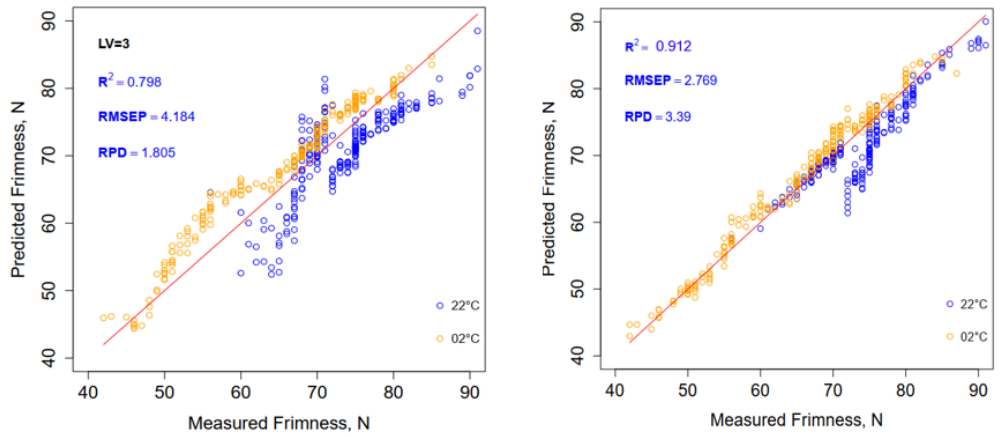

Figure 44: MVR (left) and SVM (right) prediction results for weight loss (top) and firmness (bottom) using datasets from beam and line LLBI.

Table 26: Cross-validated performance metrics of MVR and SVM models using LLBI parameters from beam and line datasets ($n_1 = 261$, $n_2 = 382$) for predicting weight loss and firmness in 'Granny Smith' apples.

Models	Parameters	R^2			RMSE			RPD		
		Mean	CI95min	CI95max	Mean	CI95min	CI95max	Mean	CI95min	CI95max
MVR	WL, %	0.906	0.903	0.909	1.216	1.194	1.238	3.219	3.164	3.275
		0.903	0.901	0.905	1.127	1.116	1.1384	3.210	3.177	3.244
	Firmness, N	0.705	0.693	0.7166	6.042	5.907	6.177	1.805	1.766	1.843
		0.798	0.791	0.805	4.184	4.144	4.224	2.237	2.202	2.273
SVM	WL, %	0.968	0.966	0.970	0.679	0.658	0.701	5.781	5.616	5.945
		0.971	0.970	0.973	0.608	0.593	0.624	6.035	5.886	6.183
	Firmness, N	0.940	0.937	0.944	2.626	2.551	2.701	4.100	3.982	4.218
		0.912	0.909	0.916	2.769	2.720	2.817	3.390	3.321	3.458

7. NEW SCIENTIFIC RESULTS

This study evaluated the application of non-destructive techniques to monitor quality changes in green asparagus, plums, and apples during post-harvest storage. The main scientific results from each practical experiment are presented as follows:

1. An optimum set of wavelengths (907, 923, 1069, 1442, and 1696 nm) was selected for the quality assessment of green asparagus during storage and shelf life. Linear Discriminant Analysis (LDA) using the selected wavelengths successfully detected the quality change in 4 days storage interval. The model achieved classification accuracies of 60.4% at 2 °C, 74.3% at 10 °C, and 76.9% at 15 °C. After 12 days, temperature-induced changes were detected with 87.7% accuracy. The SVM model demonstrated enhanced predictive accuracy compared to the PLSR model when calibrated using NIR spectra at selected wavelengths for predicting weight loss and firmness. The SVM model achieved $R^2 = 0.768$, RMSE = 5.690%, and RPD = 2.080 for weight loss, while for firmness, it achieved $R^2 = 0.829$, RMSE = 5.380 N, and RPD = 2.322.

2. Line-based Laser Light Backscattering Imaging (LLBI) analysis with a single laser module emitting at 635 nm was applied, and diffusely illuminated surfaces were captured from three positions (base, middle, tip) on asparagus spears. LLBI parameters of amplitude, shape, and FWHM were extracted using Cauchy curve fitting. The LDA model based on LLBI parameters detected quality changes in asparagus spears after 4 days across all temperature groups with 79.7% accuracy. For individual temperatures, accuracy was 81.4% at 2 °C, 89.6% at 10 °C, and 93.4% at 15 °C. MVR and MARS models were developed to predict weight loss and firmness. MARS outperformed MVR, and predicted weight loss with $R^2 = 0.846$, RMSE = 6.401%, RPD = 2.558, and firmness with $R^2 = 0.927$, RMSE = 3.266 N, RPD = 3.775.

3. An optimum set of wavelengths (909, 1064, 1323, 1447, 1650 nm) was selected for quality assessment of plum fruits during storage and shelf life. Using these wavelengths, PLSR predicted weight loss with $R^2 = 0.738$, RMSEP = 1.582%, and RPD = 1.953, and SSC with $R^2 = 0.740$, RMSEP = 0.980%, and RPD = 1.991. However, performance improved with the SVM model, which achieved $R^2 = 0.917$, RMSEP = 0.844%, and RPD = 3.492 for weight loss, and $R^2 = 0.844$, RMSEP = 0.780%, and RPD = 2.498 for SSC.

4. The beam-based LLBI technique with a Cauchy distribution function fitted on the signal of 532 nm and 780 nm was able to detect quality changes of plum. Plums stored at 1 °C showed detectable quality changes within 4 days interval, with LDA models achieving classification accuracy of 92.3% for 'Stanley' and 91.9% for 'Elena'. For storage at 5 °C, the models reached 100% accuracy across all time points and cultivars. Cultivar-specific regression models outperformed combined models. The best cross-validation results were observed for 'Elena' (Minolta chroma-based chroma: R^2 = 0.866, RMSE = 0.634; SSC: R^2 = 0.818, RMSE = 0.873%) and 'Stanley' (firmness: R^2 = 0.769, RMSE = 3.049 N; Minolta chroma-based hue angle: R^2 = 0.731, RMSE = 16.62°). This showed the potential of LLBI combined with multivariate models (i.e. LDA, MVR) for real-time quality assessment in postharvest handling and cold chain management.

5. Optimized wavelengths (908, 1080, 1358, 1450, and 1650 nm) were used to assess storage quality and shelf-life of 'Granny Smith 'apples. The SVM model showed better performance than PLSR, predicting weight loss (R^2 = 0.955, RMSEP = 0.708%, RPD = 4.852), firmness (R^2 = 0.958, RMSEP = 2.201 N, RPD = 5.088), and SSC (R^2 = 0.937, RMSEP = 0.249%, RPD = 3.932).

6. LLBI technique demonstrated the effectiveness of both line and beam laser configurations on apple quality assessment. The SVM with three LLBI parameters extracted from the modified Cauchy fitting on the LLBI profile, the system demonstrated good predictive performance for both weight loss (R^2 > 0.96) and firmness (R^2 > 0.91). Hence, line-based LLBI combined with SVM enhanced its performance in predicting weight loss (R^2 = 0.971, RMSEP = 0.608%, RPD = 6.035), while the beam laser setup yielded the best results for firmness prediction (R^2 = 0.940, RMSEP = 2.626 N, RPD = 4.100).

8. POSSIBLE APPLICATIONS AND SUGGESTIONS

8.1 Possible applications

The empirical findings of NIR and LLBI techniques demonstrate their potential applications for monitoring quality changes in fresh fruits and vegetables. Some of these applications are described as follows: -

- NIR and LLBI enable real-time quality monitoring and sorting of fruits and vegetables based on firmness, weight loss, SSC, and color, helping reduce waste.
- These techniques can predict shelf life and optimize storage conditions (temperature and duration) for produce such as asparagus, plums, and apples.
- NIR and LLBI allow nondestructive assessment of ripeness and overall quality in stores or distribution centers, supporting optimal harvest timing and ensuring high-quality produce for consumers.

8.2 Limitations and further research-

8.2.1 Limitations

- The seasonal nature of green asparagus, plums, and apples significantly limits the replication of experimental work for each crop. These fruits and vegetables are only available fresh during specific months of the year (i.e., April to June for green asparagus and July to October for plum and apple), which restricts the timeframe for conducting experiments that require fresh samples to accurately assess their quality and shelf life.
- The humidity, and gas composition for each treatment was not evaluated due to laboratory limited facility and spaces
- The maturity, cultivar differences, internal structural composition variation, and exposed storage temperature affect the consistency and accuracy of measurements, particularly for LLBI and NIR models.

8.2.2 Further research

- Expand the application of these nondestructive techniques to other fruits and vegetables. This would increase the applicability of these technologies to a broader range of agricultural products and make them more valuable for large-scale industrial adoption.

9. SUMMARY

Apples, plums, and green asparagus are widely cultivated crops, with Hungary being a major producer. These fruits and vegetables are essential to a nutritious diet, offering health benefits including a reduced risk of cancer and cardiovascular diseases(Głąbska et al., 2020; Wang et al., 2014). However, maintaining their quality during post-harvest storage poses challenges, as elevated temperature and long storage time accelerate degradation, leading to weight loss, reduced firmness, discoloration, and microbial infestation. Non-destructive methods such as NIR spectroscopy and LLBI were effective in predicting quality changes. Linear regression models like PLSR and MVR showed promising results, while non-linear models like SVM and MARS demonstrated better performance in predicting weight loss, SSC, firmness, and skin color. The full NIR spectra collected from green asparagus, plums (i.e., 'Stanley',' Elena'), and apples (i.e., 'Granny Smith') were pretreated using SNV, and the standard deviation of the normalized spectra was computed. Wavelengths were manually selected based on the local maxima peaks. The multispectral technique, utilizing selected NIR wavelengths (907, 923, 1069, 1442, and 1696 nm), was applied to evaluate the firmness and weight loss of green asparagus. Similarly, five wavelengths (909, 1064, 1323, 1447, and 1650 nm) were selected to assess the weight loss and SSC of plums. Additionally, multispectral data from five selected wavelengths (908, 1080, 1358, 1450, and 1650 nm) were used to evaluate weight loss, firmness, and SSC in 'Granny Smith' apples.

A beam- and line-based LLBI system at different wavelengths was applied to monitor the quality changes of green asparagus, plums, and 'Granny Smith' apples. The beam-based LLBI system, using a multispectral range (532-1064 nm), was optimized based on ANOVA applied to LLBI parameters extracted from the Cauchy distribution function. The data extracted from wavelengths of 532 nm and 780 nm were applied as a non-destructive approach to evaluate the firmness, SSC, and color of plums during storage. Additionally, the line-based system at 635 nm was used to assess weight loss and firmness in green asparagus and 'Granny Smith' apples. These findings underscore the potential of, NIR spectroscopy, and LLBI, as effective and reliable tools for non-destructive quality monitoring of asparagus, plum, and apple during post-harvest storage, enabling better preservation and reduced waste.

10. ACKNOWLEDGEMENT

First of all, I would like to express my deepest gratitude to my supervisors, Professor Baranyai László and Dr. Nguyen Le Phuong Lien, for their indispensable continuous support, insightful comments, encouragement, and all-encompassing guidance throughout my research work. Furthermore, I am deeply thankful to the Stipendium Hungaricum program, the Hungarian University of Agriculture and Life Sciences (MATE), and my home university, Adigrat University, for allowing me to gain better skills and broaden my knowledge. My sincere gratitude also goes to the entire Department of Food Measurements and Process Control staff, as well as the leadership of the Doctoral School of Food Sciences at the Hungarian University of Agriculture and Life Sciences, for their support and assistance in every aspect of my PhD. I would also extend my gratitude to my friends and colleagues for their invaluable advice, motivation, and encouragement throughout my studies. I want to thank my family for their love, unwavering support, and encouragement. Above all, I thank Almighty God for His protection and guidance throughout my studies.

11. REFERENCES

1. Abasi, S., Minaei, S., Jamshidi, B. and Fathi, D., 2018. Dedicated non-destructive devices for food quality measurement: A review. *Trends in Food Science and Technology*, 78, pp.197–205.
2. Abderrahim, D., Taoufiq, S., Bouchaib, I. and Rabie, R., 2023. Enhancing tomato leaf nitrogen analysis through portable NIR spectrometers combined with machine learning and chemometrics. *Chemometrics and Intelligent Laboratory Systems*, 240, p.104925. https://doi.org/10.1016/j.chemolab.2023.104925
3. Adebayo, S.E., Hashim, N., Abdan, K., Hanafi, M., Mollazade, K. (2016) Prediction of quality attributes and ripeness classification of bananas using optical properties, *Scientia Horticulturae*, 212, pp. 171–182. https://doi.org/10.1016/j.scienta.2016.09.045
4. Aghdam, M.S., Flaherty, E.J., Shelp, B.J., 2022. γ-Aminobutyrate improves the postharvest marketability of horticultural commodities: Advances and prospects. Frontiers in Plant Science, 13, 884572. https://doi.org/10.3389/fpls.2022.884572.
5. Ahmed, M.T., Villordon, A. and Kamruzzaman, M., 2024. Comparative analysis of hyperspectral image reconstruction using deep learning for agricultural and biological applications. *Results in Engineering*, 23, p.102623. https://doi.org/10.1016/j.rineng.2024.102623
6. Aispuro-Hernández, E., Vera-Guzmán, A.M., Vargas-Arispuro, I., Martínez-Téllez, M.Á., 2019. Low-temperature storage regulates the expression of genes related to peel pigments of grapefruit. Scientia Horticulturae 254, 208–214. https://doi.org/10.1016/j.scienta.2019.04.085
7. Akin, M., Eyduran, S.P., Eyduran, E., Reed, B.M., 2020. Analysis of macro nutrient related growth responses using multivariate adaptive regression splines. Plant Cell, Tissue and Organ Culture, 140, 661–670. https://doi.org/10.1007/s11240-019-01763-8.
8. Akter, T., Bhattacharya, T., Kim, J.-H., Kim, M.S., Baek, I., Chan, D.E. and Cho, B.-K., 2024. A comprehensive review of external quality measurements of fruits and vegetables using nondestructive sensing technologies. *Journal of Agriculture and Food Research*, 15, p.101068. https://doi.org/10.1016/j.jafr.2024.101068
9. Al-Dairi, M., Pathare, P.B., Al-Yahyai, R., 2021. Effect of postharvest transport and storage on color and firmness quality of tomato. Horticulturae 7, 163. https://doi.org/10.3390/horticulturae7070163

10. Alenazi, M.M., Shafiq, M., Alsadon, A.A., Alhelal, I.M., Alhamdan, A.M., Solieman, T.H.I., Ibrahim, A.A., Shady, M.R., Saad, M.A.O., 2020. Non-destructive assessment of flesh firmness and dietary antioxidants of greenhouse-grown tomato (Solanum lycopersicum L.) at different fruit maturity stages. Saudi Journal of Biological Sciences, 27, 2839–2846. https://doi.org/10.1016/j.sjbs.2020.07.004.
11. Aline, U., Bhattacharya, T., Faqeerzada, M.A., Kim, M.S., Baek, I., Cho, B.-K., 2023. Advancement of non-destructive spectral measurements for the quality of major tropical fruits and vegetables: A review. Frontiers in Plant Science, 14, 1240361. https://doi.org/10.3389/fpls.2023.1240361.
12. An, J., Zhang, M., Wang, S., Tang, J., 2008. Physical, chemical and microbiological changes in stored green asparagus spears as affected by coating of silver nanoparticles-PVP. *LWT - Food Science and Technology*, 41, 1100–1107. https://doi.org/10.1016/j.lwt.2007.06.019.
13. Anastasiadi, M., Collings, E.R., Shivembe, A., Qian, B., Terry, L.A., 2020. Seasonal and temporal changes during storage affect quality attributes of green asparagus. Postharvest Biology and Technology, 159, 111017. https://doi.org/10.1016/j.postharvbio.2019.111017
14. Antonov**,** L**.,** 2017. An alternative for the calculation of derivative spectra in the near-infrared spectroscopy. *Journal of Near Infrared Spectroscopy*, 25, pp.145–148. https://doi.org/10.1177/0967033516688222
15. Araujo, M.T., Santos, M.W.D.V., Feliciano, F.F., Costa, P.B. and Leta, F.R., 2022. Banana ripening classification using computer vision: preliminary results. In: *Systems, Signals and Image Processing, Communications in Computer and Information Science*. Springer International Publishing, Cham, pp.132–139. https://doi.org/10.1007/978-3-030-96878-6_12
16. Argenta, L.C., De Freitas, S.T., Mattheis, J.P., Vieira, M.J. and Ogoshi, C., 2021. Characterization and quantification of postharvest losses of apple fruit stored under commercial conditions. *HortScience*, 56, pp.608–616. https://doi.org/10.21273/HORTSCI15771-21.
17. Argenta, L.C., Krammes, J.G., Megguer, C.A., Amarante, C.V.T. and Mattheis, J., 2003. Ripening and quality of 'Laetitia' plums following harvest and cold storage as affected by inhibition of ethylene action. *Pesquisa Agropecuária Brasileira*, 38, pp.1139–1148. https://doi.org/10.1590/S0100-204X2003001000002 .
18. Arruda De Brito, A., Campos, F., Dos Reis Nascimento, A., Damiani, C., Alves Da Silva, F., De Almeida Teixeira, G.H., Cunha Júnior, L.C., 2022. Non-destructive determination of color,

titratable acidity, and dry matter in intact tomatoes using a portable Vis-NIR spectrometer. *Journal of Food Composition and Analysis*, 107, 104288. https://doi.org/10.1016/j.jfca.2021.104288.

19. Assaad, M., 2020. Non-destructive, non-invasive, in-line real-time phase-based reflectance for quality monitoring of fruit. *International Journal on Smart Sensing and Intelligent Systems*, 13, 1–10. https://doi.org/10.21307/ijssis-2020-009.
20. Bahaddou, Y., Tamym, L., Benyoucef, L., 2024. Ensuring Fruits and Vegetables Freshness in Sustainable Agricultural Supply Chain Networks: A Deep Learning Approach, in: Thürer, M., Riedel, R., Von Cieminski, G. (Eds.), *Advances in Production Management Systems. Production Management Systems for Volatile, Uncertain, Complex, and Ambiguous Environments*, IFIP Advances in Information and Communication Technology, Springer Nature Switzerland, Cham, pp. 364–378. https://doi.org/10.1007/978-3-031-71629-4_25.
21. Baltazar, P., Correa, E.C. and Diezma, B., 2020. Instrumental procedures for the evaluation of juiciness in peach and nectarine cultivars for fresh consumption. *Agronomy*, 10, p.152 https://doi.org/10.3390/agronomy10020152.
22. Baranyai, L., Zude, M., 2009. Analysis of laser light propagation in kiwifruit using backscattering imaging and Monte Carlo simulation. *Computers and Electronics in Agriculture*, 69, 33–39. https://doi.org/10.1016/j.compag.2009.06.011.
23. Benelli, A., Cevoli, C. and Fabbri, A., 2020. In-field hyperspectral imaging: An overview on the ground-based applications in agriculture. *Journal of Agricultural Engineering*, 51, pp.129–139. https://doi.org/10.4081/jae.2020.1030
24. Bertran, E., Blanco, M., Maspoch, S., Ortiz, M.C., Sánchez, M.S., Sarabia, L.A., 1999. Handling intrinsic non-linearity in near-infrared reflectance spectroscopy. *Chemometrics and Intelligent Laboratory Systems*, 49, 215–224. https://doi.org/10.1016/S0169-7439(99)00043-X.
25. Birth, G.S., 1978. The light scattering properties of foods. *Journal of Food Science*, 43, pp.916-925. https://doi.org/10.1111/j.1365-2621.1978.tb02455.x
26. Bizjak, J., Slatnar, A., Stampar, F. and Veberic, R., 2012. Changes in quality and biochemical parameters in 'Idared' apples during prolonged shelf life and 1-MCP treatment. *Food Science and Technology International*, 18, pp.569-577. https://doi.org/10.1177/1082013212442178
27. Bobelyn, E., Serban, A.-S., Nicu, M., Lammertyn, J., Nicolai, B.M. and Saeys, W., 2010. Postharvest quality of apple predicted by NIR-spectroscopy: Study of the effect of biological

variability on spectra and model performance. *Postharvest Biology and Technology*, 55, pp.133-143. https://doi.org/10.1016/j.postharvbio.2009.09.006

28. Bonifazi, G., Gasbarrone, R., Gattabria, D., Lendaro, E., Mosca, L., Mattioli, R., Serranti, S., 2024. Early Study on Visible (Vis) and Short-Wave Infrared (SWIR) Spectroscopy for Assessing Water Content in Olive Fruits: Towards Sustainable Land and Agricultural Practices. *Land*, 13, 2231. https://doi.org/10.3390/land13122231.
29. Boonsiriwit, A., Lee, M., Kim, M., Itkor, P., Lee, Y.S., 2021. Exogenous Melatonin Reduces Lignification and Retains Quality of Green Asparagus (Asparagus officinalis L.). *Foods*, 10, 2111. https://doi.org/10.3390/foods10092111.
30. Briano, R., Girgenti, V., Giuggioli, N.R., Peano, C., 2015. Performance of different box bags for map to preserve the quality of "angeleno" plums in transport storage conditions. *Acta Horticulturae*, 561–566. https://doi.org/10.17660/ActaHortic.2015.1079.75.
31. Büchele, F., Hivare, K., Khera, K., Thewes, F.R., Argenta, L.C., Hoffmann, T.G., Mahajan, P.V., Prange, R.K., Pareek, S., Neuwald, D.A., 2024. Novel Energy-Saving Strategies in Apple Storage: A Review. *Sustainability*, 16, 1052. https://doi.org/10.3390/su16031052.
32. Bureau, S., Ruiz, D., Reich, M., Gouble, B., Bertrand, D., Audergon, J.-M., Renard, C.M.G.C., 2009. Rapid and non-destructive analysis of apricot fruit quality using FT-near-infrared spectroscopy. *Food Chemistry*, 113, 1323–1328. https://doi.org/10.1016/j.foodchem.2008.08.066.
33. Buyukcan, M.B. and Kavdir, I., 2017. Prediction of some internal quality parameters of apricot using FT-NIR spectroscopy. *Food Measurement*, 11, pp.651-659. https://doi.org/10.1007/s11694-016-9434-9
34. Caleb, O.J., Mahajan, P.V., Opara, U.L. & Witthuhn, C.R., 2012. Modelling the respiration rates of pomegranate fruit and arils. *Postharvest Biology and Technology*, 64, pp.49–54. https://doi.org/10.1016/j.postharvbio.2011.09.013
35. Camps, C., Christen, D., 2009. Non-destructive assessment of apricot fruit quality by portable visible-near infrared spectroscopy. *LWT - Food Science and Technology*, 42, 1125–1131. https://doi.org/10.1016/j.lwt.2009.01.015.
36. Camps, C., Gilli, C., 2017. Prediction of local and global tomato texture and quality by FT-NIR spectroscopy and chemometrics. *Europ. J. Hortic. Sci.*, 82, 126–133. https://doi.org/10.17660/eJHS.2017/82.3.2.

37. Candan, A.P. and Calvo, G., 2021. Treatment with 1-MCP: an alternative to extend storage in plums harvested with advanced maturity. *Agrociencia Uruguay*, 26. https://doi.org/10.31285/AGRO.25.402

38. Cao, Y., Wang, H., Wu, W., Yang, P., Zhou, Z., Wang, Z., Li, Z., Li, X., 2021. Simple and effective characterization of Fuji apple flavor quality by ethylene and sugar content. *Food Analytical Methods*, 14, 2576–2584. https://doi.org/10.1007/s12161-021-02085-2.

39. Cárdenas, F., Fuentes-Viveros, L., Caballero, E., Soto-Maldonado, C., Ayala, A. and Olivares, A., 2024. Comparative shelf-life study in dehydrated plums: Use of potassium sorbate and its effect on microbial spoilage. *LWT-Food Science and Technology*, 213, p.117004. https://doi.org/10.1016/j.lwt.2024.117004

40. Carlini, P., Massantini, R. and Mencarelli, F., 2000. Vis-NIR measurement of soluble solids in cherry and apricot by PLS regression and wavelength selection. *Journal of Agricultural and Food Chemistry*, 48, pp.5236-5242. https://doi.org/10.1021/jf000408f

41. Cen, H. and He, Y., 2007. Theory and application of near infrared reflectance spectroscopy in determination of food quality. *Trends in Food Science & Technology*, 18, pp.72-83. https://doi.org/10.1016/j.tifs.2006.09.003

42. Cetin, B.E. and Saraçoğlu, O., 2023. Effects of different maturity stages and fruit parts on quality traits of plum (*Prunus domestica*) fruits. *Erwerbs-Obstbau*, 65, pp.1069-1077. https://doi.org/10.1007/s10341-022-00795-3

43. Chandrasekaran, I., Panigrahi, S.S., Ravikanth, L., Singh, C.B., 2019. Potential of near-infrared (NIR) spectroscopy and hyperspectral imaging for quality and safety assessment of fruits: an overview. *Food Analytical Methods*, 12, 2438–2458. https://doi.org/10.1007/s12161-019-01609-1.

44. Chauchard, F., Cogdill, R., Roussel, S., Roger, J.M., Bellon-Maurel, V., 2004. Application of LS-SVM to non-linear phenomena in NIR spectroscopy: development of a robust and portable sensor for acidity prediction in grapes. *Chemometrics and Intelligent Laboratory Systems*, 71, 141–150. https://doi.org/10.1016/j.chemolab.2004.01.003.

45. Chen, C., 2015. Overview of plant pigments, in: Chen, C. (Ed.), *Pigments in Fruits and Vegetables*. Springer New York, New York, NY, pp. 1–7. https://doi.org/10.1007/978-1-4939-2356-4_1.

46. Chen, L.-Y., Wu, C.-C., Chou, T.-I., Chiu, S.-W. and Tang, K.-T., 2018. Development of a dual MOS electronic nose/camera system for improving fruit ripeness classification. *Sensors*, 18, p.3256. https://doi.org/10.3390/s18103256

47. Chen, N., Liu, Z., Zhang, T., Lai, Q., Zhang, J., Wei, X., Liu, Y., 2024. Research on the prediction of yellow flesh peach firmness using a novel acoustic real-time detection device and Vis/NIR technology. *LWT-Food Science and Technology*, 209, 116772. https://doi.org/10.1016/j.lwt.2024.116772.

48. Chidambaram, S. and Srinivasagan, K.G., 2019. Performance evaluation of support vector machine classification approaches in data mining. *Cluster Computing*, 22, pp.189-196. https://doi.org/10.1007/s10586-018-2036-z

49. Choi, H.-S., Jung, S.-K., 2014. Effect of treatment time of 1-MCP on ripening of 'Fuji' apples stored at low and room temperature for a long period. *Journal of Food and Nutrition Research*, 2, 617–620. https://doi.org/10.12691/jfnr-2-9-14.

50. Cocco, C., Silvestre, W.P., Schildt, G.W. and Tessaro, F.A., 2022. Effect of Ethephon application on fruit quality at harvest and post-harvest storage of Japanese plum (Prunus salicina) cv. Fortune. Brazilian Archives of Biology and Technology, 65, e20210183. https://doi.org/10.1590/1678-4324-2022210183

51. Concepción, M., Sargent, D.J., Šurbanovski, N., Colgan, R.J. and Moretto, M., 2021. De novo sequencing and analysis of the transcriptome of two highbush blueberry (Vaccinium corymbosum L.) cultivars 'Bluecrop' and 'Legacy' at harvest and following post-harvest storage. PLoS ONE, 16, e0255139. https://doi.org/10.1371/journal.pone.0255139

52. Cortés, V., Blasco, J., Aleixos, N., Cubero, S. and Talens, P., 2019. Monitoring strategies for quality control of agricultural products using visible and near-infrared spectroscopy: A review. *Trends in Food Science & Technology*, 85, pp.138–148. https://doi.org/10.1016/j.tifs.2019.01.015

53. Costa, R.C., Lima, K.M.G.D., 2013. Prediction of parameters (soluble solid and pH) in intact plum using NIR spectroscopy and wavelength selection. *Journal of the Brazilian Chemical Society*. https://doi.org/10.5935/0103-5053.20130172.

54. Crisosto, C.H., Garner, D., Crisosto, G.M., Bowerman, E., 2004. Increasing 'Blackamber' plum (Prunus salicina Lindell) consumer acceptance. *Postharvest Biology and Technology*, 34, 237–244. https://doi.org/10.1016/j.postharvbio.2004.06.003.

55. Daniels, A.J., Poblete-Echeverría, C., Nieuwoudt, H.H., Botha, N., Opara, U.L., 2021. Classification of browning on intact table grape bunches using near-infrared spectroscopy coupled with partial least squares-discriminant analysis and artificial neural networks. *Frontiers in Plant Science*, 12, 768046. https://doi.org/10.3389/fpls.2021.768046.

56. Deng, H., Long, X., Wang, X., Wang, Y., Pang, C., Xia, H., Liang, D., Zhang, H., Luo, X., Wang, J., Lv, X. and Deng, Q., 2023. Comparative analysis of carotenoid profiles and biosynthetic gene expressions among ten plum cultivars. *Plants*, 12, p.2711. https://doi.org/10.3390/plants12142711

57. Díaz-Pérez, M., Hernández-García, J.J., Carreño-Ortega, Á. and Velázquez Martí, B., 2024. Post-harvest behavior of seedless conical and mini-conical peppers: weight loss, dry matter content, and total soluble solids as indicators of quality and commercial shelf-life. *Foods*, 13, p.1889. https://doi.org/10.3390/foods13121889

58. Ding, B., Li, Y.C., Li, Y.H., Liu, J., Bi, Y., 2010. Effect of intermittent warming combined with modified atmosphere packaging on chilling injury of plum. *Acta Horticulturae*, 531–537. https://doi.org/10.17660/ActaHortic.2010.877.68.

59. East, A.R., Tanner, D.J., Jobling, J.J., Maguire, K.M., Mawson, A.J., 2008. The influence of breaks in storage temperature on 'Cripps Pink' (Pink Lady™) apple physiology and quality. *HortScience*, 43, 818–824. https://doi.org/10.21273/HORTSCI.43.3.818.

60. Elmetwalli, A.H., Derbala, A., Alsudays, I.M., Al-Shahari, E.A., Elhosary, M., Elsayed, S., Al-Shuraym, L.A., Moghanm, F.S. and Elsherbiny, O., 2024. Machine learning-driven assessment of biochemical qualities in tomato and mandarin using RGB and hyperspectral sensors as nondestructive technologies. *PLoS ONE*, 19, p.e0308826. https://doi.org/10.1371/journal.pone.0308826

61. Eisenstecken, D., Panarese, A., Robatscher, P., Huck, C., Zanella, A. and Oberhuber, M., 2015. A near-infrared spectroscopy (NIRS) and chemometric approach to improve apple fruit quality management: A case study on the cultivars 'Cripps Pink' and 'Braeburn'. *Molecules*, 20, pp.13603-13619. https://doi.org/10.3390/molecules200813603

62. Fakhlaei, R., Babadi, A.A., Sun, C., Ariffin, N.M., Khatib, A., Selamat, J. and Xiaobo, Z., 2024. Application, challenges and future prospects of recent nondestructive techniques based on the electromagnetic spectrum in food quality and safety. *Food Chemistry*, 441, p.138402. https://doi.org/10.1016/j.foodchem.2024.138402

63. Falcioni, R., Antunes, W.C., Demattê, J.A.M. and Nanni, M.R., 2023. A novel method for estimating chlorophyll and carotenoid concentrations in leaves: A two hyperspectral sensor approach. *Sensors*, 23, p.3843. https://doi.org/10.3390/s23083843

64. Fan, S., Wang, Q., Tian, X., Yang, G., Xia, Y., Li, J., Huang, W., 2020. Non-destructive evaluation of soluble solids content of apples using a developed portable Vis/NIR device. *Biosystems Engineering*, 193, 138–148. https://doi.org/10.1016/j.biosystemseng.2020.02.017.

65. Fang, Y. and Wakisaka, M., 2021. A review on the modified atmosphere preservation of fruits and vegetables with cutting-edge technologies. *Agriculture*, 11, p.992. https://doi.org/10.3390/agriculture11100992

66. Farag, M., Sheashea, M., Zhao, C. and Maamoun, A., 2022. UV fingerprinting approaches for quality control analyses of food and functional food coupled to chemometrics: A comprehensive analysis of novel trends and applications. *Foods*, 11, p.2867. https://doi.org/10.3390/foods11182867

67. Fearn, T., Riccioli, C., Garrido-Varo, A. and Guerrero-Ginel, J.E., 2009. On the geometry of SNV and MSC. *Chemometrics and Intelligent Laboratory Systems*, 96, pp.22–26. https://doi.org/10.1016/j.chemolab.2008.11.006

68. Feng, Q., Wang, Z., Xiong, W., Kong, W., Huang, M., Xi, W., Zhou, K., 2024. The effect of postharvest storage temperatures on fruit flavor constituents in 'Wushancuili' plum. *Horticulturae*, 10, 414. https://doi.org/10.3390/horticulturae10040414.

69. Ferreira, I.J.S., Almeida, S.L.F.D.O., Figueiredo Neto, A., Costa, D.D.S., 2022. Determination of quality and ripening stages of 'Pacovan' bananas using Vis-NIR spectroscopy and machine learning. *Engenharia Agrícola*, 42, e20210160. https://doi.org/10.1590/1809-4430-eng.agric.v42nepe20210160/2022.

70. Fiol, A., García-Gómez, B.E., Jurado-Ruiz, F., Alexiou, K., Howad, W. and Aranzana, M.J., 2021. Characterization of Japanese plum (*Prunus salicina*) PsMYB10 alleles reveals structural variation and polymorphisms correlating with fruit skin color. *Frontiers in Plant Science*, 12, p.655267. https://doi.org/10.3389/fpls.2021.655267

71. Flores-Rojas, K., Sánchez, M.-T., Pérez-Marín, D., Guerrero, J.E., Garrido-Varo, A., 2009. Quantitative assessment of intact green asparagus quality by near infrared spectroscopy. *Postharvest Biology and Technology*, 52, 300–306. https://doi.org/10.1016/j.postharvbio.2008.12.007.

72. Fodor, M., Matkovits, A., Benes, E.L. and Jókai, Z., 2024. The role of near-infrared spectroscopy in food quality assurance: a review of the past two decades. *Foods*, 13, p.3501. https://doi.org/10.3390/foods13213501

73. Fuchs, S.J., Mattinson, D.S. and Fellman, J.K. 2008. Effect of edible coatings on postharvest quality of fresh green asparagus. *Journal of Food Processing and Preservation*, 32(6), pp.951‐971.https://doi.org/10.1111/j.1745-4549.2008.00226.x

74. Gabriëls, S.H.E.J., Mishra, P., Mensink, M.G.J., Spoelstra, P., Woltering, E.J., 2020. Non-destructive measurement of internal browning in mangoes using visible and near-infrared spectroscopy supported by artificial neural network analysis. *Postharvest Biology and Technology*, 166, 111206. https://doi.org/10.1016/j.postharvbio.2020.111206.

75. Gantner, M., Król, K. and Kopczyńska, K., 2020. Application of MAP and ethylene–vinyl alcohol copolymer (EVOH) to extend the shelf-life of green and white asparagus (*Asparagus officinalis* L.) spears. *Food Measure*, 14, pp.2030–2039. https://doi.org/10.1007/s11694-020-00449-6

76. Garrido, A., Sánchez, M.T., Cano, G., Pérez, D., López, C., 2001. Prediction of neutral and acid detergent fiber content of green asparagus stored under refrigeration and modified atmosphere conditions by near-infrared reflectance spectroscopy. *Journal of Food Quality*, 24, 539–550. https://doi.org/10.1111/j.1745-4557.2001.tb00629.x.

77. Geng, Y., Zhang, Y., Liu, Y., Hu, B., Wang, J., He, J. and Liang, M., 2020. Quality attributes and microstructure of cell walls in 'Suli' plum fruit (*Prunus salicina* Lindl.) during softening. *Food Science and Technology Research*, 26, pp.281-292. https://doi.org/10.3136/fstr.26.281

78. Gibertoni, G., Lenzini, N., Ferrari, L., Rovati, L., 2022. Design and performance of a near-infrared spectroscopy measurement system for in-field alfalfa moisture measurement. *Photonics*, 9, 178. https://doi.org/10.3390/photonics9030178.

79. Giordano, C., Benelli, C., Faraloni, C., Grifoni, D., Anichini, M., Ieri, F., Traversi, L., Beghè, D. and Petruccelli, R., 2023. Effect of postharvest UVB irradiation on the fruit of cv. Dottato (*Ficus carica* L.). *Applied Sciences*, 13, p.13003. https://doi.org/10.3390/app132413003

80. Głąbska, D., Guzek, D., Groele, B., Gutkowska, K., 2020. Fruit and vegetable intake and mental health in adults: A systematic review. *Nutrients*, 12, 115. https://doi.org/10.3390/nu12010115.

81. Golic, M. and Walsh, K.B., 2006. Robustness of calibration models based on near-infrared spectroscopy for the in-line grading of stone fruit for total soluble solids content. *Analytica Chimica Acta*, 555, pp.286-291. https://doi.org/10.1016/j.aca.2005.09.014

82. Goneli, A.L.D., Corrêa, P.C., Oliveira, A.P.L.R., Hartmann Filho, C.P., Oba, G.C., 2018. Castor beans quality subjected to different storage temperatures and periods. *Engenharia Agrícola*, 38, 361–368. https://doi.org/10.1590/1809-4430-eng.agric.v38n3p361-368/2018.

83. Guerra, M., Casquero, P.A., 2008. Effect of harvest date on cold storage and postharvest quality of plum cv. Green Gage. *Postharvest Biology and Technology*, 47, 325–332. https://doi.org/10.1016/j.postharvbio.2007.07.009.

84. Guerra, M., Sanz, M.A. and Casquero, P.A., 2010. Influence of storage conditions on the sensory quality of a high acid apple. *International Journal of Food Science & Technology*, 45, pp.2352-2357. https://doi.org/10.1111/j.1365-2621.2010.02410.x

85. Guo, H., Yan, F., Li, P. and Li, M., 2022. Determination of storage period of harvested plums by near-infrared spectroscopy and quality attributes. *Food Processing and Preservation*, 46. https://doi.org/10.1111/jfpp.16504

86. Guo, W., Li, W., Yang, B., Zhu, Z., Liu, D., Zhu, X., 2019. A novel noninvasive and cost-effective handheld detector on soluble solids content of fruits. *Journal of Food Engineering*, 257, 1–9. https://doi.org/10.1016/j.jfoodeng.2019.03.022.

87. Ha, N.T.T., Pham, T.T., Mac, H.X., Nguyen, L.L.P., Horváth-Mezofi, Z., Göb, M., Nguyen, Q.D., Baranyai, L., Zsom, T., Friedrich, L.F. and Hitka, G., 2023. Evaluation of the effect of 1-MCP treatment on flesh and surface color of selected European and Asian plum fruit using machine vision. *Horticulturae*, 9, p.341. https://doi.org/10.3390/horticulturae9030341

88. Hamilton, A., Ruiz-Llacsahuanga, B., Mendoza, M., Mattheis, J., Hanrahan, I., Critzer, F.J., 2022. Persistence of *Listeria innocua* on fresh apples during long-term controlled atmosphere cold storage with postharvest fungal decay. *Journal of Food Protection*, 85, 133–141. https://doi.org/10.4315/JFP-21-232.

89. Han, Z., Li, B., Wang, Q., Sun, Z. and Liu, Y., 2023. Detection of skin defects on loquat using hyperspectral imaging combining both band ratio and improved three-phase level set segmentation method. *Food Quality and Safety*, 7, p.fyac065. https://doi.org/10.1093/fqsafe/fyac065

90. Hasan, M.U., Singh, Z., Shah, H.M.S., Kaur, J., Woodward, A., 2024. Water loss: A postharvest quality marker in apple storage. *Food Bioprocess Technology*, 17, 2155–2180. https://doi.org/10.1007/s11947-023-03305-9.

91. Hasanzadeh, B., Abbaspour-Gilandeh, Y., Soltani-Nazarloo, A., Hernández-Hernández, M., Gallardo-Bernal, I., Hernández-Hernández, J.L., 2022. Non-destructive detection of fruit

quality parameters using hyperspectral imaging, multiple regression analysis, and artificial intelligence. *Horticulturae*, 8, 598. https://doi.org/10.3390/horticulturae8070598.

92. Hashim, N., Adebayo, S.E., Abdan, K. and Hanafi, M., 2018. Comparative study of transform-based image texture analysis for the evaluation of banana quality using an optical backscattering system. *Postharvest Biology and Technology*, 135, pp.38-50. https://doi.org/10.1016/j.postharvbio.2017.08.021
93. Hashim, N., Janius, R.B., Abdul, R., Osman, A., Shitan, M. and Zude, M., 2014. Changes of backscattering parameters during chilling injury in bananas. *Journal of Engineering Science and Technology*, 9, pp.314-325.
94. Hayati, R., Munawar, A.A., Fachruddin, F., 2020. Enhanced near infrared spectral data to improve prediction accuracy in determining quality parameters of intact mango. *Data in Brief*, 30, 105571. https://doi.org/10.1016/j.dib.2020.105571.
95. He, M., Wu, Y., Wang, Y., Hong, M., Li, T., Deng, T. and Jiang, Y., 2022. Valeric acid suppresses cell wall polysaccharides disassembly to maintain fruit firmness of harvested 'Waizuili' plum (*Prunus salicina* Lindl). *Scientia Horticulturae*, 291, p.110608. https://doi.org/10.1016/j.scienta.2021.110608
96. Hemrattrakun, P., Nakano, K., Boonyakiat, D., Ohashi, S., Maniwara, P., Theanjumpol, P. and Seehanam, P., 2021. Comparison of reflectance and interactance modes of visible and near-infrared spectroscopy for predicting persimmon fruit quality. *Food Analytical Methods*, 14, pp.117-126. https://doi.org/10.1007/s12161-020-01853-w .
97. Hend, B.T., Ghada, B., Sana, B.M., Mohamed, M., Mokhtar, T. and Amel, S.-H., 2009. Genetic relatedness among Tunisian plum cultivars by random amplified polymorphic DNA analysis and evaluation of phenotypic characters. *Scientia Horticulturae*, 121, pp.440-446. https://doi.org/10.1016/j.scienta.2009.03.009
98. He, S., Gao, L., Zhang, Z., Ming, Z., Gao, F., Ma, S., Zou, M., 2024. Diversity analysis of microorganisms on the surface of four summer fruit varieties in Baotou, Inner Mongolia, China. *PeerJ*, 12, e18752. https://doi.org/10.7717/peerj.18752.
99. Huang, Y., Lu, R., Chen, K., 2018. Prediction of firmness parameters of tomatoes by portable visible and near-infrared spectroscopy. *Journal of Food Engineering*, 222, 185–198. https://doi.org/10.1016/j.jfoodeng.2017.11.030.
100. Hung, D.V., Tong, S., Tanaka, F., Yasunaga, E., Hamanaka, D., Hiruma, N., Uchino, T., 2011. Controlling the weight loss of fresh produce during postharvest storage under a nano-size mist

environment. *Journal of Food Engineering*, 106, 325–330. https://doi.org/10.1016/j.jfoodeng.2011.05.027.

101. Hyson, D.A., 2011. A comprehensive review of apples and apple components and their relationship to human health. *Advances in Nutrition*, 2, 408–420. https://doi.org/10.3945/an.111.000513.
102. Ignat, T., Lurie, S., Nyasordzi, J., Ostrovsky, V., Egozi, H., Hoffman, A., Friedman, H., Weksler, A. and Schmilovitch, Z., 2014. Forecast of apple internal quality indices at harvest and during storage by VIS-NIR spectroscopy. *Food Bioprocess Technology*, 7, pp.2951-2961. https://doi.org/10.1007/s11947-014-1297-7
103. Igwe, E.O., Charlton, K.E., 2016. A systematic review on the health effects of plums (*Prunus domestica* and *Prunus salicina*). *Phytotherapy Research*, 30, 701–731. https://doi.org/10.1002/ptr.5581.
104. Jaramillo, S., Rodríguez, R., Jiménez, A., Guillén, R., Fernández-Bolaños, J., Heredia, A., 2007. Effects of storage conditions on the accumulation of ferulic acid derivatives in white asparagus cell walls. *Journal of the Science of Food and Agriculture*, 87, 286–296. https://doi.org/10.1002/jsfa.2718.
105. Jaywant, S.A., Singh, H., Arif, K.M., 2022. Sensors and instruments for Brix measurement: A review. *Sensors*, 22, 2290. https://doi.org/10.3390/s22062290.
106. Jha, S.N., Rai, D.R., Shrama, R., 2012. Physico-chemical quality parameters and overall quality index of apple during storage. *Journal of Food Science and Technology*, 49, 594–600. https://doi.org/10.1007/s13197-011-0415-z.
107. Jiang, B., Li, W. and Huang, Y.D., 2012. Influence of pretreatment methods of the spectra on the calibration model of the precuring degree. *Journal of Applied Polymer Science*, 124, pp.1529–1533. https://doi.org/10.1002/app.35197
108. Jiang, X., Zhu, M., Yao, J., Zhang, Y., Liu, Y., 2022. Study on the effect of apple size difference on soluble solids content model based on near-infrared (NIR) spectroscopy. *Journal of Spectroscopy*, 2022, 1–10. https://doi.org/10.1155/2022/3740527.
109. Johnston, J.W., Hewett, E.W., Banks, N.H., Harker, F.R. and Hertog, M.L.A.T.M., 2001. Physical change in apple texture with fruit temperature: effects of cultivar and time in storage. *Postharvest Biology and Technology*, 23, pp.13-21. https://doi.org/10.1016/S0925-5214(01)00101-6

110. Ju, S., Park, Y.K., 2019. Low fruit and vegetable intake is associated with depression among Korean adults in data from the 2014 Korea National Health and Nutrition Examination Survey. *Journal of Health, Population and Nutrition*, 38, 39. https://doi.org/10.1186/s41043-019-0204-2.

111. Kanchanomai, C., Nakano, K., Kittiwachana, S., Krongchai, C., Ohashi, S., Maniwara, P., Theanjumpol, P. and Naphrom, D., 2022. Seedlessness detection in 'White Malaga' table grapes using near-infrared spectroscopy. *International Food Research Journal*, 29, pp.806–813. https://doi.org/10.47836/ifrj.29.4.08

112. Kapoor, L., Simkin, A.J., George Priya Doss, C. and Siva, R., 2022. Fruit ripening: dynamics and integrated analysis of carotenoids and anthocyanins. *BMC Plant Biology*, 22, p.27. https://doi.org/10.1186/s12870-021-03411-w

113. Kapse, S., Kedia, P., Kausley, S. and Rai, B., 2023. Nondestructive evaluation of banana maturity using NIR AS7263 sensor. *Journal of Nondestructive Evaluation*, 42, p.30. https://doi.org/10.1007/s10921-023-00943-z

114. Kashef, R., 2021. A boosted SVM classifier trained by incremental learning and decremental unlearning approach. *Expert Systems with Applications*, 167, 114154. https://doi.org/10.1016/j.eswa.2020.114154.

115. Kassebi, S., Farkas, C., Székely, L., Géczy, A., Korzenszky, P., 2022. Late shelf life saturation of Golden Delicious apple parameters: TSS, weight, and colorimetry. *Applied Sciences*, 13, 159. https://doi.org/10.3390/app13010159.

116. Kaulmann, A., André, C.M., Schneider, Y.-J., Hoffmann, L. and Bohn, T., 2016. Carotenoid and polyphenol bioaccessibility and cellular uptake from plum and cabbage varieties. *Food Chemistry*, 197, pp.325-332. https://doi.org/10.1016/j.foodchem.2015.10.049

117. Kaur, K. and Dhillon, W.S., 2015. Influence of maturity and storage period on physical and biochemical characteristics of pear during post cold storage at ambient conditions. *Journal of Food Science and Technology*, 52, pp.5352–5356. https://doi.org/10.1007/s13197-014-1620-3

118. Khan, A.S., Ahmed, M.J., Singh, Z., 2011. Increased ethylene biosynthesis elevates incidence of chilling injury in cold-stored 'Amber Jewel' Japanese plum (*Prunus salicina* Lindl.) during fruit ripening. *International Journal of Food Science and Technology*, 46, 642–650. https://doi.org/10.1111/j.1365-2621.2010.02538.x.

119. Khan, M.R., 2022. *Diseases of Fruit and Plantation Crops and Their Sustainable Management*, 1st ed. Agriculture Issues and Policies Series. Nova Science Publishers, Incorporated, New York.
120. Kienle, A., Lilge, L., Patterson, M.S., Hibst, R., Steiner, R. and Wilson, B.C., 1996. Spatially resolved absolute diffuse reflectance measurements for noninvasive determination of the optical scattering and absorption coefficients of biological tissue. *Applied Optics*, 35, p.2304. https://doi.org/10.1364/AO.35.002304
121. Kitazawa, H., Motoki, S., Maeda, T., Ishikawa, Y., Hamauzu, Y., Matsushima, K., Sakai, H., Shiina, T., Kyutoku, Y., 2011. Effects of storage temperature on the postharvest quality of three asparagus cultivars harvested in spring. *Journal of the Japanese Society for Horticultural Science*, 80, 76–81. https://doi.org/10.2503/jjshs1.80.76.
122. Kodagoda, G., Hong, H.T., O'Hare, T.J., Sultanbawa, Y., Topp, B. and Netzel, M.E., 2021. Effect of storage on the nutritional quality of Queen Garnet plum. *Foods*, 10, p.352.. https://doi.org/10.3390/foods10020352
123. Kumar, P., Sethi, S., Sharma, R.R., Srivastav, M., Singh, D., Varghese, E., 2018. Edible coatings influence the cold-storage life and quality of 'Santa Rosa' plum (*Prunus salicina* Lindell). *Journal of Food Science and Technology*, 55, 2344–2350. https://doi.org/10.1007/s13197-018-3130-1.
124. Kusumiyati, Munawar, A.A. and Suhandy, D., 2021. Fast, simultaneous and contactless assessment of intact mango fruit by means of near infrared spectroscopy. *AIMS Agriculture and Food*, 6, pp.172–184. https://doi.org/10.3934/agrfood.2021011
125. Kusumiyati, Sutari, W., Farida, Mubarok, S. and Hamdani, J.S., 2019. Prediction of surface color of 'Crystal' guava using UV-Vis-NIR spectroscopy and multivariate analysis. *IOP Conference Series: Earth and Environmental Science*, 365, p.012026. https://doi.org/10.1088/1755-1315/365/1/012026
126. Kyriacou, M.C., Rouphael, Y., 2018. Towards a new definition of quality for fresh fruits and vegetables. *Scientia Horticulturae*, 234, 463–469. https://doi.org/10.1016/j.scienta.2017.09.046.
127. Lara, M.V., Bonghi, C., Famiani, F., Vizzotto, G., Walker, R.P., Drincovich, M.F., 2020. Stone fruit as biofactories of phytochemicals with potential roles in human nutrition and health. *Frontiers in Plant Science*, 11, 562252. https://doi.org/10.3389/fpls.2020.562252.

128. Lasalvia, M., Capozzi, V., Perna, G., 2022. A comparison of PCA-LDA and PLS-DA techniques for classification of vibrational spectra. *Applied Sciences*, 12, 5345. https://doi.org/10.3390/app12115345.

129. Lee, J., Mattheis, J.P., Rudell, D.R., 2019. High storage humidity affects fruit quality attributes and incidence of fruit cracking in cold-stored 'Royal Gala' apples. *HortScience*, 54, 149–154. https://doi.org/10.21273/HORTSCI13406-18.

130. Lei, F., Yang, Y., Zhang, J., Zhong, J., Yao, L., Chen, J. and Pan, T., 2019. Window optimisation PMSC–PLS with applications to NIR spectroscopic analyses. *Chemometrics and Intelligent Laboratory Systems*, 191, pp.158–167. https://doi.org/10.1016/j.chemolab.2019.07.005

131. Leng, J., Yu, L., Dai, Y., Leng, Y., Wang, C., Chen, Z., Wisniewski, M., Wu, X., Liu, J., Sui, Y., 2023. Recent advances in research on biocontrol of postharvest fungal decay in apples. *Critical Reviews in Food Science and Nutrition*, 63, 10607–10620. https://doi.org/10.1080/10408398.2022.2080638.

132. Li, B., Cobo-Medina, M., Lecourt, J., Harrison, N., Harrison, R.J. and Cross, J.V., 2018. Application of hyperspectral imaging for nondestructive measurement of plum quality attributes. *Postharvest Biology and Technology*, 141, pp.8-15. https://doi.org/10.1016/j.postharvbio.2018.03.008

133. Li, C., Li, L., Wu, Y., Lu, M., Yang, Y. and Li, L., 2018. Apple variety identification using near-infrared spectroscopy. *Journal of Spectroscopy*, 2018, pp.1–7. https://doi.org/10.1155/2018/6935197

134. Lidster, P. 1990. Storage humidity influences fruit quality and permeability to ethane in 'McIntosh' apples stored in diverse controlled atmospheres. *Journal of the American Society for Horticultural Science*, *115*(1), 94–96. https://doi.org/10.21273/JASHS.115.1.94

135. Li, H., Huang, Z., Addo, K.A., Yu, Y., 2022. Evaluation of postharvest quality of plum (*Prunus salicina* L. cv. 'French') treated with layer-by-layer edible coating during storage. *Scientia Horticulturae*, 304, 111310. https://doi.org/10.1016/j.scienta.2022.111310.

136. Li, J., Huang, W., Zhao, C., Zhang, B., 2013. A comparative study for the quantitative determination of soluble solids content, pH, and firmness of pears by Vis/NIR spectroscopy. *Journal of Food Engineering*, 116, 324–332. https://doi.org/10.1016/j.jfoodeng.2012.11.007.

137. Li, L., Jia, X., Fan, K., 2024. Recent advance in nondestructive imaging technology for detecting quality of fruits and vegetables: A review. *Critical Reviews in Food Science and Nutrition*, 1–19. https://doi.org/10.1080/10408398.2024.2404639.

138. Li, M., Han, D. and Liu, W., 2019. Non-destructive measurement of soluble solids content of three melon cultivars using portable visible/near infrared spectroscopy. *Biosystems Engineering*, 188, pp.31–39. https://doi.org/10.1016/j.biosystemseng.2019.10.003

139. Li, Q., Leng, C.Z., Wang, S.X., Li, X.H., Chen, L., Li, Y.Y., Chen, H.H., Huang, X.H., Hao, M.M., 2014. Effect of different temperatures on storage quality of fresh-cut apples. *Advanced Materials Research*, 941–944, 1188–1191. https://doi.org/10.4028/www.scientific.net/AMR.941-944.1188.

140. Lipton, W.J., 2011. Postharvest biology of fresh asparagus, in: Janick, J. (Ed.), *Horticultural Reviews*. John Wiley & Sons, Inc., Hoboken, NJ, USA, pp. 69–155. https://doi.org/10.1002/9781118060858.ch2.

141. Liu, D., Sun, D.-W. and Zeng, X.-A., 2014. Recent advances in wavelength selection techniques for hyperspectral image processing in the food industry. *Food and Bioprocess Technology*, 7, pp.307–323. https://doi.org/10.1007/s11947-013-1193-6

142. Liu, D., Wang, E., Wang, G. and Ma, G., 2022. Nondestructive determination of soluble solids content, firmness, and moisture content of "Longxiang" pears during maturation using near-infrared spectroscopy. *Food Processing and Preservation*, 46. https://doi.org/10.1111/jfpp.16332

143. Liu, Q., Chen, S., Zhou, D., Ding, C., Wang, J., Zhou, H., Tu, K., Pan, L., Li, P., 2021. Nondestructive detection of weight loss rate, surface color, vitamin C content, and firmness in mini-Chinese cabbage with nanopackaging by Fourier transform-near infrared spectroscopy. *Foods*, 10, 2309. https://doi.org/10.3390/foods10102309.

144. Liu, Q., Xin, D., Xi, L., Gu, T., Jia, Z., Zhang, B., Kou, L., 2022. Novel applications of exogenous melatonin on cold stress mitigation in postharvest cucumbers. *Journal of Agriculture and Food Research*, 10, 100459. https://doi.org/10.1016/j.jafr.2022.100459.

145. Liu, Y., Zhang, Y., Jiang, X., Liu, H., 2020. Detection of the quality of juicy peach during storage by visible/near infrared spectroscopy. *Vibrational Spectroscopy*, 111, 103152. https://doi.org/10.1016/j.vibspec.2020.103152.

146. Lockman, N.A., Hashim, N., Onwude, D.I., 2019. Laser-based imaging for cocoa pods maturity detection. *Food Bioprocess Technology*, 12, 1928–1937. https://doi.org/10.1007/s11947-019-02350-7.

147. Løkke, M.M., Seefeldt, H.F., Edwards, G., Green, O., 2011. Novel wireless sensor system for monitoring oxygen, temperature and respiration rate of horticultural crops post harvest. *Sensors*, 11, 8456–8468. https://doi.org/10.3390/s110908456.

148. Lorente, D., Zude, M., Idler, C., Gómez-Sanchis, J., Blasco, J., 2015. Laser-light backscattering imaging for early decay detection in citrus fruit using both a statistical and a physical model. *Journal of Food Engineering*, 154, 76–85. https://doi.org/10.1016/j.jfoodeng.2015.01.004.

149. Lorente, D., Zude, M., Regen, C., Palou, L., Gómez-Sanchis, J., Blasco, J., 2013. Early decay detection in citrus fruit using laser-light backscattering imaging. *Postharvest Biology and Technology*, 86, 424–430. https://doi.org/10.1016/j.postharvbio.2013.07.021.

150. Lu, R. (Ed.), 2017. *Light Scattering Technology for Food Property, Quality and Safety Assessment*, 0 ed. CRC Press. https://doi.org/10.1201/b20220.

151. Lu, R., 2004. Multispectral imaging for predicting firmness and soluble solids content of apple fruit. *Postharvest Biology and Technology*, 31, 147–157. https://doi.org/10.1016/j.postharvbio.2003.08.006.

152. Lu, R. 2009. Spectroscopic technique for measuring the texture of horticultural products: Spatially resolved. In M. Zude (Ed.), *Optical monitoring of fresh and processed agricultural crops, vol. 450* (p. 391). Boca Raton: CRC.

153. Lu, W.C., Cheng, Y.T., Lai, C.J. Chiang, B.H, Huang, Li, P.H., 2023. Mathematical modeling of modified atmosphere package/LDPE film combination and its application to design breathing cylinders for extending the shelf life of green asparagus. *Chemical and Biological Technologies in Agriculture*, 10(60). https://doi.org/10.1186/s40538-023-00386-8

154. Luo, W., Tian, P., Fan, G., Dong, W., Zhang, H. and Liu, X., 2022. Non-destructive determination of four tea polyphenols in fresh tea using visible and near-infrared spectroscopy. *Infrared Physics & Technology*, 123, p.104037. https://doi.org/10.1016/j.infrared.2022.104037

155. Luo, Z., Xie, J., Xu, T., Zhang, L., 2009. Delay ripening of 'Qingnai' plum (*Prunus salicina* Lindl.) with 1-methylcyclopropene. *Plant Science*, 177, 705–709. https://doi.org/10.1016/j.plantsci.2009.08.013.

156. Magwaza, L.S., Opara, U.L., Nieuwoudt, H., Cronje, P.J.R., Saeys, W., Nicolaï, B., 2012. NIR spectroscopy applications for internal and external quality analysis of citrus fruit—A review. *Food Bioprocess Technology*, 5, 425–444. https://doi.org/10.1007/s11947-011-0697-1.

157. Mahayothee, B., Rungpichayapichet, P., Yuwanbun, P., Khuwijitjaru, P., Nagle, M. and Müller, J., 2020. Temporal changes in the spatial distribution of physicochemical properties during postharvest ripening of mango fruit. *Food Measure*, 14, pp.992–1001. https://doi.org/10.1007/s11694-019-00348-5

158. Manganaris, G.A., Vicente, A.R., Crisosto, C.H., 2008. Effect of pre-harvest and post-harvest conditions and treatments on plum fruit quality. *CABI Reviews*. https://doi.org/10.1079/PAVSNNR20083009.

159. Mariani, N.C.T., Da Costa, R.C., De Lima, K.M.G., Nardini, V., Cunha Júnior, L.C., Teixeira, G.H.D.A., 2014. Predicting soluble solid content in intact jaboticaba [*Myrciaria jaboticaba* (Vell.) O. Berg] fruit using near-infrared spectroscopy and chemometrics. *Food Chemistry*, 159, 458–462. https://doi.org/10.1016/j.foodchem.2014.03.066.

160. Martins, D.R., Barbosa, N.C. and Resende, E.D., 2014. Respiration rate of Golden papaya stored under refrigeration and with different controlled atmospheres. *Scientia Agricola*, 71(5), pp.369–373: https://doi.org/10.1590/0103-9016-2013-0334

161. Martineli, M., Castricini, A., Empresa de Pesquisa Agropecuária de Minas Gerais, Maia, V.M., Universidade Estadual de Montes Claros and Maranhão, C.M.D.A., Universidade Estadual de Montes Claros, 2021. Post-harvest physiology of pitaya at different ripening stages. *Semina: Ciências Agrárias*, 42, pp.1033–1048. https://doi.org/10.5433/1679-0359.2021v42n3p1033

162. Martineli, M., Castricini, A., Oliveira Santos, J.L., Pereira, L.D. and Maida De Albuquerque Maranhão, C., 2022. Quality of *Butia capitata* fruits harvested at different maturity stages. *Agronomía Colombiana*, 40, pp.69–76. https://doi.org/10.15446/agron.colomb.v40n1.99651

163. Mason-D'Croz, D., Bogard, J.R., Sulser, T.B., Cenacchi, N., Dunston, S., Herrero, M., Wiebe, K., 2019. Gaps between fruit and vegetable production, demand, and recommended consumption at global and national levels: an integrated modelling study. *The Lancet Planetary Health*, 3, e318–e329. https://doi.org/10.1016/S2542-5196(19)30095-6.

164. Matabura, V.V., 2022. Modelling of firmness variability of Jonagold apple during postharvest storage. *Journal of Food Science Technology*, 59, 1487-1498. https://doi.org/10.1007/s13197-021-05159-5

165. Matsumoto, K., Sato, S., Fujita, T., Kougo, T. and Kobayashi, T., 2021. Physiological characterization of the yellow-skinned 'Koukou' apples (*Malus* × *domestica* Borkh.) retaining green color with low Brix values, and approaches for decreasing their production. *European Journal of Horticultural Science*, 86, pp.441-449. https://doi.org/10.17660/eJHS.2021/86.4.12
166. Megías, Z., Manzano, S., Martínez, C., Barrera, A., Garrido, D., Valenzuela, J.L., Jamilena, M., 2015. Effects of 1-MCP on different postharvest quality parameters in zucchini. *Acta Horticulturae*, 83–89. https://doi.org/10.17660/ActaHortic.2015.1091.9.
167. Melnyk, O., Drozd, O., Boicheva, N., Zhmudenko, Y., Melnyk, I., Khudik, L., Remeniuk, L., Vykhvatniuk, L., 2014. Ethylene emission of apples treated with 1-methylcyclopropene during storage. *Journal of Horticultural Research*, 22, 109–112. https://doi.org/10.2478/johr-2014-0013.
168. Meng, Q., Shang, J., Huang, R. and Zhang, Y., 2021. Determination of soluble solids content and firmness in plum using hyperspectral imaging and chemometric algorithms. *Journal of Food Process Engineering*, 44, p.e13597. https://doi.org/10.1111/jfpe.13597
169. Mireei, S.A., Mohtasebi, S.S., Massudi, R., Rafiee, S., Arabanian, S., Berardinelli, A., 2010. Non-destructive measurement of moisture and soluble solids content of Mazafati date fruit by NIR spectroscopy. *Australian Journal of Crop Science*, 4, 175–179.
170. Mishra, P., Brouwer, B., Meesters, L., 2022. Improved understanding and prediction of pear fruit firmness with variation partitioning and sequential multi-block modelling. *Chemometrics and Intelligent Laboratory Systems*, 222, 104517. https://doi.org/10.1016/j.chemolab.2022.104517.
171. Mishra, P., Rutledge, D.N., Roger, J.-M., Wali, K. and Khan, H.A., 2021. Chemometric pre-processing can negatively affect the performance of near-infrared spectroscopy models for fruit quality prediction. *Talanta*, 229, p.122303. https://doi.org/10.1016/j.talanta.2021.122303
172. Moggia, C., Graell, J., Lara, I., González, G. and Lobos, G.A., 2017. Firmness at harvest impacts postharvest fruit softening and internal browning development in mechanically damaged and non-damaged highbush blueberries (*Vaccinium corymbosum* L.). *Frontiers in Plant Science*, 8, p.535. https://doi.org/10.3389/fpls.2017.00535
173. Mohd Ali, M., Hashim, N., Bejo, S.K., Shamsudin, R., 2017. Determination of the difference on color changes of watermelons by laser light backscattering imaging. *Journal of Food Science Technology,* 54, 3650-3657. https://doi.org/10.1007/s13197-017-2826-y

174. Mollazade, K., Omid, M., Tab, F.A., Mohtasebi, S.S., 2012. Principles and applications of light backscattering imaging in quality evaluation of agro-food products: a review. *Food Bioprocess Technology*, 5, 1465–1485. https://doi.org/10.1007/s11947-012-0821-x.

175. Mozaffari, M., Sadeghi, S., Asefi, N., 2022. Prediction of the quality properties and maturity of apricot by laser light backscattering imaging. *Postharvest Biology and Technology*, 186, 111842. https://doi.org/10.1016/j.postharvbio.2022.111842.

176. Ncama, K., Magwaza, L.S., 2022. Application of spectroscopy for assessing quality and safety of fresh horticultural produce, in: *Nondestructive Quality Assessment Techniques for Fresh Fruits and Vegetables*. Springer Nature Singapore, Singapore, pp. 85–102. https://doi.org/10.1007/978-981-19-5422-1_5.

177. Neri, L., Santarelli, V., Di Mattia, C.D., Sacchetti, G., Faieta, M., Mastrocola, D., Pittia, P., 2019. Effect of Dipping and Vacuum Impregnation Pretreatments on the Quality of Frozen Apples: A Comparative Study on Organic and Conventional Fruits. *Journal of Food Science*, 84, 798-806

178. Nguyen, C.-N., Lam, V.-L., Le, P.-H., Ho, H.-T. and Nguyen, C.-N., 2022. Early detection of slight bruises in apples by cost-efficient near-infrared imaging. *International Journal of Electrical and Computer Engineering (IJECE)*, 12, p.349. https://doi.org/10.11591/ijece.v12i1.pp349-357

179. Nguyen, L.L.P., Baranyai, L., Nagy, D., Mahajan, P.V., Zsom-Muha, V. and Zsom, T., 2021. Color analysis of horticultural produces using hue spectra fingerprinting. *MethodsX*, 8(2-3), p.101594. https://doi.org/10.1016/j.mex.2021.101594 .

180. Nguyen, N.H., Michaud, J., Mogollon, R., Zhang, H., Hargarten, H., Leisso, R., Torres, C.A., Honaas, L., Ficklin, S., 2024. Rating pome fruit quality traits using deep learning and image processing. *Plant Direct*, 8, e70005. https://doi.org/10.1002/pld3.70005.

181. Nicolaï, B.M., Beullens, K., Bobelyn, E., Peirs, A., Saeys, W., Theron, K.I., Lammertyn, J., 2007. Nondestructive measurement of fruit and vegetable quality by means of NIR spectroscopy: A review. *Postharvest Biology and Technology*, 46, 99–118. https://doi.org/10.1016/j.postharvbio.2007.06.024.

182. Nikzadfar, M., Rashvand, M., Zhang, H., Shenfield, A., Genovese, F., Altieri, G., Matera, A., Tornese, I., Laveglia, S., Paterna, G., Lovallo, C., Mammadov, O., Aykanat, B. and Di Renzo, G.C., 2024. Hyperspectral imaging aiding artificial intelligence: A reliable approach for food qualification and safety. *Applied Sciences*, 14, p.9821. https://doi.org/10.3390/app14219821

183. Noh, H.K., Lu, R., 2007. Hyperspectral laser-induced fluorescence imaging for assessing apple fruit quality. *Postharvest Biology and Technology*, 43, 193–201. https://doi.org/10.1016/j.postharvbio.2006.09.006.

184. Okere, E.E., Ambaw, A., Perold, W.J. and Opara, U.L., 2023. Vis-NIR and SWIR hyperspectral imaging method to detect bruises in pomegranate fruit. *Frontiers in Plant Science*, 14, p.1151697. https://doi.org/10.3389/fpls.2023.1151697

185. Orihuel-Iranzo, B., Miranda, M., Zacarías, L., Lafuente, M.T., 2010. Temperature and ultra low oxygen effects and involvement of ethylene in chilling injury of 'Rojo Brillante' persimmon fruit. *Food Science and Technology International*, 16, 159–167. https://doi.org/10.1177/1082013209353221.

186. Ozturk, B., Yıldız, K., Ozkan, Y., 2015. Effects of Pre-Harvest Methyl Jasmonate Treatments on Bioactive Compounds and Peel Color Development of 'Fuji' Apples. *International Journal of Food Properties*, 18, 954-962. https://doi.org/10.1080/10942912.2014.911312

187. Pandiselvam, R., Prithviraj, V., Manikantan, M.R., Kothakota, A., Rusu, A.V., Trif, M. and Mousavi Khaneghah, A., 2022. Recent advancements in NIR spectroscopy for assessing the quality and safety of horticultural products: A comprehensive review. *Frontiers in Nutrition*, 9, p.97345. https://doi.org/10.3389/fnut.2022.973457

188. Paz, P., Sánchez, M.-T., Pérez-Marín, D., Guerrero, J.-E., Garrido-Varo, A., 2008. Nondestructive determination of total soluble solid content and firmness in plums using near-infrared reflectance spectroscopy. *Journal of Agricultural and Food Chemistry*, 56, 2565–2570. https://doi.org/10.1021/jf073369h.

189. Pegiou, E., Mumm, R., Acharya, P., De Vos, R.C.H., Hall, R.D., 2019. Green and white asparagus (*Asparagus officinalis*): A source of developmental, chemical and urinary intrigue. *Metabolites*, 10, 17. https://doi.org/10.3390/metabo10010017.

190. Peng, Lu, 2006. New approaches of analyzing multispectral scattering profiles for predicting apple fruit firmness and soluble solids content, in: *2006 Portland, Oregon, July 9-12, 2006*. Presented at the 2006 Portland, Oregon, July 9-12, 2006, American Society of Agricultural and Biological Engineers. https://doi.org/10.13031/2013.21559.

191. Peng, Lu, 2005. Modeling multispectral scattering profiles for prediction of apple fruit firmness. *Transactions of the ASAE*, 48, 235–242. https://doi.org/10.13031/2013.17923.

192. Perez, D., Sanchez, M.T., Cano, G., Garrido, A., 2002. Prediction of texture in green asparagus by near infrared spectroscopy (NIRS). *Journal of Food Quality*, 25, 277–287. https://doi.org/10.1111/j.1745-4557.2002.tb01025.x.

193. Pérez-Marín, D., Paz, P., Guerrero, J.-E., Garrido-Varo, A., Sánchez, M.-T., 2010. Miniature handheld NIR sensor for the on-site non-destructive assessment of post-harvest quality and refrigerated storage behavior in plums. *Journal of Food Engineering*, 99, 294–302. https://doi.org/10.1016/j.jfoodeng.2010.03.002.

194. Pham, T.T., Nguyen, T.B., Dam, M.S., Nguyen, L.L.P., Baranyai, L., 2024. A review of the application of the laser-light backscattering imaging technique to agricultural products. *Agriculture*, 14, 1782. https://doi.org/10.3390/agriculture14101782.

195. Phillips, K.M., McGinty, R.C., Couture, G., Pehrsson, P.R., McKillop, K. and Fukagawa, N.K., 2021. Dietary fiber, starch, and sugars in bananas at different stages of ripeness in the retail market. *PLoS ONE*, 16, e0253366. https://doi.org/10.1371/journal.pone.0253366

196. Pimienta, J.R.-, Oyola, J.L.-, Bote, M.E., Yuste, M.C.A.-, Bernalte, M.J., Velardo, B., Adamez, J.D.-, 2020. Influence of storage period and shelf-life on the incidence of chilling injury and microbial load in "Angeleno" and "Larry Ann" plums. *Emirates Journal of Food and Agriculture*, 376. https://doi.org/10.9755/ejfa.2020.v32.i5.2108.

197. Pokhrel, D.R., Sirisomboon, P., Khurnpoon, L., Posom, J., Saechua, W., 2023. Comparing Machine Learning and PLSDA Algorithms for Durian Pulp Classification Using Inline NIR Spectra. *Sensors*, 23, 5327. https://doi.org/10.3390/s23115327

198. Praiphui, A., Lopin, K.V., Kielar, F., 2023. Construction and evaluation of a low-cost NIR-spectrometer for the determination of mango quality parameters. *Food Measurement*, 17, 4125–4139. https://doi.org/10.1007/s11694-023-01948-y.

199. Prange, R.K., Wright, A.H., 2023. A review of storage temperature recommendations for apples and pears. *Foods*, 12, 466. https://doi.org/10.3390/foods12030466.

200. Pratiwi, E.Z.D., Pahlawan, M.F.R., Rahmi, D.N., Amanah, H.Z., Masithoh, R.E., 2023. Non-destructive evaluation of soluble solid content in fruits with various skin thicknesses using visible–shortwave near-infrared spectroscopy. *Open Agriculture*, 8, 20220183. https://doi.org/10.1515/opag-2022-0183.

201. Priss, O., Hutsol, T., Glowacki, S., Bulhakov, P., Bakhlukova, K., Osokina, N., Nurek, T., Horetska, I. and Mykhailova, L., 2024. Effect of asparagus chitosan-rutin coating on losses and

waste reduction during storage. *Agricultural Engineering*, 28, pp.99–118. https://doi.org/10.2478/agriceng-2024-0008.

202. Priss, O., Yevlash, V., Zhukova, V., Kiurchev, S., Verkholantseva, V., Kalugina, I., Kolesnichenko, S., Salavelis, A., Zolovska, O. and Bandurenko, H., 2017. Effect of abiotic factors on the respiration intensity of fruit vegetables during storage. *Eastern-European Journal of Enterprise Technologies (EEJET)*, 6, pp.27–34. https://doi.org/10.15587/1729-4061.2017.117617
203. Qin, J., Lu, R., 2008. Measurement of the optical properties of fruits and vegetables using spatially resolved hyperspectral diffuse reflectance imaging technique. *Postharvest Biology and Technology*, 49, 355–365. https://doi.org/10.1016/j.postharvbio.2008.03.010.
204. Qing, Ji, B., Zude, M., 2007a. Wavelength selection for predicting physicochemical properties of apple fruit based on near-infrared spectroscopy. *Journal of Food Quality*, 30, 511–526. https://doi.org/10.1111/j.1745-4557.2007.00139.x.
205. Qing, Z., Ji, B., Zude, M., 2008. Non-destructive analyses of apple quality parameters by means of laser-induced light backscattering imaging. *Postharvest Biology and Technology*, 48, 215–222. https://doi.org/10.1016/j.postharvbio.2007.10.004.
206. Qing, Z., Ji, B., Zude, M., 2007b. Predicting soluble solid content and firmness in apple fruit by means of laser light backscattering image analysis. *Journal of Food Engineering*, 82, 58–67. https://doi.org/10.1016/j.jfoodeng.2007.01.016.
207. Rabasco-Vílchez, L., Jiménez-Jiménez, F., Possas, A., Brunner, M., Fleck, C., Pérez-Rodríguez, F., 2024. Evaluating the shelf life of strawberries using a portable Vis-NIR spectrophotometer and a Reflectance Quality Index (RQI). *Postharvest Biology and Technology*, 218, 113189. https://doi.org/10.1016/j.postharvbio.2024.113189.
208. Radzevičius, A., Viškelis, J., Karklelienė, R., Juškevičienė, D., Viškelis, P., 2016. Determination of tomato quality attributes using near infrared spectroscopy and reference analysis. *Zemdirbyste-Agriculture*, 103, 443–448. https://doi.org/10.13080/z-a.2016.103.012.
209. Rajkumar, D., Künnemeyer, R., Kaur, H., Longdell, J., McGlone, A., 2022. Interactions of Linearly Polarized and Unpolarized Light on Kiwifruit Using Aquaphotomics. *Molecules*, 27, 494. https://doi.org/10.3390/molecules27020494
210. Ravikanth, L., Jayas, D.S., White, N.D.G., Fields, P.G., Sun, D.-W., 2017. Extraction of spectral information from hyperspectral data and application of hyperspectral imaging for food

and agricultural products. *Food Bioprocess Technology*, 10, 1–33. https://doi.org/10.1007/s11947-016-1817-8.

211. Ravindra, M.R., Goswami, T.K., 2008. Modelling the respiration rate of green mature mango under aerobic conditions. *Biosystems Engineering*, 99, 239–248. https://doi.org/10.1016/j.biosystemseng.2007.10.005.
212. Rezaei Kalaj, Y., Mollazade, K., Herppich, W., Regen, C., Geyer, M., 2016. Changes of backscattering imaging parameter during plum fruit development on the tree and during storage. *Scientia Horticulturae*, 202, 63–69. https://doi.org/10.1016/j.scienta.2016.02.029.
213. Riccioli, C., Pérez-Marín, D. and Garrido-Varo, A., 2021. Optimizing spatial data reduction in hyperspectral imaging for the prediction of quality parameters in intact oranges. *Postharvest Biology and Technology*, 176, p.111504. https://doi.org/10.1016/j.postharvbio.2021.111504
214. Rinnan, Å., Berg, F.V.D., Engelsen, S.B., 2009. Review of the most common pre-processing techniques for near-infrared spectra. *TrAC Trends in Analytical Chemistry*, 28, 1201–1222. https://doi.org/10.1016/j.trac.2009.07.007.
215. Robertson, J.A., Meredith, F.I., Lyon, B.G., Norton, J.D., 1991. Effect of cold storage on the quality characteristics of "Au-Rubrum" plums. *Journal of Food Quality*, 14, 107–117. https://doi.org/10.1111/j.1745-4557.1991.tb00052.x.
216. Rodríguez, R., Jaramillo, S., Heredia, A., Guillén, R., Jiménez, A., Fernández-Bolaños, J., 2004. Mechanical properties of white and green asparagus: changes related to modifications of cell wall components. *Journal of the Science of Food and Agriculture*, 84, 1478–1486. https://doi.org/10.1002/jsfa.1762.
217. Romano, G., Argyropoulos, D., Gottschalk, K., Cerruto, E., Müller, J., 2010. Influence of colour changes and moisture content during banana drying on laser backscattering. *International Journal of Agricultural & Biological Engineering*, 3. https://doi.org/10.3965/j.issn.1934-6344.2010.02.046-051.
218. Romano, G., Argyropoulos, D., Nagle, M., Khan, M.T., Müller, J., 2012. Combination of digital images and laser light to predict moisture content and color of bell pepper simultaneously during drying. *Journal of Food Engineering*, 109, 438–448. https://doi.org/10.1016/j.jfoodeng.2011.10.037.
219. Romano, G., Argyropoulos, D., Gottschalk, K., Cerruto, E. and Müller, J., 2010. Influence of colour changes and moisture content during banana drying on laser backscattering.

International Journal of Agricultural and Biological Engineering, 3(2), pp.46–51. https://doi.org/10.3965/j.issn.1934-6344.2010.02.046-051

220. Romano, G., Nagle, M., Argyropoulos, D., Müller, J., 2011. Laser light backscattering to monitor moisture content, soluble solid content and hardness of apple tissue during drying. *Journal of Food Engineering*, 104, 657-662. https://doi.org/10.1016/j.jfoodeng.2011.01.026
221. Romano, G., Baranyai, L., Gottschalk, K. and Zude, M., 2008. An approach for monitoring the moisture content changes of drying banana slices with laser light backscattering imaging. *Food and Bioprocess Technology*, 1, pp.410–414. https://doi.org/10.1007/s11947-008-0113-7
222. Rosipal, R., Krämer, N., 2006. Overview and recent advances in partial least squares, in: Saunders, C., Grobelnik, M., Gunn, S., Shawe-Taylor, J. (Eds.), *Subspace, Latent Structure and Feature Selection, Lecture Notes in Computer Science*. Springer Berlin Heidelberg, Berlin, Heidelberg, pp. 34–51. https://doi.org/10.1007/11752790_2.
223. Rudell, D.R., Mattinson, D.S., Fellman, J.K. and Mattheis, J.P., 2000. The progression of ethylene production and respiration in the tissues of ripening 'Fuji' apple fruit. *HortScience*, 35, pp.1300-1303. https://doi.org/10.21273/HORTSCI.35.7.1300
224. Ruiz-López, M.D., García-Villanova Ruiz, B., 2023. Fruits and vegetables, in: *Encyclopedia of Human Nutrition*. Elsevier, pp. 397–411. https://doi.org/10.1016/B978-0-12-821848-8.00124-4.
225. Saad, A., Azam, M.M. and Amer, B.M.A., 2022. Quality analysis prediction and discriminating strawberry maturity with a hand-held Vis–NIR spectrometer. *Food Analytical Methods*, 15, pp.689–699. https://doi.org/10.1007/s12161-021-02166-2
226. Salehi, F., 2020. Recent advances in the modeling and predicting quality parameters of fruits and vegetables during postharvest storage: A review. *International Journal of Fruit Science*, 20, pp.506–520. https://doi.org/10.1080/15538362.2019.1653810
227. Sanad, R.A., Yarlagadda, P. and Karim, A., 2023. An empirical model for predicting the fresh food quality changes during storage. *Foods*, 12, p.2113. https://doi.org/10.3390/foods12112113
228. Sánchez, M.-T., Pérez-Marín, D., Flores-Rojas, K., Guerrero, J.-E., Garrido-Varo, A., 2009. Use of near-infrared reflectance spectroscopy for shelf-life discrimination of green asparagus stored in a cool room under controlled atmosphere. *Talanta*, 78, 530–536. https://doi.org/10.1016/j.talanta.2008.12.004.

229. Sarrwy, S., 2021. Thermal poststorage treatment for maintaining fruit quality and extending storage life of pomegranate 'Wonderful' cultivars. *Egyptian Journal of Chemistry*, 0, pp.0–0. https://doi.org/10.21608/ejchem.2021.77765.3798

230. Sayin, C., Karaman, S., Mencet, M.N., Tascioglu, Y., Karaşahin, I.Y., 2010. Determining the role of cold storage practices for apple marketing in Turkey. *Acta Horticulturae*, 979–987. https://doi.org/10.17660/ActaHortic.2010.877.132.

231. Scheper, R.W.A., Rogers, D.J., Walker, J.T.S., Manning, M.A., Wood, P.N., 2007. The incidence of storage rots after postharvest apple washing. *New Zealand Plant Protection*, 60, 7–14. https://doi.org/10.30843/nzpp.2007.60.4626.

232. Schiavon, A.V., Leivas, G.L.D., Silva, G.F.D., Malgarim, M.B. and Herter, F.G., 2023. Refrigerated storage of blackberry cultivar 'BRS Cainguá' harvested at different ripeness stages. *Revista Ceres*, 70, pp.32–40. https://doi.org/10.1590/0034-737x202370020004

233. Seasholtz, M.B., Kowalski, B.R., 1992. The effect of mean centering on prediction in multivariate calibration. *Journal of Chemometrics*, 6, 103–111. https://doi.org/10.1002/cem.1180060208.

234. Sergio, L., Boari, F., Di Venere, D., Gonnella, M., Cantore, V., Renna, M., 2021. Quality evaluation of wild and cultivated asparagus: A comparison between raw and steamed spears. *Agriculture*, 11, 1213. https://doi.org/10.3390/agriculture11121213.

235. Shafiq, M., Singh, Z., Khan, A.S., 2011. Delayed harvest and cold storage period influence ethylene production, fruit firmness and quality of 'Cripps Pink' apple: Harvest date affects apple cold storage life. *International Journal of Food Science & Technology*, 46, 2520–2529. https://doi.org/10.1111/j.1365-2621.2011.02776.x.

236. Sharma, R., Pal, R., Singh, D., Samuel, D., Sethi, S., & Kumar, A. 2013. Evaluation of heat shrinkable films for shelf life, and quality of individually wrapped Royal Delicious apples under ambient conditions. *Journal of Food Science and Technology, 50*(3), 590–594. https://doi.org/10.1007/s13197-011-0332-1

237. Shen, F., Zhang, B., Cao, C., Jiang, X., 2018. On-line discrimination of storage shelf-life and prediction of post-harvest quality for strawberry fruit by visible and near infrared spectroscopy. *Journal of Food Process Engineering*, 41, e12866. https://doi.org/10.1111/jfpe.12866.

238. Shen, M., Li, H., Zhang, B., Zhang, M., Pu, Y., Chen, A., Zhao, J., 2021. Study on quality model of apple during controlled atmosphere storage based on VIS/NIR spectroscopy, in: *2021 ASABE Annual International Virtual Meeting, July 12-16, 2021*. Presented at the 2021 ASABE

Annual International Virtual Meeting, July 12-16, 2021, American Society of Agricultural and Biological Engineers. https://doi.org/10.13031/aim.202100325.

239. Singh, Z., Khan, A.S., 2010. Physiology of plum fruit ripening. *Stewart Postharvest Review*, 6, 1–10. https://doi.org/10.2212/spr.2010.2.3.

240. Song, D.-J., Chun, S.-W., Kim, M.-J., Park, S.-H., Ahn, C.-K., Mo, C., 2024. Performance improvement of partial least squares regression soluble solid content prediction model based on adjusting distance between light source and spectral sensor according to apple size. *Sensors*, 24, 316. https://doi.org/10.3390/s24020316.

241. Stratton, A.E., Finley, J.W., Gustafson, D.I., Mitcham, E.J., Myers, S.S., Naylor, R.L., Otten, J.J., Palm, C.A., 2021. Mitigating sustainability tradeoffs as global fruit and vegetable systems expand to meet dietary recommendations. *Environmental Research Letters*, 16, 055010. https://doi.org/10.1088/1748-9326/abe25a.

242. Subedi, P.P., Walsh, K.B., Hopkins, D.W., 2012. Assessment of titratable acidity in fruit using short wave near infrared spectroscopy. Part A: Establishing a detection limit based on model solutions. *Journal of Near Infrared Spectroscopy*, 20, 449–457. https://doi.org/10.1255/jnirs.1010.

243. Sun, X., Zhang, H., Pan, Y. and Liu, Y., 2009. Nondestructive measurement of soluble solids content of apple by portable and online near-infrared spectroscopy. In: Jäger, D.S., Wu, H., Jian, S., Jiang, D., Liu, D., Dong, W., Sun, Q. and Xiao, X., eds. *Photonics and Optoelectronics Meetings 2009*, Wuhan, China, p.75140P. https://doi.org/10.1117/12.843390

244. Szparaga, A., Kopeć, A., Czerwińska, E., 2014. Effect of osmotic dehydration and frozen storage on microbiological condition of plums defrosted in vacuum-steam chamber. *Zywnosc Nauka Technologia Jakosc*. https://doi.org/10.15193/zntj/2014/92/137-147.

245. Tasioulas, S., Watson, J., Kasampalis, D.S. and Tsouvaltzis, P., 2024. Postharvest tomato fruit shelf life and quality assessment based on color, firmness and visNIR spectroscopy combined with chemometrics.https://doi.org/10.20944/preprints202412.2315.v1

246. Tian, S., Xu, H., 2023. Mechanical-based and optical-based methods for nondestructive evaluation of fruit firmness. *Food Reviews International*, 39, 4009–4039. https://doi.org/10.1080/87559129.2021.2015376.

247. Tian, S., Xu, H., 2022. Nondestructive methods for the quality assessment of fruits and vegetables considering their physical and biological variability. *Food Engineering Reviews*, 14, 380–407. https://doi.org/10.1007/s12393-021-09300-0.

248. Tokala, V.Y., Singh, Z., Kyaw, P.N., 2022. Postharvest quality of 'Cripps Pink' apple fruit influenced by ethylene antagonists during controlled atmosphere storage with photocatalytic oxidation. *Journal of the Science of Food and Agriculture*, 102, 4484–4490. https://doi.org/10.1002/jsfa.11803.

249. Tomar, M.S. and Pradhan, R.C., 2024. Effect of storage temperatures on physicochemical, textural, bioactive, and microstructure changes in amla fruit. *Food Measure*, 18, pp.9658–9668. https://doi.org/10.1007/s11694-024-02911-1

250. Tong, C., McKay, S.J., Luby, J.J., Beaudry, R., Contreras, C., Nock, J.F. and Watkins, C.B., 2013. Using mixed-effects models to estimate the effect of harvest date and its interactions with post-harvest storage regime on apple fruit firmness. *The Journal of Horticultural Science and Biotechnology*, 88, pp.29–36. https://doi.org/10.1080/14620316.2013.11512932

251. Torrieri, E., Cavella, S. & Masi, P., 2009. Modelling the respiration rate of fresh-cut Annurca apples to develop modified atmosphere packaging. *International Journal of Food Science and Technology*, 44(5), pp.890–899. https://doi.org/10.1111/j.1365-2621.2007.01615.x

252. Träger, F., ed., 2012. *Springer Handbook of Lasers and Optics*. Berlin, Heidelberg: Springer Berlin Heidelberg. https://doi.org/10.1007/978-3-642-19409-2

253. Toscano, S., Rizzo, V., Licciardello, F., Romano, D. and Muratore, G., 2021. Packaging solutions to extend the shelf life of green asparagus (*Asparagus officinalis* L.) 'Vegalim'. *Foods*, 10, p.478. https://doi.org/10.3390/foods10020478

254. Tzoumaki, M.V., Biliaderis, C.G., Vasilakakis, M., 2009. Impact of edible coatings and packaging on quality of white asparagus (*Asparagus officinalis*, L.) during cold storage. *Food Chemistry*, 117, 55–63. https://doi.org/10.1016/j.foodchem.2009.03.076.

255. Udomkun, P., Nagle, M., Mahayothee, B., Müller, J., 2014. Laser-based imaging system for non-invasive monitoring of quality changes of papaya during drying. *Food Control*, 42, 225-233. https://doi.org/10.1016/j.foodcont.2014.02.010

256. Valenzuela, J.Á.L., Valverde Juárez, F.J., Mejía Torres, S.L., López Angulo, G. and Vega García, M.O., 2011. Effect of controlled atmosphere storage on the postharvest and nutritional quality of tomato fruit. *Revista Chapingo Serie Horticultura*, 17, pp.115–128. https://doi.org/10.5154/r.rchsh.2011.17.014

257. Valero, A., Carrasco, E., Pérez-Rodríguez, F., García-Gimeno, R., Blanco, C., Zurera, G., 2006. Monitoring the sensorial and microbiological quality of pasteurized white asparagus at different storage temperatures. *Journal of the Science of Food and Agriculture*, 86, 1281–1288. https://doi.org/10.1002/jsfa.2489.

258. Van Dijk, C., Boeriu, C., Peter, F., Stolle-Smits, T., Tijskens, L.M.M., 2006. The firmness of stored tomatoes (cv. Tradiro). 1. Kinetic and near infrared models to describe firmness and moisture loss. *Journal of Food Engineering*, 77, 575–584. https://doi.org/10.1016/j.jfoodeng.2005.07.029.

259. Vestergaard, R.-J., Vasava, H., Aspinall, D., Chen, S., Gillespie, A., Adamchuk, V., Biswas, A., 2021. Evaluation of optimized preprocessing and modeling algorithms for prediction of soil properties using VIS-NIR spectroscopy. *Sensors*, 21, 6745. https://doi.org/10.3390/s21206745.

260. Vignati, S., Tugnolo, A., Giovenzana, V., Pampuri, A., Casson, A., Guidetti, R., Beghi, R., 2023. Hyperspectral imaging for fresh-cut fruit and vegetable quality assessment: Basic concepts and applications. *Applied Sciences*, 13, 9740. https://doi.org/10.3390/app13179740.

261. Villanueva, M.J., Tenorio, M.D., Sagardoy, M., Redondo, A., Saco, M.D., 2005. Physical, chemical, histological and microbiological changes in fresh green asparagus (*Asparagus officinalis*, L.) stored in modified atmosphere packaging. *Food Chemistry*, 91, 609–619. https://doi.org/10.1016/j.foodchem.2004.06.030.

262. Vitalis, F., Muncan, J., Anantawittayanon, S., Kovacs, Z., Tsenkova, R., 2023. Aquaphotomics monitoring of lettuce freshness during cold storage. *Foods*, 12, 258. https://doi.org/10.3390/foods12020258.

263. Vitalis, F., Tjandra Nugraha, D., Aouadi, B., Aguinaga Bósquez, J.P., Bodor, Z., Zaukuu, J.-L.Z., Kocsis, T., Zsom-Muha, V., Gillay, Z., Kovacs, Z., 2021. Detection of Monilia contamination in plum and plum juice with NIR spectroscopy and electronic tongue. *Chemosensors*, 9, 355. https://doi.org/10.3390/chemosensors9120355.

264. Walsh, K.B., Blasco, J., Zude-Sasse, M., Sun, X., 2020. Visible-NIR 'point' spectroscopy in postharvest fruit and vegetable assessment: The science behind three decades of commercial use. *Postharvest Biology and Technology*, 168, 111246. https://doi.org/10.1016/j.postharvbio.2020.111246.

265. Wang, A., Xie, L., 2014. Technology using near infrared spectroscopic and multivariate analysis to determine the soluble solids content of citrus fruit. *Journal of Food Engineering*, 143, 17-24. https://doi.org/10.1016/j.jfoodeng.2014.06.023

266. Wang, H., Peng, J., Xie, C., Bao, Y., He, Y., 2015. Fruit quality evaluation using spectroscopy technology: A review. *Sensors*, 15, 11889–11927. https://doi.org/10.3390/s150511889.

267. Wang, H., Yuan, J., Chen, L., Ban, Z., Zheng, Y., Jiang, Yuqian, Jiang, Yunbin, Li, X., 2022. Effects of Fruit Storage Temperature and Time on Cloud Stability of Not from Concentrated Apple Juice. *Foods*, 11, 2568. https://doi.org/10.3390/foods11172568

268. Wang, J., Pan, H., Wang, R., Hong, K., Cao, J., 2016. Patterns of flesh reddening, translucency, ethylene production and storability of 'Friar' plum fruit harvested at three maturity stages as affected by the storage temperature. *Postharvest Biology and Technology*, 121, 9–18. https://doi.org/10.1016/j.postharvbio.2016.07.009.

269. Wang, L., Sang, W., Xu, R., Cao, J., 2020. Alteration of flesh color and enhancement of bioactive substances via the stimulation of anthocyanin biosynthesis in 'Friar' plum fruit by low temperature and the removal. *Food Chemistry*, 310, 125862. https://doi.org/10.1016/j.foodchem.2019.125862

270. Wang, L.-X., Choi, I.-L., Kang, H.-M., 2021. Antifungal effects of cold plasma, coupled with modified atmosphere packaging on asparagus during cold storage. *Journal of Soil Management*, 50, 2537–2548. https://doi.org/10.17576/jsm-2021-5009-04.

271. Wang, X., Ouyang, Y., Liu, J., Zhu, M., Zhao, G., Bao, W., Hu, F.B., 2014. Fruit and vegetable consumption and mortality from all causes, cardiovascular disease, and cancer: Systematic review and dose-response meta-analysis of prospective cohort studies. *BMJ*, 349, g4490–g4490. https://doi.org/10.1136/bmj.g4490.

272. Watanabe, T., Sekiyama, Y., Kawamura, T., Fukuda, Y. and Nagata, M., 2023. Tissue structural analysis for internal browning sweet potatoes using magnetic resonance imaging and bio-electrochemical impedance spectroscopy. *Journal of Food Engineering*, 349, p.111451. https://doi.org/10.1016/j.jfoodeng.2023.111451

273. Wei, X., Xie, D., Mao, L., Xu, C., Luo, Z., Xia, M., Zhao, X., Han, X., Lu, W., 2019. Excess water loss induced by simulated transport vibration in postharvest kiwifruit. *Scientia Horticulturae*, 250, 113-120. https://doi.org/10.1016/j.scienta.2019.02.009

274. Weng, S., Yu, S., Guo, B., Tang, P. and Liang, D., 2020. Non-destructive detection of strawberry quality using multi-features of hyperspectral imaging and multivariate methods. *Sensors*, 20, p.3074. https://doi.org/10.3390/s20113074

275. Whale, S.K., Singh, Z., 2007. Endogenous ethylene and color development in the skin of 'Pink Lady' apple. *Journal of the American Society for Horticultural Science*, 132, 20–28. https://doi.org/10.21273/JASHS.132.1.20.

276. Wieme, J., Mollazade, K., Malounas, I., Zude-Sasse, M., Zhao, M., Gowen, A., Argyropoulos, D., Fountas, S., Van Beek, J., 2022. Application of hyperspectral imaging systems and artificial intelligence for quality assessment of fruit, vegetables and mushrooms: A review. *Biosystems Engineering*, 222, 156–176. https://doi.org/10.1016/j.biosystemseng.2022.07.013.

277. Workman, J. Jr. and Weyer, L., 2007. *Practical guide to interpretive near-infrared spectroscopy*. 1st ed. Boca Raton, FL: CRC Press. https://doi.org/10.1201/9781420018318

278. Wu, Z., Ouyang, G., Shi, X., Ma, Q., Wan, G., Qiao, Y., 2014. Absorption and quantitative characteristics of C-H bond and O-H bond of NIR. *Optics and Spectroscopy*, 117, 703–709. https://doi.org/10.1134/S0030400X1411023X.

279. Xia, Y., Zhang, W., Che, T., Hu, J., Cao, S., Liu, W., Kang, J., Tang, W. and Li, H., 2024. Comparison of diffuse reflectance and diffuse transmittance Vis/NIR spectroscopy for assessing soluble solids content in kiwifruit coupled with chemometrics. *Applied Sciences*, 14, p.10001. https://doi.org/10.3390/app142110001

280. Yahia, E.M., García-Solís, P., Celis, M.E.M., 2019. Contribution of fruits and vegetables to human nutrition and health, in: *Postharvest Physiology and Biochemistry of Fruits and Vegetables*. Elsevier, pp. 19–45. https://doi.org/10.1016/B978-0-12-813278-4.00002-6.

281. Yang, Y., Jin, Y., Wu, Y. and Chen, Y., 2016. Application of near infrared spectroscopy combined with competitive adaptive reweighted sampling partial least squares for on-line monitoring of the concentration process of Wangbi tablets. *Journal of Near Infrared Spectroscopy*, 24, pp.171–178. https://doi.org/10.1255/jnirs.1209

282. Yang, Z., Li, M., East, A.R., Zude-Sasse, M., 2021. Application of absorption and scattering properties obtained through image pre-classification method using a laser backscattering imaging system to detect kiwifruit chilling injury. *Foods*, 10, 1446. https://doi.org/10.3390/foods10071446.

283. Yang, Z., Li, M., Zhang, J., Li, J., Zhao, L., 2024. Optical property mapping and early-bruise identification in apples using spatial frequency domain imaging. *Postharvest Biology and Technology*, 217, 113120. https://doi.org/10.1016/j.postharvbio.2024.113120.

284. Yao, Y., Ma, K., Zhu, J., Huang, F., Kuang, L., Wang, X., Li, S., 2023. Non-destructive determination of soluble solids content in intact apples using a self-made portable NIR diffuse reflectance instrument. *Infrared Physics & Technology*, 132, 104714. https://doi.org/10.1016/j.infrared.2023.104714.

285. Yoo, J., Lee, S.-Y., Win, N.M., Kwon, S.-I., Jung, H.-Y., Cho, Y.-J., Kang, I.-K., 2018. Effects of cold storage temperature treatments on fruit quality attributes in "Hongro" apples. *Korean Journal of Food Preservation*, 25, 779–785. https://doi.org/10.11002/kjfp.2018.25.7.779.

286. Yu, Y., Yao, M., 2023. Is this pear sweeter than this apple? A universal SSC model for fruits with similar physicochemical properties. *Biosystems Engineering*, 226, 116–131. https://doi.org/10.1016/j.biosystemseng.2023.01.002.

287. Zareef, M., Chen, Q., Hassan, M.M., Arslan, M., Hashim, M.M., Ahmad, W., Kutsanedzie, F.Y.H. and Agyekum, A.A., 2020. An overview on the applications of typical non-linear algorithms coupled with NIR spectroscopy in food analysis. *Food Engineering Reviews*, 12, pp.173-190. https://doi.org/10.1007/s12393-020-09210-7

288. Zeb, A., Qureshi, W.S., Ghafoor, A., Malik, A., Imran, M., Mirza, A., Tiwana, M.I., Alanazi, E., 2023. Towards sweetness classification of orange cultivars using short-wave NIR spectroscopy. *Scientific Reports*, 13, 325. https://doi.org/10.1038/s41598-022-27297-2.

289. Zeng, S., Zhang, Z., Cheng, X., Cai, X., Cao, M., Guo, W., 2024. Prediction of soluble solids content using near-infrared spectra and optical properties of intact apple and pulp applying PLSR and CNN. *Spectrochimica Acta Part A: Molecular and Biomolecular Spectroscopy*, 304, 123402. https://doi.org/10.1016/j.saa.2023.123402.

290. Zhang, B., Chen, X., Wang, N., Guo, S., Jiang, W., Yu, M., Ma, R., 2022. Effects of harvest maturity on the fruit quality of different flesh-type peach stored at near-freezing point temperature. *Foods*, 11, 2200. https://doi.org/10.3390/foods11152200.

291. Zhang, B., Dai, D., Huang, J., Zhou, J., Gui, Q., and Dai, F. (2018). Influence of physical and biological variability and solution methods in fruit and vegetable quality nondestructive inspection by using imaging and near-infrared spectroscopy techniques: A review, *Critical Reviews in Food Science and Nutrition*, 58(13), pp. 2099–2118. https://doi.org/10.1080/10408398.2017.130078.

292. Zhang, B., Zhang, M., Shen, M., Li, H., Zhang, Z., Zhang, H., Zhou, Z., Ren, X., Ding, Y., Xing, L. and Zhao, J., 2021. Quality monitoring method for apples of different maturity under

long-term cold storage. *Infrared Physics & Technology*, 112, p.103580. https://doi.org/10.1016/j.infrared.2020.103580

293. Zhang, D., Xu, L., Liang, D., Xu, C., Jin, X., Weng, S., 2018. Fast prediction of sugar content in Dangshan pear (*Pyrus spp.*) using hyperspectral imagery data. *Food Analytical Methods*, 11, 2336–2345. https://doi.org/10.1007/s12161-018-1212-3.
294. Zhang, J., Liang, Y., He, L., Kaliaperumal, K., Tan, H., Jiang, Y., Zhong, B. and Zhang, Jun, 2022. Effects of storage time and temperature on the chemical composition and organoleptic quality of Gannan navel orange (*Citrus sinensis* Osbeck cv. Newhall). *Food Measure*, 16, pp.935–944. https://doi.org/10.1007/s11694-021-01218-9
295. Zhao, P., Ndayambaje, J.P., Liu, X. and Xia, X., 2022. Microbial spoilage of fruits: a review on causes and prevention methods. *Food Reviews International*, 38, pp.225–246. https://doi.org/10.1080/87559129.2020.1858859
296. Zhao, Y., Kang, Z., Chen, L., Guo, Y., Mu, Q., Wang, S., Zhao, B., Feng, C., 2023. Quality classification of kiwifruit under different storage conditions based on deep learning and hyperspectral imaging technology. *Food Measurement*, 17, 289–305. https://doi.org/10.1007/s11694-022-01554-4.
297. Zhu, L., Spachos, P., Pensini, E., Plataniotis, K.N., 2021. Deep learning and machine vision for food processing: A survey. *Current Research in Food Science*, 4, 233–249. https://doi.org/10.1016/j.crfs.2021.03.009.
298. Zulkifli, N., Hashim, N., Abdan, K., Hanafi, M., 2019. Application of laser-induced backscattering imaging for predicting and classifying ripening stages of "Berangan" bananas. *Computers and Electronics in Agriculture*, 160, 100–107. https://doi.org/10.1016/j.compag.2019.02.031

Website References

1. FAO, 2025. Global production value of fruits and vegetables. *Food and Agriculture Organization of the United Nations.* https://www.fao.org/faostat/en/#data/QV/ (Accessed: 07/03/ 2025).
2. WHO, 2025. Increasing fruit and vegetable consumption to reduce the risk of noncommunicable diseases. *World Health Organization*. (Accessed: 7 March 2025).

3. Hungarian Central Statistical Office, 2024. Production of main vegetables. *Hungarian Central Statistical Office.* https://www.ksh.hu/stadat_files/mez/en/mez0016.html (accessed on 10/09/2024).
4. Hungarian Central Statistical Office, 2024. Production of main fruits and grapes. *Hungarian Central Statistical Office*. https://www.ksh.hu/stadat_files/mez/en/mez0017.html (accessed on 15/09/2024) .
5. Cantwell, M. and Suslow, T., 2002. Asparagus (Green): Recommendations for maintaining postharvest quality. *Postharvest Research and Extension Center, University of California, Davis*. https://postharvest.ucdavis.edu/produce-facts-sheets/asparagus-green [Accessed 14 Jul. 2025].
6. Cantwell, M. and Suslow, T., 2002. Plum. Recommendations for maintaining postharvest quality. *Postharvest Research and Extension Center, University of California, Davis*. https://postharvest.ucdavis.edu/produce-facts-sheets/plum [Accessed 14 Jul. 2025].

12. APPENDIX

Appendix 12. 1 – Pictures

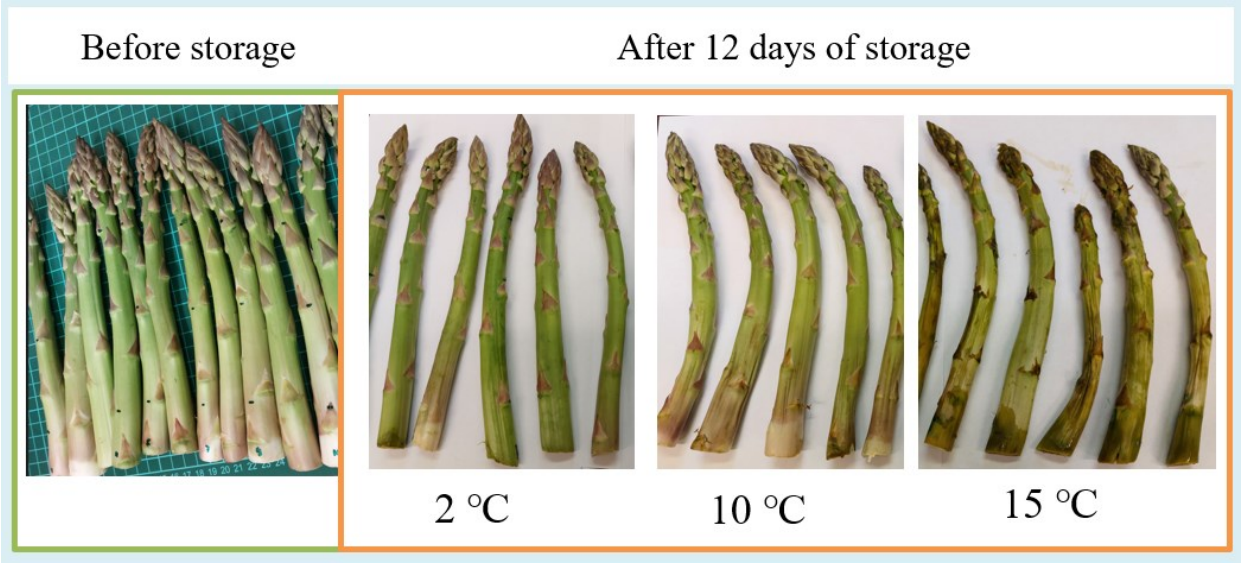

Figure 12.1.1: Green asparagus before storage (left) and exposed at different storage temperatures after 12 days of storage period (right)

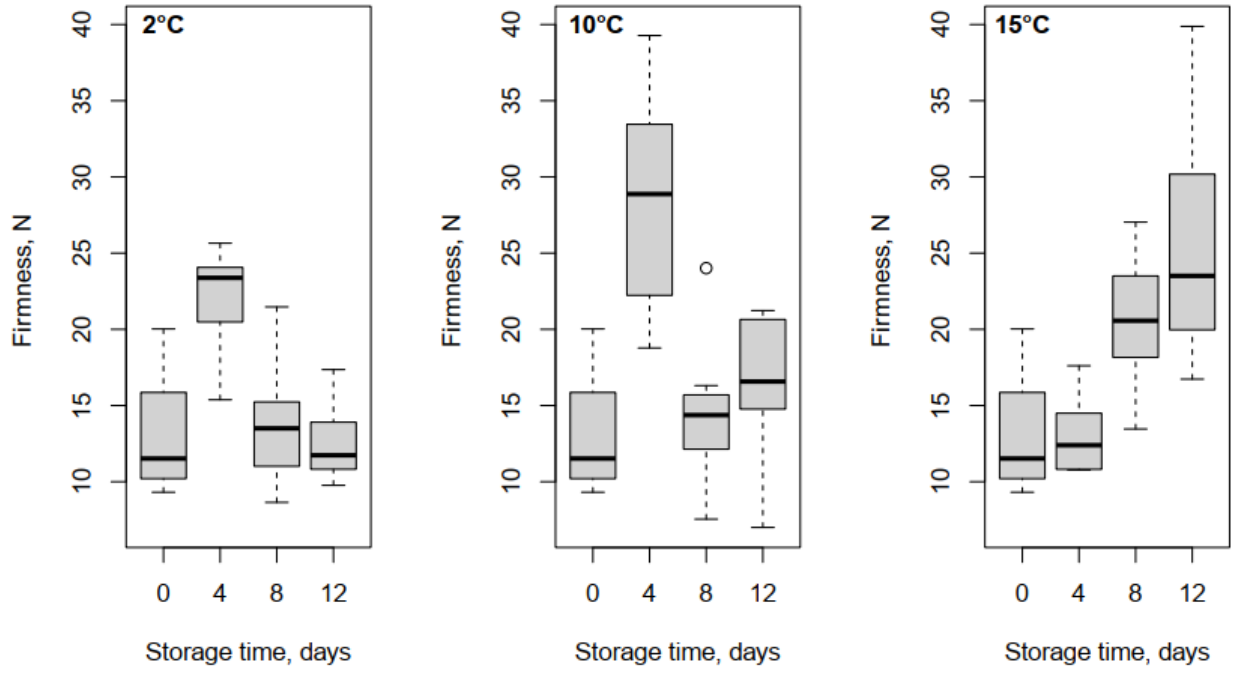

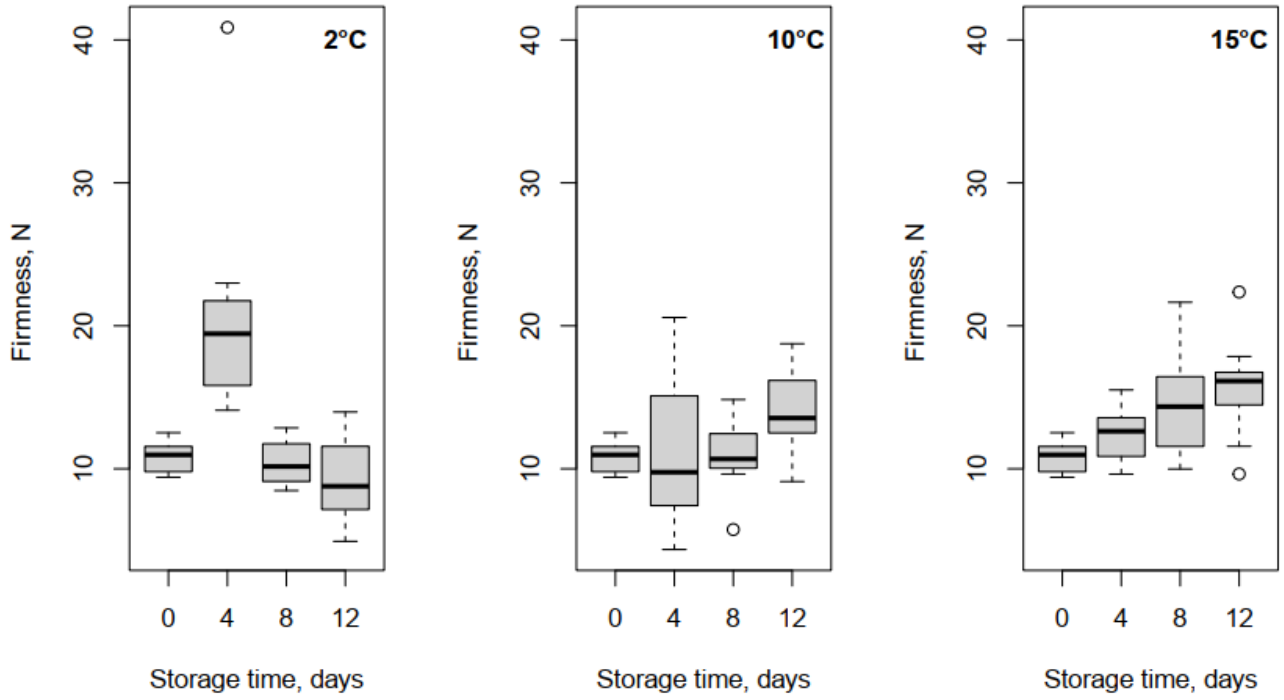

Figure 12.1.2. Changes in firmness of green asparagus after exposure to different temperatures and durations, shown at the middle (top) and peak (bottom) positions of the spears.

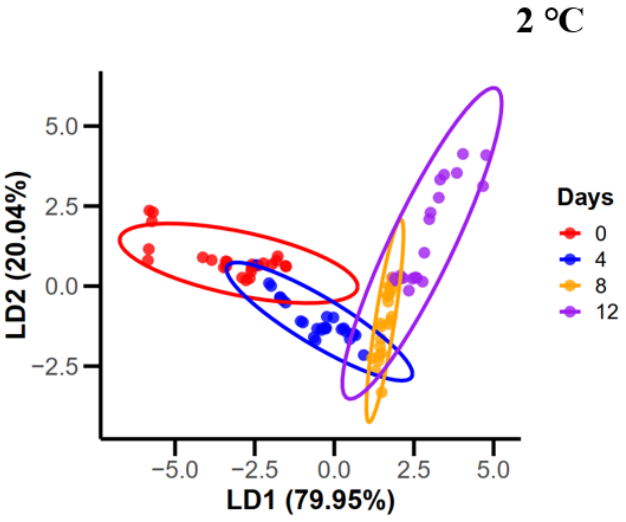

Training set(n=91, LV=3), accuracy= 85.8%

	0d	4d	8d	12d
0d	100	0	0	0
4d	11.5	73.1	15.4	0
8d	0	0	100	0
12d	0	0	23.8	76.2

Validation set (n=23, LV=3), accuracy =81.4%

	0d	4d	8d	12d
0d	100	0	0	0
4d	25	75	0	0
8d	0	0	100	0
12d	0	0	20	80

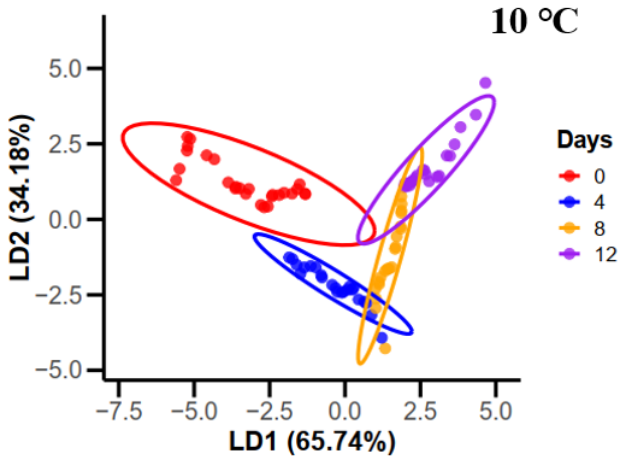

Training set (n=92, LV=3), accuracy= 92.7%

	0d	4d	8d	12d
0d	100	0	0	0
4d	0	100	0	0
8d	0	0	100	0
12d	0	0	28.6	71.4

Validation set (n=24, LV=3), accuracy = 89.6%

	0d	4d	8d	12d
0d	100	0	0	0
4d	0	100	0	0
8d	0	40	60	0
12d	0	0	0	100

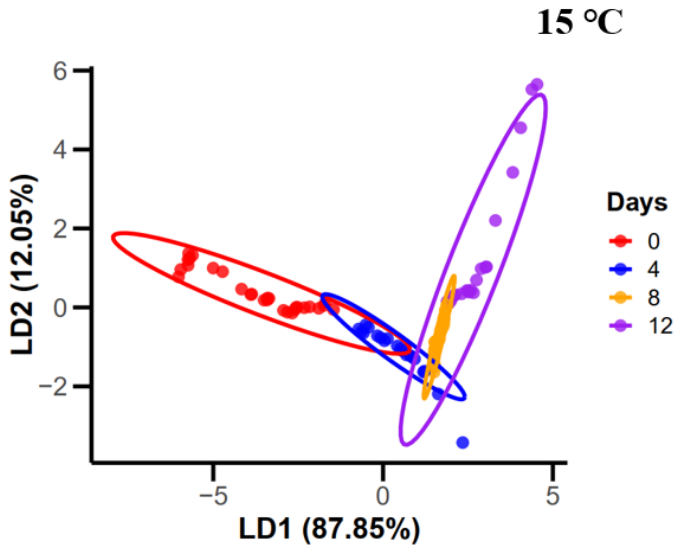

Training set (n=91, LV=3), accuracy=95.6%

	0d	4d	8d	12d
0d	100	0	0	0
4d	0	100	0	0
8d	0	4	96	0
12d	0	0	17.4	82.6

Validation set (n=23,LV=3), accuracy=93.4%

	0d	4d	8d	12d
0d	100	0	0	0
4d	0	83.3	16.7	0
8d	0	0	83.3	16.7
12d	0	0	0	100

Figure 12.1.3. LDA plot (left) of the training set and confusion matrix tables (right) for both training and validation sets, showing classification performance across storage temperature groups for detecting quality changes in green asparagus at 4-day storage intervals using three LLBI parameters.

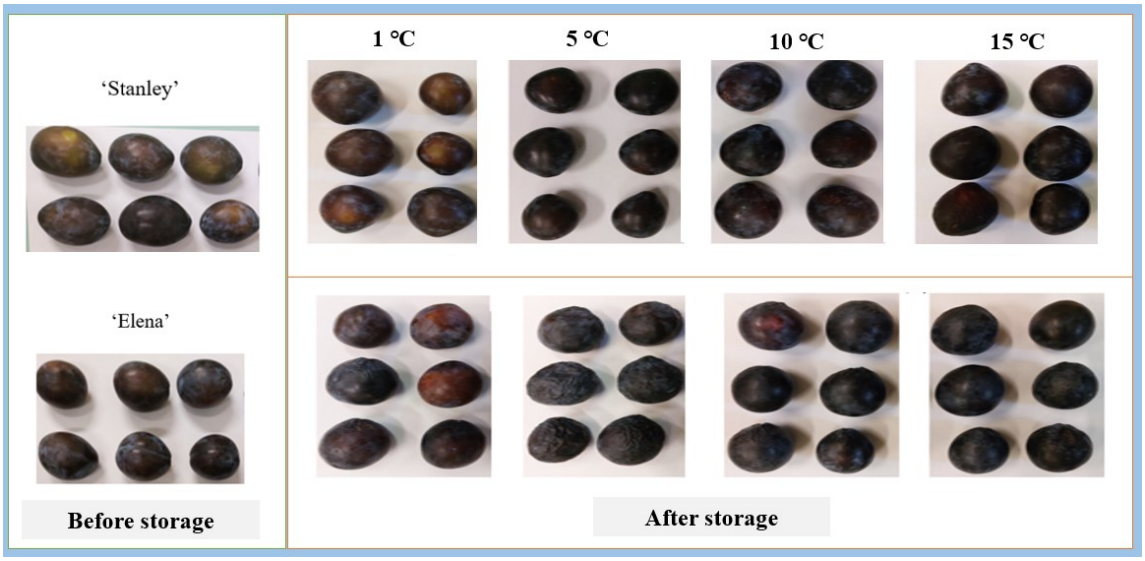

Figure 12.1.4: Photos of plums (top-'Stanley', bottom- Elena') taken before storage (left) and after storage (right) at different temperatures.

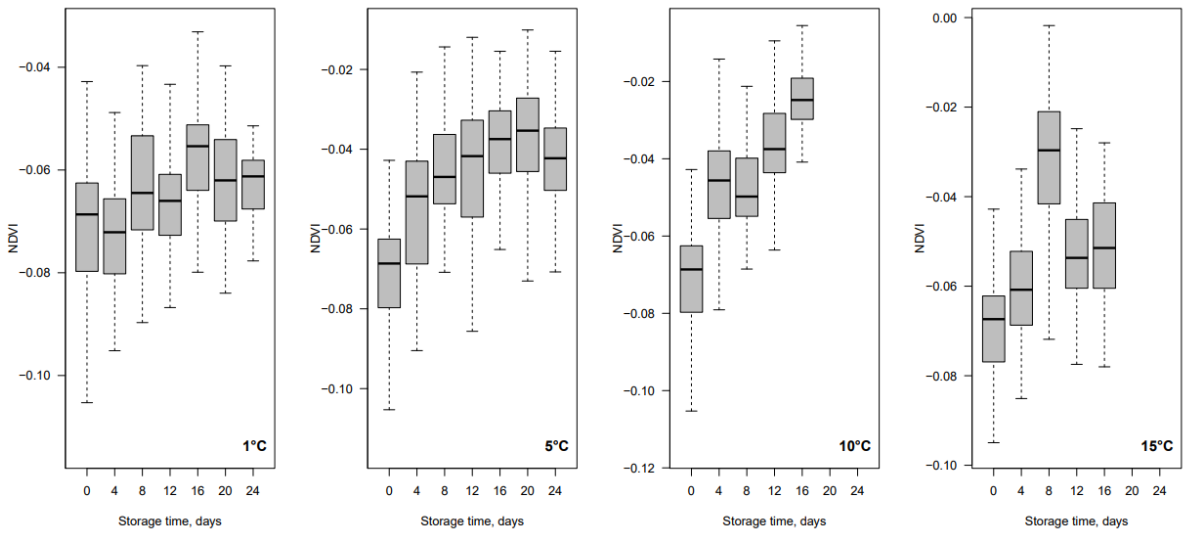

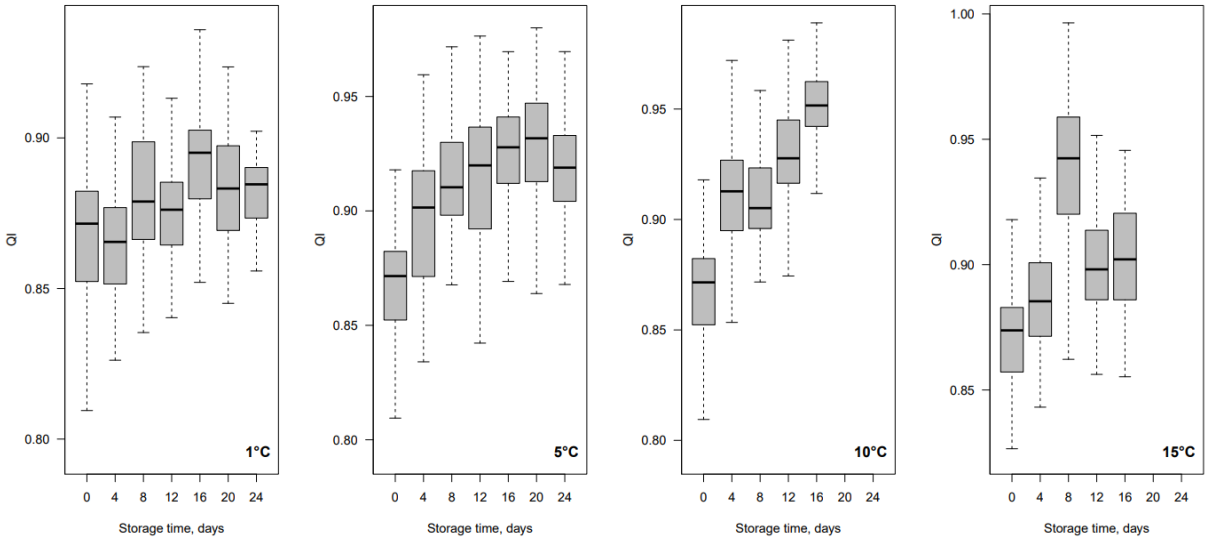

Figure 12.1.5 Changes in sample plums' NDI (top) and QI (bottom) with storage time and temperature at 1650 nm

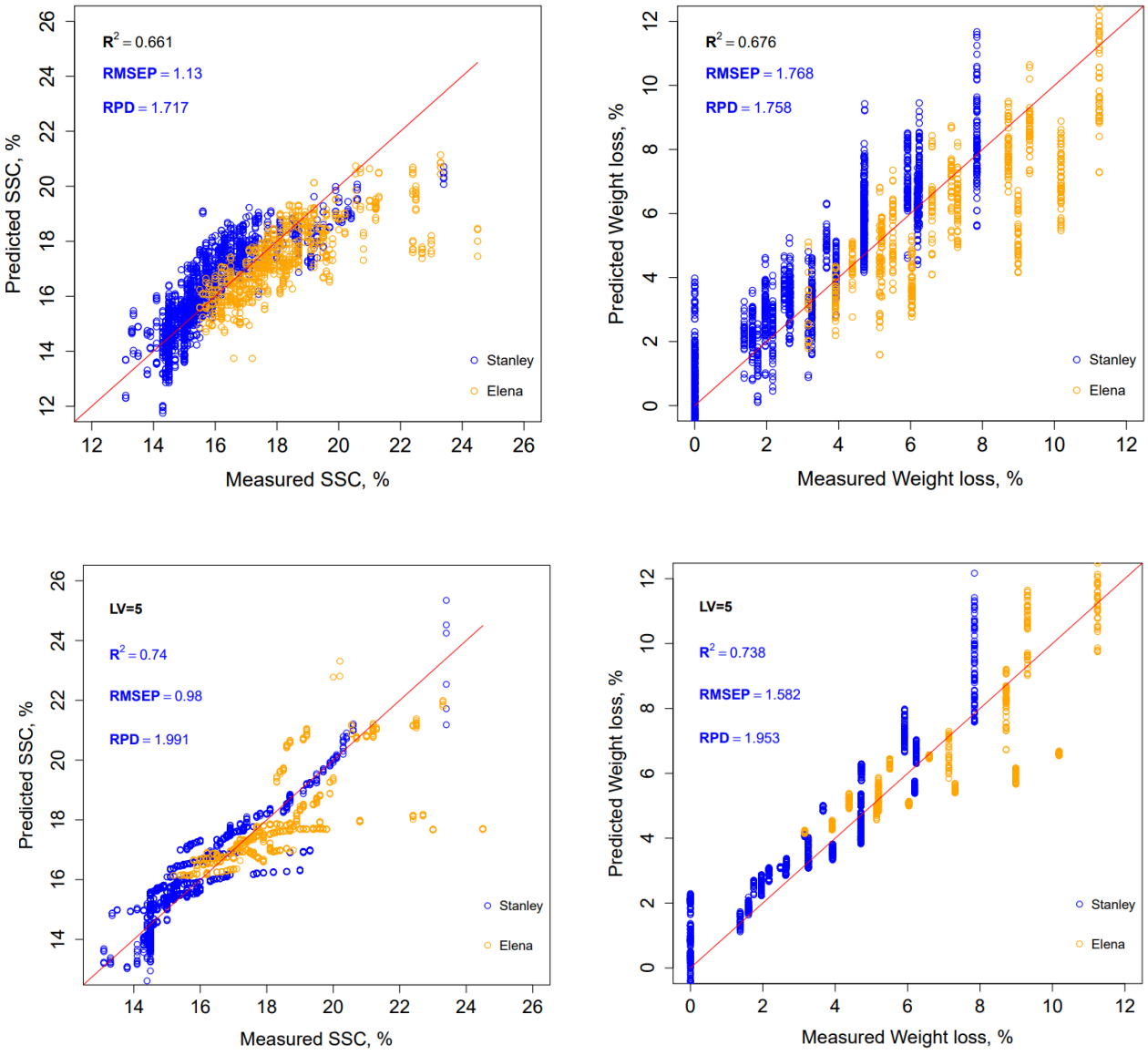

Figure 12.1.6. PLSR model predictions for SSC (left) and WL (right) using full spectra (top) and selected wavelengths (bottom).

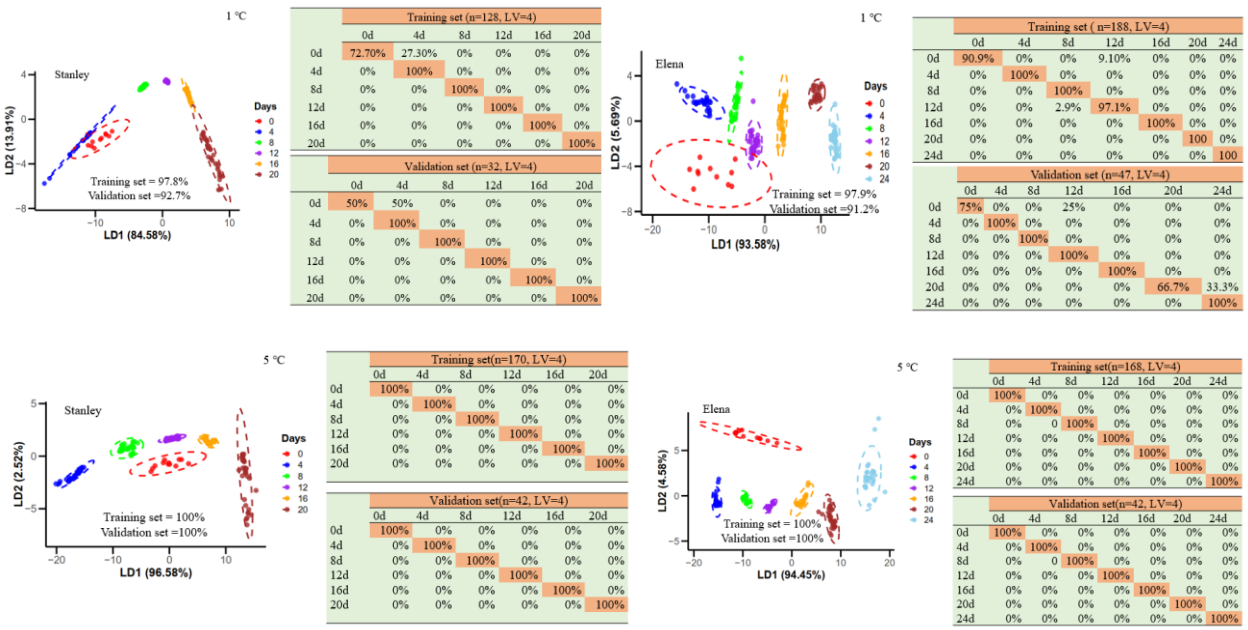

Figure 12.1.7: Cross-validated LDA model performance (left) in detecting quality changes in plum cultivars 'Stanley' and 'Elena' stored at 1 °C (top row) and 5 °C (bottom row), based on four-day storage intervals. The confusion matrix tables (right) summarize the training and validation set accuracies across different storage durations.

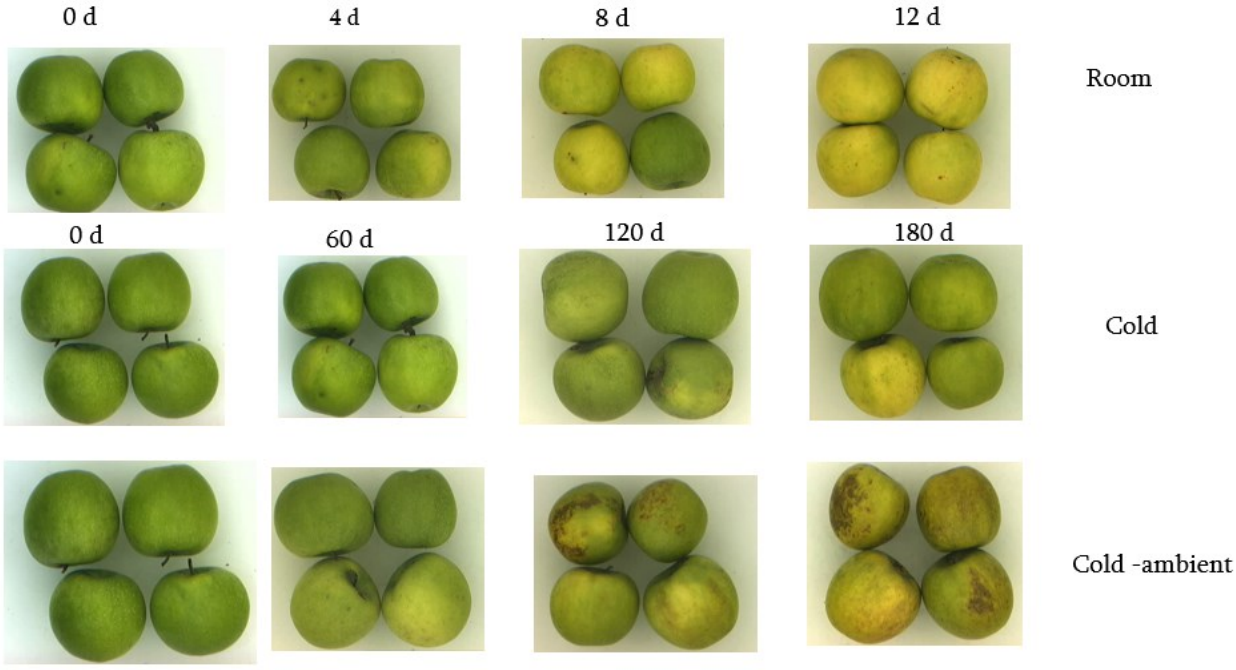

Figure 12.1.8 'Granny Smith' apple stored at room, cold and cold-ambient at room temperature

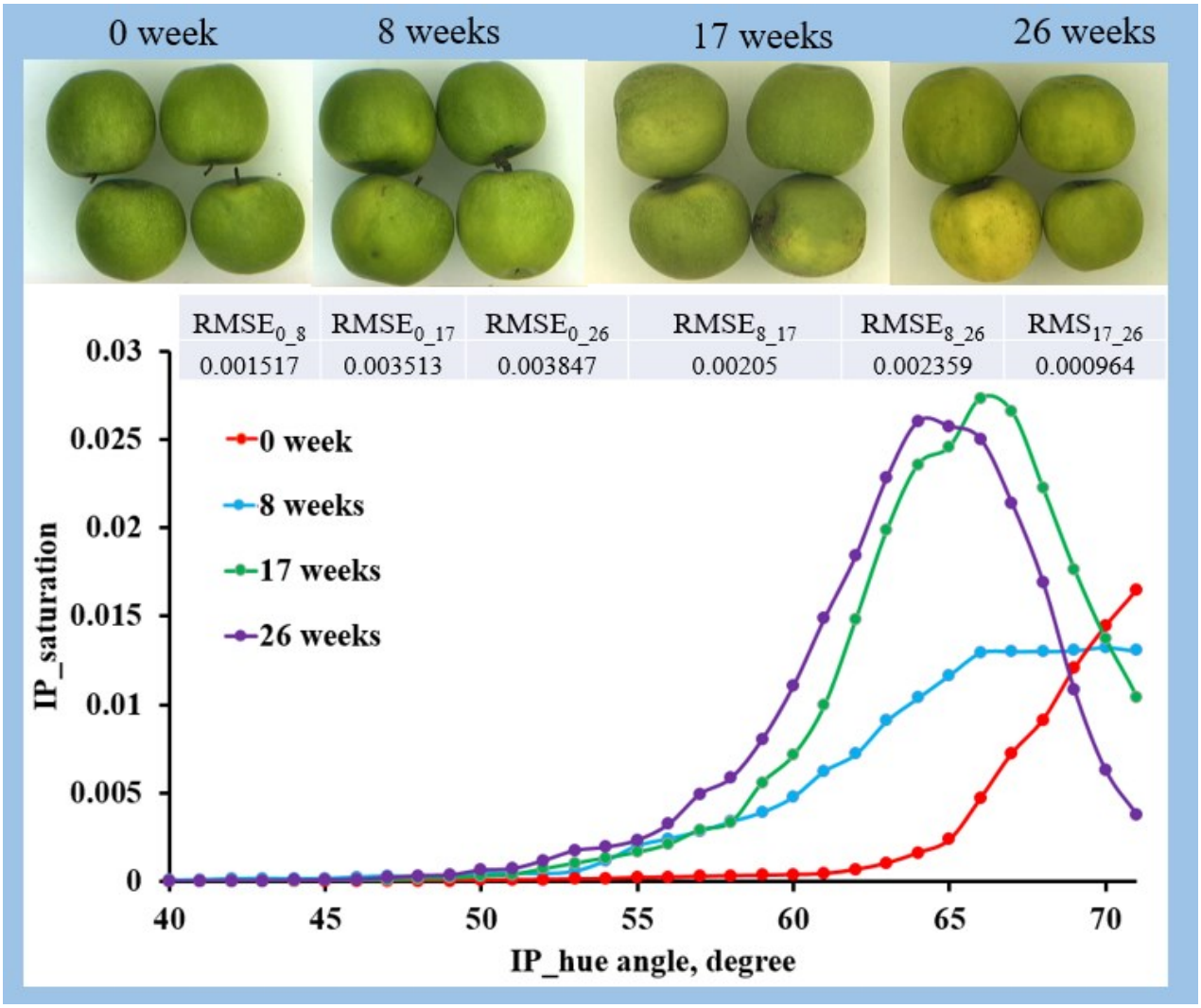

Figure 12.1.9 Changes in skin color and corresponding hue spectra of 'Granny Smith' apples under different storage durations and temperatures: Hue-saturation of samples at storage .

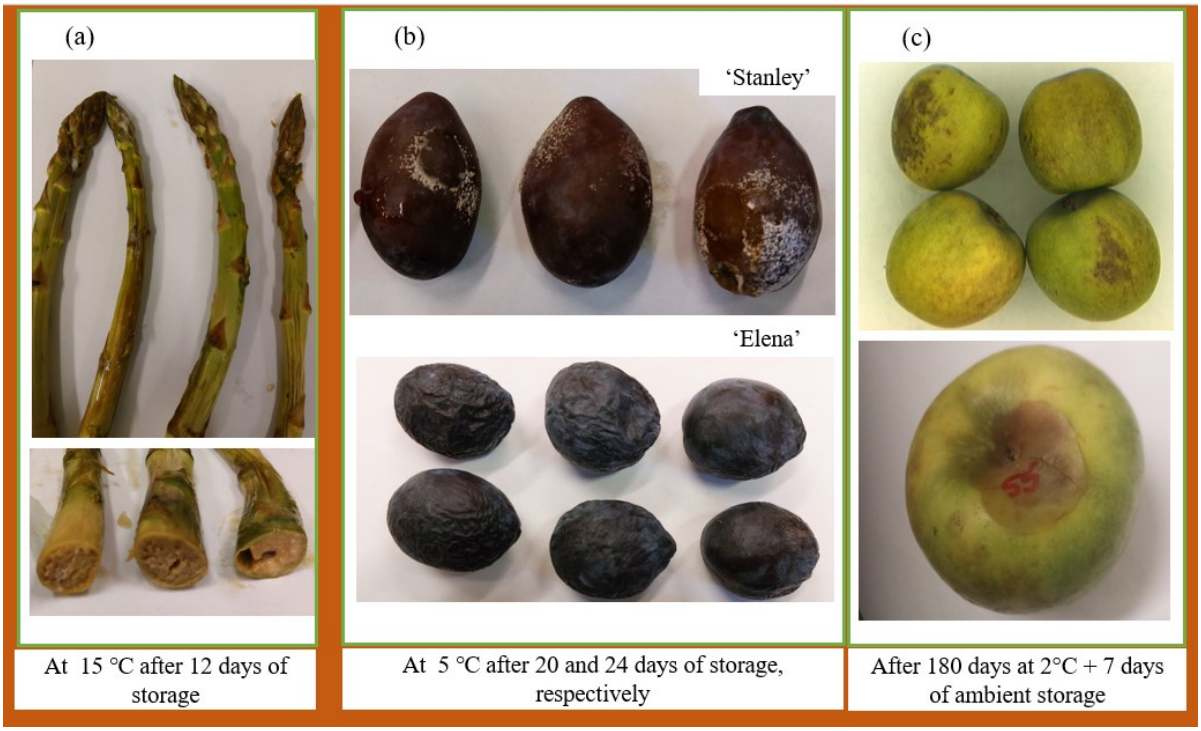

Figure 12.1.10 Decayed green asparagus(a) and plums (b) and 'Granny Smith' apple(c) during Storage

Appendix 12.2 – Tables

Table 12.2.1: Performance metrics for the PLS-DA model, including equations for sensitivity, specificity, precision, accuracy, and F-score.

Equation	Description
$\text{Sensitivity} = \frac{TP}{TP + FN}$	Sensitivity indicates the model's ability to correctly identify true positives out of all positive observations.
$\text{Specificity} = \frac{TN}{TN + FP}$	Specificity is a measure of a model's ability to correctly identify true negatives from all negative observations.
$\text{Precision} = \frac{TP}{TP + FP}$	Precision reflects the accuracy of positive predictions, measuring the ratio of true positives to all predicted positive cases.
$\text{Accuracy} = \frac{(TP + TN)}{(TP + TN + FP + FN)}$	Accuracy assesses the overall correctness of a model by calculating the ratio of correctly predicted cases to the total number of cases.
$\text{F-score} = \frac{2 \times \text{Precision} \times \text{Sensitivity}}{\text{Precision} + \text{Sensitivity}}$	F-score is used for evaluating the model's ability to correctly classify both positive and negative cases by considering precision and sensitivity.

Table 12.2.2: Cross-validation performance metrics of the PLS-DA model using full spectra in detecting quality changes of green asparagus within 4-day storage intervals at different storage temperature groups.

2 °C

	Training set (n=182)			Validation set (n=46)		
Metric	Mean	CI95.Min	CI95.Max	Mean	CI95.Min	CI95.Max
Accuracy	47.9%	44.4%	51.1%	46.6%	40.4%	53.2%
Sensitivity	38.9%	27.8%	49.9%	39.0%	24.0%	59.2%
Specificity	85.0%	84.0%	86.1%	84.8%	81.9%	87.7%
Precision	49.2%	45.8%	52.3%	47.7%	41.4%	54.2%
F-score	43.7%	34.8%	55.5%	50.8%	39.1%	66.6%
Balanced Accuracy	62.5%	56.4%	68.3%	62.0%	54.4%	74.6%

10 °C

	Training set (n=187)			Validation set(n=47)		
Metric	Mean	CI95.Min	CI95.Max	Mean	CI95.Min	CI95.Max
Accuracy	50.5%	48.1%	53.3%	49.2%	44.5%	54.3%
Sensitivity	52.1%	40.2%	62.4%	46.7%	28.6%	68.5%
Specificity	86.7%	85.9%	87.3%	86.5%	84.1%	88.1%
Precision	50.4%	48.1%	53.1%	49.2%	44.5%	54.2%
F-score	48.7%	37.4%	56.1%	57.8%	46.3%	71.2%
Balanced Accuracy	70.9%	64.4%	76.4%	68.7%	57.9%	69.8%

15 °C

	Training set(n=177)			Validation set(n=45)		
Metric	Mean	CI95.Min	CI95.ax	Mean	CI95.Min	CI95.Max
Accuracy	52.1%	46.9%	57.9%	51.9%	42.2%	54.4%
Sensitivity	55.9%	41.6%	62.5%	57.4%	38.9%	74.8%
Specificity	86.1%	84.4%	88.0%	86.2%	82.2%	90.5%
Precision	51.0%	45.7%	56.9%	51.0%	41.1%	63.7%
F-score	57.5%	49.3%	65.6%	57.9%	44.1%	75.3%
Balanced Accuracy	73.5%	63.6%	77.3%	72.7%	62.3%	74.4%

Table 12.2.3: Cross-validation performance metrics of the LDA model using spectra at selected wavelengths in detecting quality changes of green asparagus within 4-day storage intervals at different storage temperature groups.

2 °C

	Training set (n=182)			Validation set (n=46)		
Metric	Mean	CI95.Min	CI95.Max	Mean	CI95.Min	CI95.Max
Accuracy	63.9%	59.6%	67.5%	60.4%	48.9%	68.9%
Sensitivity	61.8%	57.4%	66.2%	59.2%	46.4%	69.4%
Specificity	88.3%	86.8%	89.5%	87.3%	83.1%	90.7%
Precision	63.1%	58.8%	66.9%	59.8%	48.1%	68.4%

F-score	61.9%	57.9%	65.6%	58.6%	47.7%	67.4%
Balanced Accuracy	75.1%	72.1%	77.7%	73.2%	65.4%	79.6%

10 ℃

	Training set (n=187)			Validation set(n=47)		
Metric	Mean	CI95.Min	CI95.Max	Mean	CI95.Min	CI95.Max
Accuracy	75.5%	72.2%	78.6%	74.3%	66.0%	84.1%
Sensitivity	76.1%	72.5%	79.6%	75.8%	64.4%	85.7%
Specificity	91.8%	90.8%	92.9%	91.6%	88.8%	94.9%
Precison	75.2%	71.8%	78.6%	74.1%	65.1%	84.1%
F-score	75.4%	72.0%	78.8%	73.9%	63.7%	84.0%
Balanced Accuracy	83.9%	81.7%	86.3%	83.7%	76.8%	90.3%

15 ℃

	Training set(n=177)			Validation set(n=45)		
Metric	Mean	CI95.Min	CI95.ax	Mean	CI95.Min	CI95.Max
Accuracy	81.1%	77.7%	84.1%	76.9%	67.4%	88.1%
Sensitivity	80.4%	76.7%	83.3%	77.0%	65.9%	89.5%
Specificity	93.8%	92.7%	94.8%	92.5%	89.3%	96.3%
Precision	80.4%	76.9%	83.4%	76.4%	66.3%	87.8%
F-score	80.3%	76.8%	83.3%	76.0%	65.6%	87.6%
Balanced Accuracy	87.1%	84.7%	89.0%	84.7%	77.7%	92.9%